WEI ZHANG

Performance of lead anodes used for zinc electrowinning and their effects on energy consumption and cathode impurities

Thèse présentée
à la Faculté des études supérieures de l'Université Laval
dans le cadre du programme de maîtrise en génie de la métallurgie
pour l'obtention du grade de Philosophiæ Doctor (Ph.D)

FACULTÉ DES SCIENCES ET DE GÉNIE
UNIVERSITÉ LAVAL
QUÉBEC

2010

RÉSUMÉ

Dans cette thèse, les performances de différentes anodes Pb-Ag utilisées pour l'extraction électrolytique du zinc « electrowinning » ont été étudiées dans un électrolyte acide de sulfate de zinc avec ou sans la présence d'ions Mn^{2+} à 38°C, à l'aide de méthodes conventionnelles et plus récentes telles le bruit électrochimique et la spectroscopie d'impédance électrochimique. En outre, l'influence de la gélatine, de l'acide malonique et d'autres additifs sur l'efficacité du courant, la surtension anodique et la morphologie du dépôt de zinc a été examinée pendant l'extraction électrolytique du zinc dans des solutions acides de sulfate de zinc contenant des ions de manganèse avec ou sans impuretés sous une densité de courant de 50 mA/cm^2 à 38°C.

On a montré, par voltammétrie cyclique, que l'utilisation d'une anode en alliage Pb-0,7%Ag pour l'extraction électrolytique du zinc dans un électrolyte acide de sulfate de zinc permettrait de diminuer le pic d'oxydation $Pb \rightarrow PbSO_4$ par 40% et d'augmenter la hauteur du pic d'oxydation de $PbSO_4 \rightarrow \beta\text{-}PbO_2$ de 40%. (Chapitre 4)

Le comportement de trois anodes en alliage Pb-Ag (avec 0,5%Ag, 0,6%Ag et 0,7%Ag) a été évalué par des mesures galvanostatiques, potentiodynamiques et du bruit électrochimique pendant l'extraction électrolytique du zinc. On a observé que l'anode Pb-0,5%Ag avait la plus haute surtension anodique, suivie par celles contenant 0,6%Ag et 0,7%Ag. En comparaison, l'anode de Pb-0,5%Ag présentait plus de produits de corrosion pendant la polarisation (ou l'électrolyse), avec un plateau important d'une valeur moyenne de 1,61 V/SHE pendant la plus longue période (45 minutes), alors que l'anode en alliage Pb-0,7%Ag a montré la formation de cellules galvaniques plus actives en début de chute de potentiel (11-16 h de chute de potentiel) pouvant correspondre à une corrosion localisée plus importante dû à la présence en plus grande quantité des phases contenant Ag et ce, après 24 h d'électrolyse. Durant la décroissance du potentiel électrochimique, un contenu plus élevé en Ag dans l'anode favorise donc une meilleure résistance à la corrosion. Toutefois, à la toute fin de la chute du potentiel, on a observé qu'une teneur plus élevée en argent dans l'anode augmentait légèrement la vitesse de corrosion. (Chapitre 5)

À l'aide de la technique du bruit électrochimique, on a pu montrer que la valeur absolue des pentes reliées à la puissance de la densité spectrale « PDS » des trois anodes Pb-Ag pouvait correspondre à différentes réactions de corrosion et/ou types de corrosion. En effet, l'anode de

plomb contenant 0,5%Ag montre une corrosion uniforme en début d'analyse (première heure) et une corrosion localisée à la fin d'une chute de potentiel de 16 h, alors qu'avec une anode contenant 0,7%Ag, on observe une corrosion localisée importante au début, suivie d'une corrosion uniforme, pour revenir finalement à une corrosion localisée. En comparant les paramètres du bruit électrochimique avec les résultats obtenus par les méthodes conventionnelles, on constate que cette nouvelle approche constitue une technique très valable pour étudier l'influence de l'argent comme élément d'alliage sur la vitesse de corrosion des anodes en plomb. (Chapitre 6)

Une anode de l'alliage Pb contenant 0,56%Ag a été étudiée par spectroscopie d'impédance électrochimique « SIE » dans un électrolyte acide de sulfate de zinc conventionnel contenant $MnSO_4$ pour évaluer son activité électrochimique pendant et après l'électrolyse. La polarisation galvanostatique sous 50 mA/cm^2 et à 38°C a été effectuée pendant 5 h. Une chute de potentiel de 6 h a été observée. Durant la première heure de la chute de potentiel, le procédé de diffusion ionique contrôle la réaction électrochimique, alors que durant la période suivante de la chute du potentiel (2 à 6 h), la capacité électrochimique de la couche double et celle du film en surface diminuent en fonction du temps d'immersion. Par contre, la résistance de la couche externe ainsi que la charge de transfert augmentent en fonction du temps. (Chapitre 7)

Une anode de l'alliage Pb-0,25%Ag-0,1%Ca et trois anodes commerciales en plomb contenant 0,56%Ag, 0,6%Ag et 0,69%Ag ont aussi été étudiées dans un électrolyte acide de sulfate de zinc avec ou sans additions de $MnSO_4$ utilisant les méthodes électrochimiques conventionnelles et la spectroscopie d'impédance électrochimique « SIE » afin d'évaluer leur activité et comportement à la corrosion durant la chute de potentiel après une électrolyse de 5 h. Un examen des surfaces polies des échantillons ont montré que l'anode renfermant un contenu le plus élevé en Ag possédait le plus bas courant de corrosion parmi les quatre types d'anode examinés, suivie par les anodes contenant 0,6%Ag, 0,25%Ag-0,1%Ca et 0,56%Ag. (Chapitre 8)

On a constaté que l'addition d'acide malonique pouvait augmenter l'efficacité de courant d'électrolyse et diminuer les potentiels anodique et cathodique ainsi que le potentiel de la cellule électrolytique dans un électrolyte standard. De plus, dans le cas d'un électrolyte industriel contenant de l'antimoine comme impureté, l'ajout de l'acide malonique « MA » a conduit à une augmentation du pourcentage d'efficacité de courant non négligeable. Le chlorure de Triethylbenzylammonium « TEBACl » est le meilleur additif pour favoriser une efficacité de

courant en présence d'impuretés Ni^{2+} (concentration de ~5 mg/L). On a aussi observé que le TEBACl contrecarrait mieux l'effet délétère du Sb^{3+} que les autres additifs tels que le polyéthylène glycol, le sulfate laurique de sodium, l'acide de perfluoroheptanoique et l'acide malonique, mais pas aussi efficace que la colle et le chlorure ensemble. L'ajout de 2 mg/L de « TEBACl » à la solution d'acide sulfurique en présence d'ions nickel a augmenté le potentiel cathodique de la réaction d'évolution de l'hydrogène sur le dépôt de zinc de façon plus importante qu'avec une solution contenant 100 mg/L d'acide malonique. (Chapitre 9)

L'analyse du bruit électrochimique dans le domaine des temps (paramètres de skewness et de kurtosis) était appropriée pour indiquer l'effet combiné de différentes concentrations de gélatine et d'antimoine sur le procédé d'extraction électrolytique du zinc. Les valeurs des pentes de skewness et de kurtosis tout autour de la moyenne « 0 » signifient que la distribution des données est symétrique autour de la valeur moyenne et que la forme des courbes est semblable à celle d'une distribution normale. Cela semble correspondre à la meilleure combinaison de l'effet synergique de l'impureté et de l'additif pour une efficacité de courant plus élevée, des surtensions anodique et cathodique faibles et de meilleurs dépôts denses et uniformes. (Chapitre 10)

ABSTRACT

In this thesis, the performance of different Pb-Ag anodes used for zinc electrowinning has been studied in acid zinc sulphate electrolyte with or without the presence of Mn^{2+} at 38°C, using conventional and recent methods such as electrochemical noise and electrochemical impedance spectroscopy measurements. Moreover, the influence of gelatine, malonic acid and other additives on current efficiency, anodic overpotential and morphology of zinc deposit has been investigated during zinc electrowinning in acid zinc sulphate solutions containing manganese ions, with or without impurities, under 50 mA/cm^2 current density at 38°C.

It was found, by cyclic voltammetry, that the used of Pb-0.7%Ag anode for zinc electrowinning in acid zinc sulphate electrolyte decreased the oxidation peak ($Pb \rightarrow PbSO_4$) by ~40% and increased the height of oxidation peak of ($PbSO_4 \rightarrow \beta\text{-}PbO_2$) by ~40%. (Chapter 4)

Behaviour of three Pb-Ag alloy anodes (with 0.5%Ag, 0.6%Ag and 0.7%Ag) was evaluated during electrowinning by galvanostatic, potentiodynamic and electrochemical noise measurements. It was observed that Pb-0.5%Ag anode had the highest anodic overpotential, followed by those of anodes containing 0.6%Ag and 0.7%Ag. Comparatively, the Pb-0.5%Ag anode had more corrosion products during polarization (or electrolysis) with an important potential plateau at the average value of 1.61 V/SHE for the longest time (45 min), while Pb-0.7%Ag anode showed the formation of more active galvanic cells at the beginning of the potential decay (11-16 h of potential decay) that could correspond to more localised corrosion due to the presence of a greater quantity of phases containing Ag after 24 h of electrolysis. During the potential decay, higher Ag content in the anode then promoted the best corrosion resistance. However, at the far end of the potential decay, it was observed that a greater silver content in the anode slightly increased the corrosion rates. (Chapter 5)

Using the electrochemical noise technique, it was possible to show that the absolute value related to the power spectral density « PSD » slopes of the three Pb-Ag anodes can correspond to different corrosion reactions and/or corrosion types. Indeed, Pb-0.5%Ag anode shows uniform corrosion at the beginning (first hour) and localised corrosion at the end of the 16 h potential decay, while Pb-0.7%Ag anode shows high localised corrosion at the beginning followed possibly by uniform corrosion and then finally back to localised corrosion. Comparing the

electrochemical noise parameters, it is then found that this technique is a good approach to investigate the influence of silver as alloying element on the corrosion rate of lead anodes. (Chapter 6)

One Pb-0.56%Ag anode was studied by electrochemical impedance spectroscopy « EIS » in typical acid zinc sulphate electrolyte containing $MnSO_4$ to evaluate its electrochemical activity during and after electrolysis. Galvanostatic polarization under 50 mA/cm^2 and at 38°C was carried out for 5 h and a potential decay period of 6 h was evaluated. During the first hour of potential decay, the diffusion process controlled the electrochemical reaction and during the following period of potential decay (2 h to 6 h), the double layer and film capacities decreased with immersion time. However, the surface layer and the charge transfer resistance increased with time. (Chapter 7)

One Pb-0.25%Ag-0.1%Ca anode and three commercial lead alloy anodes containing 0.56%Ag, 0.6%Ag, and 0.69%Ag have been also studied in acid zinc sulphate electrolyte with or without $MnSO_4$ additions using conventional electrochemical methods and electrochemical impedance spectroscopy (EIS) technique to evaluate their activity and corrosion behaviour during the potential decay period after 5 h of electrolysis. The polished surfaces examined showed that anode with the highest silver content (0.69%Ag) had the lowest corrosion current among the four examined anodes, followed by anodes containing 0.6%Ag, 0.25% Ag-0.1% Ca and 0.56%Ag. (Chapter 8)

It was found that adding Malonic acid could increase current efficiency, decrease anodic and cathodic potentials and cell voltage in the standard electrolyte. Moreover, in the case of industrial zinc electrolyte containing antimony impurity, adding Malonic acid « MA » led to an increase in the current efficiency percentage. Triethylbenzylammonium chloride « TEBACl » is the best additive to promote current efficiency in presence of Ni^{2+} impurity (concentration ~5 mg/L). It has been also observed that TEBACl counteracted the deleterious effect of Sb^{3+} better than the other additives such as Polyethyleneglycol, Sodium lauryl sulphate, Perfluoroheptanoic acid and Malonic acid, but not as good as Glue and chloride together. Adding 2 mg/L of TEBACl to sulphuric acid solution in presence of nickel ions increased the cathodic potential of hydrogen evolution reaction on zinc deposit, much more than that of 100 mg/L Malonic acid. (Chapter 9)

The electrochemical noise analysis in the time domain (skewness and kurtosis parameters) was appropriate to reveal the combined effect of different concentrations of gelatin and antimony on zinc electrowinning process. Skewness and kurtosis slope values around 0 mean that the distribution of data is symmetric around the mean value and that the curve shape is similar to that of a normal distribution. This seems to correspond to the best synergetic effect of impurity and additive leading to higher current efficiency, lower overpotentials and better smooth and compact deposits. (Chapter 10)

PREAMBLE

The Chapters 4, 5, 6, 7, 8, 9, 10 of this thesis are articles for scientific Journal or Conference Proceedings. The contribution of each co-author can be summarised as follows:

Publication 1 (Chapter 4):

Co-authors: W. Zhang, S. Jin, E. Ghali, G. Houlachi

Title: Cyclic voltammetric studies of the behaviour of lead-silver anodes in zinc electrolytes, Accepted subject to revision by Journal of Materials Engineering and Performance, ASM, U.S.A.

W. Zhang was responsible for doing all the experiments and assumed the statistical analyses of the data, the interpretation of the results and the writing of the manuscript. Drs. Ghali, Jin, and Mr. Houlachi supervised and revised the work.

Publication 2 (Chapter 5):

Co-authors: W. Zhang, A-M. Lafront, E. Ghali, G. Houlachi, G. Monteith, G. Champoux

Title: Effect of silver content in Pb-Ag anodes on the performance of the anodes during zinc electrowinnig, CMQ, Vol. 48, 2009, pp. 327-336.

The same content is already published in proceeding as: W. Zhang, A-M. Lafront, E. Ghali, G. Houlachi, G. Monteith, G. Champoux (2008), Effect of Silver content in Pb-Ag Anodes on the performance of the Anodes during Zinc Electrowinning, METSOC, Zinc and Lead Metallurgy, Winnipeg, Canada, 47th Annual Conference of Metallurgists of CIM .

W. Zhang did all the experiments and was responsible for the statistical analyses of the data, the interpretation of the results and writing of the manuscript. Dr Anne-Marie Lafront, Mr. Houlachi, Monteith, Champoux and Dr Ghali supervised and revised the work. W. Zhang was the speaker at METSOC conference.

Publication 3 (Chapter 6):

Co-authors: W. Zhang, A-M. Lafront, E. Ghali, G. Houlachi

Title: Influence of silver content on corrosion resistance of lead anodes during potential decay by electrochemical noise measurements, METSOC, Development & Performance of Sulphur Capture Plants, Sudbury, Ontario, Canada, 48th Annual Conf. of Metallurgists of CIM (Aug. 23-26, 2009), pp. 101-115.

W. Zhang did all the experiments and was responsible for the statistical analyses of the data, the interpretation of the results and writing of the manuscript. Dr Lafront, Mr. Houlachi and Dr Ghali supervised and revised the work. W. Zhang was the speaker at METSOC conference.

Publication 4 (Chapter 7):

Co-authors: W. Zhang, M. Bounoughaz, E. Ghali, G. Houlachi

Title: Electrochemical impedance spectroscopy evaluation of the corrosion behaviour of Pb-Ag alloys, it will be sent to Hydrometallurgy.

W. Zhang did all the experiment and was responsible for the statistical analyses of the data, the interpretation of the results and writing of the manuscript. Drs. Bounoughaz, Gu, Ghali, Mr. Houlachi supervised and revised the work.

Publication 5 (Chapter 9):

Co-authors: W. Zhang, A-M. Lafront, E. Ghali, G. Houlachi

Title: Influence of Malonic acid and Triethylbenzylammonium chloride on Zn Electrowinning in zinc electrolyte, Hydrometallurgy, Vol. 99, 2009, pp. 181-188.

W. Zhang did all the experiment and was responsible for the statistical analyses of the data, the interpretation of the results and writing of the manuscript. Drs. Lafront, Ghali, Mr. Houlachi supervised and revised the work.

Publication 6 (Chapter 10):

Co-authors: A-M. Lafront, W. Zhang, E. Ghali, G. Houlachi

Title: Effect of gelatin and antimony on zinc electrowinning by electrochemical noise measurements, CMQ, Vol. 48, 2009, pp. 337-346.

W. Zhang did all the experiments. Statistical analyses of the data, the interpretation of the results and the writing of the manuscript were performed by Dr Anne-Marie Lafront and W. Zhang. Dr Ghali and Mr Houlachi supervised and revised the work.

ACKNOWLEDGEMENTS

I would like to express my utmost appreciation to my principal supervisor, Professor Edward Ghali, for his valuable advice and dedication. Without his support, the completion of this thesis would not have been possible. I am also grateful to Professors Réal Tremblay, Dominique Dubé and members of the Department of Mining, Metallurgical, and Materials Engineering for their help and guidance.

It gives me great pleasure to acknowledge the constant support and guidance provided by Mr. Georges Houlachi and Mr. Gilles Champoux (Hydro-Quebec) and Mr. Gary Monteith (Zinc Électrolytique du Canada Ltée, Montréal).

I am very grateful to Dr. Anne-Marie Lafront and Dr. Shize Jin for their valuable and simulative discussions and their important contribution. I am also very thankful to Dr. Gordon Ping Gu and Mr. Bounoughaz Moussa for teaching me the impedance skills and to Dr. Marc Choquette, Mr. André Ferland, and Mrs. Maude Larouche for their contribution in microstructural analysis. I also would like to thank Mr. Jean Frenette for his help in advanced analysis of X-rays and to Mr. Carl Moniz and Mr. Francois Gilbert, students in engineering programs, for their help with computers.

I am grateful to the Natural Sciences and Engineering Research Council of Canada (NSERC) and the industrial partners LTE, Hydro-Québec, and Zinc Électrolytique du Canada Ltée (Valleyfield, Québec) for their financial support.

No words can adequately express my heartfelt gratitude and thanks to my wife Jianying and daughter Peiyin, Susan for their understanding and unfailing support during this work.

TABLE OF CONTENTS

LIST OF SYMBOLS AND ABBREVIATION

Ag-AgCl/KCl	Silver chloride electrode
A_v, A_i, and A_r	Noise intensity of potential, current and ratio of PSD plots
b	Tafel slope
C^o	Initial concentration, mole cm^{-3}
C_{dl}	Double layer capacitor
D	Diffusion coefficient, cm^2sec^{-1}
E	Electrode potential
$\overline{E}$	Mean potential
E^o	Standard potential
E_{corr}	Corrosion potential
$E_n(k)$	Potential in function of time at each instant k
$E_{1/2}$	Half-wave potential
F	Faraday constant, 96487 C
f	Frequency
G	Gelatin
I	Total cell current (A)
I_A	Anodic current
I_c	Cathodic current
I_{corr}	Corrosion current in amps
i_{corr}	Corrosion current
k_s	Electrochemical specific rate constant
M	Molecular weight
MA	Malonic acid
n	Change electron numbers in electrochemical reaction
N	Number of points in the time record
PFHA	Perfluoroheptanoic acid
R	Gas constant, 8.314 J / mol.^oK
R_p	Polarization resistance
R_n	Noise resistance

R_{ct}	Charge transfer resistance
R_s,	Solution resistor
Ref.	Reference electrode
v	Sweep rate, volt sec^{-1}
SE	Acid electrolyte
SLS	Sodium lauryl sulphate
S_v, S_i and S_r	Slope of potential, current and ratio of PSD plots
T	Absolute temperature
t	Time of deposition
TEBACl	Triethy-benzyl-ammonium chloride
W	Weight of deposit (g)
W_O	Warburg impedance
XRD	X-Ray diffraction
XPS	X-Ray photoelectron spectroscopy
β_a	Anodic Beta Tafel Constant in volt/decade
β_c	Cathodic Beta Constant in volts/decade
σ_v	Standard deviation of potential noise
σ_I	Standard deviation of current noise
ACS	Active corrosion state
CPR	Corrosion potential region
CV	Cell voltage
CE	Current efficiency
EDX	Energy dispersive X-ray analyzer
EIS	Electrochemical impedance spectroscopy
EN	Electrochemical noise
FFT	Fast Fourier Transform
GOB	Good Ordinary Brand
HER	Hydrogen evolution reaction
NOP	Nucleation Overpotential region
OCP	Open circuit potential
PAM	Positive active mass

PC	Power consumption
PSD	Power spectral density
SEM	Scanning electron microscope
SHE	Standard hydrogen electrode
WE	Working electrodes
ZRA	Zero resistance ammeter

LIST OF FIGURES

LIST OF TABLES

CHAPTER 1

Introduction and scope of the work

1.1 Introduction

1.1.1 Background

Zinc is one of the oldest metals and has been an important material in development of civilization. Today, world consumption of zinc is nearly 10 million tonnes per annum and is growing at 2-3% per annum. This growth rate for the world commodity is steady and upwards [1].

Zinc is the twenty-third most abundant element in the Earth's crust. There are zinc mines around the world, with the largest producers being Australia, Canada, China, Peru, and the United States. Mines in Europe include Vieille Montagne in Belgium; Hill of Tara, Galmoy, and Lisheen in Ireland; and Zinkgruvan in Sweden [1].

Minerals from which zinc is extracted include sphalerite (zinc sulfide), smithsonite (zinc carbonate), hemimorphite (zinc silicate), and franklinite (a zinc spinel). The most heavily mined ores (particularly sphalerite) almost contain roughly 10 percent iron as well as 40-50 percent zinc [1].

1.1.2 Extraction of zinc from ores

A sphalerite or zinc sulphide (ZnS) concentrate contains 50-60% zinc, ~ 30% sulphur and other gangue components, impurities and minor metals. Several steps are used to make high purity zinc from ZnS. Firstly the zinc sulphide must be roasted to burn off the sulphur, leaving the zinc in the form of impure zinc oxide (ZnO). Secondly the zinc oxide must be reduced to metallic zinc, and this always is required the use of large quantities of energy since zinc is a highly reactive metal. Finally the zinc must be separated from the gangue and other impurities and from minor metals [2].

Zinc metal is produced at zinc smelters which need the use of heat and energy, as was universally the case when the recovery of zinc first started. The word smelting now includes zinc production by hydrometallurgical means, i.e. production from solutions and suspensions in water. In practical terms the zinc is recovered by electrolysis, which is by applying an electric current through a solution of zinc sulphate ($ZnSO_4$) [3].

In the western world, there are approximately 50 zinc smelters; the most common size of these smelters is in the range 100,000 to 150,000 tonnes per year. [1]

The extractive metallurgy is used to produce the zinc metal. Zinc sulfide (sphalerite) minerals are concentrated by the "froth flotation" method and then usually "pyrometallurgy" method is used to oxidize the zinc sulfide to zinc oxide. The zinc oxide is leached in several stages to increase stronger sulfuric acid. Iron is usually removed as jarosite or goethite, other impurities also are taken off at the same time. It is the final purification to use zinc dust to remove copper, cadmium, and cobalt. The zinc is then extracted from the sulphate acid solution during electrowinning (large-scale electroplating) as cathodic deposits [3].

1.1.3 Zinc quality

The standard zinc product is Special High Grade zinc, with an assay of 99.995% zinc, i.e. it can contain a maximum of 50 parts per million of impurities. However, this quality is difficult to be obtained for some zinc smelters. There is also a grade of 98.5% zinc, the main impurity being lead, and this is used to be the standard grade, called GOB (Good Ordinary Brand) or PW (Prime Western) [4].

1.1.4 Applications of zinc and its alloys

The uses of zinc can be divided into six major categories: (a) coating, (b) casting alloys, (c) alloying element in brass and other alloys, (d) wrought zinc alloys, (e) zinc oxide, and (f) zinc chemicals. The most important application is the use of zinc coatings for corrosion of steel structure because of high corrosion resistance of zinc in atmospheric and other environments. Nearly half of the zinc produced is used for this purpose. The position of zinc in the electromotive series of metals means that zinc coating provides not only a barrier layer to prevent contact between the coated steel and the environment but also a sacrificial protection if discontinuities in the coating occur [5].

1.15 Basic properties

1.1.5.1 Physical properties

Zinc is a silvery blue-gray metal with a relatively low melting point (419.5°C) and boiling point (907°C), the density of zinc at 20°C is 7.14 g/cm^3 [6].

Zinc crystals have a close-packed hexagonal structure. The lattice constants a and c that are 0.2664 and 0.4947 nm, respectively. The axial ratio c/a is 1.856, which is considerably greater than the theoretical value of 1.633 for the system. Although each zinc atom has 12 near neighbors, 6 of them are at a distance of 0.2664 nm and the other 6 are at 0.2907 nm. Thus, the bonds between the atoms in the hexagonal basal layers are appreciably stronger than those between the layers. This is considered for much of the deformation behavior and anisotropy of zinc crystal [6].

The grain structure in a polycrystalline zinc product has preferred orientations depending on the casting and mechanical working conditions. The <0001> direction is in perpendicular to the axis of the cast columnar crystals for cast products; the (0001) plane is parallel to the rolling plane for wire; also the <1120> direction is parallel to the rolling direction for sheet rolled at 20°C [7].

1.1.5.2 Mechanical properties

The strength and hardness of unalloyed zinc are greater than those of tin or lead but much less than those of aluminum or copper. The pure zinc cannot be used in stressed applications since its creep resistance is low. Except zinc very pure, it is brittle at ordinary temperatures, but it is ductile at about 100°C [1].

Since the distance between atoms in the basal plane is shorter than that between atoms in adjoining layers, bonding between atoms in adjoining layers, bonding between basal planes is relatively weak. Under stress, the lattice tends to first slip along this plane. At higher temperature, slip may also occur along the (1010) plane. Twinning is another major deformation mode of zinc crystal and it tends to occur along one of the (1012) pyramidal planes [6].

Pure zinc recrystallizes rapidly after deformation at room temperature because of the high mobility of atoms within the lattice. Thus, zinc cannot be work-hardened at room temperature. Zinc has low resistance to creep due to grain boundary migration. The temperature for recrystallization and the creep resistance can be increased by alloying [6].

Zn-Al eutectoid alloy has very fine grain size, on the order of 1 μm, at temperatures of 200-270°C, and it can obtain superplasticity, with an extension of up to 1000%, [6]. The deformation under this condition appears to take place by slip of the small grains over each other, with little distortion of the grains.

1.1.6 Electrowinning of zinc

Electrowinning is a process of transferring metal ion in the electrolyte to elemental metal by passage of electrical current through a conducting circuit consisting of electrolyte, anode, cathode and connecting wire. The basic features of an electrowinning cell are shown in Figure 1.1. The zinc electrolyte is contained in an electrolytic cell. The cell is fitted with electrodes that are immersed in the electrolyte. The external electrical circuit connected to the electrodes causes an electrical current to flow in a controlled manner between the electrodes through the electrolyte [8]. This results in electrochemical reactions to occur at the interfaces between the electrolyte and the electrodes. Zinc is formed and deposited on the cathode through the transfer of electrons to zinc ions [9].

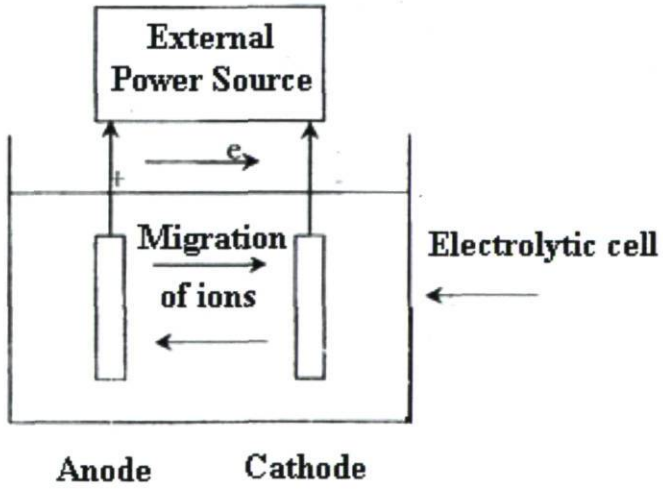

Figure 1.1: Basic features of an electrowinning cell [9].

In zinc electrowinning, zinc is deposited at the cathode and oxygen evolution is on the anode. Inert Pb-alloys and aluminum are often used as anode and cathode, respectively. The main reaction at the cathode involves the conversion of the zinc ions to a metallic state via an electron transfer process. There are also other side reactions at the cathode during the electrowinning process due to the presence of other ionic species in the electrolyte.

At the cathode:

$$Zn^{2+} + 2e^- \rightarrow Zn\ (s) \qquad E^o_{cathode}\ (SHE) = -\ 0.763 \qquad (1.1)$$

$$M^{n+}\ (aq) + ne^- \rightarrow M\ (s) \qquad (1.2)$$

The main reaction occurring at the anode is the oxidation of water to oxygen.

$$2H_2O \rightarrow O_2 + 4H^+ + 4e^-,\ E^o_{anode\ (oxidation)}\ (SHE) = -1.23\ V \qquad (1.3)$$

The overall reaction for the electrowinning of zinc from zinc electrolyte is:

$$2Zn^{2+} + 2H_2O \rightarrow 2Zn + O_2 + 4H^+ \qquad (1.4)$$

The products in zinc electrowinning are (i) zinc metal at the cathode, (ii) oxygen gas at the anode, and regenerated sulphuric acid in the solution [9].

The theoretical potential for the total reaction is given by:

$$E^o_{cell} = E^o_{anode} + E^o_{cathode} = (-1.23) + (-0.763) = -1.993\ V \qquad (1.5)$$

As given by Eq (1.5), the theoretical cell potential for the overall zinc electrowinning reaction is E^o_{cell} = -1.993. In practice, a considerably larger amount of energy is required to overcome factors such as electrical resistance in the circuit, ionic resistance as well as polarization at the anode and cathode. These added voltage requirements are called overpotentials.

1.1.7 Anode

In electrowinning applications, lead and its alloys have been the preferred anode material for a long time. Ivanov et al. (2000) suggested that a useful anode material must meet three requirements: electrical conductivity, electrocatalysis, stability and certain

resistance of the formation of PbO_2 [10]. Good electrical conductivity is essential for energy efficiency. Good electrocatalytical properties are essential to improve product yield. Long-term stability is also an important property because electrode wear and corrosion may cause product contamination, increasing energy consumption and material and labor costs due to the need for periodical maintenance. Also, the anode should have fine, uniform grains with little or no segregation of alloying elements to the grain boundary [11]. Pure lead is a weak material and it tends to creep and warp during use. Therefore, lead must be alloyed in order to improve its mechanical properties. Lead has a relatively low melting point, which facilitates its casting, and it is also a very ductile material and can be machined with ease. In zinc electrowinning plants, lead-silver alloy has been widely used as an insoluble anode material. The lead-silver alloy anode in acidic sulphate bath has the following favourable features [12], small amounts of Ag (0.7-1.0%) alloyed with lead decrease the oxygen overvoltage, and increase the corrosion resistance of material during electrolysis. A well established custom in the most electrolytic zinc plants is to use Pb-Ag alloys containing 0.7-1.0 percent Ag as the anode material. The resulting benefits are a longer anode life and a lower Pb content in the cathodic zinc [13].

The lead-silver alloy anode in acidic sulphate bath has many favourable features, for example, alloying of silver in the alloys resulted in suppression of anodic oxidation of the materials, decrease in the anode potential, formation of dense oxide layer closely adhering to electrode and appearance of β-PbO_2 in the anodic oxide layer, so the lead-silver alloy anode has been employed in electrolytic production of zinc for 50 years [12]

Presently, most of zinc plants use lead-silver alloy as anodes [14]. The stability of the anodes is related to the cathode quality – the lead contamination level of the cathode deposits. To improve the performance of the lead anodes, some manufactories of insoluble anodes, such as RSR Technologies (USA), change the composition and the process of the anodes fabrication, for example, by introducing Ca or Sn in the Pb-Ag alloy and rolling lead anode plates to diminish the number of the holes, voids and laps [15]. But there are some difficulties in their use that can create problems; one is concerned with the incorporation of lead corrosion products in cathode which decreases the purity. Also the oxygen overpotential becomes relatively high which increases the cell voltage and decreases energy efficiency. Due to these problems there is always

interest in finding ways to improve anode performance and minimize the corrosion and overpotential problems [14].

Corrosion resistance of lead anodes is improved by alloying. The beneficial effect can be achieved by better mechanical properties or by a finer grained and more homogeneous microstructure. It was found that the following alloys show the best results with respect to resistance: Pb–Ag 1%; Pb–Ag–As and Pb–Ag–Sn. Several kinds of Pb alloy electrodes containing 1–30% Ag, 5–30% Sn and 5–30% Sb have been casted. The anode composed of 70% Pb, 10% Ag and 20% Sn is most favorable but the bath stability during electrolysis is still too low to be employed industrially [10].

The standard life of an anode in a tank house is approximately 5 to 8 years. The anodes used in the electrowinning process can be considered theoretically insoluble.

1.1.8 Cathode

Aluminum is used as the cathode because it forms no alloys with zinc, thus facilitating zinc deposit separation at the end of the electrolysis, and given its low density, it is easy to handle [16].

1.1.9 Current efficiency

The current efficiency was calculated as CE% = (WFn/ItM) x100%; where W is the weight of deposit (g), n is the number of e^-, F is the faraday constant, M is a molecular weight, I is the total cell current (A) and t is the time of deposition.

Most plants operate over 90% CE. The presence of iron or antimony impurities in the zinc electrolyte has negative impact on the current efficiency, so organic additives are widely employed to counteract their harmful effects. Sometimes, the counteracting can play a beneficial producing optimum current efficiency and acceptable surface morphology of the deposit [17].

1.1.10 Optimum electrowinning conditions

There are numbers of processes and operational parameters that must be maintained to achieve optimum electrowinning conditions [9].

Anode Maintenance- anode should be cleaned regularly. The cleaning is to remove flake on the anode but not to restore a bright surface to the anode.

The composition of the electrolyte used by the refining industry of Valleyfield, Montreal (Noranda) is as follows: 60 g/L of Zn^{2+}, 180 g/L of H_2SO_4, 8 g/L of Mn^{2+}, 250 mg/L Cl^-, 3 mg/L glue.

Zinc sulfate ($ZnSO_4 \cdot 7H_2O$), manganese sulfate ($MnSO_4 \cdot H_2O$) from Sigma-Aldrich Fine Chemicals, sodium chloride and sulfuric acid of Merck KGaA were used to prepare the supporting electrolyte with double distilled water. Gelatin (glue) was product of BDH Inc. The chemicals meet ACS specifications (except gelatin) and were used as received without further treatment.

Temperature (38°C): The setting and the stability of temperature are important to the operation.

Current Density (50 mA/cm^2): Scott et al. (1988) found that at higher current densities a larger driving force is required, and both cathode and anode potentials rise with increasing current density [18].

1.1.11 Organic additives

Malonic acid belongs to the poly acid family. The effect of malonic acid on zinc electrowinning has been studied by Jin et al. (2003). They have found that adding 500 mg/L malonic acid $CH_2(COOH)_2$ to the acid electrolyte (SE) obtained an excellent current efficiency 94.8% and decreased the cell potential by 51 mV of zinc deposits during 12 hours of electrowinning [19]. Gamburge, et al. (2002) have added malonic acid to the electrolyte designed for deposition of Ni coating to increase the buffer properties of the electrolyte and decrease the passivation of nickel anode. The deposits can be obtained in wide range of the current densities with high current efficiency in comparison to boric and succinic acid electrolyte [20].

The beneficial effect of triethy-benzyl-ammonium chloride (TEBACl) in nickel-containing electrolytes has been related to a decrease in the screening effect of hydrogen bubbles where local galvanic cell can be generated [21]. This additive has been shown to

increase the reduction period which precedes the reverse dissolution of zinc deposits obtained under galvanostatic conditions in nickel-containing electrolytes [22].

Gelatin alone is a polarizing agent and its addition in zinc electrowinning baths leads generally to smooth deposits by polarizing the deposition potential of Zn. Also, it has been stated that polarization increases with gelatin concentration [23].

1.2 Scope of the work

1.2.1 Objectives and detailed approaches

The aim of this thesis is to study the influence of silver content on corrosion performance of Pb-Ag alloy anodes and effect of organic additives on current efficiency, cell voltage and quality of zinc deposit. Special and great attentions are devoted to the behaviour of anodes during interruption of electrolysis for maintenance purposes, accompanied by decay of potential. Some techniques of electrochemistry (e.g. Potentiodynamic measurements such as cyclic voltammetry, electrochemical impedance measurements), and surface analyses, e.g. optical microscope scanning electron microscope techniques, X-Ray diffraction (XRD) and X-Ray photoelectron spectroscopy (XPS) are chosen for this purpose. Electrochemical noise measurements are selected also for important potential applications in situ. Detailed description of this thesis work can be related to four main aspects:

A. Anode choice and performance

This necessitates the understanding of the redox mechanism of Pb-Ag alloy anode in the zinc electrolyte conditions of industrial practice at 38°C and 50 mA / cm^2. The influence of high silver content in the Pb-Ag alloy anode should consider the following:

a) Corrosion rate during polarization and at short and long periods of maintenance (decay).

b) The decrease of the amount of corrosion products during electrolysis.

c) Determine the decrease in overpotential during polarization.

d) Evaluate the higher current efficiency.

B. Influence of organic additives

Organic additives can lead to an increase of the current efficiency and a decrease of the cell voltage, and the major parameters to evaluate the performance of additives are:

a) Better counteract the impurities such as: antimony, nickel, etc.

b) Lower overpotentials.

c) Higher current efficiency.

d) Better deposit morphology.

C. Evaluation of gelatin as additive in presence of antimony

Gelatin or Glue interacts in a beneficial way with impurities such as antimony to optimize zinc deposition, increase current efficiency CE% and modify the zinc deposit morphology. The synergetic effect of glue and antimony will be examined by electrochemical noise considering:

a. The highest current efficiency CE%.

b. The lowest overpotentials.

c. Smooth and compact deposits with preferred orientation.

d. Suitable parameters of electrochemical noise measurements to monitor the synergetic effect for optimal concentrations of gelatin additive and antimony impurity.

D. Creative work in corrosion science and engineering

The influence of the Ag content in the lead anode after 2 cycles of 5 h polarization (Ch. 5) and 24 h of polarization (Ch. 6) of the anodes in the zinc electrolyte at 38 $^{\circ}$C and 50 mA / cm^2 and the potential evolution during potential decay periods (up to 16 h) will be considered. This can indicate different performance and mechanisms of corrosion that have been rarely studied by other authors. These chosen periods of decay reflect the practice of electrowinning processes, the corrosion forms of Pb-Ag anodes during the decay will be examined by well established potentiodynamic electrochemical methods and electrochemical noise measurements for the 1st time to our knowledge.

1.2.2. Methodology

This research work was applied the following methods of investigation to accomplish the detailed described planning:

- Cyclic voltammetry studies were carried out to investigate the mechanism of the reactions taking place on Pb-Ag alloy anodes in a sulphuric acid and acidic zinc sulphate electrolytes, and to interpret the peaks appearing on the CV diagrams of lead-silver alloy electrodes in the whole scanned potential region in zinc electrolyte. (Chapter 4)
- It was important to study the performance of different Pb-Ag anodes during and after electrowinning. The potential decay or self discharge method (OPC) following 5 hours polarization in conjunction with the scanning electron microscopy technique are employed to evaluate the influence of Ag concentration on the electrochemical activity, O_2 overpotential and corrosion behaviour. The electrochemical measurements and corrosion behaviour are then related to the microstructure and chemical composition of the anodes. (Chapter 5)
- After 24 hours of polarization, electrochemical noise technique in situ during 16 h of decay was chosen to characterize the electrochemical reaction of the lead anode and the influence of silver on the reduction and oxidation reactions on the surface of the lead anode. (Chapter 6)
- Impedance spectroscopic studies were also used as innovative method in this area to examine the corrosion behaviour of different Pb-Ag alloy anodes, especially during decay periods. Different periods of anode decay and corrosion behaviour were then found and characterised by their mechanisms and kinetics. (Chapter 7)
- The influence of manganese sulphate addition to the electrolyte on the overpotential during electrolysis and its influence on decay periods were investigated and clarified by potentiodynamic and impedance metods. (Chapter 8)
- Conventional measurements were carried out to: 1) optimize the malonic acid concentration since the addition of 500 mg/L to the acid electrolyte (SE) seems excessive and 2) investigate the influence malonic acid, Triethylbenzylammonium

chloride (TEBACl) and other additives on the current efficiency CE%, anodic and cathodic potentials, cell voltage and deposit morphology during the electrowinning of zinc. This was carried out in the same operational conditions from acid sulphate solutions containing manganese ions and metallic impurities such as $Sb^{3+}$and Ni^{2+}. Also, it was important to examine the influence of the promising additives on the competing hydrogen overvoltage reaction "HER" alone in the same operational conditions of electrowinning, since some of these additives as Malonic acid or Triethylbenzylammonium chloride decreases the zinc deposition overvoltage during elecrowinning. (Chapter 9)

- The effect of glue and antimony on the morphology of zinc deposits was evaluated by Electrochemical Noise Analyses "ENA". Analysis of the potential noise in the time domain (skewness and kurtosis values) was carried out to see the effect of the additive (glue) and impurities (antimony) on the quality of the deposit accompanied by scanning electron microscopy "SEM" evaluation. A comparison with current efficiency CE% and cathodic potential measurements after 2 hours of galvanostatic experiments has been done. (Chapter 10)

1.3 References

[1] **Porter, F.**, Zinc Handbook, Faulkener, L.L. (Ed), Marcel dekker, New York, 1991. ISBN 9780824783402.

[2] **Rosenqvist, T.,** Principles of Extractive Metallurgy (2 ed.). Tapir Academic Press. 1992, pp. 7, 16, 186. ISBN 8251919223.

[3] **Bodsworth, C.**, The Extraction and Refining of Metals. CRC Press. 1994, pp. 148-161. ISBN 0849344336.

[4] http://www.williamhunter.co.uk/ZINC/background.htm, 12 Nov. 2009.

[5] **Zhang, X. G.**, Corrosion and Electrochemistry of Zinc, Schulich science & engineering, publisher: plenum pub, seller: landmark ltd, 1996, ISBN: 0306453347.

[6] **Morgan, S. W. K.**, Zinc and Its Alloys and Compounds, John Wiley & Sons, Toronto, 1985.

[7] **Morrow, H.**, Encyclopedia of Materials Science and Engineering, Vol. 7, M.B. Bever (ed), MIT Press, Cambridge, Massachusetts, 1986.

[8] **Woollacott, L. C., Eric, R. H.**, Electrometallurgy, Mineral and Metal Extraction An Overview, The South African Institute of Mining and Metallurgy, Johannesburg, 1994, pp. 371-379.

[9] **Nguyen, T. K. T.,** A Study of the Mechanism by which Cobalt Ions Minimize Corrosion of Lead Alloy Anodes During Electrowinning of Base Metals, Ph.D Thesis, University of Queensland, Australia, 2007.

[10] **Ivanov, I., Stefanov, Y., Noncheva, Z., Petrova, M., Dobrev, Ts., Mirkova, L., Vermeersch, R., and Demaerel, J.-P.,** Insoluble Anodes Used in Hydrometallurgy Part I. Corrosion Resistance of Lead and Lead Alloy Anodes, Hydrometallurgy, vol. 57, 2000, pp. 109-124.

[11] **Prengaman, R.D.,** The Metallurgy of Lead Alloys for Electrowinning Anodes, in: D.J. Robinson, S.E. James (Eds), Proceedings of the sessions sponsored by The electrolytic Procersses Committee of the Metallurgical Society of AIME, The Metallurgical Society of AIME, Los Angles, California, Feb. 28, 1984, pp.49-55.

[12] **Umetsu, Y., Nozoka H. and Tozawa, K.**, Anodic Behaviour of Pb-Ag Alloys in Sulfuric Acid Solution, Proceedings of the International Symposium on Extract. Metall. Zinc, MMJ, Tokyo, Japan, 1985. pp. 265-279.

[13] **Tikkanen, M.H. and Hyvarinen, O.**, On the Anodic Behaviour of Pb-Ag Alloys in Sulfuric Acid Solutions, Proc. Int. Congr. Metai. Corros., 4th (1972), Meeting data 1969, pp. 669-675.

[14] **Yu. P. and O'Keefe**, T.J., Evaluation of Lead Anode Reactions in Acid Sulfate Electrolytes. I. Lead Alloys with Cobalt Additives, J. Electrochem. Soc., vol. 146, 1999, pp. 1361-1369.

[15] **Prengaman R.D. and Siegmund, A.**, New Wrought Pb-Ag-Ca Anodes for Zinc Electrowinning to Protective Oxide Coating Rapidly, LEAD-ZINC 2000, Ed. J.E. Dutrizac, J.A. Gonzalez, D.M. Henke, S.E. James and A.H.-J. Siegmund, Warrendale, PA: The Metallurgical Society of AIME, 2000, pp. 589-597.

[16] **Recéndiz, A., Gonzàlez, I., Nava, J. L.**, Current Efficiency Studies of the Zinc Electrowinning Process on Aluminum Rotating Cylinder Electrode (RCE) in Sulfuric Acid Medium: Influence of Different Additives, Electrochimica Acta 52, 2007, pp. 6880-6887.

[17] **Tripathy, B.C., Das, S.C., Misra, V.N.**, Effect of Antimony(III) on the Electrocrystallisation of Zinc from Sulphate Solutions Containing SLS, Hydrometallurgy, 69, 2003, pp. 81-88.

[18] **Scott, A.C., Pitblado, R.M., Barton, G.W., Ault, A.R.**, Experimental Determination of the Factors Affecting Zinc Electrowinning Efficiency, Journal of Applied Electrochemistry 18, 1988, pp. 120-127.

[19] **Jin, S., Ghali, E., St-Amant, G., Houlachi, G.**, Effect of Some Polyols and Organic Acids on the Current Efficiency and the Cell Voltage During Zinc Electrowinning, in Hydrometallurgy 2003: edited by C. Young, A. Alfantazi, C. Anderson, A. James, D. Dreisinger, and B. Harris, TMS, Warrendale, PA, USA, Vol. 2, 2003, pp. 1219-1231.

[20] **Gamburg, Y.D., Grosheva, M.Y., Biallozor, S., Hass, M.**, The Electrochemical Deposition of Nickel from Electrolytes Containing Malonic Acid. Surface and Coatings Technology 150, 2002, pp. 95-100.

[21] **Bozhkov, C., Petrova, M., Rashkov, St.**, Nickel and Cobalt Synergism Effect in Zinc Electrowinning from Sulphate Electrolytes, Journal of Applied Electrochemistry 22, 1992, pp. 73-81.

[22] **Cachet, C., Wiart, R., Ivanov, I., Stefanov, Y., Rashkov, S.**, Mechanism of the Reverse Dissolution of Zinc in the Presence of Nickel Part II: Influence of Triethylbenzylammonium Chloride, Journal of Applied Electrochemistry 24, 1994, pp. 713-718.

[23] **Ivanov, I., Stefanov, Y.**, Electroextraction of Zinc from Sulphate Electrolytes Containing Antimony and Hydroxyethylated-butine-2-diol-1,4: Part 2: Deposition on A Specpure Aluminium Cathode, Hydrometallurgy, 64, 2002, pp. 111-117.

CHAPTER 2

Literature review

2.1 Lead alloy anodes during electrowinning

General description

Insoluble anodes are widely used in industrial hydrometallurgical processes. A useful anode material must meet: electrical conductivity, electrocatalysis and stability. Good electrical conductivity is beneficial for energy savings. Good electrocatalytical property is essential to improve product yield. Long-term stability is also an important property since electrode wear and corrosion may cause the contamination of deposit, increasing energy consumption, material and labour costs due to the need for periodical maintenance [1].

2.1.1 Alloying elements in lead alloy

The mechanical properties of lead and its creep behaviour in particular, are generally inadequate for this application; however, they may be improved by a suitable arrangement of the structure or by adding alloying elements. Due to creeping of the lead under its own weight at operating temperature, the brittle lead oxide coating is broken up, and dissolves in the electrolyte to cause anode corrosion. The movement of the electrolyte may cause the oxide particles detached from the surface to migrate to cathode. The oxide particles are subsequently reduced at the cathodes, thus increasing the lead content of the zinc cathode. Thus, lead alloys (Pb-Ag, Pb-Sn and Pb-Ca-Sn) are used to improve the mechanical properties and corrosion behaviour of the anode [1].

According to Koenig et al. [2], it is useful to add Ag and other alloying metals in Pb because during their dissolution, the increase of anodic surface leads to the decrease of anodic current density and the corrosion rate. It was established that formation of microelements on the alloy surface is one of the reasons for the increase in resistance of some Pb alloys during corrosion in hot H_2SO_4 without anodic polarization. Thus, silver or other added elements improve not only the mechanical properties of the anodes, but also the corrosion behaviour of the lead alloys [1].

The corrosion resistance of Pb alloys has been studied for many years. The following alloys show the best results with respect to the corrosion resistance: Pb-Ag1%;

Pb-Ag-As and Pb-Ag-Sn. The reason was that the protective action of Ag and other alloying additives in Pb with the formation of good quality of dense lead oxides layers on the anode. Also the inclusion of Tl leads to a more fine-grained structure of Pb [1]. Tizpar and Ghasemi [3] reported that Ag is one of the most attractive of these grid alloying elements, with claims that it can improve both the corrosion stability and the creep strength, even at a comparatively low concentration of 0.01–0.1 wt.%.

Several kinds of Pb alloy electrodes containing 1-30% Ag, and 5-30% Sn have been casted. The anode composed of 70% Pb, 10% Ag and 20% Sn is the most favourable but the stability of bath during polarization is still too low to be employed industrially. Ag in the Pb anode greatly decreases the corrosion rate of lead during electrolysis. The amount of the anode slime is increased by acidity, independent of the temperature. The Pb impurity in the Zn deposit is uniformly distributed over the cathode and it is proportional to the amount of the slime. Pb impurity is always less than 0.01% if the Pb-Ag anode contains more than 0.5% Ag. The impurity tends to gather at the top of the cathode at lower temperatures and at the lower part of cathode at higher temperature. Mn concentration has great influence on Pb contamination of zinc deposit, when the anode contains more than 0.51% Ag content, Pb content in the cathode deposit decreases with increasing Mn^{2+} concentration. When the anode contain less than 0.20% Ag content, the distribution of Pb in the cathode deposit is affected by Mn^{2+} concentration and by the slime formation [1]. Also, Cl^- in the electrolyte has an influence on the anode slime, the amount of anode slime of Ag-Pb anode containing more 0.5% Ag is not affected by less than 40 mg/L Cl^-, larger amount of Cl^- appreciably decreases the anode slime.

The corrosion resistance of Pb and Pb-alloy anodes (determined by the decrease of their weight) has been studied during electrolysis in 1 M H_2SO_4 at a current density of 400 A/m^2 and 25°C. The experiments show that the Pb-1% Ag alloy has considerably more resistant than pure Pb and Pb- 0.5% Ag. Also, a large amount of Se in the Pb-Ag alloy increase resistance, low concentrations of 0.5% Ca or 0.2% Se improve the resistance but their action decreases with time.

Kiryakov and Korchmarek [4] have proved that the protective layer on Pb-1% Ag is thinner than that on the anodes with other compositions. The Pb-1% Ag alloy shows

slower corrosion rate and lower contamination of Pb from the anode than that of Pb-1% Ag - 0.3% Sn - 0.02% Co or Pb-1% Ag - 0.03% Co - 0.2% Sn. Therefore, it can be considered that the thickness of the layer does not affect the corrosion rate of Pb anode. The corrosion behaviour of lead alloys is of great importance. In the case of Pb-1% Ag alloy, a considerable part of Pb^{2+} passes through the loose layer of PbO_2 in 1 M H_2SO_4 solution and then discharge on the cathode. When Pb-1% Ag contains one of the other additions such as Sn, Co, Sb, Mn, the most important reaction is the oxidation of Pb^{2+} to Pb^{4+} in the pores of the layer. By hydrolysis, these ions form a PbO_2 layer covering the anode surface. Concerning the loss in the weight of alloys, it has been found that after two-week electrolysis, the alloys composed of four elements (without Ag) have lost in their weight 10 times more than that of Pb-Ag anodes under the same conditions. The quaternary anode alloys containing Ag show nearly equal resistance to that of Pb-Ag alloy, it means that Ag has a beneficial influence on lead alloys performance [1, 4].

2.1.2 Performances of Pb-Ag anodes during polarization

2.1.2.1 Oxygen overpotential of lead alloys

During the electrowinning, the Pb-Ag alloys are immersed in the zinc electrolyte, the reaction (2.1) takes place on the fresh anode surface at first.

$$Pb + SO_4^{2-} - 2e = PbSO_4 \quad E = -0.356 \text{ V/SHE} \qquad (2.1)$$

Non-conducting layer of $PbSO_4$ covers gradually the anode surface. The anodic current density and the potential on the bare surface increase. The reaction (2.2) occurs on the Pb surface instead of (2.3):

$$PbSO_4 + 2H_2O - 2e = PbO_2 + H_2SO_4 + 2H^+ \quad E = 1.685 \text{ V/SHE} \qquad (2.2)$$

$$4OH^- - 4e = O_2 + 2H_2O \quad E = 0.401 \text{ V/SHE} \qquad (2.3)$$

Thus, a well-conducting PbO_2 covers the surface of anode instead of $PbSO_4$, so the current density and the anodic potential decrease. The reaction of the O_2 evolution (2.3) starts on the layer of PbO_2 and sulphuric acid in the electrolyte renews. After the well conducting PbO_2 film formation, 99.2% of the electricity goes to the oxygen evolution, 0.67% for obtaining PbO_2 and 0.13% for the other reactions [4].

The overpotential of oxygen of can be reduced if a good anode is used. The major alloy used for anodes is lead-silver. It was found that the quality of Zn deposit is best when Pb-1% Ag anodes are used and the anodic potential is decreased by 0.12 V as compared to that of pure lead by Koenig et al. [2]. Several kinds of cast Pb alloy electrodes containing 1-30% Ag, 5-30% Sn or 5-30% Sb have been studied [1]. The addition of Ag reduces the anode potential and suppresses the formation of PbO_2. Also, other factors influence the overpotential of oxygen. For example: the acidity of bath increase from 50 to 200 g/L H_2SO_4 leads to the increase of anodic potential. At a constant concentration of Zn of 60 g/L, the addition of Ag to the Pb anode leads to a lower anodic potential at the acid bath. The anode potential decreases with increasing temperature (20-50 °C). The polarization curves for different Pb alloys (initially anodized at 10,000 A/m^2, at 30°C in 1.8 M H_2SO_4 at 1.5 h) have been measured by Newnham [5]. He has established that the Pb-Sn-Ca alloy shows the highest potential while Pb-Ag-Ca shows the lowest one (Table 2.1). It has been shown that anodic potential of Pb and Pb-Ag anodes becomes more positive with the increase in electrolyte acidity. Pb-1% Ag alloy anodes have less overpotential (0.08-0.12 V) than pure lead.

Table 2.1 Electrode potential (V/SHE) vs. current density (A/m^2) of anodes from lead and its alloys in 1.8 M H_2SO_4 at 30°C [5]

Current density (A/m^2)	Electrode potential VS. SCE (V)					
	Pb-1% Sn -0.07% Ca	Pb	Pb-0.37%Ag -0.12%Ca -0.99%Tl	Pb-0.97%Ag -0.63%Sn	Pb-0.76Ag	Pb-0.9%Ag -0.04%Ca
250	1.925	1.915	1.880	1.850	1.835	1.810
500	1.955	1.940	1.915	1.885	1.870	1.850
1000	1.980	1.975	1.945	1.925	1.915	1.885

The behaviour of Pb-Ag anodes has been investigated. Generally, the anodic potential (E_A) increases within the first few days, and it reaches a maximum value and then decreases continuously [6].

The values of anode potential "E_A" of Pb and lead alloys can be obtained during the stationary phase to form the following sequence under any investigated conditions:

$E_A(Pb) > E_A(Pb\text{-}0.2\%\ Ag) > E_A(Pb\text{-}0.8\%\ Ag)$

After 1-2 weeks, the differences between the anodic potentials were stabilized and the values were as the following:

$\Delta E_A(Pb/Pb\text{-}0.8\%\ Ag) = 140\text{-}170$ mV

$\Delta E_A(Pb/Pb\text{-}0.2\%\ Ag) = 70\text{-}110$ mV

The absolute values of the potentials increase by 170-200 mV when the current density changes from 400 to 800 A/m^2, at 35°C (in 120 g/L H_2SO_4). Also, many small variations can be observed when change of temperature is from 35°C to 45°C as well as the sulphuric acid concentration from 120 to 150 g/L. The time needed by the anodes to reach the maximum value of E_A is higher for pure Pb than that for Pb alloys.

$MnSO_4$ is added to the industrial electrolyte and has an effect on the anodic potential. The reactions of Mn^{2+} on the anode are as follows:

$$MnSO_4 + 2H_2O\text{-}2e = MnO_2 + H_2SO_4 + 2H^+ \quad E = 1.28 \text{ V/SHE} \qquad (2.4)$$

$$MnSO_4 + 4H_2O\ \text{-}5e = MnO_4^- + H_2SO_4 + 6H^+ \quad E = 1.52 \text{ V/SHE} \qquad (2.5)$$

$$PbO_2 + MnSO_4 + 2H_2O = PbSO_4 + HMnO_4 + 3H^+ \qquad (2.6)$$

$$3MnSO_4 + 2HMnO_4 + 2H_2O = 5MnO_2 + 3H_2SO_4 \qquad (2.7)$$

The lead anode was protected from corrosion by MnO_2 and PbO_2 since the well adherent oxide film (MnO_2) increased the thickness and density of oxide layer (PbO_2-MnO_2) which protect the lead anode from corrosion. The presence of Mn^{2+} slightly affects the anodic potential since the potential decreases as a result of depolarization effect during the oxidation of Mn^{2+} on the anode and, moreover, the potential increases as a result of the formation of a protective layer composed of Mn oxides. The presence of Cl^- in the electrolyte leads to a considerable decrease of the anodic potentials of Pb and its alloys. This depolarization effect exerts less influence on the more resistant anodes containing pure Pb or Pb-Ag alloy. The increase of temperature results in a considerable decrease of the anodic potential in the presence of Cl^- [6].

2.1.2.2 Effect of Ag additives on the performance of lead alloy anode

Umetsu et al. [7] has found that the lead-silver alloy anode in acidic sulphate bath had favourable features; silver element added to the lead base resulted in suppression of anodic oxidation of the anode, decrease in the anode potential, formation of dense oxide layer closely adhering to electrode and appearance of β-PbO_2 in the anodic oxide layer. During the anodization of the alloy, the surface of Pb-Ag alloy was coated by a layer of PbO_2, formed anodically and is stable in acidic sulphate solution at a high potential region where oxygen evolution is a major anode reaction. It was also observed that this Pb-Ag alloy can be melted and cast at a low temperature, and most important is that Pb-Ag alloys are spontaneously repaired by anodic oxidation of the underlying material even on accidental destruction of the anodic oxide layer.

Tizpar and Ghasemi [3] thought that Ag is one of the most attractive of these grid alloying elements, because it can improve both the corrosion stability and the creep strength, even at a comparatively low concentration of 0.01–0.1 wt.%. Also, the oxygen evolution is accelerated by the introduction of silver in the alloy and the enhancement is proportional to the Ag content. These results show that either Ag increases the number of active centers available for the oxygen evolution or it decreases the activation energy needed for reaction to proceed. This is an electrocatalytic effect of silver on reaction.

It was found that Ag from the metal surface is oxidized and Ag ions are incorporated into the PbO_2 layer, and Ag changes the α/β PbO_2 ratio and the structure of the PbO_2 layer [8].

Silver is often used as an alloying additive for preparation of grids for lead-acid batteries since Pb–Ag alloys have a higher corrosion resistance [9, 10] and better mechanical properties. Batteries with Pb–Ag grids have good deep cycling behaviour [11]. It has been found that additions of silver accelerate oxygen evolution on the battery grids [12] and decrease the oxygen overvoltage [13,14]. Ag changes the structure of PbO [13] and increases the value of the ratio α/β-PbO_2 in the corrosion layer [14].

The current values for lead 0.05% Ag and 0.1% Ag alloy electrodes are very close to that for the pure Pb electrode at the same potential. The voltammograms at the

potential of 1.5-2.1 V/SHE for the Pb–0.28% Ag and Pb–0.56% Ag electrodes have higher current values than that for the pure Pb electrode. The influence of Ag increases with temperature [6].

Some of the anode potential-polarization time curves are shown in Figure 2.1 for rapidly solidified alloys respectively.

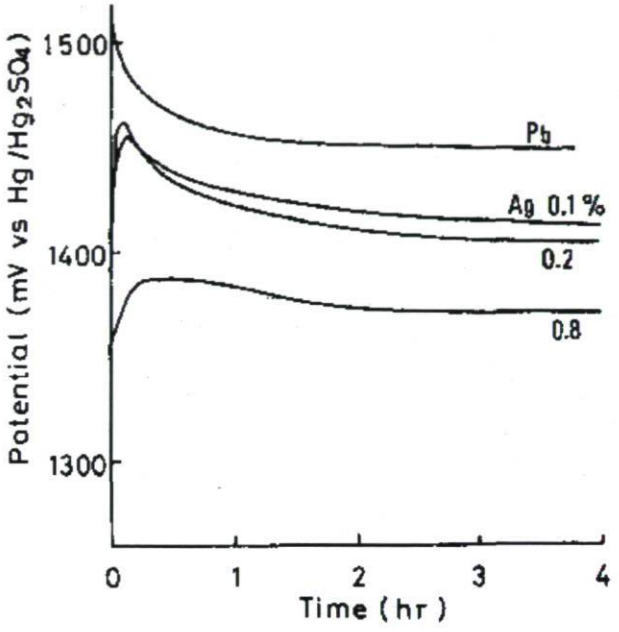

Figure 2.1 Potential transient curves (polarization at current density = 50 mA/cm^2) for some rapidly solidified Pb-Ag alloys [7].

As shown in Figure 2.1, electrode potential of rapidly solidified specimens sharply increased up to a maximum value and then approached gradually respective values depending on Ag-content.

The Pb-Ag alloy anodes become resistant to corrosion when a small amount of Ag is added. The corrosion rate decreases gradually with the increase of Ag content in the range higher than 1%. The corrosion rate is related to overvoltage, i.e. lower overvoltage leads to lower corrosion rate during electrolysis (Figure 2.2).

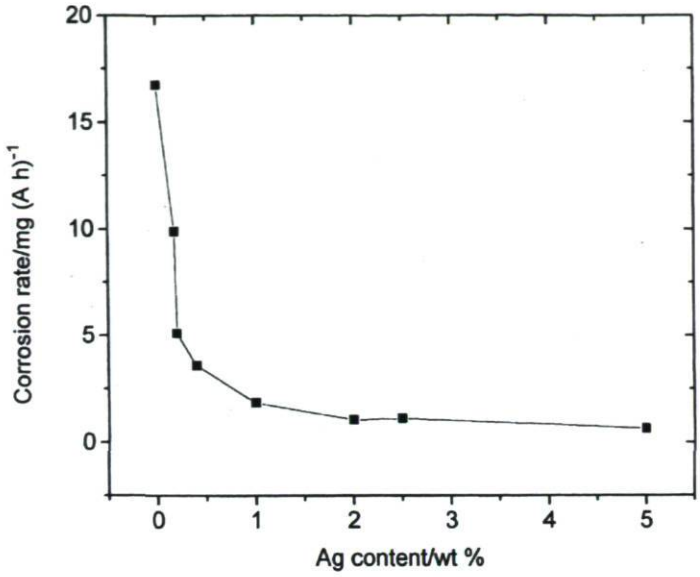

Figure 2.2 Effect of Ag addition on the corrosion rate of the Pb alloy anode in 1 M H_2SO_4, Current density: 10, 000 A/m^2; temperature: 55-60°C [15].

2.1.2.3 Current efficiency of Pb-Ag alloys

The insoluble Pb-Ag alloy anodes normally contain minor amounts of antimony, calcium, iron, etc., the impurities- antimony and iron will dissolve in the zinc electrolyte to decrease the current efficiency when the Pb-Ag anodes was immersed in the solution [16].

2.1.2.4 Influence of some factors on corrosion rates of Pb-Ag alloys

The corrosion rates of pure lead and the alloys containing 0.1-5.0% Ag were examined by Hine at al. [15]. The corrosion rate is higher in the initial stage compared to that in the final stage. This difference is attributed to the gradual formation and build-up of the oxide on the anode surface at relatively low current densities. The oxide layer control anode corrosion, the bulk metal is still exposed to and attacked by the solution through its pores (Figure 2.3).

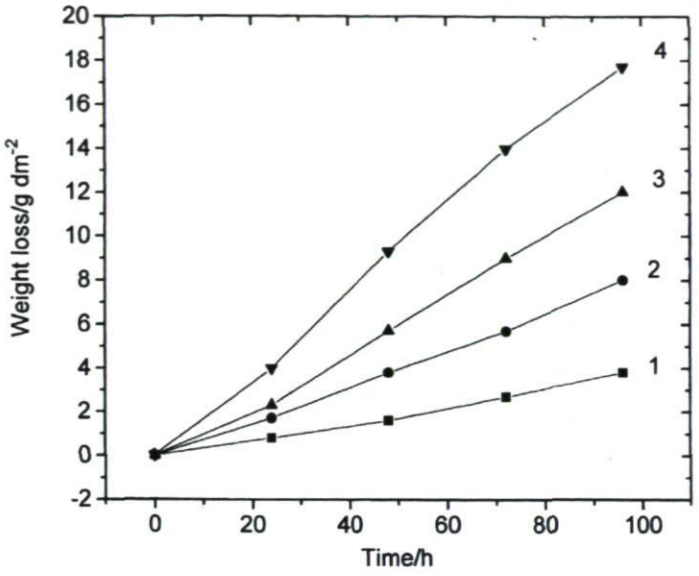

Figure 2.3 Influence of current density on weight loss of Pb-1% Ag alloy anode in 1 M H_2SO_4 at 30-60°C: (1) 2500 A/m^2; (2) 5000 A/m^2; (3) 7500 A/m^2; (4) 10,000 A/m^2 [15].

The corrosion rate increases with current density up to 5000 A/m^2 and is almost unchanged in ranges higher than this (Figure 2.4).

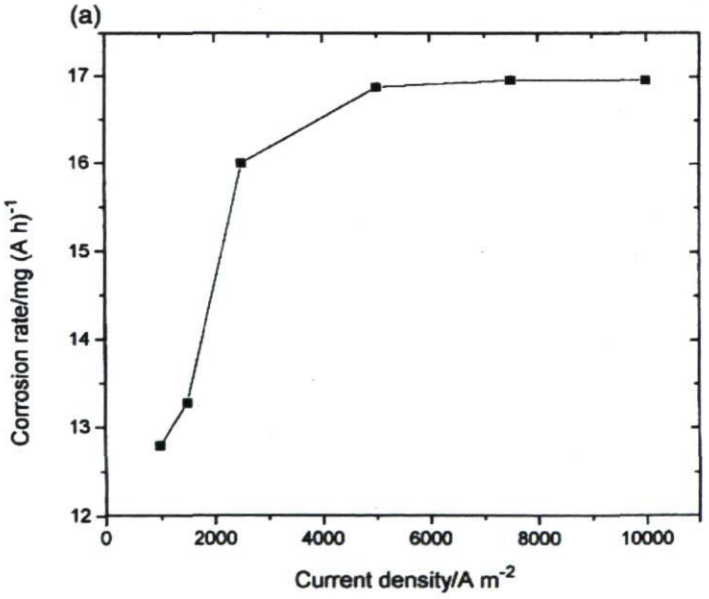

Figure 2.4 Corrosion rate of lead anodes in 1M H_2SO_4 as a function of current density, at 30-60°C [15].

The effect of the acid concentration on the corrosion rate was investigated by the corrosion test in the mixed solutions of Na_2SO_4 and H_2SO_4 conducted in a wide range of

concentrations. It was found that below 1 M H_2SO_4, the SO_4^{2-} ion concentration of the mixed solutions was kept constant at 1 M, while the single solution of H_2SO_4 was employed in the concentration range higher than 1 M. It was observed that the higher the H^+ concentration leads to the higher corrosion rate. The corrosion rate of lead anodes was independent of the SO_4^{2-} concentration by the corrosion test which was carried out in acidified solutions (0.1 M H_2SO_4) with various concentrations of Na_2SO_4 (0.2-1.0M) [15].

The corrosion rate of lead alloy anodes was accelerated by the current density (higher than 50 A/dm^2) and the H_2SO_4 concentration did not affect the mechanism of the anode reaction. This corrosion rate was obtained from the slope of the weight loss vs time curve since the weight loss was fairly proportional to the time. All the corrosion tests were conducted with 1 M H_2SO_4 at the solution temperature rose to 50-60 °C and 100 A/dm^2 [15].

The corrosion rate of Pb-Ag anodes during electrolysis in 1.8 M H_2SO_4 decreases significantly with increasing Ag content up to 1.5% with or without the presence of Mn [16]. A low effect on the corrosion rate was observed by the increase of Ag content beyond 1.5%. A thin layer of MnO_2 on the anode was formed in the presence of Mn^{2+} at current densities of 400-600 A/m^2 and 10000 A/m^2 and it becomes more dense and adherent as the temperature is increased and acts as an additional physical barrier to the corrosion of the Pb-Ag substrate [6].

In the absence of Mn^{2+}, the corrosion rate of alloys with Ag content below 1% increases slightly and the corrosion rate with Ag content greater than 1% increases significantly in at temperature above 50°C. In the presence of Mn^{2+} (10 g/L), the corrosion rate increases significantly with increasing temperature at all concentrations of Ag. Also, the corrosion rate increases greatly at higher acid concentrations for Mn^{2+} containing solutions [6].

In the absence of Mn^{2+}, the corrosion rate increases markedly as the acid and Zn^{2+} levels increase. If sulphate concentration is up to approximately 2.8 M, the corrosion rates are independent of the Zn^{2+}. However, the corrosion rates are considerably higher in the presence of Zn^{2+} when sulphate levels are over 2.8 M [6].

The corrosion tests of the other Pb alloys in the presence or absence of Mn^{2+} in the electrolyte were conducted at 50 °C in 1.8 M H_2SO_4 at 5000 A/m^2. Addition of Sn into the Pb-Ca alloy resulted in decreasing the corrosion rate two times; however this rate was higher than that of Pb-Ag alloys [6]. It was reported that anodic behaviour of Pb-Ag-Ca alloy anodes was polarization in the acid sulphate solution at 50 mA/cm^2 and 40°C, the Ag-content was 0.2-1.0wt% and Ca content was varied in the range up to 1.0wt%, after 48 h experiment, it was found that alloying of silver led to suppress the anodic oxidation of the material and brought about appearance of β-PbO_2, and the calcium in the alloy made more pronounced effect than that of silver [7].

In the case of pure lead, the maximum value of the electrode potential was reached immediately after the application of the current and the electrode potential was a subsequent rapid decrease. For Pb-Ag alloys, the maximum value of anode potential was depressed and the polarization time to reach the maximum was longer as Ag-content increased [6].

2.1.2.5 Deposition of lead dioxide layer

PbO_2 formation is the main possible way that reduces the energy consumption of the anode during electrowinning; and improves the electrocatalytical properties by surface modifications of the lead anodes. The improvement of the electrocatalytical properties of the anode will result in a lower anode potential at constant current density. This can be either due to a surface area effect or to a change in the reaction mechanism [17].

According to many papers, PbO_2 exist in two crystal structures – rhombic (α) and tetragonal (β). They are formed on Pb anode during electrolysis in H_2SO_4 solutions and show different mechanical properties. It was reported that the density of α-PbO_2 is slightly higher than that of β-PbO_2 [17].

The layer grows due to the reaction between Pb and oxygen from boundary oxide solution. A thin layer of β-PbO_2 is formed from sulphate on the boundary with the solution. On further polarization of Pb at potentials over equilibrium potentials for this system, an inclusion of O_2 in the Pb through the layer of β-PbO_2 is realized; and α-PbO_2 is formed close to the surface. It can be observed that transition of α-PbO_2 to tetragonal

Pb and to Pb when the oxygen content decreases with increased distance from boundary. Probably, an oxide layer with intermediate composition is formed between α-PbO_2 and tet-PbO (tetragonal) or PbO_x (where x ranges from 1.4 to 1.6), since the β-PbO_2 is more resistant than α-PbO_2 at normal conditions. At a potential near the equilibrium potential and in solution saturated with $PbSO_4$, the electrochemical recrystallization is also possible:

α-PbO_2 → $PbSO_4$ →β-PbO_2.

It was found that α–PbO_2 is formed from PbO, and β–PbO_2 is formed from $PbSO_4$ after the following reactions [17].

$$\alpha\text{–}PbO_2 + 2\,H^+ + 2\,e^- \rightarrow PbO + H_2O \qquad (2.8)$$

$$\beta\text{–}PbO_2 + H_2SO_4 + 2\,H^+ + 2\,e^- \rightarrow PbSO_4 + 2\,H_2O \qquad (2.9)$$

As reported by Tikkanen and Hyvarinen [18] and Bode [19], Ag favours the occurrence of β-PbO_2 in the oxide film. The curves in Figures 2.5 and 2.6 show X-ray diffraction intensity values for Pb and Pb-2.5% Ag as a function of the anode potential, measured after 24 hours exposure. It can be observed that on surface of pure Pb, α-PbO_2 is the main constituent of thin anodic layer at potentials higher than +1800 mV. Silver increases the relative amount of β-PbO_2 and broadens its stability region. Alloying Ag into the lead promotes β-PbO_2 formation, also silver helps to transform the typical pure Pb intercrystalline corrosion into a more planar one [18].

Considering the practical consequences of the results, it is clearly shown that alloying Ag into the lead results in the surface of Pb-Ag alloys which is converted into β-PbO_2 more easily than that of pure Pb during the electrolytic process. The stability of the β-PbO_2 film is also increased, a factor of the utmost importance in the electrolysis of zinc where the anodic current density is a regulating factor [18].

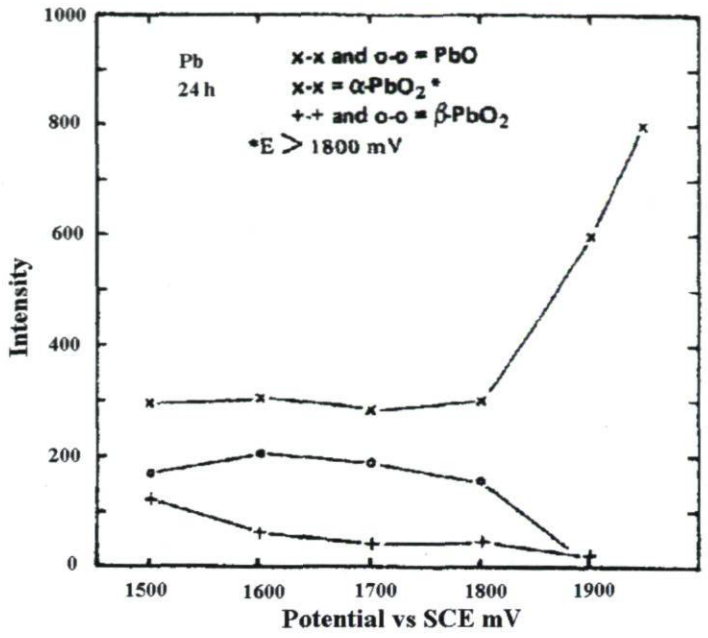

Figure 2.5 X-ray diffraction intensity versus electrode potential curves for Pb; 24 h, 2 N H_2SO_4, 25°C [18].

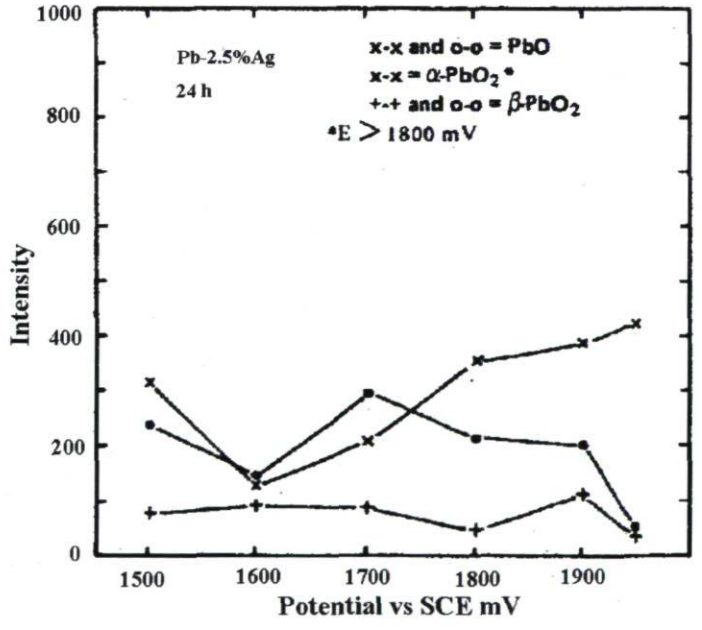

Figure 2.6 X-ray diffraction intensity versus electrode potential curves for Pb-2.5% Ag alloy; 24 h, 2 N H_2SO_4, 25°C [18].

Electrodeposited β-PbO_2 prepared by Ruetschi and Cahan [20] exhibited a stable potential about 7 mV below that of α-PbO_2 in 4.4 M H_2SO_4. β-PbO_2 electrodes prepared by pressing β-PbO_2 powder into perforated lead sheet also exhibited potentials lower than those of α-PbO_2 prepared in the same manner, although these electrodes exhibited limited stability because of the self-discharge effects.

It has been pointed out that the properties of α-PbO_2 suggest that its free energy of formation would be higher than that of β-PbO_2 [21], so a higher electrode potential would be expected for α-PbO_2 than for β- PbO_2.

Four potential regions for dissolution of lead anode in sulphuric acid solution can be divided by Dawson [22] as shown in Figure 2.7. The first region is the formation of a denser layer of $PbSO_4$ crystals which is initially formed on a fresh surface of lead anode. As the film grows, the intercrystalline space between the crystals decreases progressively.

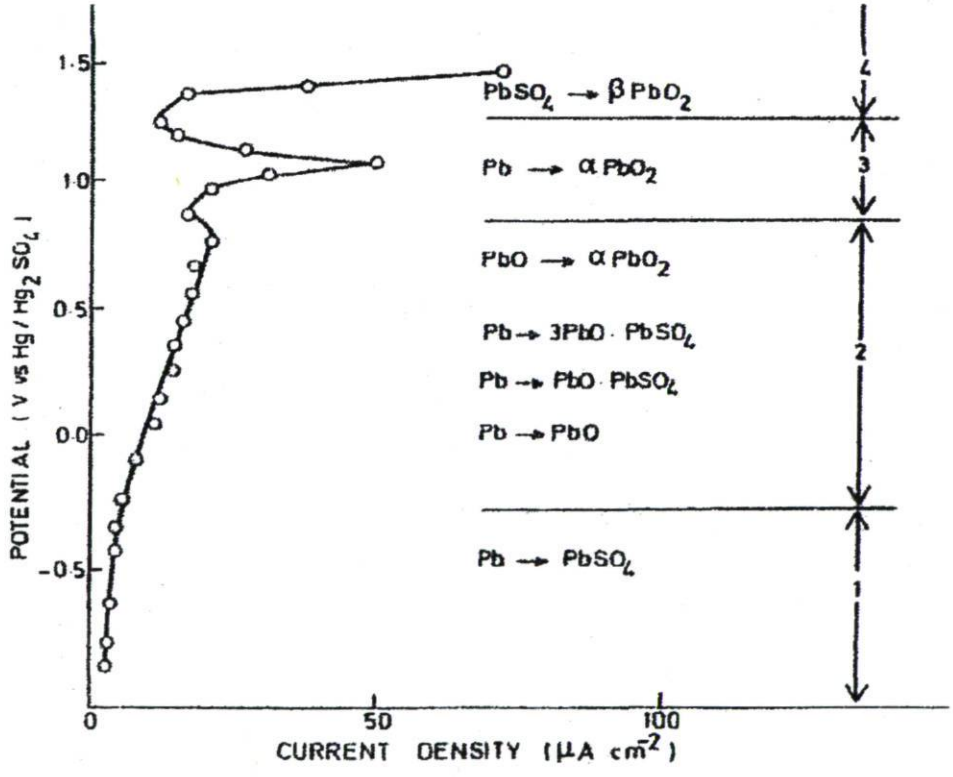

Figure 2.7 Steady state oxidation of lead after 4 h in 4.5M H_2SO_4 [22].

In the second region, the film consists of many products. Basic lead sulphate (such as $PbO.PbSO_4$, $3PbO.PbSO_4.H_2O$, $5PbO.2H_2O$), lead hydroxides and lead monoxide (PbO) are formed as a sequence of the local alkalinisation at the $Pb/PbSO_4$ interface. These products are formed both underneath and within the pores of the initial sulphate film, possibly by the reaction of diffusion OH^- species or water. For the lead monoxide, there are two identified forms: ort-PbO (orthorhombic) and tet-PbO (tetragonal). There is limited formation of α-PbO_2 in this region presumably from the intermediate oxides $PbO\text{-}xPbO_2$, basic lead sulphuric and underlying lead [22, 17].

In the third region, it is the formation of the electronically conducting film of α-PbO_2, which is produced directly from lead. In the fourth region, β-PbO_2 is produced from the lead sulphate. At still higher potential, oxygen evolution occurs and the oxidation increases rapidly with potential [22].

The α-PbO_2 forms stronger deposits composed of large and closely packed crystals whereas, the β-PbO_2 deposits are considerably less strong and composed of badly bonded, fine, needle-shaped crystals. The formation of different forms of PbO_2 is caused by different electrochemical steps, the solution pH influences the formation of α-PbO_2 or β-PbO_2; the α-PbO_2 can only be obtained in alkaline or neutral solutions and the β-PbO_2 can only be formed in acidic solution [17].

It was found that α-PbO_2 is formed close to the surface of lead metal and that β-PbO_2 is formed on top of the corrosion product and further away from the surface of metal [23]. The formation of β-PbO_2 is by the conversion of $PbSO_4$ whereas α-PbO_2 is formed by the direct oxidation of the underlying metal [20, 24]. Initially the lead surface was passivated by a continuous lead sulphate layer, and then a thin film of β-PbO_2 was formed on top of the sulphate layer. Since the pore exists in the layer of β-PbO_2, further polarization allowed oxygen to diffuse through the pore of the layer of β-PbO_2, leading to the formation of α-PbO_2 under the β-PbO_2 layer. Under the α-PbO_2 layer, close to the lead surface, PbO and probably the intermediate compounds PbO_x ($x = 1.3\text{-}1.6$) were formed.

2.2 Potential decay of lead alloy anodes after electrowinning

In some zinc industries, there is a significant period of time where the current is off, 2 hours once a week and 12-16 hours every 3 months which affect the stability of the anodes for maintenance. The process of corrosion of lead anode (in zinc electrowinning electrolyte) on open-circuit following anodic polarization is analogous to the self-discharge of lead acid batteries following the charging state. This means that the results found for lead acid batteries can be taken in consideration with some restrictions. The rate of self-discharge, in time, is determined by the potential-decay procedure (diminution of cell voltage) and called the shelf life of battery. Self-discharge, by definition, involves progressive, time-dependent loss of charge, the state-of-charge (SOC) continuously diminishes with time, usually at progressively diminishing rate [25].

2.2.1 Layer of lead dioxide

High capacity for batteries represents a low self discharge (high electromotive force "EMF", low potential decay and longer discharge time). The contrary is desired during the discharge of the anode at least for the first hour that involves high potential decay $\Delta E/\Delta t$ and the corrosion potential reaches low values very quickly with less intermediate states corresponding to better performance and less corrosion products of the anode during electrolysis [25].

For the batteries, the interparticle contact is an important aspect for the capacity of all lead dioxide electrodes. It can be discussed with respect to the ratio of the two lead dioxide phases, α- and β- PbO_2. Of the two phases, the α-PbO_2 has a more compact structure compared to the more porous β-PbO_2, resulting in a better contact between the particles [26]. The more compact structure makes the α-PbO_2 more difficult to discharge compared to the β-PbO_2. For battery application, it is important to produce lead dioxide with high discharge capacity and a good ability active material and the current collector is an important aspect for the capacity of the battery. These phenomena can be discussed in terms of interparticle contact and porosity [16].

X-ray powder diffraction has been used to identify the α- and β-PbO_2 phases in the samples. Recently, the positive lead dioxide active mass (PAM) has been treated as a gel-crystal system composed by crystal zones surrounded by amorphous lead hydroxide [27-30]. The crystallinity of this oxide (α-PbO_2) was tested by comparing its X-ray spectra with that of chemically formed β-PbO_2 (p.a., MERCK). The intensity of the diffraction peaks for the electrochemically formed α-PbO_2 was found to be lower than those for the chemically formed β-PbO_2.

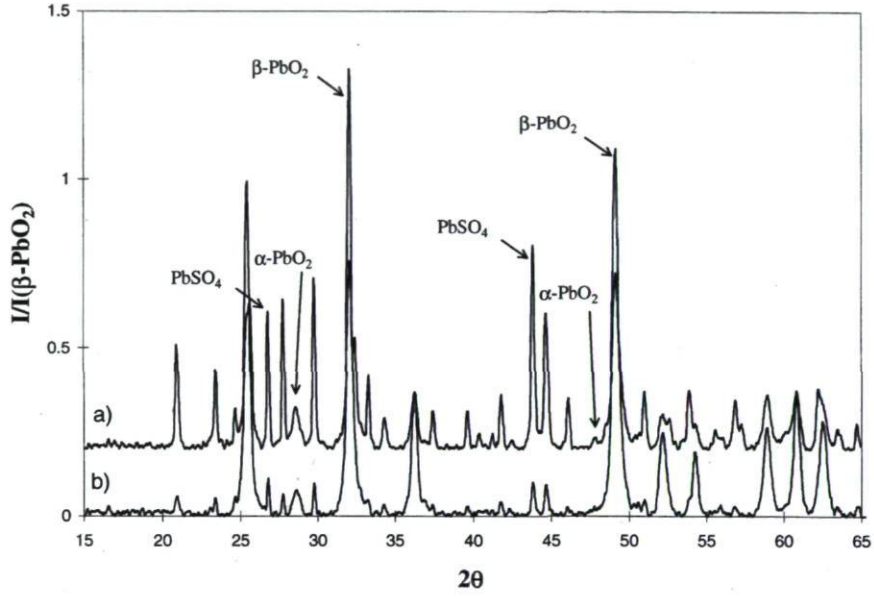

Figure 2.8. X-ray powder diffraction, using CuKa radiation, of the two different lead dioxide phases, α- and β-PbO_2, and lead sulphate [26].

Figure 2.8 shows two spectra, one with the two lead dioxide structures, α and β, and a minor lead sulphate peak, and the other one when a larger ratio of lead sulphate is present in the sample. The corresponding peaks at 28.6 and 47.5° (α- PbO_2), 32.6 and 49° (β-PbO_2) and 26.7 and 43.7 ($PbSO_4$) were used for integration of the respective phase [26].

Lead dioxide particles comprise crystal (PbO_2) and hydrated (gel) zones ($PbO(OH)_2$) [31]. PbO_2 reduction (called discharge or positive active mass "PAM" reduction for batteries) takes place in gel zone [32-34] in a bulk of the particles, probably at the interface crystal and hydrated structure [35]. Gel zone connect the crystal and thus create electron and proton conductivities in PAM [36]. Gel zone is electrochemically

active. Electron conductivity is related to crystal PbO_2 zone and polymer chains in the gel zone. Proton conductivity depends only on the gel zone [35].

Gel/crystal ratio, numbers of chains that interconnect the crystal zone (density of PAM) and additives (dopants) [35, 36] decide conductivity of gel-crystal system (active mass). Discharge capacity was related to film structure and internal resistance of PbO_2 [36]. Gel structure which is a compact caused lower internal resistance because of higher conductivity [36] and thus to higher capacity [34, 37]. Moreover some authors state that increasing α-PbO_2/β-PbO_2 ratio leads to higher capacity too, i.e. α-PbO_2 has more compact structure than β-PbO_2 and is longer to discharge [38, 39]. α-PbO_2 retards PCL (premature capacity loss) [40]. The greater amount of α-PbO_2 in the PAM corresponds to the longer the life of the plate [41].

Since PAM particles and agglomerates contain gel zones, and then an ion-exchange process is possible between the gel zones and the solution [35].

In presence of gel zones in its structure, PAM seems to be a good proton conductor. The discharge behaviour of positive battery plates confirms this conjecture. The reaction of discharge involves hydrogen ions and if PAM were not a good proton conductor, the polarization of the positive plates would be high.

Gel zones allow the reaction of PbO_2 reduction to proceed in the bulk of the particles and agglomerates, probably at the interface between the crystal and hydrated zones.

It has been understood over 100 years [42] that high valent lead oxides form polymer chains of the type:

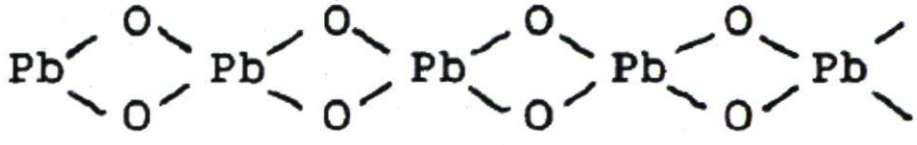

It can be proved that gel zones consist of similar polymer chains that are hydrated as follow:

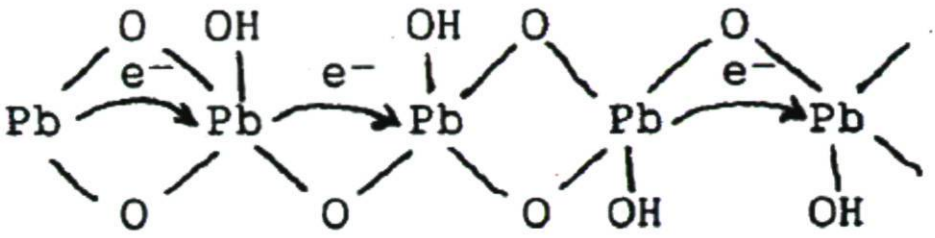

Generally, the mechanism of the electron conductivity in the gel-crystal systems is as follows. Crystal zones are 'islands' in which electrons move freely within the whole volume (conductivity band of degenerated n-type semiconductors). Gel polymer chains forming 'bridges' along which electrons move between the crystals zones (Figure 2.9) interconnected these 'islands'. The gel polymer chains are comprised of a certain amount of free electrons which are electro-neutralized by free protons in the gel chains [35].

An optimum capacity of PAM can be obtained at an optimum ratio between the crystal and gel zones, and optimum electron and proton conductivities. Service life is one of the major tasks of the technology and designs of lead/ acid batteries which determine these optimum ratios and maintain them throughout the battery [35].

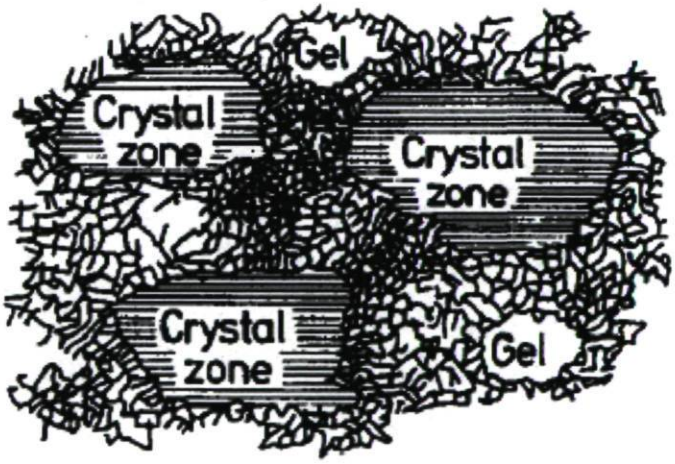

Figure 2.9 A model of the structure of the gel-crystal system characterized by an 'island-bridge' conductivity mechanism of the electron movement in the agglomerates and particles of PAM [35].

2.2.2 Decay of lead dioxide layer

The self-discharge (electrochemical power source) of lead acid batteries must take place through coupled anodic and cathodic processes, passing parasitic currents at one or both individual negative and positive electrodes. During discharge, chemical energy stored in a lead acid battery can be converted into electrical energy. The positive electrode consists of lead oxide, while the negative electrode comprises of lead. Both are converted to lead sulphate in the discharge process [43].

The reversible potentials in a lead battery are:

Positive electrode:

$$PbO_2 + 4\,H^+ + SO_4^{2-} + 2\,e^- \rightarrow PbSO_4 + 2\,H_2O \qquad E^0 = +1.685V \qquad (2.10)$$

Negative electrode:

$$Pb + SO_4^{2-} \rightarrow PbSO_4 + 2\,e^- \qquad E^0 = -0.356V \qquad (2.11)$$

The overall cell reaction is:

$$PbO_2 + 2H_2SO_4 + Pb \rightarrow (\text{discharge}) \leftarrow (\text{charge})\ 2\,PbSO_4 + 2\,H_2O \qquad (2.13)$$

The cell voltage (potential measured between the 2 electrodes) is the available charge of the battery and gives an open circuit potential EMF = 2.041 V.

The lead–acid battery derives its power from the electrochemical energy released during the conversion both on the positive plate, and the negative plate. As cycle life proceeds, the positive active mass (PAM) becomes increasingly soft and finable. The decrease in the cohesion of the PAM is accompanied by an increase in electrical resistance. It has been believed [44] that the gradual decline in plate capacity is caused by this resistance increase, together with increased grid corrosion [34]. Two stages can be divided during the process of PAM discharge [45]. The first stage includes an electrochemical reaction with the transfer of two electrons according to:

$$PbO_2 + 2H^+ + 2e^- \rightarrow Pb(OH)_2 \qquad (2.14)$$

Or discharge of positive active material, the reduction of $PbO(OH)_2$, present in the gel zones,

$$PbO(OH)_2 + 2H^+ + 2e^- = Pb(OH)_2 + H_2O \quad (2.15)$$

During the second stage, a chemical reaction proceeds between the particles and H_2SO_4:

$$Pb(OH)_2 + H_2SO_4 \rightarrow PbSO_4 + 2H_2O \quad (2.16)$$

The formation of $PbSO_4$ weakens the bonds between the PbO_2 crystals and reduces the conductivity of battery. This phenomenon causes one of the major problems encountered when the mechanism of PbO_2 reduction is studied in H_2SO_4 solutions.

Also, Fitas et al. [34] found that the process of PAM reduction includes two electrochemical stages (one electron is consumed during each stage) taking place in the gel zones according to a proton-electron mechanism or a double-injection process:

$$PbO_2 + H^+ + e^- \rightarrow PbOOH, \text{ first plateau,} \quad (2.17)$$

$$PbOOH + H^+ + e^- \rightarrow Pb(OH)_2, \text{ second plateau.} \quad (2.18)$$

By these considerations, it follows that such a mechanism may be possible only if PbO_2 is both electron and proton conductive. Also, the maxima of the proton and electron conductivities of the gel-crystal system determine the PAM capacity.

Zerroual et al. [33] suggested the mechanism of PbO_2 reduction taking place in the gel zones. The ratio between the two forms of lead dioxide determines the capacity of the positive plate. Pavlov [35] showed that lead dioxide active mass is a gel–crystal system with proton and electron conductivity. Using XPS technique, it was found by Pavlov [27] that more than 30% of the surface layer of PbO_2 is hydrated.

Self-discharge reactions of the positive electrode in the lead/acid system are caused from the thermodynamic point of view, by instabilities. These instabilities can be illustrated by a Pourbaix diagram (Figure 2.10). It can be seen that reactions between (i) PbO_2 and H_2O, (ii) PbO_2 and Pb, and (iii) PbO_2 and H_2 are possible. The reaction, between PbO_2 and Hydrogen, is, however, very low (i.e., 5×10^{-5} -10^{-6}), and thus the important reactions are (i) and (ii) [46].

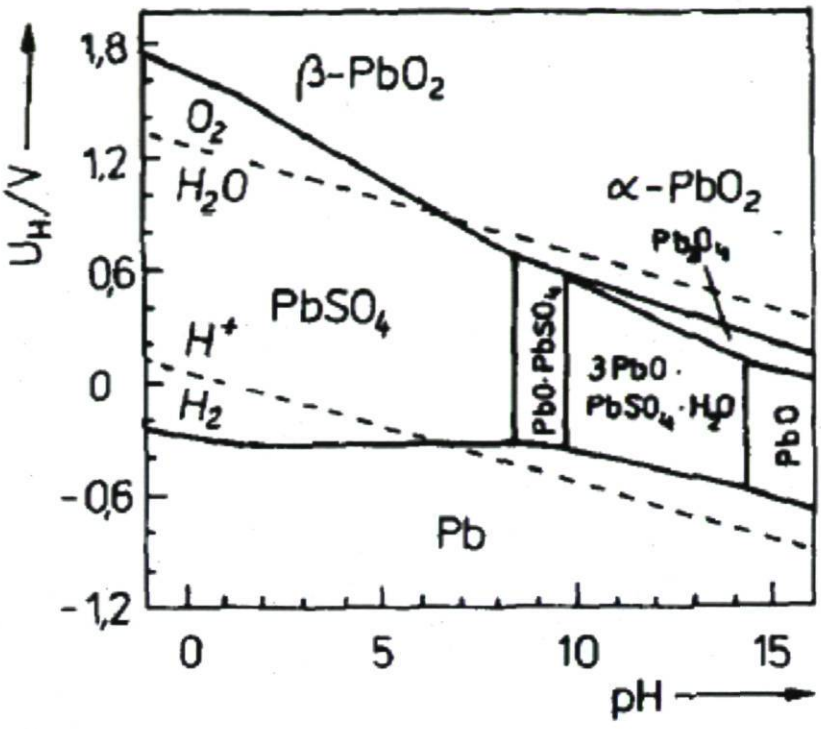

Figure 2.10 Pourbaix diagram of Pb/H_2O system ($\alpha_{SO4}^{2-} = \alpha_{HSO4}^{-} = 1$) [46].

The cathodic reaction takes place in the PbO_2 region of the corrosion layer and in the active mass. The first step is the electrochemical reduction of PbO_2, i.e.

$$PbO_2 + 2\,(2 - x)\,H^+ + 2\,(2 - x)\,e^- \rightarrow PbO_x + (2 - x)\,H_2O \qquad (2.19)$$

In simple terms, *i.e.*, $x = 1$, eqn. (2.19) becomes:

$$PbO_2 + 2H^+ + 2e^- \rightarrow PbO + H_2O \qquad (2.20)$$

The second step in the cathodic reaction is purely chemical, *i.e.*,

$$PbO + H_2SO_4 \rightarrow PbSO_4 + H_2O \qquad (2.21)$$

If the pH of the electrolyte is relatively high, then the rate of the chemical stage, eqn. (2.21), is low, and a PbO-layer is formed in the corrosion-layer region. The cathodic reaction can also take place in the solid state, especially if the reaction temperature is relatively high, *i.e.*, > 100°C. Under this condition, oxygen species are transported from the PbO_2 region in the direction of the grid [47, 48].

The anodic reaction occurs at the phase boundary of the grid/corrosion layer, and results in the formation of Pb^{2+} ions:

$$Pb \rightarrow Pb^{2+} + 2e^- \quad (2.22)$$

The formation of lead compounds was examined by means of potential decay transients for the lead oxidised at 1.85, 1.9, and 1.95 V/SHE. Nguyen and Atrens [49] obtained that the potential remained for some time period at a potential plateau corresponding to the presence of lead dioxide, then decreased sharply to the $PbSO_4$ potential.

Figure 2.11 presents the potential transients for a freshly polished Pb-Ca-Sn electrode after oxidation at a current density of 285 A/m^2 in a 170 g/L H_2SO_4 solution. During oxidation, the surface of the lead anode is oxidised to PbO_2 [50]. When the oxidising current is switched off, the lead dioxide transforms to lead sulphate because thermodynamically lead dioxide is unstable on the surface of lead in the sulphuric acid solutions. At the surface of the film at the electrolyte, PbO_2 is electrochemically reduced according to the following reaction

$$PbO_2 + HSO_4^- + 3H^+ + 2e^- \rightarrow PbSO_4 + 2H_2O \quad E^\circ = 1.685 \quad (2.23)$$

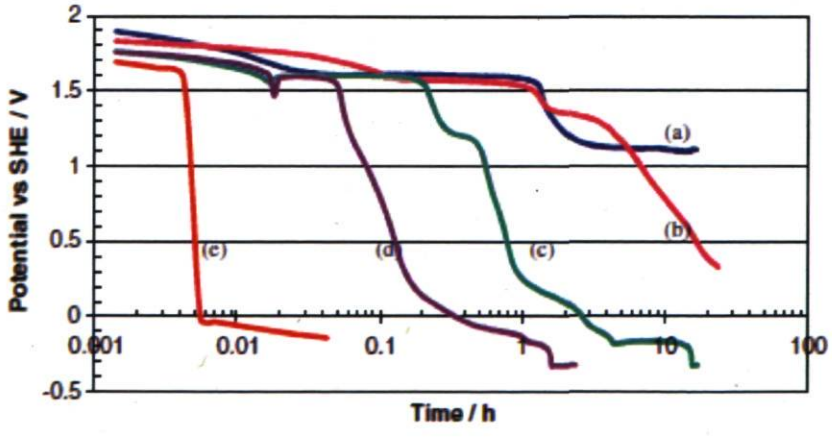

Figure 2.11 The potential of the Pb-Ca-Sn alloy, after oxidation for 24 h at 285 A/m^2, measured in the same solution. The 170 g/L H_2SO_4 solution contained cobalt ion concentrations of (a) 0 mg/L, (b) 100 mg/L, (c) 500 mg/L, (d) 2000 mg/L (e) 5000 mg/L [50].

The oxidized anode at open circuit potential presents two possible interfaces (lead and its semi-conductor dioxide) that is driven by simultaneous cathodic reduction of PbO_2 (active material) at 1) PbO_2/electrolyte interface and 2) PbO_2/Pb (anode) interface. PbO_2 is instable in acid solution [51]:

$$PbO_2 + 4\,H^+ + 2\,e^- \rightarrow Pb^{2+} + 2\,H_2O \quad PbO_2/Pb^2 \qquad E^0 = 1.449 \tag{2.24}$$

It was found that the potential falls quickly after the first plateau from the Figure 2. 11. Garche et al. [52] thought that the potential fall quickly since $PbSO_4$ [PbO_2] is formed during the discharge. The main reaction is as follows

$$2PbO_2 + 4H^+ + SO_4^- + 2e^- \rightarrow PbSO_4[PbO_2] + 2H_2O \tag{2.25}$$

Volume of $2PbO_2$= 2 X 25 cm^3/mol, and volume of $PbSO_4$=49 cm^3/mol and [PbO_2] = 25 cm^3/mol, i.e ther is increase of 24 cm^3/mol.

At the end of discharge, the further discharge of PbO_2 will be blocked by $PbSO_4$, and the remaining $PbSO_4$ ([PbO_2]) will be electrochemically inactive, i.e., $PbSO_4$ [PbO_2] is formed and the potential will fall [52]. However, the dense passivating layer of lead sulphate will be made porous by the formation of lead because the molar volume relation of the compounds is Volume of $PbSO_4$/ Volume of PbO_2 = 1.96: 1. Therefore, inactive lead dioxide ([PbO_2]) comes into contact with the electrolyte and can be reduced to lead sulphate.

Also, the dissolution of the lead appears in the pores of PbO_2 and $PbSO_4$ is formed in the pore or in the cracks of PbO_2 [53]. The anodic reaction could be the following one:

$$Pb + HSO_4^- \leftrightarrow PbSO_4 + H^+ + 2\,e^- \tag{2.26}$$

$PbSO_4$/Pb $\quad E^0$=–0.300 V

The time for which the potential remained at plateau at ~1.6V is a measure of the time taken to convert the PbO_2 to $PbSO_4$. This time relates to the amount of PbO_2 present as well as to the difficulty to converting the PbO_2 into $PbSO_4$. The origin of the second plateau at about 1.1 V may be associated with the reduction of PbO_2 to form basic lead sulphate:

$2PbO_2 + HSO_4^- + 5H^+ + 4e^- \rightarrow PbO.PbSO_4 + 3H_2O \quad E^o = 1.375$ (2.27)

Also, some authors [53, 54] found that the cathodic reaction, the transformation of PbO_2 to $PbSO_4$, could proceed by electrochemical sulphate reaction giving basic lead sulphates intermediate compound followed by chemical sulphate reaction (acid-base reaction)

$2\ PbO_2 + 6\ H^+ + SO_4^{2-} + 4\ e^- \rightarrow PbOPbSO_4 + 3\ H_2O$ (2.28)

$PbO_2 / PbOPbSO_4 \qquad E^0 = 1.468$ V

$4\ PbO_2 + 10\ H^+ + SO_4^{2-} + 8\ e^- \rightarrow 3\ PbOPbSO_4\ H_2O + 4\ H_2O$ (2.29)

$PbO_2 / 3PbOPbSO_4\ H_2O \quad E^0 = 1.325$ V

$PbOPbSO_4 + H_2SO_4 \rightarrow 2\ PbSO_4 + H_2O$ (2.30)

Equations (2.28) and (2.30) give the total reaction:

$2\ PbO_2 + 6\ H^+ + SO_4^{2-} + 4\ e^- + H_2\ SO_4 \rightarrow 2\ PbSO_4 + 4\ H_2O$ (2.31)

$3\ PbOPbSO_4\ H_2O + H_2SO_4 \rightarrow 2\ (PbOPbSO_4) + H_2O$ (2.32)

Equations (2.29) and (2.32) give the total reaction:

$PbOPbSO_4 + H_2SO_4 \rightarrow 2PbSO_4 + H_2O$ (2.33)

The transformation of PbO_2 to $PbSO_4$ could proceed by hydrolysis reaction of the produced oxide to hydroxide (intermediate compounds) followed by chemical sulphate reaction (acid-base reaction)

$PbO_2 + 2\ H^+ + 2\ e^- \rightarrow PbO + H_2O$ (2.34)

$PbO_2 / PbO \qquad E^0 = 1.107$

$Pb(OH)_2 + H_2SO_4 \rightarrow PbSO_4 + 2\ H_2O$ (2.35)

Equations (2.34) and (2.35) give the total reaction:

$PbO_2 + 2\ H^+ + 2\ e^- + H_2SO_4 \rightarrow PbSO_4 + 2\ H_2O$ (2.36)

From Figure 2.11 (c, d), the potential of plateau is around or below 0.5 V vs SHE, it is possible that the conventional corrosion mechanism of Pb occurs at the H_2O/Pb interface (Pb, $PbSO_4$ /aqueous H_2SO_4 /H_2). Diffusion of oxygen to cathodic sites can depolarise the

cathodic reaction and produce water instead of H_2. When dissolved oxygen is available at the interface, it could be coupled to all reactions of Pb oxidation since it is a strong depolarizer [51].

$$Pb+HSO_4^- \leftrightarrow PbSO_4+ H^+ +2\ e^- \quad (2.37)$$

$PbSO_4/Pb$ $\quad E^0=-0.300$

$$Pb+H_2O \leftrightarrow PbO+2\ H^+ +2\ e^- \quad (2.38)$$

PbO/Pb $\quad E^0 = 0.248$

$$2\ Pb+H_2O+SO_4^{2-} \rightarrow PbOPbSO_4 \cdot +2\ H^+ +4\ e^- \quad (2.39)$$

$PbOPbSO_4/Pb$ $\quad E^0=-0.113$

$$4\ Pb+H_2O+SO_4^{2-} \rightarrow 3\ PbOPbSO_4 \cdot H_2O+6\ H^+ +8\ e^- \quad (2.40)$$

$3PbOPbSO_4 \cdot H_2O\ /Pb$ $\quad E^0=0.030$

The cathodic site for O_2 reduction (followed by H_2) could be the alloying element in lead alloy. More alloying nobler elements lead to more corrosion since it increases the limited number of cathodic sites [55].

2.3 Zinc deposit

Many factors influence the zinc electrowinning. Also, it is reported that some of the principal problems encountered in electrowinning of zinc from acid sulphate electrolytes are (a) maintaining high current efficiency and low energy consumption, (b) producing smoother level deposits at high current densities [56].

2.3.1 Experimental determination of the factors affecting zinc electrowinning efficiency

The two parameters directly outline the energy consumption are current efficiency and cell voltage. The major variables affecting these two parameters are: zinc and acid concentrations, current density, temperature, impurities and additive levels. The time of deposition can also be important if impurities are present in the electrolyte solution. Hence for the model to be capable of predicting current efficiency, cell voltage and hence

energy consumption, it must accurately describe the effects of each of these major variables [57].

Zinc concentration

The effect of increasing the concentration of zinc in the cell from 20 g/L to 85 g/L is illustrated in Figure 2.12. It can be observed that the current efficiency increases rapidly at concentrations between 20-50 g/L, since the reaction rate for the zinc deposition reaction increases as the number of zinc ions in solution rises.

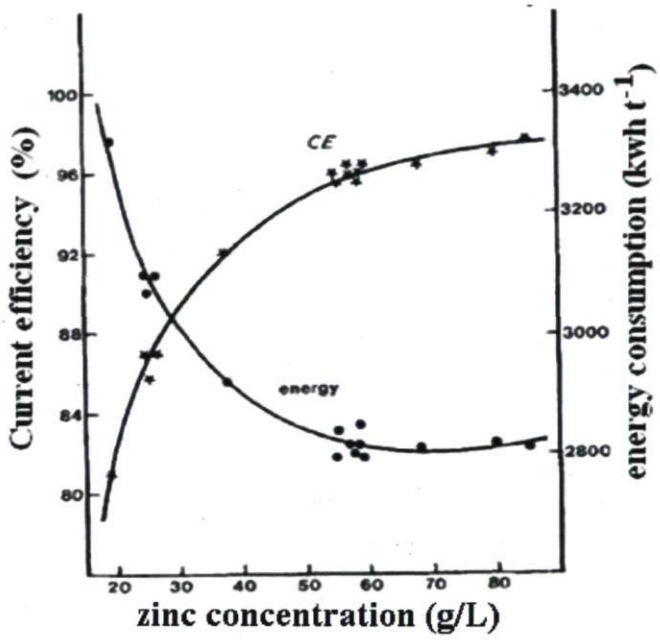

Figure 2.12. Effect of zinc concentration on electrowinning performance (H_2SO_4 = 110 g/L, temperature = 35°C, current density = 500 A/m^2, t = time in hours) [57].

Acidity of electrolyte

The current efficiency decreased linearly from 97.4% at 65 g/L sulphuric acid to 94.0% at 155 g/L acid (Figure 2.13), at the range of concentrations of sulphuric acid, the effect on the current efficiency is not significant. However, the rate of hydrogen evolution becomes greater as the concentration of hydrogen ions increases. Since hydrogen evolution and zinc deposition reactions are both competing for each unit of available current at the cathode, any increase in the rate of one of them, must be associated with a decrease in the

rate of the other reaction. So the rate of zinc deposition must decrease with increasing acidity, which results in a lower cell current efficiency.

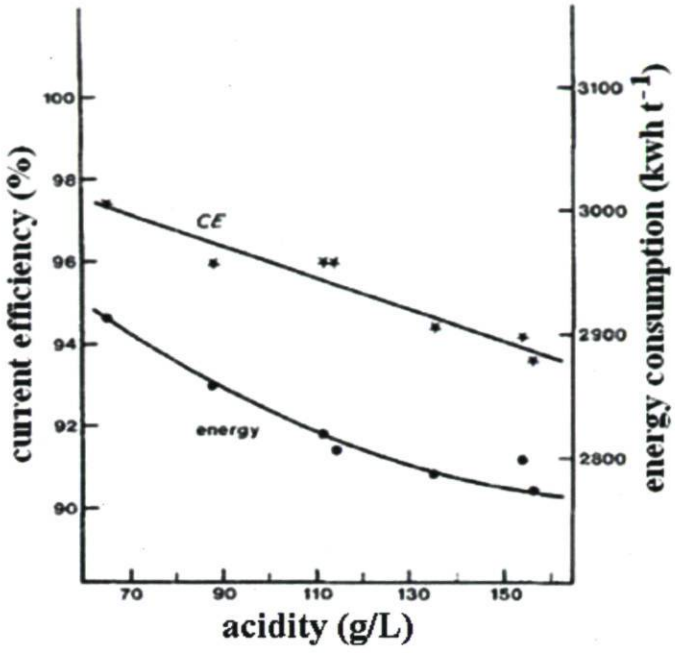

Figure 2.13. Effect of acid concentration on electrowinning performance (Zinc concentration (Zinc concentration = 55 g/L; temperature = 35°C, current density = 500 A/m^2, t = time in hours) [57].

Cell temperature

The current efficiency increased with temperature from 94.0% at 25°C to 97.7% at 50°C (Figure 2.14) [57]. The specific energy consumption declines rapidly with increasing temperature (Figure 2.14) from 2960 $kWht^{-1}$ at 25°C to 2700 $kWht^{-1}$ at 50°C. The reason for this decrease is due to both the increasing current efficiency and the decreasing cell voltage as the temperature rises. Cell voltage decreased from 3.39 V at 25°C to 3.21 V at 45°C.

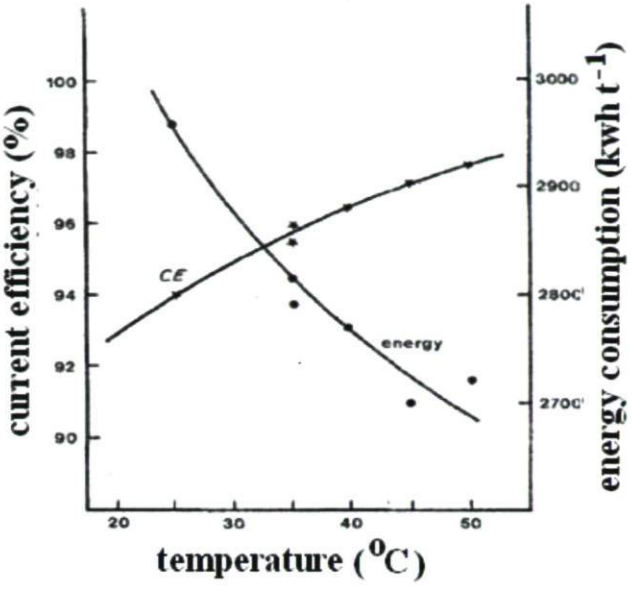

Figure 2.14 Effect of temperature on electrowinning performance (Zinc concentration = 55 g/L; H_2SO_4 = 110 g/L; current density = 500 A/m^2, t = time in hours) [57].

Current density

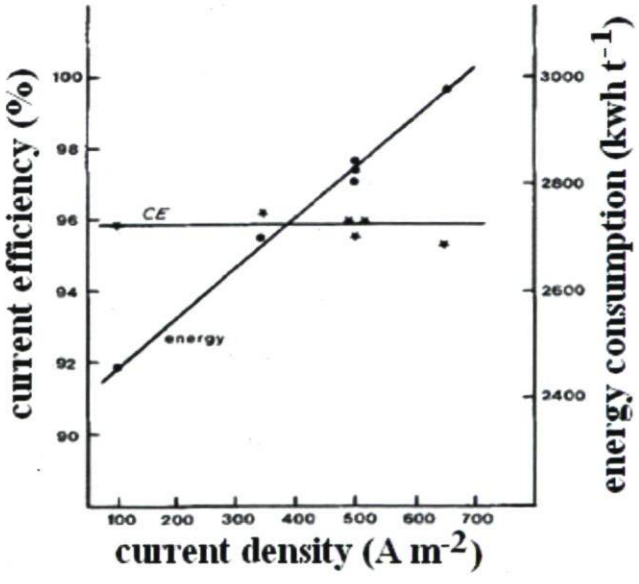

Figure 2.15 Effect of current density on electrowinning performance (zinc concentration = 55 g/L; H_2SO_4 = 110 g/L; temperature = 35°C, t = time in hours) [57].

These experiments were carried out at constant coulombs passed in order to separate coulombic and current density effects. Current efficiency was found to be independent of current density over the range 100-650 Am^{-2} as shown in Figure 2.15.

Additive rate

Animal glue is added to the electrolyte containing antimony as impurity to control the deposit morphology, however the mechanism of action is not well known. Under standard conditions (55 g/L Zn, 110 g/L H_2SO_4), the additive (25 mg/L animal glue) was added to the electrolyte containing Sb impurity (0.04 mg/L) [57].

2.3.2 Impurities

The zinc electrowinning process is very sensitive to the presence of impurities in the electrolyte. Until now, the impurity behaviour in the zinc electrolyte is not well understood, but many researchers have studied the work which characterizes impurity effects on zinc deposit morphology and orientation and on zinc deposition polarization [58].

It is serious problem that hydrogen ions can be reduced in solution in the presence of the impurity. Some impurities such as Ge, Sb are hydride formers and the formation of which could serve as the cathodic reaction for localized corrosion, it is possible for the zinc to redissolve even while cathodically polarization. Since Ge, Sb etc have low hydrogen overpotentials, they may facilitate the reduction of hydrogen ions in the electrolyte. Other impurities such as Ni and Co cause mild re-dissolution of the zinc deposit, but this occurs only after an incubation period that is dependent on the impurity concentration and on the zinc to acid ratio. Finally, a synergism often occurs when the impurities and organic additives present in the electrolyte and this complicates the prediction of impurity effects on the CE [58].

The effect of the elements listed in Table 2.2 on the electrowinning of 1-h zinc deposits from industrial acid sulphate electrolyte have been characterized in terms of deposit morphology and preferred orientation and in terms of zinc deposition current

efficiency and polarization. The factors such as the elements studied, their atomic number and their position in the periodic table are shown in Table 2.2 [58].

Table 2.2 Partial periodic classification of elements and their atomic numbers [58]

VIII		*IB*	*IIB*	*IIIA*	*IVA*	*VA*	*VIA*
Co	Ni	Cu	Zn	Ga	Ge	As	Se
27	28	29	30	31	32	33	34
			Cd	In	Sn	Sb	Te
			48	49	50	51	52
				Tl	Pb	Bi	
				81	82	83	

During zinc electrowinning, when antimony is introduced into the electrolyte, a process of reverse dissolution of zinc starts soon. Antimony is a very active impurity because of its uniform deposition on the zinc surface in the form of an electrolytic alloy. It partially interacts with hydrogen ions absorbed onto the separate crystal faces of zinc or combines with hydrogen ions in the double layer forming a volatile hydride. A large specific surface is created by antimony, and the actual current density of this surface is very low and the local antimony-zinc galvanic pairs are numerous [59]. It was found that the amount of antimony in zinc deposit is proportional to its concentration in the electrolyte. During the first few minutes of electrolysis, antimony deposition on the zinc is more intensive. Due to the process of reverse dissolution, it can be observed that rounding of the hexagonal, flat zinc crystallites and fine pitting and pores occur at the grain boundaries [56]. When antimony ion concentrations are higher than 0.1 mg/L, only a thin zinc layer is observed on the cathode since corrosion on the part of the aluminum substrate is so strong [60].

Antimony (at concentrations > 0.02 mg/L) has long been recognized as one of the most detrimental impurities with respect to zinc deposition CE [61], and its effects have most recently been studied by Ault and Frazer [62]. Without additive/impurity in the zinc electrolyte (Blank), the CE was 89.3%. It was reported that when Sb (III) was introduced into the solution alone, it decreased the current efficiency and deteriorated the deposit quality. When Sb (III) concentration in the electrolysis bath was 0.08 mg/L, the effect

was worst and CE showed a significant decrease by about 26% [63]. Figure 2.16 shows the effects of Ge, Sb, Se, Te and Sn on the CE over the concentration range 0 to 2.0 mg/L.

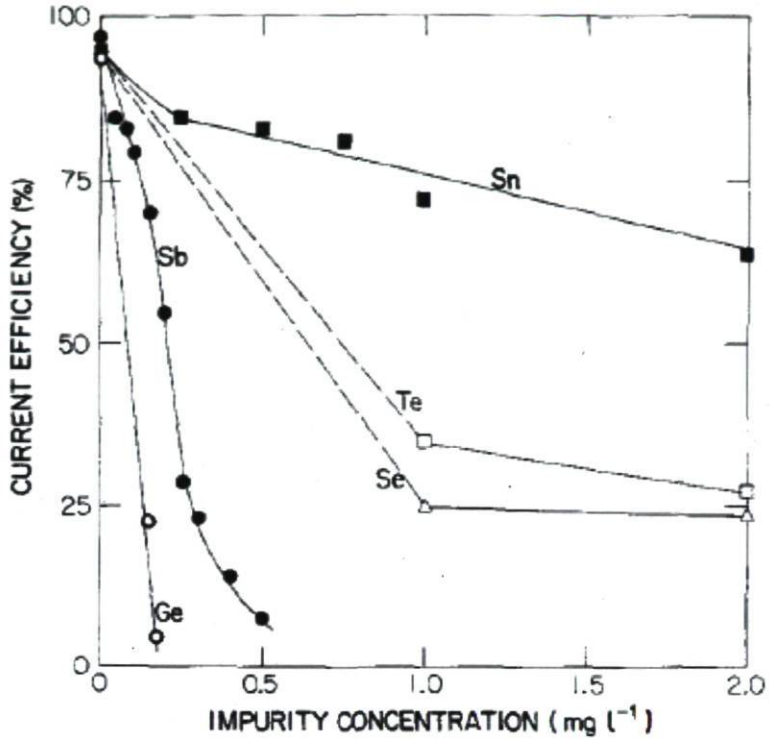

Figure 2.16 The effect of increasing impurities concentration (Ge, Sb, Se, Te, and Sn) on the current efficiency for 1 h zinc deposit, electrowon at 430 A/m^2 from industrial acid sulphate electrolyte [58].

It was observed from Figure 2.16 that both Ge and Sb are very detrimental to zinc deposition CE [58]. For Ge, it was found that the CE decreased from 96 to 86% with the addition of 0.15 mg/L Ge. At 0.3 mg/L Ge, the CE was 0%, i.e. it means that the zinc deposit was completely redissolved [58].

2.3.3 Glue and antimony

The addition of animal gelatin (glue) to the zinc electrolyte used in zinc electrowinning plant serves several purposes [64]. Gelatin increases zinc deposition polarization, decreases the current efficiency and reduces the deposit grain size. Certain combinations of antimony and gelatin optimize zinc deposition current efficiency and decrease acid

mist evolution [60]. It was also observed that the glue additions control cathode growth to give smooth cathode zinc deposits, inhibit the deleterious effects that impurities such as antimony have on the current efficiency of zinc electrodeposition, and decrease acid mist evolution by forming stable foam layers on the electrolytic cell tops in conjunction with additives [64].

A large number of solid and liquid animal glue are available commercially with variation in physical and chemical properties due to different raw material sources and method preparation. Before their use in the zinc tankrooms, these animal glues are often evaluated for use in zinc electrowinning by testing in small pilot electrolysis cell [64].

Gelatin or glue (G) is an animal protein that consists of a complicated mixture of polypeptides and is used as levelling agent. In acid solution and at 65°C, the protein breaks up in polypeptides and peptides. With an additional hydrolysis, the polypeptides and peptides become oligoelements and amino acids [65]. Gelatin is completely degraded in twenty hours [66].

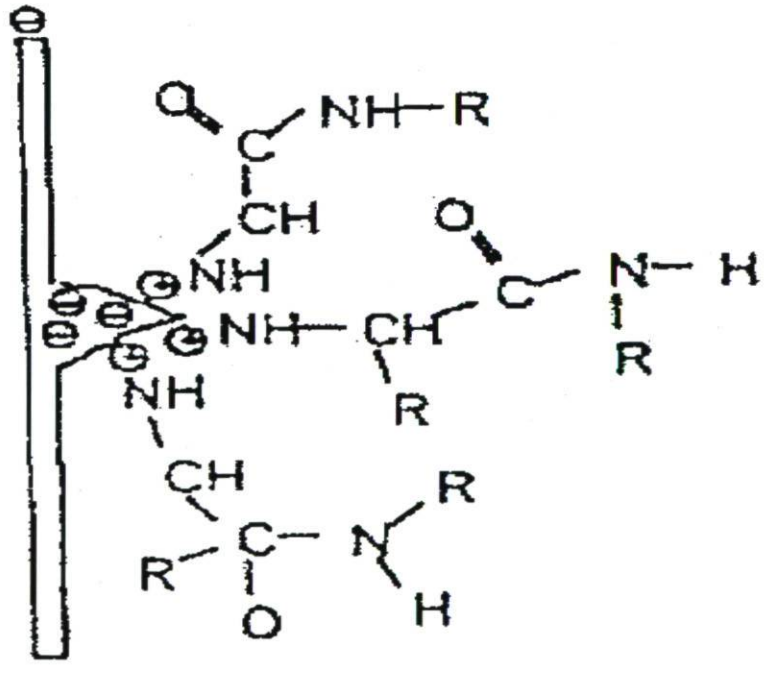

Figure 2.17 Gelatin adsorption on a cathode [66].

Adsorption of gelatin occurs at locations of the cathode with high field strength such as edges, nodules and needles. Electro-adsorption of polar gelatin molecular takes

place at these preferred sites, which forms an isolating layer (see Figure 2.17). It can result in preventing zinc electrodeposition. When the normal zinc layer has grown up it also desorbs the gelatin. Also, gelatin may then be adsorbed again on another place with high field strength.

During electrorefining, gelatin is consumed by incorporation into deposit [65], and by adsorption onto the slimes. Thus, fresh gelatin solution is added to the sulphate acid solution at a rate that ensures a smooth deposit on the cathode with minimal entrapment of electrolyte and slime.

Glue, however, also interacts in a beneficial way with certain impurities or additives in the electrolytic; for example, antimony, to optimize zinc deposition CE and modify the zinc deposit morphology and preferred orientation [61].

In spite of the detrimental effect of antimony on CE, a small concentration of antimony is usually added to the zinc electrolyte because it is thought to reduce zinc deposit adherence to the aluminum cathode blank and because of its beneficial interaction with glue.

In addition to optimizing CE and modifying the zinc deposit morphology, glue and antimony also have a signification effect on the zinc deposition overpotential [61]. The addition of glue to the electrolyte increases the overpotential; that is, it polarizes zinc deposition whereas increasing concentrations of antimony decrease the overpotential. Balanced additions of glue and antimony produce a zinc deposition overpotential that results in an optimum value of the CE.

Antimony exhibits an induction period before it becomes detrimental to the zinc electrowinning process. Atimony in the zinc electrolyte causes redissolution of deposited zinc and decrease the current efficiency, the redissolution starts in the pits formed in the deposit [67]. The induction period is extended to obtain better current efficiencies for longer time is to maintain a smooth, level deposit free from dendrites or pores. Add organic reagents such as glue to the electrolyte is one method of improving the physical character of the deposit. These organic reagents tend to produce a smooth level deposit, possibly by depositing in clusters on points of high current density, thereby reducing the amount of current at these points.

Since there is a relationship between the zinc deposit structure and current efficiency, proper control of crystal growth could yield high current efficiencies (≥90%) and longer plating cycles. The effects of impurities and addition agent on zinc deposit morphology, orientation and smoothness have been studied by development of the scanning electron microscope (SEM) which has provided a suitable means for characterizing the often rough deposit surfaces [59].

Sato studied the effects of various impurities and additives on the morphology and orientation of electrodeposited zinc [68]. He observed that increasing concentrations of most cationic impurities tend to produce (002) preferred orientations whereas organic additives polarized additives and shifted the orientation to (101). He also observed that the deposit morphology was characteristic of the type and concentration of the impurity present in the electrolyte. Thus it was possible to determine approximately the impurities that are active in the electrolyte by examining the deposits using SEM.

Robinson and O'Keefe interpreted the fact that at the zinc plant of Cominco Ltd at Trail, B.C., 15-30 mg/L of animal glue and 0.04-0.08 mg/L of antimony are added to the purified electrolyte to obtain an empirically determined maximum metal recovery [69]. They have observed that correlation of SEM observation with current efficiency results can provide an insight into what constitutes the desirable deposit structure characteristics. When antimony-glue consists of 0.04 mg/L Sb + 15 mg/L glue, the current efficiency was maximized, a characteristic zinc deposit morphology results at these conditions was obtained. Robinson and O'Keefe also observed characteristic zinc deposit morphologies for addition-free, antimony-addition and glue-addition electrolytes [56].

Large hexagonal platelets which grew at random angles to the aluminum substrate were observed from zinc deposits obtained from addition-free electrolytes. The preferred orientations were (101) (102) (103). Glue additions (50 mg/L) caused a decrease in the zinc platelet size and the platelets were oriented at 90°C angles to the substrate. The observed orientation was (110). Antimony additions (0.04 mg/L) also resulted in a decrease in size platelet size and the platelets were aligned parallel to the substrate. The preferred orientation was (002). Combinations of antimony and glue in solution gave platelets with intermediate angles.

It was reported that the ex-situ cyclic voltametric technique (CV) has been employed to identify and quantitatively evaluate the effects of antimony, gelatin or combinations of the two [64]. This technique has shown that the Nucleation Overpotential region (NOP) (difference between *the crossover potential,* the start of the dissolution, and the point at which Zn begins to deposit) could be a useful parameter to identify the best gelatin and antimony ratio [61]. It was observed that addition of gelatin to the zinc electrolyte leads to a gradual proportional increase of NOP. However, addition of antimony to the zinc electrolyte shows a significant decrease in the NOP since antimony is a strong depolarizing agent. The synergetic effect of gelatin and antimony can be evaluated by the cyclic voltammetry technique. For each Sb concentration there is an optimum gelatin value at which the current efficiency "CE" is maximum, for e.g. for Sb 0.02 and 0.04 mg/L concentrations, the corresponding ones of gelatin are 5 mg/L and 20 mg/L respectively. The relationship between the additives - gelatin and antimony can be observed between CE and NOP for zinc deposition in a way that the CE was maximal when the NOP of the initial cell electrolyte was 756-766 mV/SHE, and /or NOP of the final cell electrolyte was 736-746 mV/SHE [61].

2.3.4 Other organic additives

Organic additives are widely employed to counteract the harmful effects of these metallic impurities such as Sb^{3+}, Ge, etc. In combination with some glue, antimony also plays a beneficial role producing optimum current efficiency and acceptable surface morphology of the deposit [70-72]. Glue is the most common organic additive used industrially. Nevertheless, some authors have investigated the use of other additives like ammonium ion, various polyols and also anionic additives like perfluorocarboxylic acid and alkyl sulphates as alternatives to glue.

In the electrolyte for zinc electrowinning, organic compounds are generally added to control the adverse effect of metal impurities on the efficiency [73, 74]. Generally, organic additives influence the zinc electrode polarization and they modify the morphology and preferred orientation of zinc deposits. For example, triethyl-benzyl-ammonium chloride (TEBACl) added into the nickel-containing electrolytes has the

beneficial effect to decrease the screening effect of hydrogen bubbles where local galvanic cell can be generated [75]. This additive has been shown to increase the reduction period which precedes the reverse dissolution of zinc deposits obtained under galvanostatic conditions in nickel-containing electrolytes [76].

The influence of an organic additive, triethyl-benzyl-ammonium chloride on zinc deposition could be summarized: (1) Inhibiting the hydrogen evolution taking place on a Ni/Zn-containing surface compound and inhibiting the reaction of zinc deposition. (2) Increasing the charge transfer resistance and decreasing the double layer capacitance over a wide potential domain.

The effects of TEBACl alone or in the presence of antimony, on power consumption (PC) and current efficiency are also summarized in Table 2.3 [77].

Table 2.3 The effect of TEBACl alone or in the presence of antimony, on power consumption (PC) and current efficiency [77]

[*Additive*]/mg dm^{-3}	[*Sb*(III)]/mg dm^{-3}	*CE*/%	*PC*/kWh t^{-1}
TEBACl			
0	0	89.3	2608
1.0	0	90.9	2463
1.5	0	92.6	2436
2.0	0	92.8	2430
2.5	0	92.6	2445
5.0	0	91.3	2497
40	0	89.7	2588
2.0	0.01	95.6	2291
2.0	0.02	94.1	2336
5.0	0.01	92.2	2402
5.0	0.02	90.1	2449

t = hour

It can be observed from Table 2.3 that with TEBACl alone, a maximum reduction in PC of ~180 kWht^{-1} was obtained at an additive concentration of 2 mg/dm^3. A further reduction of ~140 kWht^{-1} was achieved on the addition of 0.01 mg/dm^3 of Sb (III). Also, addition of antimony to the electrolyte was found to play a beneficial role when combined with organic additives, and producing high current efficiencies and good deposit morphologies [62]. When antimony is combined with TEBACl, a similar

beneficial effect has been obtained. Thus, in presence of 0.01 mg/dm^3 antimony (III) the addition of TEBACl up to 2 mg/dm^3 results in an increase in the CE up to 95.6%.

Perfluorinated carboxylic acids and their salts show unusually low surface tension [78]. This property in electrodeposition is very well since it imparts excellent levelling effectiveness. The applications of perfluorinated compounds have been reported recently [79]. Fluorinated organic compounds have been used as a suppressant of hydrogen evolution on zinc and have been reported to be efficient inhibitors for the growth of zinc moss and dendrites and for zinc corrosion. Also perfluorinated surfactants can be used in the acidic sulphate electrolytes for zinc electrowinning to counteract the deleterious effect of metal impurities such as antimony on the CE of zinc deposition [80].

During zinc electrodeposition, the effect of the perfluoroheptanoic acid "PFHA" on CE and PC has been studied in the electrolyte with and without Sb (III) (Table 2.4). The CE obtained for zinc deposition was 89.3% in the electrolyte without any addition [70]. Addition of the 1 mg/dm^3 PFHA to the electrolyte increased the CE up to ~95.4% (Table 2.4), and this can be attributed to the suppression of hydrogen evolution during zinc electrodeposition by blocking the active sites through adsorption [81]. It was also found that addition of 1 mg/dm^3 PFHA to the electrolyte can decrease PC of ~ 80 kWht^{-1} less than addition-free electrolyte [70]. The effects of the addition of Sb (III) in the presence of the PFHA on the CE are also shown in Table 2.4. It means that addition of PFHA is beneficial to both of current efficiency and energy consumption. In marked contrast to most organic additives, the addition of Sb (III) to the electrolyte containing PFHA decreases the CE. Thus even with 0.01 mg/dm^3 Sb (III) a decrease in CE by 1-2% was observed in all cases and it falls drastically with further increase in the Sb (III) concentration. This is very probable because PFHA cannot counteract the harmful effect of antimony.

Table 2.4 Effects of perfluoroheptanoic acid "PFHA" on CV, CE and PC during electrodeposition of zinc from acidic zinc sulphate solution in presence and absence of Sb (III) [80]

[PFHA] (mg dm^{-3})	[Sb(III)] (mg dm^{-3})	CV (V)	CE (%)	PC (kW h t^{-1})
0.5	0.00	2.94	95.3	2530
1	0.00	2.94	95.4	2528
5	0.00	2.95	95.2	2542
10	0.00	2.94	95.0	2538
40	0.00	2.94	94.8	2544
1	0.01	2.93	93.4	2573
1	0.02	2.93	90.2	2664
1	0.04	2.94	83.6	2884
1	0.08	2.93	67.7	3550
5	0.01	2.94	92.3	2613
5	0.02	2.93	90.3	2661
40	0.01	2.94	93.3	2585
40	0.02	2.93	91.7	2621

In industrial zinc deposition, recently, several synthetic surfactant of the cationic type have been tested in zinc electrowinning. Anionic surfactants usually contain polar and solubilizing group like carboxylates, surfactants, sulphate and phosphates. The alkyl sulphates containing eight or more carbon atoms are often used among these compounds, [82]. These anionic surfactants adsorb on the surface of the substrate to reduce the interfacial tension. Sodium lauryl sulphate "SLS" and sodium lauryl ethoxy sulfonates "SLES", which belong to that category, have been used commercially in the electrowinning [70]. The effects of Sb variation at different SLS concentrations are given in Figure 2.18.

It can be observed from Figure 2.18 that the addition of Sb has a beneficial effect on the current efficiency in the presence of SLS. The advantage is most pronounced at lower concentrations of SLS particularly at around 1 mg/dm^3 of SLS where the CE first increases with increasing Sb concentration. The maximum CE (~97%) occurs at around 0.02 mg/dm^3 Sb and then gradually decreased. Without Sb (III), the maximum CE% (~93) appears with 1 mg/dm^3 SLS. Without additives, the CE drops rapidly as Sb concentration is increased.

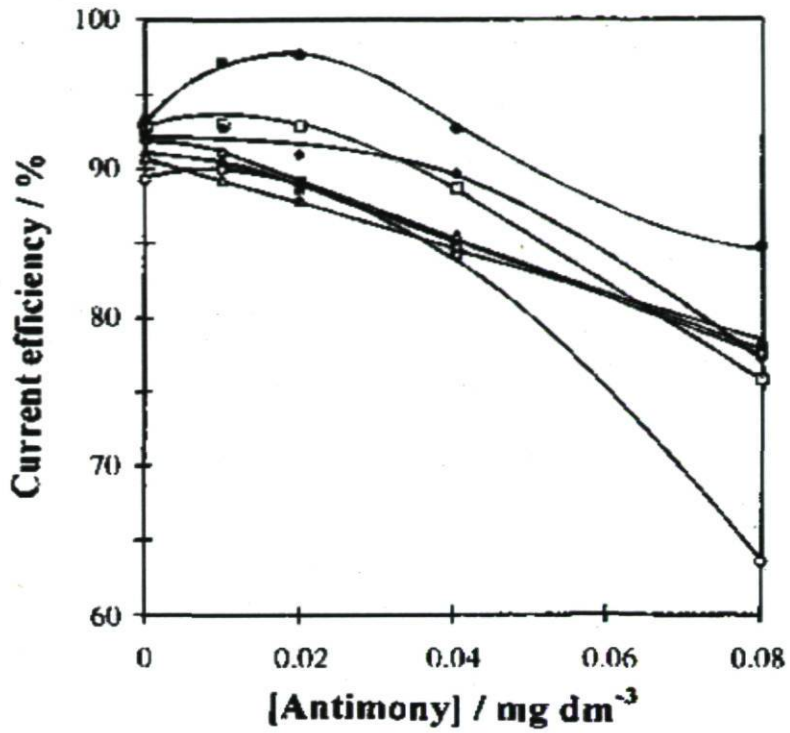

Figure 2.18 Effect of antimony on current efficiency during zinc electrowinning in presence of: (O) blank, (□) 0.05, (●) 1.0, (♦) 1.5, (◊) 2.0, (▲) 5 and (Δ) 10 mg/dm^3 SLS [70].

2.4 Anode degradation using electrochemical techniques

Introduction

Different electrochemcial measurement techniques have been applied to corrosion system in order to determine the corrosion rate because of the electrochemical nature of corrosion processes. The great advantages of electrochemical techniques are the relatively short measuring time, the high accuracy and possibility of continuous corrosion monitoring. Indeed, rapid and accurate methods for measuring corrosion rates are of tremendous importance, especially for practical applications [83, 84]. Direct analytical methods, such as weight loss measurements, require relatively long exposure times of the corroding systems, and they are restricted to systems which do not form adherent layers of corrosion products [83].

2.4.1 Cyclic voltammetry

2.4.1.1 Theory of cyclic voltammetry

In cyclic voltammetry, the potential applied to an electrode (by means of a potentiostat) is changed linearly with time in a repetitive manner. The current is measured as a function of a potential or time. If only a single anodic or cathodic sweep is performed, the technique is usually referred to as the linear potential-sweep method. In both cases, the experiment is conducted in unstirred solutions, where convection is eliminated as far as possible [85].

The fundamental equations for linear potential sweep and cyclic voltammetry have been developed by Delahay [86], Shain [87] and others. The appearance of a current peak is the basic feature of a voltammogram (i.e. a plot of current vs potential during cyclic voltammetry or linear potential sweep) at a potential characteristic of the electrode reaction taking place (Figure 2.19). Sweep rate, electrode material, solution composition and the concentration of reactants can influence on the position and the shape of a given peak. Cyclic voltammetry alone is studied relevant only to the specific experimental conditions chosen in no stirring solutions.

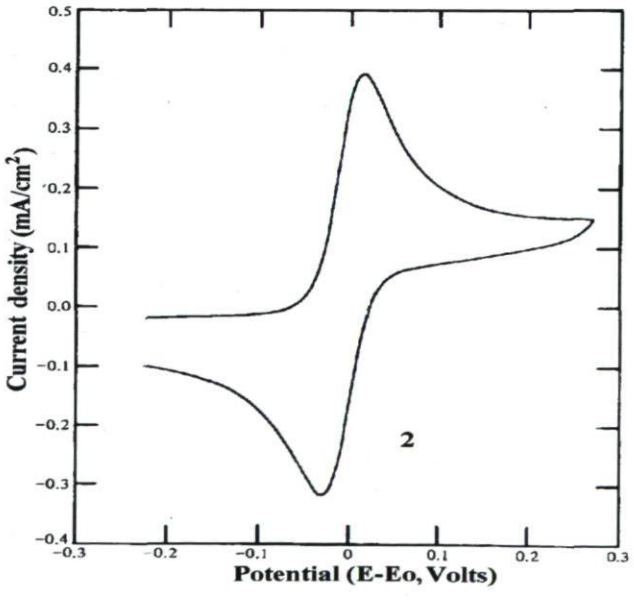

Figure 2.19. Typical cyclic voltammogram 3 mM Fe^{2+} in 1 M H_2SO_4 v = 50 mV/sec [85].

Both reactants and products are soluble for a simple cathodic charge-transfer process under reversible conditions, i_p in Amp cm^{-2} at 25°C is given by

$$i_p = 2.72 \times 10^5 \, n^{3/2} D^{1/2} C^o v^{1/2} \quad (2.41)$$

where D is the diffusion coefficient of Fe^{2+}, cm2/sec, C^o is the initial concentration of Fe^{2+}, mole/cm^3 and v is the sweep rate, volt/sec, n is the change in electron numbers in electrochemical reaction.

2.4.1.2 Application of cyclic voltammetry

Typical curves of a cyclic voltammogram for lead electrode in sulphuric acid solution

Cyclic voltammetry has been used to study the electrochemical redox behaviour of the $Pb/PbO_{n(1,2)}/PbSO_4$ system on the lead electrode in aqueous H_2SO_4 solutions. The polarization behaviour of Pb electrode in H_2SO_4 has been investigated to observe the oxidation and reduction peaks [88]. The typical curves of a cyclic voltammogram for the lead electrode in a sulphuric acid solution are shown by the solid line and the dotted line in Figure 2.20.

In the Figure 2.20, seven peaks a, b, c, d, e, f, g can be observed. Each peak corresponds to one electrochemical reaction of the lead electrode. The oxidation peak a ($Pb \rightarrow PbSO_4$) [89] can be observed during the anodic sweep. The oxidation peak b ($PbO \rightarrow \alpha\text{-}PbO_2$) appeared on the dotted line; the oxidation peak c ($PbSO_4 \rightarrow \beta\text{-}PbO_2$) also can be observed on the dotted line. Then, the irregular and sharp oxidation peak d (Pb, $PbO_2 \rightarrow PbSO_4$) appeared at the outset in reversing the potential cathodically from a region of the oxygen evolution to the starting potential [90], the reduction peak e (β-$PbO_2 \rightarrow PbSO_4$, $\alpha\text{-}PbO_2 \rightarrow PbSO_4$) appeared on the solid line, the last two reduction peaks f ($PbO \rightarrow Pb$, $PbSO_4 \rightarrow PbO$) and reduction g ($PbSO_4 \rightarrow Pb$) appeared [91].

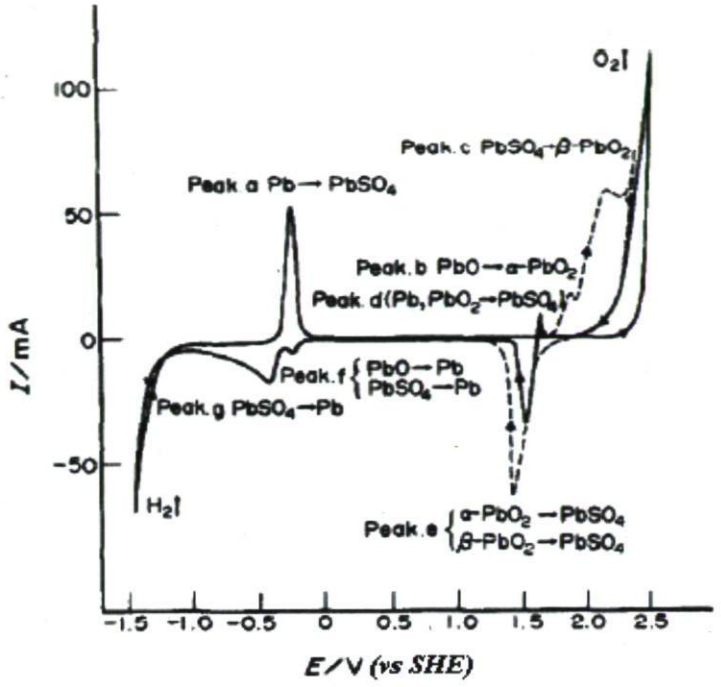

Figure 2.20 Typical cyclic voltammograms for a lead electrode in aqueous H_2SO_4 solution. Solid line was traced in a region from the potential of hydrogen evolution to the potential of oxygen evolution. Dotted line was traced in a region from 0.62 V to the potential of oxygen evolution. Sweep rate: 41.7 mV/Fs [88].

The molar volume of the β-PbO_2 is 25 cm^3/mol, much smaller value than the molar volume of $PbSO_4$, which equals 48 cm^3/mol and, for this reason, this transition can result in a large increase of the molar volume of the surface layer. This, in turn, might cause cracks in the surface layer, thus exposing a bare metal surface, which is instantly oxidized [92].

The studies of reduction process of the anodic PbO_2 film formed at 1.4 V (vs MSE) in sulfuric acid using linear sweep voltammetry were given by Cai et al. [93]. The pure lead anode was oxidized in 4.5 M H_2SO_4 solution for 1 h at 1.4 V. The XRD analysis indicated that the anodic film was composed of β-PbO_2, α-PbO_2, PbO and small amount of $PbSO_4$. Most of the β-PbO_2 and part of the α-PbO_2 in the film were reduced to $PbSO_4$ at the reduction potential of 0.9 V. The results showed that the rest of α-PbO_2 was reduced at lower potentials. Extra charge was required for the reduction of α-PbO_2 at 0.6 V possibly due to higher pH in the inner part of the anodic film [93]:

$$PbO_2 + SO_4^{2-} + 4H^+ + 2e^- = PbSO_4 + 2H_2O \quad (2.42)$$

The consumption of H^+ and SO_4^{2-} by reaction increased the pH of the inner part of the film. The film became alkaline which lowered the reduction potential of oxide film.

The influence of cyclic numbers

Typical cyclic voltammogram of the lead electrode in 0.5 M H_2SO_4 solution are shown in Figure 2.21 as a function of cycle number. It shows the growing process of the redox peaks in the potential region of the lead positive electrode from 1.0 V to the oxygen evolution potential. After the fifth cycle, a peak current ascribed to β-PbO_2 formation was clearly detected at 1.85 V due to potential positive slight of the oxygen evolution reaction [94].

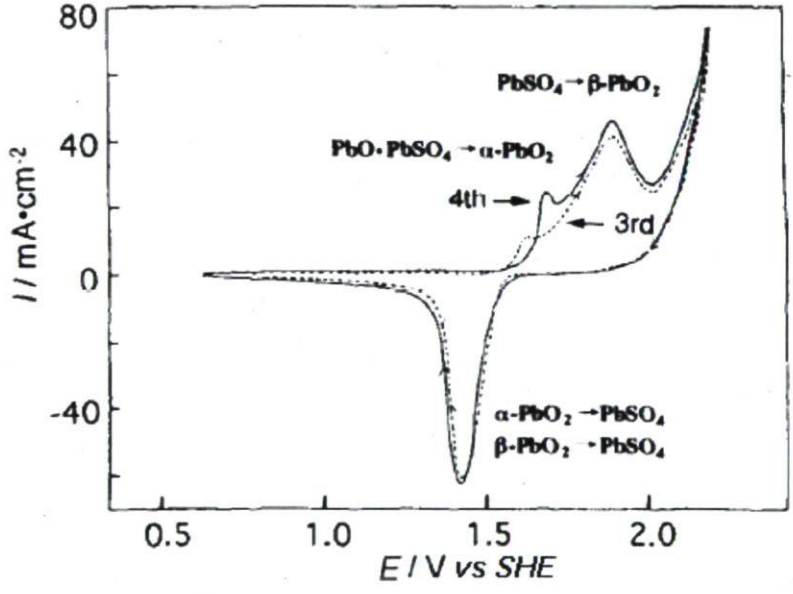

Figure 2.21. (a) Typical cyclic voltammograms for the lead electrode in the potential range of 0.6 V to the oxygen evolution potential in 0.5 M H_2SO_4 solution. The first positive going potential scan was started from the hydrogen evolution potential after holding the electrode in the potential region of hydrogen evolution [94].

Factors influencing the redox reactions occurring on Pb electrode

The redox reactions occurring on the Pb electrode in sulfuric acid solutions are complex and depend on many factors, such as the concentration of the acid, the sweep rate in CV experiments and the temperature (Figure 2.22) [95].

One of the curiosities of the redox reactions of the lead electrode is the appearance of small oxidation peaks that accompany the main reduction process, i.e., the reduction of the lead dioxide to lead sulphate. These small anodic peaks, sometimes called "anodic excursion" peaks, appear either before or after the main reduction peak and depend significantly on the condition of the experiment.

The "anodic excursion" peaks proposed by Deutscher et al. [92], situated on CVs obtained in 5 M H_2SO_4 after the main reduction peaks, are related to the reduction reaction, in which β-lead oxide is reduced to lead sulphate. A large increase of molar volume occurs in this reaction, from 25 cm^3/mol for β-PbO_2 to 48 cm^3/mol for $PbSO_4$. Such change in the molar dimensions of the surface layer might generate cracks on the electrode surface and the exposure of the metallic lead, which is instantly oxidized by sulphuric acid, giving rise to the "anodic excursion" current.

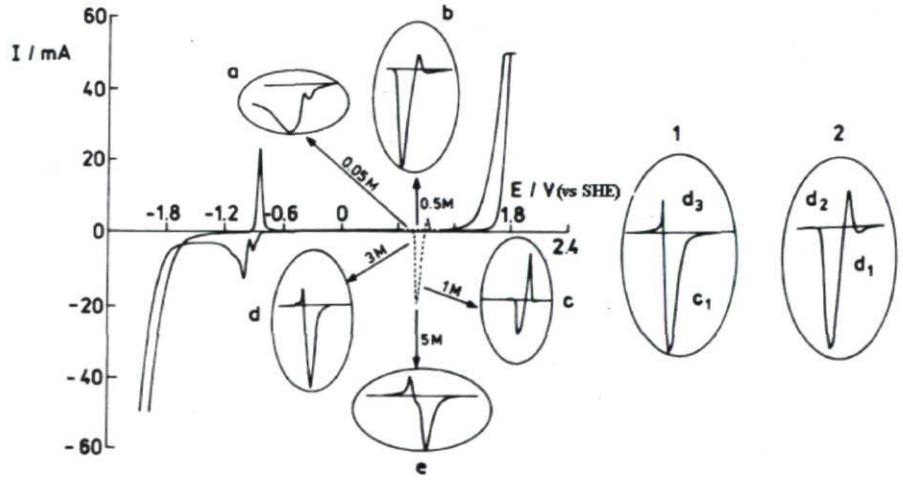

Figure 2.22: Cyclic voltammogram at 40 mV/s, of the Pb electrode in various H_2SO_4 solutions (a) 0.05 M, (b) 0.5 M, (c) 1.0 M, (d) 3.0 M, (e) 5.0 M. The "anodic excursion" peaks are separated and magnified in circles. In separated circles labelled as 1 and 2 the possibilities of "anodic excursion" peak locations are shown [95].

Czerwinski et al. [95] studied the anodic excursions in a wide range of sulphuric acid concentrations (0.05-5.0 M), at different sweep rates (50 mV/s to 10 mV/s) and in various potential regions. Both anodic excursion peaks, one occurring before (d_2) and the other after (d_3) the main reduction peak (peak c_1) occurred on cyclic voltammograms under certain experimental conditions.

2.4.2 Potentiodynamic method

Potentiodynamic polarization techniques permit the measurement of polarization behaviour by continuously scanning the potential while monitoring the current response. Also, this experimental method permits the easy automation of curves and real time plots of the experimental data. Potentiodynamic polarization techniques have become much more popular than the potentiostatic techniques or galvanostatic for drawing polarization curves since its ability is to automate data taking. For potentiodynamic measurements, several important considerations, such as selection of a sweep rate, selection of a data acquisition system, and selection of a starting potential also are presented [96]. Potentiodynamic tests were carried out by a classical three-electrode electrochemical cell. For example, the tested specimen was used as working electrode, a platinum electrode was used as counter electrode and Ag, AgCl/KCl $_{sat.}$ reference electrode.

The sweep rate selection is very important, especially if near steady-state conditions are desired. ASTM Standard G5 specifies a sweep rate of 0.6 V/h (10 mV/min), however, other rates could be considered depending on steady states of the reactions and reproducibility of the results, etc [97].

2.4.2.1 Theory of potentiodynamic

Figure 2.23 shows a typical potentiodynamic polarization curve. This curve represents the evolution of net current with potential. The net current, I_{net} is defined as:

$$I_{net} = I_A - I_c \qquad (2.43)$$

where I_A and I_c are the anodic and the cathodic currents, respectively [98].

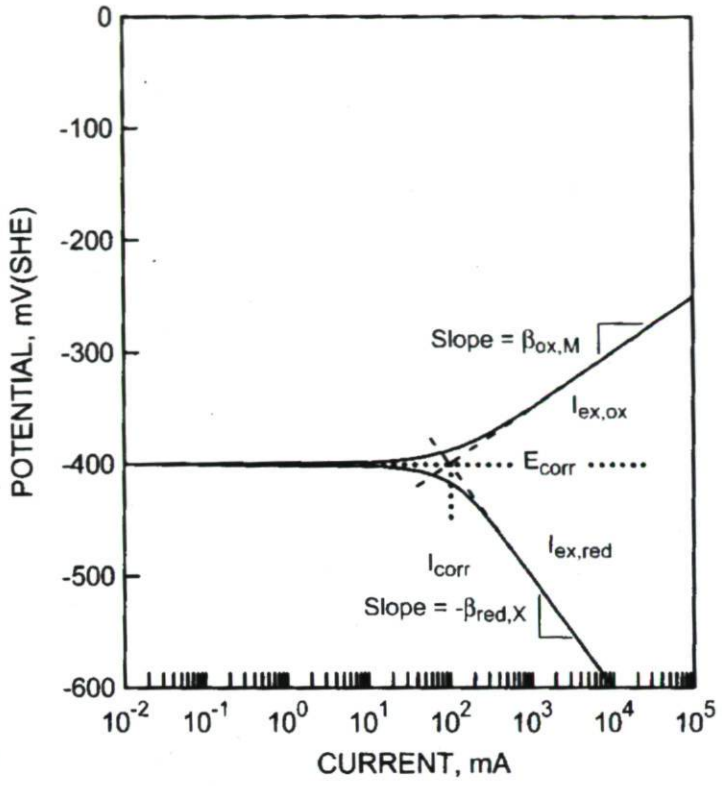

Figure 2.23 Potentiodynamic polarization curve showing anodic and cathodic current components [98]

The open circuit potential, E_{oc} is the equilibrium potential assumed by no current flowing the circuit [84]. The value of either the anodic or cathodic current at E_{oc} is called the corrosion current, I_{corr}. The rates of both, the anodic and cathodic processes, are controlled by the kinetics of the charge transfer reaction at the metal surface (Figure 2.23) [84]. The Butler-Volmer equation can be used to describe an electrochemical reaction under kinetics control (2.44):

$$I = I_{corr}(\exp(2.303(E-E_{corr})/\beta_a) - \exp(-2.303(E-E_{corr})/\beta_{corr}) \quad (2.44)$$

where

I is the measured cell current in amps;

I_{corr} is the corrosion current in amps;

E is the electrode potential, and is expressed as a function of $I_{ex,\,red}$ and $I_{ex,\,ox}$.

E_{corr} is the corrosion potential in volts;

β_a is the anodic Beta Tafel Constant in volt/decade;

β_c is the cathodic Beta Constant in volts/decade.

The corrosion current I_{corr} can be then easily calculated from (2.44).

2.4.2.2 Characteristics of potentiodynamic measurements

The starting potential for a polarization curve depends on the purpose of the test. If only an anodic curve is not to be determined, a starting potential approximately 50 mV more negative than the corrosion potential should be used. The initial current will be cathodic, and current will be switched to anodic potentials at values more positive than the corrosion potential.

The advantage of potentiodynamic polarization is that it acts as an accelerated electrochemical test, which makes it possible to provide information and parameters relating to corrosion. These parameters are as follows [96]:

- Corrosion potential E_{corr}: it is this potential which the electrode instantaneously undergoes a corrosion in the absence of the external current. The parameter indicates the tendency to corrosion. Thus, more the potential of corrosion increases nobler leads to more decrease of the tendency to corrosion. However, the corrosion potential does not provide any information on the speed of corrosion since this depends on Evans diagram.

- Corrosion current of i_{corr}: the density of corrosion current i_{corr} thus makes it possible to calculate the rate of corrosion employing the Faraday's law. i_{corr} is generally considered for corrosion current/cm^2.

- The pitting potential is the potential at which pitting will initiate on the surface of a metal. The pitting potential also has been referred to as the breakdown potential. Pitting corrosion occurs due to the breakdown of the passive surface film. Pitting is characterized by a rapid increase in current with only a small change in potential. The potential, at which this current increase initiates, is termed the pitting potential.

- Passivation potential (sometimes called repassivation potential) is that potential where repassivation occurs (pitting or crevice corrosion ceases) during the reverse scan and the current decreases back to, or below, the original passive current density.

For lead alloys, the potentiodynamic polarization, with scanning speed of 1 mV/s, begins with a potential of -1.5 V, and ends with a potential of 2.3 V/SHE. Figure 2.24 shows the potentiodynamic polarization curves of Pb-Sn alloys. The oxidation part shows the characteristics of passivation property of Pb-Sn alloys [99].

After the passivation process, the continuous passive layer is destroyed and pitting occurs. Corresponding electrochemical parameters, equilibrium potential (E^0), pitting potential (E_p or E_{pit}), and the difference between E^0 and E_p, which are derived from the experimental data, are collected in Table 2.5. According to the test results, the value of E_p is around 1.65 V while interzone spanning from E_p to E_0 is more than 2 V. This data indicates that all tested Pb-Sn alloys have good anti-corrosive properties, although pitting does occur after compact passive layers are penetrated. Once pitting starts, the sulfuric acid, which acts as an electrolyte, infiltrates the protective layers and promotes the electrochemical reaction acting as so-called self-catalysis [100].

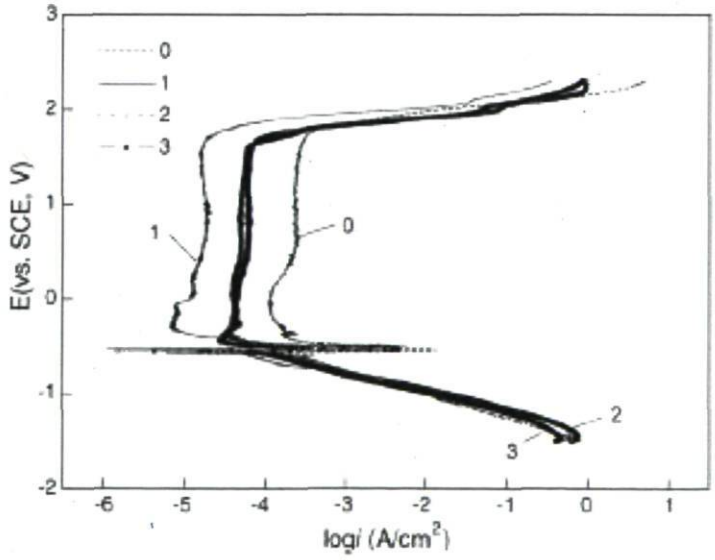

Figure 2.24. Potentiodynamic polarization curves of Pb-Sn alloys in 4 M H_2SO_4 solution. (0), pure Pb; (1) Pb-0.532wt.% Sn; (2) Pb-0.82wt.% Sn; (3) Pb-1.06wt.% Sn [99].

Table 2.5 Characteristic parameters of polarization curves of Pb-Sn alloys in 4 M H_2SO_4 solution [99]

	Sample no.			
	0	1	2	3
Equilibrium potential E^0 (V vs. SCE)	−0.577	−0.531	−0.554	−0.556
Pitting potential E_p (V vs. SCE)	1.722	1.692	1.622	1.621
Difference between E_p and E^0 (V)	2.299	2.223	2.162	2.193

2.4.2.3 Linear polarization resistance or polarization resistance

Linear polarization resistance (LPR) and polarization resistance (PR) are analogous terms that refer to a linear approximation of the polarization behaviour at potentials near corrosion potential (Stern-Geary relationship) [101]. The polarizing current is assumed to change linearly (not logarithmically) with a small vary in the potential from the Stern-Geary equation, In general, this assumption becomes a good approximation ($\sim \pm$10-20 mV), and the corrosion rate can be estimated. The relationship of Stern-Geary describes the change in potential as a function of change in net (polarizing) current, dE/di, close to the corrosion potential, and it is given in Equation 2.45:

$$R_p = dE/di = (\beta_A\beta_C)/2.3(\beta_A + \beta_C)i_{corr} \quad (2.45)$$

where β_A and β_C are the anodic and cathodic Tafel slopes given as absolute values in volts per decade of current, i_{corr} is the corrosion current density with units of A/m^2, and the polarization resistance, R_p, is defined as dE/di at the corrosion potential with units of $ohm.m^2$. When the potential close to the corrosion potential is plotted on a linear graph vs current, the slope of this curve is equal to R_p (dE/di), this analysis typically is performed within $\pm$10-20 mV of the corrosion potential. It is good method that R_p is calculated as equal to the slope of the tangent of this curve at the corrosion potential where the current is zero (Figure 2.25).

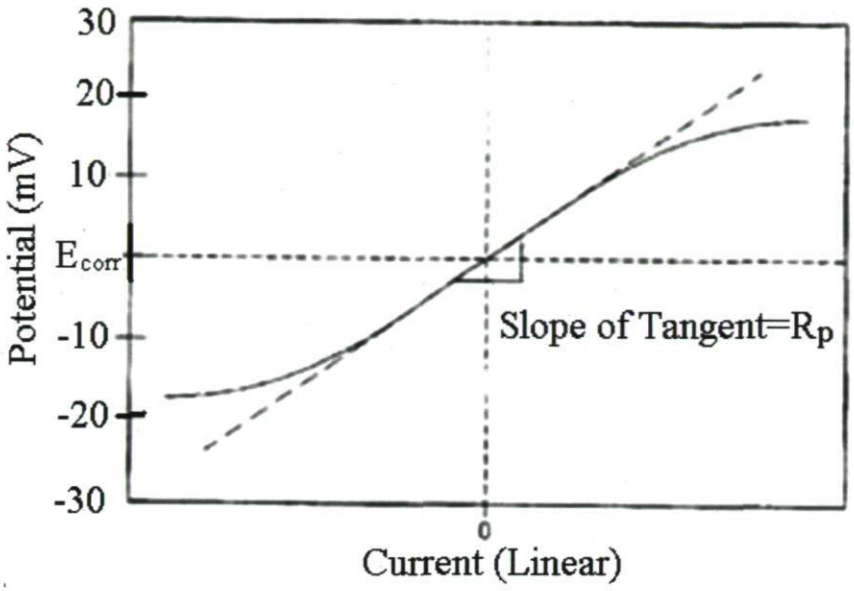

Figure 2.25 –Illustration of typical linear polarization resistance curve [96].

For lead alloys, linear polarization resistance was used to evaluate the corrosion resistance, the linear polarization starts usually from a cathodic potential of about -25 mV relative to the corrosion potential and stopped at an anodic potential for the active specimens. The scanning rate used in the experiments is 0.166 mV/s.

2.4.3 Galvanostat

The purpose of a galvanoststic measurements studies is to supply a constant current to the working electrode independent of voltage and impedance changes at the electrode surface. The operation of a galvanostat is similar to that of a potentiostat, and the basic circuit component is an operational amplifier [102].

In galvanostatic techniques, a constant current is applied, and the potential is monitored as function of time. It is also possible to record an entire polarization curve in the galvanostatic mode.

For lead alloys, the galvanostatic measurements were used to evaluate the anodic polarization, the anodic current density was 50 mA/cm^2 for 5 h and the anodic overpotential during anodic polarization was measured.

2.4.4 Electrochemical noise

General

Electrochemical noise (EN) technique has been used to study corrosion related processes since the early 1980s. Sensitivity of this electrochemical technique has been established for the detection of spontaneous changes in localized corrosion processes, in particular pitting and cavitation attack.

2.4.4.1 History

At the beginning, the term "electrochemical noise" was associated with spontaneous fluctuation in the potential with time. It was observed many times ago, certain types of corrosion processes, in particular localized corrosion phenomena, had characteristic signatures. Changes in the free corrosion potential could be observed and correlated with localized attack. In itself, this proved to be a practically useful tool, and could be used to identify changes in the behaviour of materials in particular environments.

Over the years, fundamental principles and methodology behind EN measurements have not been changed much. However, the developments of computers and data acquisition systems have allowed simultaneous measurement of current and potential noise signals associated with the evolving corrosion processes. It is now possible to use EN techniques both in laboratory and in 'real world' applications [103].

2.4.4.2 System description of electrochemical noise

A set-up in zero resistance ammeter (ZRA) mode (Figure 2.26) was used to carry out the electrochemical noise measurements in experimental medium. The electrochemical current noise was measured as the galvanic coupling current between two nominally identical working electrodes (WE) kept at the same potential. It ensures that the two similar electrodes were at the same potential by measuring the current using a ZRA. This coupled potential was measured via a reference electrode (Ref.), a saturated silver chloride electrode Ag-AgCl/$KCl_{sat.}$ (0.202 V vs SHE). Potential and current values

sampled at a scan rate of f_s = 10 Hz for 102.4 s giving a total of 1024 points were recorded by a potentiostat (GAMRY model PC4/300) linked to a personal computer. Also, the GAMRY ESA400 software was used to conduct EN experiments and data treatment. The noise data were collected for all the immersion time period [103].

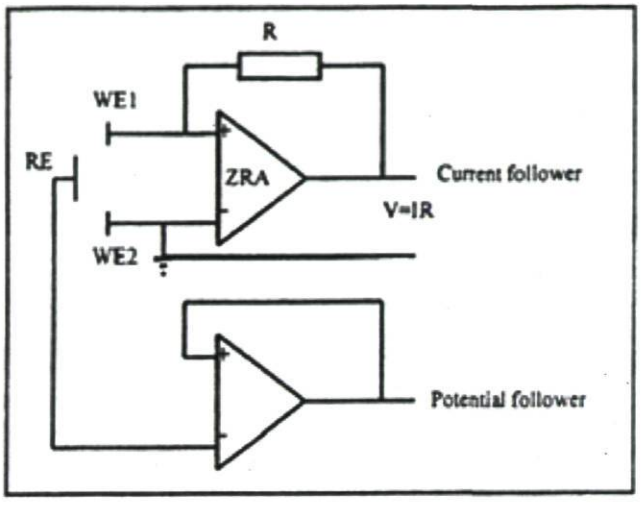

Figure 2.26 Interface for simultaneous monitoring of potential and current noises comprising a zero resistance ammeter (ZRA) [103].

The analysis of electrochemical noise data can be carried out in both time and frequency domains. In the time domain, the noise resistance (R_n) is the most important parameter of the statistical analysis, it is defined as the ratio of a standard deviation of the potential noise to that of current noise that can be associated to the polarization resistance (R_p). The ratio $1/R_n$ is proportional to the corrosion rate. Noise data were transformed into the frequency domain using Fast Fourier Transform (FFT) algorithm and presented as power spectral density (PSD), calculated in a frequency domain from $5x10^{-3}$ to 5 Hz. The data were recorded immediately after the immersion of the working electrodes in the solution [103].

Figure 2.27 illustrates a typical configuration of electrodes used for noise measurements at the corrosion potential, such that naturally occurring current and potential fluctuations may be monitored simultaneously. This type of arrangement is to study the evolution of naturally occurring corrosion processes and is widely used in plant monitoring/surveillance.

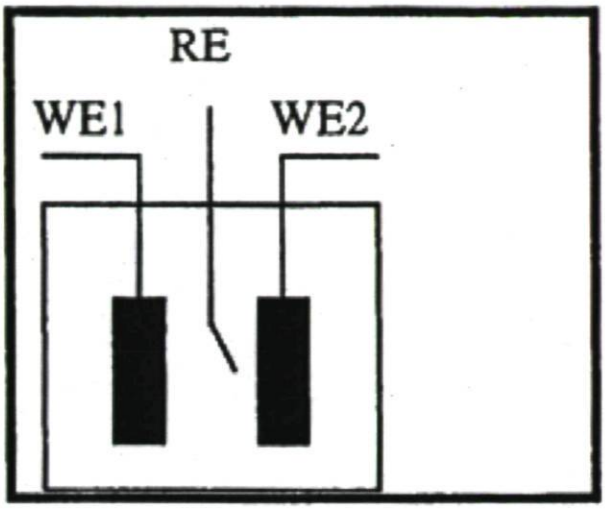

Figure 2.27 Electrode arrangements for electrochemical noise measurements at the corrosion potential [103].

In the analysis of electrical circuits and their electrochemical equivalents, it is convenient to examine various domains. The time domain analyzes the fluctuation of the instantaneous potential or current as a function of time. This is the normal mode in which the noise signals are recorded and is probably the most natural way of viewing the data. However, the frequency domain considers the noise signals in terms of power present at various frequencies [103].

2.4.4.3 Statistical analyses

Statistical analyzes are usually used to process the batch data. However, it is possible to make semi-continuous calculations by data blocking, or discounting of the past. For batch processing, the following statistics can be described as follows: [102-105]

Mean

The mathematical formula calculating the mean of a series of data is presented in equation 2.46 [102]. It can give the mean current with a rough estimate of the rate of the process and the mean potential which is significant when it is measured with respect to a reference electrode [102, 104, 105].

$$\bar{x}_n = \frac{1}{n}\sum_{i=1}^{n} x_i \qquad (2.46)$$

Variance

The mathematical formula calculating the variance of a series of data is presented in equation 2.47. The variance of signal relates to the noise power in the data [102, 104, 105].

$$M_{2,n} = \frac{1}{n}\sum_{i=1}^{n} (x_i - \bar{x}_n)^2 \qquad (2.47)$$

Standard deviation

The mathematical formula calculating the standard deviation of a series of data is presented in equation 2.58 [102, 104]. The standard deviation is the square root of the variance. Its Interpretation was essentially equivalent to those of the variance, but is slightly more intuitive than the variance [102, 104, 105].

$$\sigma = (m_{2,n})^{1/2} \qquad (2.48)$$

Coefficient of variance

The mathematical formula calculating the coefficient of variance of a series of data is presented in equation 2.59. The coefficient of variance represents a measure of the noisiness of the signal compared to its mean value [102, 104, 105].

$$\text{Coefficient of variance} = \frac{\sigma}{\bar{X}} \qquad (2.40)$$

Root mean square

The mathematical formula calculating the root mean square of a series of data is presented in equation 2.50. The rms is always used to the power available from the signal, including the effect of mean potential or current [102, 104, 105].

$$\text{rms} = \frac{1}{n}\sum_{i=1}^{n}(X_i^2) \qquad (2.50)$$

Localization index

The mathematical formula calculating the L.I. of a series of data is presented in equation 2.51. Uniform corrosion processes typically have small L.I. values (1×10^{-3}) [102, 104, 105].

$$L.I. = \sigma_i / i_{rms} \tag{2.51}$$

Noise resistance

The mathematical formula calculating the noise resistance of a series of data is presented in equation 2.52. Noise resistance gives useful information for only uniform corrosion processes [102, 104, 105].

$$R_n = \sigma_v / \sigma_i \tag{2.52}$$

Skewness and kurtosis

A dimensionless measure of the symmetry of the distribution of data around the mean value of the data is called the skewness or skew. When the distribution of data is symmetric around the mean value, skewness is zero. A positive skew means that a tail of the distribution of data deviates to the positive direction, and a negative skew means that a tail of the distribution of data deviates to the negative direction (Figure 2.28 a).

$$\text{Skewness} = \frac{1}{N}\sum_{k=1}^{N}\left(\frac{E_n[k]-\bar{E}}{\sqrt{E_n[k]^2}}\right)^3 \tag{2.53}$$

A dimensionless measure of whether data are peaked or flat relative to a normal distribution is called kurtosis. When the distribution has a shape similar to that of the normal distribution, kurtosis is zero. A positive kurtosis means a more sharply peaked distribution than the normal distribution, while a negative kurtosis means a more flat topped distribution than the normal distribution (Figure 2.28 b).

$$\text{Kurtosis} = \frac{1}{N}\sum_{k=1}^{N}\left(\frac{E_n[k]-\bar{E}}{\sqrt{E_n[k]^2}}\right)^4 - 3 \tag{2.54}$$

where N is the number of points in the time record, $\overline{E}$ is the mean potential, and $E_n(k)$ is the potential of function of time at each instant k.

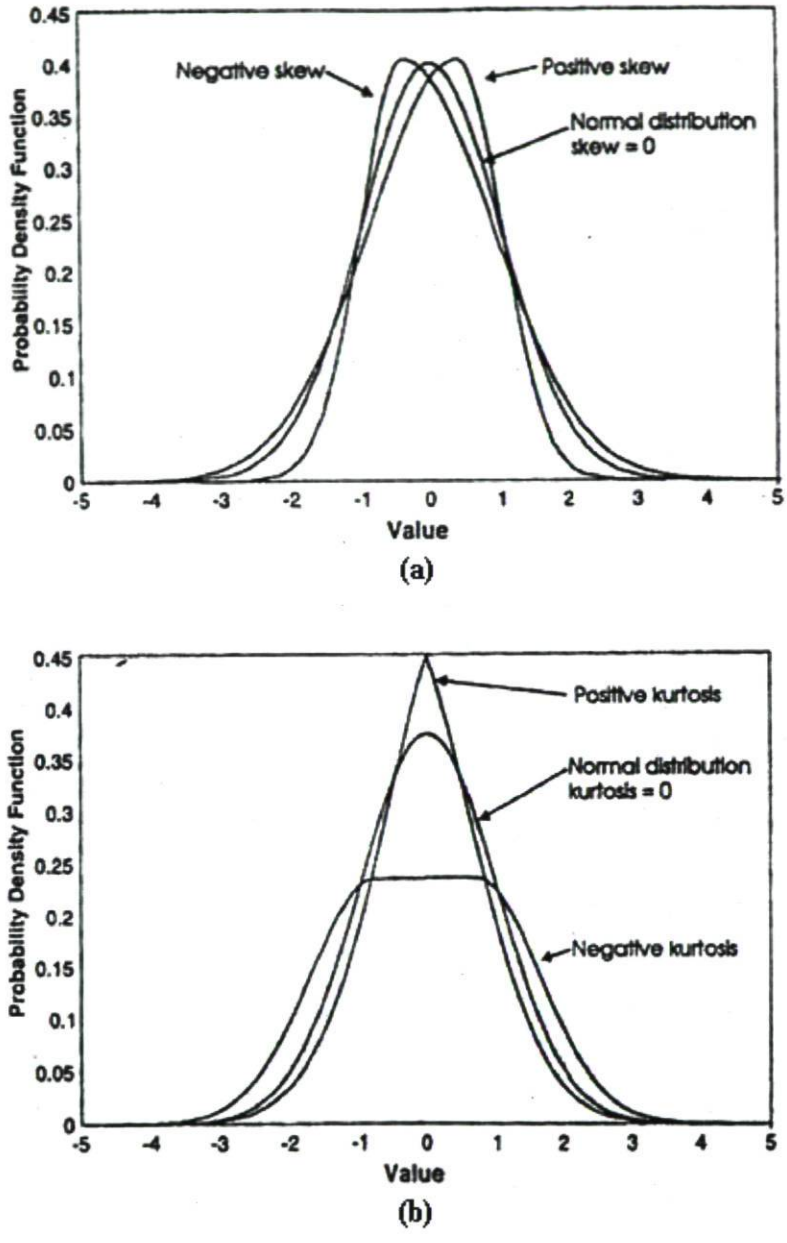

Figure 2.28: Skew (a) and kurtosis (b) of distribution [104].

2.4.4.4 Frequency domain transforms

A powerful analysis of EN acquisitions can be performed by transposing data in the frequency domain. The Fast Fourier Transform (FFT) is the method that can provide this transformation [106] and performs a spectral analysis of the random transient of the EN

signal in a frequency analysis of the random transient of the EN signal in a frequency range through the sampling time and the length of the data recording [104]. Power spectral density (PSD) is estimated by transforming of experimental EN data from the time domain to the frequency and can be obtained by the periodgram method based on the Cooley Tuckey FFT algorithm [106]:

$$\Phi(f) = \frac{2}{T}\frac{1}{N}\sum_{j=1}^{N} \left| I_j(f) \right|^2 \tag{2.55}$$

where f is the frequency, T is acquisition time, $I_j(f)$ is the Fourier transform of the elementary time recording $I_j(t)$, and N is the number of time recordings.

The analysis in the frequency domain by introducing spectral noise plots in which the ratio of the FFT of potential and current noise is plotted as a function of frequency f in the Bode plot format has been extended. Simultaneous collection of potential and current noise fluctuation is required for this type of electrochemical noise analysis (ENA) requires [107, 108]. Also, the spectral noise plots ($R_{sn}(f)$) can be calculated from the ratio of PSD plots according to [109]:

$$R_{sn}(f) = \left| V_{FFT}(f)/I_{FFT}(f) \right| = \left| V_{PSD}(f)/I_{PSD}(f) \right|^{1/2} \tag{2.56}$$

where $V_{FFT}(f)$ and $I_{FFT}(f)$ are the FFT of the potential and current fluctuations, respectively and $V_{PSD}(f)$ and $I_{PSD}(f)$ are the PSD data. Bertocci et al. [110] made a theoretical analysis and provided experimental data which have been compared to that of impedance spectra studies [111]. Mansfeld et al. [112] have found that the bandwidth $\Delta f = f_{max} - f_{min}$ of the noise spectra was suitable and quite limited in these cases with a maximum $f_{max} = 1/2f_s$, where f_s is the sampling frequency and $f_{min} = 1/T$, where T is the measurement time. Usually, f_s was 2 Hz, while T was 1024 s.

Analysis of EN data in the frequency domain involves the calculation of the noise power spectral density (PSD). The power spectral densities of potential (PSD_v), of current (PSD_i), and of the ratio (PSD_{sn}) are calculated as follows:

$$\log PSD_V = A_V + S_V \log f, \tag{2.57}$$

$$\log PSD_I = A_I + S_I \log f, \tag{2.58}$$

$$A_r = A_v - A_i,\ S_r = S_v - S_i \qquad (2.59)$$

where S_v and A_v, S_i and A_i, S_r and A_r are respectively the slope and the noise intensity of potential, current and ratio of PSD plots [108].

PSD plots were used to study the corrosion behaviour by evaluation of the absolute magnitude of PSD current of different Pb-Ag alloys showed in Figure 2.29.

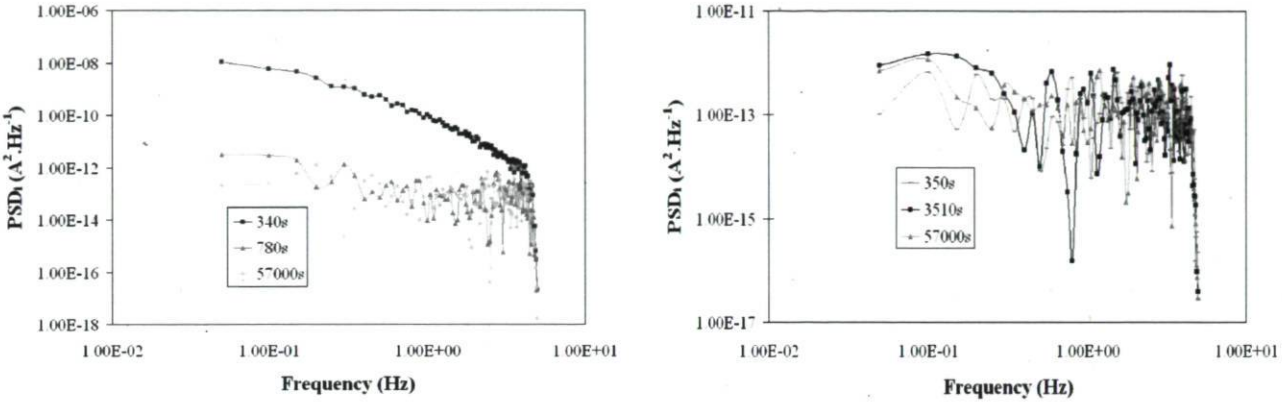

(a) (b)

Figure 2.29: PSD_i plots for (a) 0.7wt.% Ag for 20 s of the three points observed at 340 s, 780 s, 57000 s and (b) 0.5 wt.% Ag lead anode for 20 s of the three points observed at 350 s, 3510 s, 57000 s in zinc electrolyte [25].

Comparing the data of frequency analysis of 0.5% Ag and 0.7% Ag lead anodes in Figure 2.29 it was found that the ratio intensity at the first point of the lead anode containing 0.7% Ag was higher than that containing 0.5% Ag. Comparison of the slopes of PSD of the first point of the two specimens, it was also found that the absolute magnitudes of the slopes of current and potential PSD of 0.5% Ag lead anode are also lower than that of 0.7% Ag lead anode. It means that 0.5% Ag lead anode should be possible to show the passive state [113], while 0.7% Ag lead anode is much quicker to potential and current decay than that of 0.5% Ag lead anode.

2.4.5 Electrochemical impedance spectroscopy

2.4.5.1 Theory of electrochemical impedance spectroscopy

An electrochemical reaction at the electrode-electrolyte can be understood by using Electrochemical Impedance Spectroscopy "EIS". A simple interface is described by an equivalent circuit [114].

Representations of electrified interface have gradually evolved from repeated modifications (Figure 2.30a) of the model first proposed by Helmholtz [115]. In a simple case, an equivalent circuit (Figure 2.30b) can model the interface and is made of a double-layer in parallel with a polarization resistor (also known as a charge-transfer resistor with certain constraints) and a Warburg impedance, connected in series with a resistor that measures the resistance of electrolyte solution [116]. In general, the equivalent circuit can be much more complicated.

Impedance is a totally complex resistance encountered when a current flows through a circuit made of resistors, capacitors, or inductors, or any combination of these. The simple equivalent circuit is shown in Figure 2.30b without an inductive effect which is not usually encountered in electrochemistry.

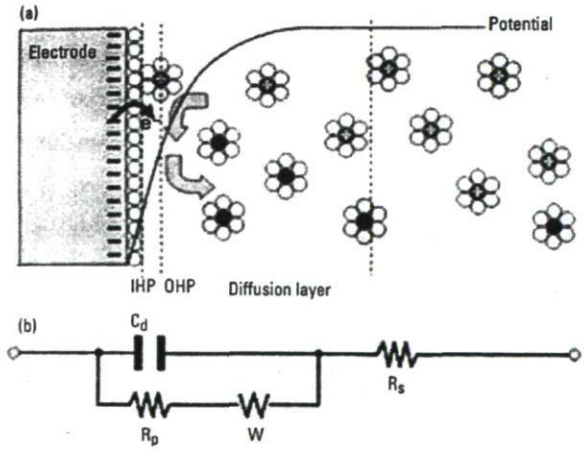

Figure 2.30. A simple electrified interface, in which the vertical dotted lines in (a) are represented by the electronic components in (b) [114].

(a) The oxidants with a positive charge diffuse toward the negatively charged electrode, accept electrons from the electrode at the interface, become the reductants, and diffuse to

the bulk of the solution. The oxidation is also a counter ion to the electrode. No specific adsorption is considered at the interface. IHP and OHP are the inner and outer Helmholtz planes, respectively.

(b) An equivalent circuit representing each component at the interface and in the solution during an electrochemical reaction is shown for comparison with the physical components: C_d double layer capacitor; R_p, polarization resistor; W, Warburg resistor; R_s, solution resistor [114].

For an equivalent circuit (Figure 2.30b), a straightforward impedance expression can be derived by applying Ohm's law to two components connected in parallel. One of these is R_p, and the other is $1/(j\omega C_d)$, in which C_d is the double-layer capacitance.

$$Z(\omega) = R_s + R_p/(1+j\omega R_p C_d) = R_s + R_p/(1+\omega^2 R_p^2 C_d^2) - j\omega^2 R_p^2 C_d/(1+\omega^2 R_p^2 C_d^2)$$

$$= Z' + jZ'' \qquad (2.60)$$

Without the Warburg component, the derivation of the equation and its interpretation are straightforward, the impedance of the interface consists of two parts, a real number Z' and an imaginary number Z" with a complex representation, $Z(\omega) = Z'(\omega) + jZ''(\omega)$ with Ø (the phase angle) $= \tan^{-1}[Z''(\omega)/ Z'(\omega)]$. Although the capacitance is relatively constant over the potential at a given electrode, the R_p varies as a function of η_{bias} applied to the electrode [114].

Bard and Faulkner [117] described the impedance as: Voltage is linked to the current through a vector $Z = R - jX_C$ called the impedance. The relationships between these various quantities can be observed in Figure 2.31. In general the impedance can be represented as:

$$Z(\omega) = Z_{Re} - jZ_{Im} \qquad (2.61)$$

where Z_{Re} and Z_{Im} are the real and imaginary parts of the impedance. For example here, $Z_{Re} = R$ and $Z_{Im} = X_C = 1/\omega C$. The magnitude of Z, written of Z, written $|Z|$ or Z, is given by

$$|Z|^2 = R^2 + X^2_C = (Z_{Re})^2 + (Z_{Im})^2 \qquad (2.62)$$

and the phase angle, Ø, is given by

$$\tan \emptyset = Z_{Im}/ Z_{Re} = X_C/R = 1/\omega RC \qquad (2.63)$$

A series of Z(w) data are obtained in the range of frequencies, typically 100 kHz-$1x10^{-4}$ Hz by giving dc bias potential,. The impedance varies with frequencies, and is also always plotted in different ways as a function of frequency (making it a spectroscopic technique), hence, the name EIS [118].

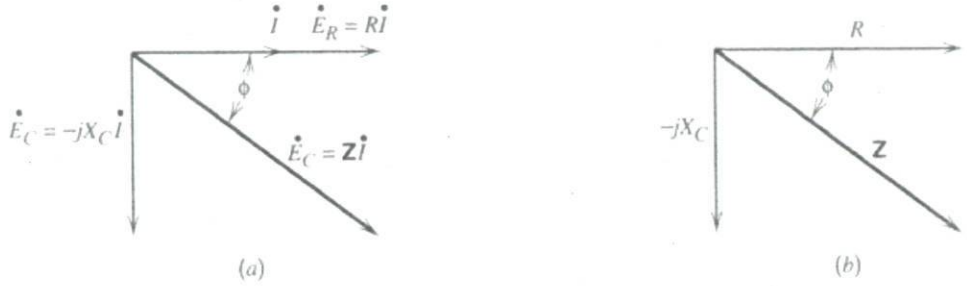

Figure 2.31 (a) Phasor diagram showing the relationship between the current and the voltages in a series RC network. The voltage across the whole network is $\dot{E}$, and $\dot{E}_R$ and $\dot{E}_C$ are its components across the resistance and the capacitance; (b) An impedance vector diagram derived from the phasor diagram in (a) [117].

By treating the impedance data in such a frequency range, system characteristic for an electrochemical reaction (i,e, R_s, R_p, and C_d) can be obtained, R_p is a function of potential; however, at η=0, it becomes the charge-transfer resistance R_{CT}. Two convenient ways of treating the impedance data are Nyquist plot, in which imaginary number $Z^{'}(\omega)$ are plotted against real numbers $Z(\omega)$, and the Bode plot, in which absolute values of impedance or phase angle are plotted against the frequency.

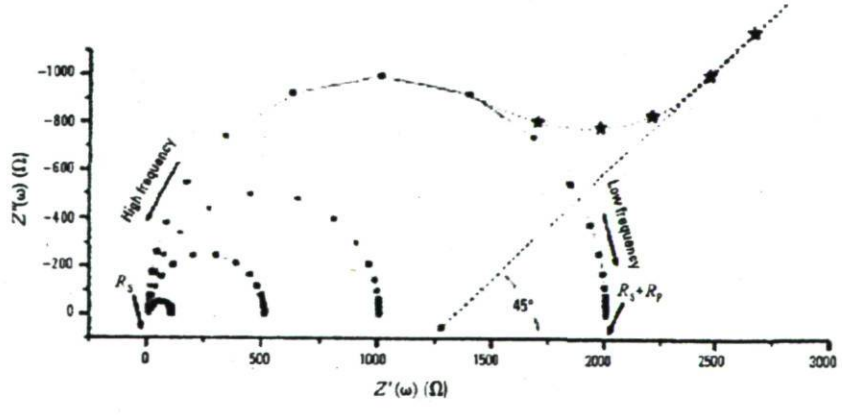

Figure 2.32. Nyquist plot [114].

The Nyquist plot (Figure 2.32) can be interpreted according to Equation 2.65. At high frequencies, Equation 2.60 is as $Z(\omega) = Z'(\omega) = R_s$. For $\omega \rightarrow 0$, Equation 2.60 becomes $Z(\omega) = R_s + R_p$. At the frequency where a maximum $Z''(\omega)$ is observed, the straightforward relationship $R_p.C_d = 1/\omega_{max} = 1/(2\pi f_{max}) = \Gamma_{rxn}$, which is the time constant of the electrochemical reaction, can be shown and indicates how fast the reaction takes place. Also, C_d can be obtained since R_p is already known from the low-frequency intercept on th $Z'(\omega)$ axis. The Nyquist plot can obtain all the necessary information about the electrode-electrolyte interface and reaction [114].

Comparison of the Bode diagram (Figure 2.33) to Equation 2.60, similar information is gotten. $LogR_s$ and $\log(R_p + R_s)$ are obtained straightforwardly from the $Z(\omega)$ versus $\log \omega$ plot at high and low frequencies from the same argument as Nyquist plot. By ignoring the frequency-independent term, R_s and 1 in the denominator, the equation 2.60 becomes:

$$Z(\omega) = R_s + R_p/(1+jwR_pC_d) \qquad (2.64)$$

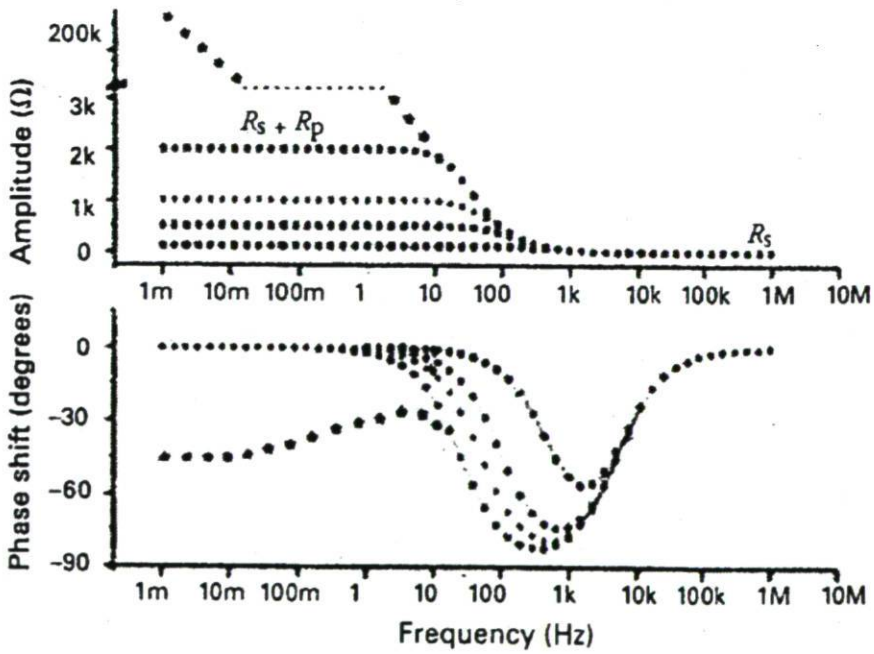

Figure 2.33 Bode plot [114].

The Bode plot provides the same information as Nyquist plot by taking the logarithm on both sides of the resulting equation yields $\log Z(\omega) = -\log \omega - \log C_d$, which

defines that $\log|Z(\omega)|$ versus log ω would have a slope of -1, and C_d can be obtained from the intercept of this line with the Z(ω) axis when –log ω = 0 at ω=1.

Thus far, the equivalent circuit has been discussed without considering the effect of the Warburg impedance; however, its contribution can be important at low frequencies because the mass transport of the electroactive species may limit the electron-transfer process [119]. The Warburg impedance [119] is imparted by mass transfer and can be derived by

$$Z(\omega) = R_s + R_p[1 + \lambda/\sqrt{2\omega}] - R_p^2 \lambda^2 C_d - jR_p \lambda/\sqrt{2\omega} \qquad (2.65)$$

In which $\lambda = k_f/\sqrt{D}_o + k_b\sqrt{D}_R$, and k_f and k_b are the forward and backward electron-transfer rate constants, respectively, and D_o and D_R are the diffusion coefficients for the oxidant O and the reductant R, respectively. So the Warburg impedance is the frequency-dependent terms $\lambda/2\omega$, appearing in both the real and the imaginary terms in Equation 2. 65 [119].

2.4.5.2 Application of electrochemical impedance spectroscopy

The electrochemical impedance spectroscopy (EIS) is useful technique in the study of corrosion. Indeed, EIS is appropriate for the rapid estimation of corrosion rates (within 30 min to 24 hours), the estimation of extremely low corrosion rates and metal contamination rates ($<10^{-4}$ mm/year), the estimation of corrosion rates in low conductivity media and the rapid evaluation of coating [120].

Brinic et al. [121] used EIS to study the corrosion resistance of Pb-Sb alloys. The impedance spectra for Pb-Sb alloys were measured in the potential region where the anodic film was expected to be composed of $PbSO_4$ and oxide film, e.g. et potentials $E_i \geq$ -0.2 V. Figure 2.34 shows the Nyquist diagrams corresponding to the impedance of Pb-Sb alloys in 0.5 M H_2SO_4 solution at -0.2 V and for the sake of comparison, the impedance of pure lead is also represented. The spectra, of the same shape as the one for pure lead, include a high frequency loop and a low frequency linear part with a slope which is almost exactly 45°, being characteristic of the Warburg impedance.

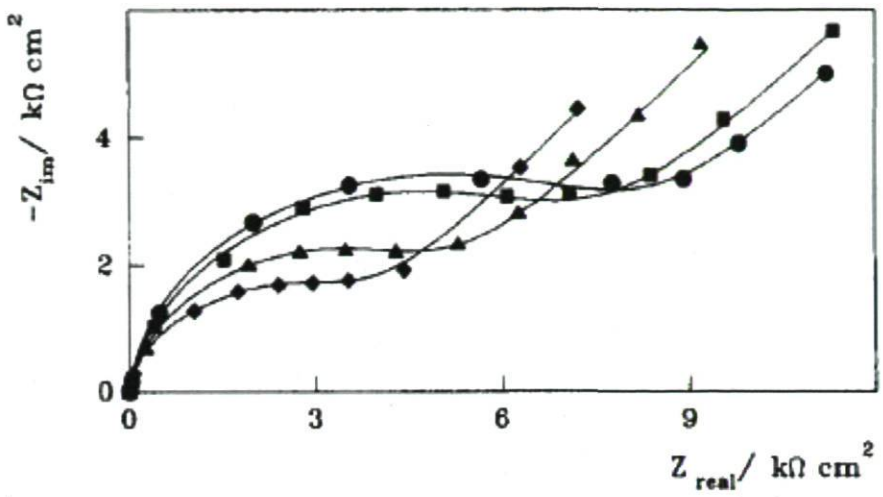

Figure 2.34. Nyquist plots for (●) Pb and Pb-Sb alloys (■) 1.3wt.% Sb; (▲) 2.7wt.% Sb; (◆) 3.7wt% Sb in a 0.5 M H_2SO_4 solution at -0.2 V vs SCE [121].

The results obtained show that the resistance values slightly decrease with an increase of the Sb content in the alloy.

2.4.6 Optical and SEM observations

Optical microscope (OM) and scanning electron microscope (SEM) techniques were used to characterize the microstructure of the alloys and the corrosion products. SEM analyses were conducted using JEOL JSM-25s III model Scanning Electron Microscope equipped with TN 5700 model energy dispersive X-ray analyzer (EDX). The microstructure of the anode surface was characterized using an optical microscope (ZEISS Model).

For example, initially, each specimen was examined by optical microscope equipped with an image analyzer after etching in order to reveal the phases, grain boundaries, inclusions and porosity. Following 16 h potential decay, after 24 h polarization in the zinc electrolyte, surface of specimen was examined by SEM equipped with energy dispersive X-ray analyzer to identify the corrosion products. The pits were investigated using the ASTM G64-94 standard [122].

2.5 References

[1] **Ivanov, I., Stefanov, Y., Noncheva, Z., Petrova, M., Dobrev, Ts., Mirkova, L., Vermeersch R., and Demaerel, J. P.**, Insoluble Anodes Used in Hydrometallurgy: Part I. Corrosion Resistance of Lead and Lead Alloy Anodes, Hydrometallurgy, vol. 57, 2000, pp. 109-124.

[2] **Koenig, A.E., MacEwan, J.U. and Larssen, E.C.**, Investigation of Lead Anodes in the Electrolysis of Zinc Sulfate Solutions, Trans. Electrochem. Soc. 79, 1941, pp. 331-345.

[3] **Tizpar, A., Ghasemi, Z.**, Influence of Silver on the Anodic Corrosion and Gas Evolution of Pb–Sb–As–Se Alloys as Positive Grids in Lead Acid Batteries, Applied Surface Science 252, 2006, pp. 7801–7808.

[4] **Kiryakov, G.Z. and Korchmarek, I.A.**, Role of Lead Dioxide Film, J. Appl. Chem. (Russian), 26 (9), 1953, pp. 1263-1266.

[5] **Newnham, R.H.**, Corrosion Rates of Lead Based Anodes for Zinc Electrowinning at High Current Densities, J. Appl. Electrochem. 22, 1992, pp. 116-124.

[6] **Ivanov, I., Stefanov, Y., Noncheva, Z., Petrova, M., Dobrev, Ts., Mirkova, L., Vermeersch, R. and Demaerel, J.-P.**, Insoluble Anodes Used in Hydrometallurgy: Part II. Anodic Behaviour of Lead and Lead-Alloy Anodes, Hydrometallurgy, vol. 57, 2000, pp. 125-139.

[7] **Umetsu, Y., Nozoka H. and Tozawa, K.**, Anodic Behaviour of Pb-Ag Alloys in Sulfuric Acid Solution, Proceedings of the International Symposium on Extract. Metall. Zinc, MMJ, Tokyo, Japan, 1985. pp. 265-279.

[8] **Monahov, B., Pavlov, D., Petrov, D.**, Influence of Ag as Alloy Additive on the Oxygen Evolution Reaction on Pb/PbO_2 Electrode, Journal of Power Sources 85, 2000, pp. 59–62.

[9] **Fink, C., Dornblatt, A.**, The Effect of Silver (0.05 to 0.15 per cent) on Some Properties and the Performance of Antimonial Lead Storage Battery Grids, Trans. Electrochem. Soc. 79, 1941. pp. 269-305.

[10] **Pavlov, D., Rogachev, T.**, Mechanism of the Action of Ag and As on the Anodic Corrosion of Lead and Oxygen Evolution at the $Pb/PbO_{(2-x)}/H_2O/O_2/H_2SO_4$ Electrode System, Electrochim. Acta 31, 1986. pp. 241-252.

[11] **Bagshaw, N.E.**, Grid Alloys for Maintenance-Free Deep-Cycling Batteries, J. Power Sources 33, 1991, pp. 3-11.

[12] **Lam, L.T., Douglas, J.D., Pillig, R., Rand, D.A.J.**, Minor Elements in Lead Materials Used for Lead/Acid Batteries- Hydrogen- and Oxygen-Gassing Characteristics, J. Power Sources 48, 1994. pp. 219-232.

[13] **Hein, K., Schierle, T.**, Oxygen Overvoltage at Insoluble Anodes in the System Pb-Ag-Ca (German), Erzmetall, Leadscan 44, 1992. pp. 447-451.

[14] **Pavlov, D., Monahov, B., Petrov, D.**, Effect of Ag Element on the Formation of Lead Oxide Layer, 6th European Lead Battery Conference, Prague, 21–25 September 1998, p. 3.2-1, Abstracts.

[15] **Hine, F., Ogata, Y., Yasuda, M.**, Consumption of Lead-Silver Alloy Anodes in Sulfuric Acid Solution, B. Electrochem., 4(1), 1988, pp. 61-65.

[16] **Moskalyk, R.R., Alfantazi, A., Tombalakian A.S., Valic, D.**, Anode Effects in Electrowinning, Materials Engineering, Vol. 12, No. 1, 1999, pp. 65-73.

[17] **Nguyen T., Atrens, A.**, Influence of Lead Dioxide Surface Films on Anodic Oxidation of A lead Alloy Under Conditions Typical of Copper Electrowinning, J. Appl. Electrochem. 38, 2008, pp. 569-577.

[18] **Tikkanen, M.H. and Hyvarinen, O.**, On the Anodic Behaviour of Pb-Ag Alloys in Sulfuric Acid Solutions, Proc. Int. Congr. Metai. Corros., 4^{th} (1972), Meeting data 1969, pp. 669-675.

[19] **Bode, H.**, Lead-Acid Batteries, Wiley, New York, 1977.

[20] **Ruetschi, P. J. and Cahan, B. D.**, Electrochemical Properties of PbO_2 and the Anodic Corrosion of Lead and Lead Alloys, J. Electrochem. Soc., 105, 1958. pp. 369-376.

[21] **Bone, S.J., Singh, K. P., and Wynne-Jones, W. F. K.**, Some Potential and Exchange Studies of α-Lead Dioxide, Electrochim. Acta., 4, 1961. pp. 288-293.

[22] **Dawson, J.L.**, Principles of Lead Corrosion in Sulphuric Acid, in: A.T. Kuhn (Ed.), The electrochemistry of lead, Academic Press, 1979.

[23] **Burbank, J., Simon, A.C., Willihnganz, E.**, The Lead-Acid Cell, in: C.W. Tobias (Ed), Advances in electrochemistry and electrochemical engineering, Vol. 8, Wiley-Interscience, New York, London, Sydney, Toronoto, 1971, pp. 157-164.

[24] **Ruetschi, P., Cahan, B.D.**, Anodic Corrosion and Hydrogen and Oxygen Overvoltage on Lead and Lead Antimony Alloys, J. Electrochem. Soc. 104, 1957, pp. 406-413.

[25] **Zhang, W., Lafront, A-M., Ghali, E., Houlachi, G.**, Influence of Silver Content on Corrosion Resistance of Lead Anodes During Potential Decay by Electrochemical Noise Measurements, METSOC, Development & Perfromance of Sulphur Capture Plants, Sudbury, Ontario, Canada, 48th Annual Conf. of Metallurgists of CIM, 2009, pp. 101-115.

[26] **Petersson, I., Ahlberg, E., Berghult, B.**, Parameters Influencing the Ratio between Electrochemically Formed α- and β-PbO_2, Journal of Power Sources 76, 1998, pp. 98–105

[27] **Pavlov, D., Balkanov, I., Halachev, T., Rachev, P.**, Hydration and Amorphization of Active Mass PbO_2 Particles and Their Influence on the Electrical Properties of the Lead-Acid Battery Positive Plate, J. Electrochem. Soc. 136, 1989. pp. 3189-3197.

[28] **Pavlov, D., Balkanov, I.**, The PbO_2 Particle: Exchange Reactions between Ions of the Electrolyte and the PbO_2 Particles of the Lead-Acid Battery Positive Active Mass, J. Electrochem. Soc. 139, 1992. pp. 1830-1835.

[29] **Pavlov, D.**, Influence of Crystal and Gel Zones on the Capacity of the Lead Dioxide Active Aass (extended abstract), Journal of Power Sources, 40, 1992, pp. 169-173.

[30] **Monahov, B., Pavlov, D.**, Hydrated Structures in the Anodic Layer Formed on Lead Electrodes in H_2SO_4 Solution, J. Appl. Electrochem. 23, 1993. pp. 1244-1250.

[31] **Pavlov, D., Petkova, G., Dimitrov, M., Shiomi, M., Tsubota, M.**, Influence of Fast Charge on the Life Cycle of Positive Lead–Acid Battery Plates, J. Power Sources 87, 2000, pp. 39-56.

[32] **Rogachev, T., Pavlov, D.**, Influence of Cycling on the Nature of the Positive Active Mass of Lead/Acid Batteries and Effect of $CaSO_4$ on the Behaviour of the Positive Plates, J. Power Sources 64, 1997, pp. 51-56.

[33] **Zerroual, L., Fitas, R., Djellouli, B., Chelali, N.**, Relationship between Water Departure and Capacity Loss of α and β-PbO_2 Using An All Solid-State System: Estimation of Proton Diffusion Coefficient, Journal of Power Sources 158, 2006, pp. 837–840.

[34] **Fitas, R., Chelali, N., Zerroual, L., Djellouli, B.**, Mechanism of the Reduction of α- and β-PbO_2 Electrodes Using An All-Solid-State System, Solid State Ionics 127, 2000, pp. 49–54

[35] **Pavlov, D.**, The Lead-Acid Battery Lead Dioxide Active Mass: A Gel-Crystal System with Proton and Electron Conductivity, J. Electrochem. Soc. 139 (11), 1992, pp. 3075-3080.

[36] **Pavlov, D.**, Effect of Corrosion Layer on Phenomena that Cause Premature Capacity Loss in Lead/Acid Batteries, J. Power Sources 48, 1994, pp. 179-193.

[37] **Zhou, D., Gao, L.**, Effect of Electrochemical Preparation Methods on Structure and Properties of PbO_2 Anodic Layer, Electrochim. Acta 53, 2007, pp. 2060-2064.

[38] **Shen, P.K., Xiao, L.W.**, Morphologic Study of Electrochemically Formed Lead Dioxide, Electrochim. Acta 48, 2003, pp. 1743-1747.

[39] **Li, X., Pletcher, D., Walsh, F.C.**, A novel Flow Battery: A Lead Acid Battery Based on An Electrolyte with Soluble Lead (II): Part VII. Further Studies of the Lead Dioxide Positive Electrode, Electrochim. Acta 54, 2009, pp. 4688-4695.

[40] **Sawai, K., Tsuboi, Y., Okada, Y., Shiomi, M., Osumi, S.**, New Approach to Prevent Premature Capacity Loss of Lead-Acid Battery in Cycle Use, J. Power Sources 179, 2008, pp. 799-807.

[41] **Pavlov, D.**, Premature Capacity Loss (PCL) of the Positive Lead/Acid Battery Plate: A New Concept to Describe the Phenomenon, J. Power Sources 42, 1993, pp. 345-363.

[42] **Mellor, J. M.**, A Comprehensive Treatise on Inorganic and Theoretical Chemistry, Vol. 7, Longmans, London, 1960, pp. 685-695.

[43] **Niu, J., Conway, B.E., Pell, W. G.**, Comparative Studies of Self-Discharge by Potential Decay and Float-Current Measurements at C Double-Layer Capacitor and Battery Electrodes, J. Power Sources 135, 2004, pp. 332-343.

[44] **Caulder, S.M., Simon, A.C.**, Thermal Decomposition Mechanism of Formed and Cycled Lead Dioxide Electrodes and Its Relationship to Capacity Loss and Battery Failure, J. Electrochem. Soc. 121, 1974, pp. 1546-1551.

[45] **Pavlov, D.**, Effect of Chemisorbed Water on the Electrical Capacity of the Lead—Acid Battery Positive Plate, J. Power Sources 19, 1987, pp. 15-24.

[46] **Garche, J.**, Passivation of the Positive Electrode of the Lead/Acid Battery: A Consequence of Self-Discharge, Journal of Power Sources, 3o, 1990, pp. 47 – 54.

[47] **Garche, J.**, The Redox Cycling of Lead Alloys, Dissertation Dr. SC., TU Dresden, 1982.

[48] **Wiesener, K., Garche J. and Anastaeijevic, N.**, The Decay of the Anode of Lead Acid Battery, in J. Thompson (ed.), Power Sources 9, Academic Press, London, 1983, pp. 13-16.

[49] **Nguyen, T., Atrens, A.**, Composition and Morphology of the Film Formed on A Lead Alloy under Conditions Typical of the Electro-winning of Copper, Hydrometallurgy 96, 2009, pp. 14-26.

[50] **Nguyen T., Guresin, N., Nicol, M., Atrens, A.**, Influence of Cobalt Ions on the Anodic Oxidation of A Lead Alloy under Conditions Typical of Copper Electrowinning, J. Appl. Electrochem. 38, 2008, pp. 215-224.

[51] **Pourbaix, M.**, Altas of Electrochemical Equilibrium in Aqueous Solution, NACE, Houston, TX, 1974, pp. 141-145.

[52] **Garche, J., Jossen, A., Dijring, H.**,The Influence of Different Operating Conditions, Especially Over-Discharge, on the Lifetime and Performance of Lead/Acid Batteries for Photovoltaic Systems, Journal of Power Sources 67, 1997, pp. 201-212.

[53] **Barnes, S.C., Mathieson, R.T.**, The potential pH Diagram of Lead in the Presence of Sulphate Ions and Some of Its Implications in Lead-Acid Battery Studies, in "Batteries", D. H. Collins, (Ed). Pergamon Press, New York, 1963, pp. 41-54.

[54] **Cifuentes, G., Cifuents, L., Crisostomo, G.**, A Lead-Acid Analogue to In Situ Anode Degradation in Copper Electrometallurgy, Corrosion science,Vol. 40, 1998, pp. 225-234.

[55] **Xu, J., Liu, X., Li, X., Barbero, E., Dong, C.**, Effect of Sn Concentration on the Corrosion Resistance of Pb-Sn Alloys in H_2SO_4 Solution, Journal of Power Sources 155, 2006, pp. 420–427.

[56] **Robinson, D. J., O'Keefe, T. J.**, On the Effects of Antimony and Glue on Zinc Electrocrystallization Behaviour, Journal of applied electrochemistry, Vol. 6, 1976, pp. 1-7.

[57] **Scott, A.C., Pitblado, R.M., Barton G.W. and Ault, A.R.**, Experimental Determination of the Factors Affecting Zinc Electrowinning Efficiency, Journal of Applied Electrochemistry 18, 1988, pp. 120-127.

[58] **Mackinnon, D.J., Brannen, J. M., Fenn, P. L.**, Characterization of Impurity Effects in Zinc Electrowinning from Industrial Acid Sulphate Electrolyte, Journal of Applied Electrochemistry 17, 1987, pp. 1129-1143.

[59] **Mackinnon, D.J., Brannen, J.M.**, Zinc Deposit Structures Obtained from High Purity Synthetic and Industrial Acid Sulphate Electrolytes with and without

Antimony and Glue Additions, Journal of Applied electrochemistry 7, 1977, pp. 451-459.

[60] **Ivanov, I., Stefanov, Y.**, Electroextraction of Zinc from Sulphate Electrolytes Containing Antimony and Hydroxyethylated-Butine-2-diol-1,4: Part 2: Deposition on A Specpure Aluminium Cathode, Hydrometallurgy 64, 2002, pp. 111-117.

[61] **Mackinnon, D.J., Morrison, R.M., Mouland, J.E., and Warren, P.E.**, The Effects of Antimony and Glue on Zinc Electrowinning from Kidd Creek Electrolyte, Journal of applied electrochemistry 20, 1990, pp. 728-736.

[62] **Ault A.R. and Frazer, E. J.**, Effects of Certain Impurities on Zinc Electrowinning in High-Purity Synthetic Solutions, J. Appl. Electrochem. 18, 1988, pp. 583-589.

[63] **Tripathy, B.C., Das, S.C., Misra, V.N.**, Effect of Antimony(III) on the Electrocrystallisation of Zinc from Sulphate Solutions Containing SLS, Hydrometallurgy 69, 2003, pp. 81-88.

[64] **Kerby, R. C., Jackson, H. E., O'Keefe, T. J. and Wang, Y-M.**, Evaluation of Organic Additives for Use in Zinc Electrowinning, Metall. Trans., 1977, vol. 8B, pp. 661-668.

[65] **Pajdowski, L.**, Effect of Organic Additive in Electrowinning, Problemy I metody chemii koordynacyjnej, 1981, pp. 327-343.

[66] **Krzewska, S., Pajdowski, L., Podsiadly, H., Podsiadly, J.**, Electrochemical Determination of Thiourea and Glue in the Industrial Copper Electrolyte, Metallurgical Transaction B, Volume 15B, September 1981, pp. 451-459.

[67] **Maja M. and Spinelli, P.**, Detection of Metallic Impurities in Acid Zinc Plating Baths, J. Electrochem. Soc. 118, 1971, pp. 1538-1540.

[68] **Sato R.**, Crystal Growth of Electrodeposited Zinc, J. Electrochem. Soc. 106, 1959, pp. 206-211.

[69] **Bushell, C.H. G., Krauss C.J. and Liang, S.C.**, Effect of Some Trace Impurities on the Zinc Electrowinning Process, Paper presented at CIMM Conference of Metallurgist, Ottwa, Sep. 1-3 1965.

[70] **Tripathy, B. C., Das, S. C., Hefter, G. T., Singh, P.**, Zinc Electrowinning from Acidic Sulfate Solutions: Part I: Effects of Sodium Lauryl Sulfate, Journal of Applied Electrochemistry 27, 1997, pp. 673-678.

[71] **Recéndiz, A., Gonzàlez, I., Nava, J. L.**, Current Efficiency Studies of the Zinc Electrowinning Process on Aluminum Rotating Cylinder Electrode (RCE) in Sulfuric Acid Medium: Influence of Different Additives, Electrochimica Acta 52, 2007, pp. 6880-6887

[72] **Stefanov, Y., Ivanov, I., Rashkov, S.**, Electro-Extraction of Zinc from Sulphate Electrolytes Containing Antimony and Hydroxyethylated-butyne-2-diol-1,4. Part 1: Deposition on An Aluminium Cathode Containing Iron Impurities, Hydrometallurgy 44, 1997, pp. 71- 81.

[73] **O'Keefe, T.J., Chen, S.F., Cole E.R. and Dattilo, M.**, Electrochemical Monitoring of Electrogalvanizing Solutions, J. Appl. Electrochem. 16, 1986, pp. 913-918

[74] **Sider M. and Piron, D.L.**, The Effects of Metallic Impurities and 2-Butyne-1,4-Diol on Zinc Electrowinning from Chloride Solutions, J. Appl. Electrochem. 18, 1988, pp.54-61.

[75] **Bozhkov, C., Ivanov I., and Rashkov, S.**, The Relationship between the Growth Rate of Hydrogen Bubbles and the Duration of the Induction Period' in the Electrowinning of Zinc from Sulphate Electrolytes, J. Appl. Electrochem. 20, 1990, pp. 447-453.

[76] **Cachet, C., Wiart, R., Ivanov, I., Stefanov, Y., Rashkov, S.**, Mechanism of the Reverse Dissolution of Zinc in the Presence of Nickel, Journal of Applied Electrochemistry 24, 1994, pp. 713-718.

[77] **Tripathy, B.C., Das, S.C., Hefter, G., Singh, P.**, Zinc Electrowinning from Acidic Sulphate Solutions, part II: Effects of Triethylbenzylammonium Chloride, Journal of Applied Electrochemistry 28, 1998, pp. 915-920.

[78] **Kirk, R.E., Othmer, D.F.**, Encyclopedia of Chemical Technology, Vol. 22, third ed., 1979, pp. 348-356.

[79] **Cachet, C., Wiart, R.,** Influence of A Perfluorinated Surfactant on the Mechanism of Zinc Deposition in Acidic Electrolytes, Electrochim. Acta 44, 1990, pp. 4743-4751.

[80] **Tripathy B.C., Das, S.C., Singh, P., Hefter, G.T., Misra, V.N.**, Zinc Electrowinning from Acidic Sulphate Solutions Part IV: Effects of Perfluorocarboxylic Acids, Journal of Electroanalytical Chemistry 565, 2004, pp. 49-56.

[81] **Juhel, G., Beden, B., Lamy, C., Leger, J.M., Vignaud, R.**, Effect of the Surfactant "Forafac" on Hydrogen Evolution on a Zinc Electrode, Electrochim. Acta 35, 1990, pp. 479-481.

[82] **Schwartz A.M., and Perry, J.W.**, Surface Active Agents Vol 1, Interscience Publishers, New York, 1963, pp. 53-55.

[83] **Lorenz, W.J. and Mansfeld, F.**, Determination of Corrosion Rates by Electrochemical DC and AC Methods, Corrosion Science, Vol. 21 (9-10), 1981, pp. 647-672.

[84] **Shreir, L.L., Jarman, R.A., and Burstein, G.T.**, Corrosion, Edsited by Butterworth-Heinemann, Vol.2, 1994, pp. 19:76-19:95.

[85] **Gileadi, E., Kirowa-Eisner E. and Penciner, J.**, Interfacial Electrochemistry, (Addison-Wesley Publishing Company, INC.), Ontario, 1975, ISBN 0-201-02399-7.

[86] **Delahay, A.**, New Instrumental Methods in Electrochemistry, Interscience Publishers Inc., New York, 1966, Chap. 6.

[87] **Nicholson, R.S. and Shain, I.**, Theory of Stationary Electrode Polarography: Single Scan and Cyclic Methods Applied to Reversible, Irreversible, and Kinetic Systems, Anal. Chem. 36. 1964. pp. 706-717.

[88] **Yamamoto, Y., Fumino, K., Ueda T. and Nambu, M.**, A Potentiodynamic Study of the Lead Electrode in Sulphuric Acid Solution, Electochemica Acta 37, 1992. pp. 199-203.

[89] **Mahata, B. K.,** The Cyclic Corrosion of the Lead-Acid Battery Positive, J. Electrochem. Soc. 126. 1979. pp. 365-374.

[90] **Sharpe, T. F.**, Low-Rate Cathodic Linear Sweep Voltammetry (LSV) Studies on Anodized Lead, J. electrochem. Soc. 122, 1975, pp. 845-849.

[91] **Mahato, B. K.**, Lead-Acid Battery Expander, J. electrochem. Soc. 127, 1980. pp. 1679-1686.

[92] **Deutscher, R.L., Fletcher, S., Hamilton, J.A.**, Invention of Cyclic Resistometry, Electrochim. Acta 31, 1986. pp. 585-589.

[93] **Cai, W.-B., Wan, Y.-Q., Liu, H.-T., Zhou, W.-F.**, A Study of the Reduction Process of Anodic PbO_2 Film on Pb in Sulfuric Acid Solution, Journal of Electroanalytical chemistry 387 (1-2), 1995, pp. 95-103.

[94] **Yamamoto, Y., Matsuoka, M., Kimoto, M., Uemura M. and Iwakura, C.**, Potentiodynamic Reactivation of A Passivated Lead Negative Electrode in Sulphuric Acid Solution, Electrochimica Acta, Vol. 41. No. 3 1996, pp. 439-444.

[95] **Czerwinski, A., Zelazowska, M., Grden, M., Kuc, K., Milewski, J,D., Nowacki, A., Wojcik, G., Kopczyk, M.**, Electrochemical Behavior of Lead in Sulfuric Acid Solutions, Journal of power 85, 2000, pp.49-55.

[96] **Thompson, N.G and Payer, J.H.**, DC Electrochemical Test Methods, in Corrosion Testing Made Easy, B. C. Syrett, (series Ed), NACE International, Houston, Texas, 1998, Volume 6.

[97] **ASTM Publication, ASTM G5-94**, Standard Reference Test Method for Making Potentiostatic and Potentiodynamic Anodic Polarization Measurements, 2001, Vol. 03.02, Philadelphia, PA, pp. 54-69.

[98] **Stansbury, E.E. and Buchanan, R.A.** Fundamental of Electrochemical Corrosion, ASM International, Material Park, OH, USA, 2000, pp. 88-108.

[99] **Xu, J., Liu, X., Li, X., Barbero, E., Dong, C.**, Effect of Sn Concentration on the Corrosion Resistance of Pb-Sn Alloys in H_2SO_4 Solution, Journal of Power Sources 155, 2006, pp. 420-427

[100] **Yang, D., Shen, Z.**, Metallurgical Corrosion, second ed., Metallurgical Press, Beijing, 1999, pp. 19–41.

[101] **Stern, M., Geary, A.L.**, Electrochemical Polarization, Journal of Electrochemical Society 104, 1957, pp. 56-63.

[102] **Eden, D.A.,** Electrochemical noise, National Association of Corrosion Engineers, Corrosion 98 (USA), pp. 386/1-386/31, Mar. 1998.

[103] **Eden, D.**A., Electrochemical Noise, Ch. 69, ed. R.W. Revie, Uhlig's Corr. Handbook, 2000, pp. 1227-1237.

[104] **Cottis, R. and Turgoose, S.**, Electrochemical Impedance and Noise, NACE International TX, USA, 1999.

[105] **Veilleux, B.,** Effect of various Additives Ratios and Concentrations on Cathode Quality during Copper Electrorefinning under High Current Densities, Ph.D thesis, Laval University, Quebec, Canada, 2000.

[106] **Gusmano, G., Montesperelli, G., Pacetti, S., Petitti, A. and D'amico, A.**, Electrochemical Noise Resistance as A Tool for Corrosion Rate Prediction, Corrosion, Vol. 53 (11), 1997, pp. 860-868.

[107] **Mansfeld, F. and Xiao, H.**, Electrochemical Noise Analysis of Iron Exposed to NaCl Solutions of Different Corrosivity, J. Electrochem. Soc., Vol. 140, 1993, pp. 2205-2211.

[108] **Xiao, H. and Manfeld, F.**, Evaluation of Coating Degradation with Electrochemical Impedance Spectroscopy and Electrochemical Noise Analysis, J. Electrochem. Soc., Vol. 141, 1994, pp. 2332-2337

[109] **Lee C.C., and Mansfeld, F.**, Analysis of Electrochemical Noise Data for A Passive System in the Frequency Domain, corrosion science, Vol. 40, No. 6, 1998, pp. 959-962.

[110] **Bertocci, U., Gabrielli, C., Huet, F. and Keddam, M.**, Noise Resistance Applied to Corrosion Measurements, J. Electrochem. Soc., Vol. 144, 1997a, pp. 31-37.

[111] **Bertocci, U., Gabrielli, C., Huet, F. and Keddam, M. and Rousseau. P.**, Noise Resistance Applied to Corrosion Measurements, J. Electrochem. Soc. Vol. 144, 1997b, pp. 37-43.

[112] **Mansfeld, F., Han, L.T. and Lee. C.C.**, Analysis of Electrochemical Noise Data for Polymer Coated Steel in the Time and Frequency Domains, J. Electrochem. Soc. Vol. 143, 1996, pp. L286-295.

[113] **Girija, S., Kamachi Mudali, U., Raju, V. R., Dayal, R. K., Khatak, H. S., Raj, B.**, Determination of Corrosion Types for AISI Type 304L Stainless Steel Using Electrochemical Noise Method, Materials Science and Engineering A 407, 2005, 188-195.

[114] **Park, S.M. and Yoo, J.S.**, Electrochemical Impedance Spectroscopy, In Analytical Chemistry, American Chemical Society, 2003, November 1, pp. 455A-461A.

[115] **Stansbury, E.E. and Buchanan, R.A.**, Fundamental of Electrochemical Corrosion, ASM International, Material Park, OH, USA, 2000, pp. 3-4.

[116] **Randles, J.E.B.**, A Cathode Ray Polarograph. Part II.—The Current-Voltage Curves, Trans. Faraday. Soc. 44, 1948, pp. 327-337.

[117] **Bard, R.J. and Faulkner, L. R.**, Electrochemical Methods; Wiley & Sons: New York, Chapters 10, 2001, pp. 368-416.

[118] **Macdonald, J.R.**, Impedance Spectroscopy; Wiley/Interscience : New York, 1987.

[119] **Sluyters-Rehback, M. and Sluyters., J.H.**, The Warburg Impedance in Electrochemical Reaction, in Electrochemical Chemistry; Bard, A. J., Ed.; Marcel Dekker: New York, 1970; Vol. 4.

[120] **Silverman, D.C.**, Practical Corrosion Prediction Using Electrochemical Techniques, in Uhlig's Corrosion Handbook, John Wiley & Sons, 2000, pp. 1179-1224.

[121] **Brinic, S., Metikos-Hukovic, M., Babic, R.**, Characterization of Anodic Films on Lead and Lead Alloys by Impedance Spectroscopy, Journal of Power Sources 55, 1995, pp. 19-24.

[122] **ASTM Publication**, **ASTM G64-94**, Standard Guide for Examination and Evaluation of Pitting Corrosion, Wear and Erosion, Metal Corrosion, Philadelphia, PA, 03.02, 2001, pp. 178-184.

CHAPTER 3

Experimental procedures

3.1 Lead alloys used in this work

The newly developed laminated Pb-Ag and Pb-Ag-Ca alloys selected in this study were divided two groups. The first group has six Pb-Ag specimens, and their chemical composition is given in Table 3.1. At least 45 elements were analysed by fluorescence X and only the elements where the wt% is higher than 0.05% are given. Ag, Ca and Fe contents were analysed quantitatively by atomic absorption technique. These six specimens were provided by Fonderie Générale du Canada (Montréal).

Table 3.1 – Chemical composition (wt %) of the six experimental anodes (Studies of chapters 5, 6, 9)

Anode	Ag (wt %)	Fe (wt %)	Ca (wt %)	Al (wt %)	Mn (wt %)	S (wt %)	Si (wt %)	Ti (wt %)	Zr (wt %)	Pb (wt %)
#1	0.516	0.007	< 0.001	0.29	< 0.05	0.13	1.4	< 0.05	0.21	bal.
#2	0.512	0.007	< 0.001	0.11	< 0.05	0.12	0.4	0.4	0.19	bal.
#3	0.574	0.021	< 0.001	0.09	0.15	0.4	0.29	0.26	0.18	bal.
#4	0.600	0.013	< 0.001	< 0.05	< 0.05	0.08	0.3	0.18	0.22	bal.
#5	0.684	0.015	< 0.001	< 0.05	< 0.05	< 0.05	0.23	0.19	0.2	bal.
#6	0.672	0.009	< 0.001	< 0.05	< 0.05	0.07	0.07	0.25	0.19	bal.

The second group has four Pb-Ag-Ca and Pb-Ag specimens. The anode #1 is a Pb-0.25%Ag-0.1%Ca alloy; the anodes #2 and #3 are Pb-0.6%Ag alloys, while anode #4 is a Pb-0.7%Ag alloys, but they have different impurities such as Fe. Their complete chemical composition is given in Table 3.2.

Table 3.2 Chemical composition (wt%) of the four commercial lead alloy anodes (Studies of chapters 4, 7, 8, 10)

Anodes	Ag	Zr	Ca	Al	Au	Fe	Cu	Ba	Ni	W	S	Pb
#1	0.25	0.22	0.1	<0.05	<0.01	<0.05	<0.05	<0.05	<0.05	0.10	0.12	bal.
#2	0.60	0.23	0.05	<0.05	<0.01	<0.05	<0.05	<0.05	<0.05	0.10	0.09	bal.
#3	0.56	0.24	0.06	<0.05	<0.01	<0.05	<0.05	<0.05	<0.05	<0.05	<0.05	bal.
#4	0.69	0.22	<0.05	<0.05	<0.01	<0.05	<0.05	<0.05	<0.05	<0.05	<0.05	bal.

Anodes #1 and #2 were provided by RSR (Texas, USA); anodes #3 and #4 were provided by Goslar (Germany) and Fonderie Générale du Canada (Montréal), respectively.

3.2 Preparation of specimens used for anode studies

Electrode specimens used for zinc electrowinning were cut into small pieces of 1 x 1 x 1 cm then connected with a plastic isolated copper wire and cast in acrylic resin leaving 1 cm^2 exposed area surface. Two types of working anode, original and polished surfaces were washed with alcohol and dried immediately before being introduced into the electrolytic cell. The polished anode surfaces were obtained ground with 600 soft grid SiC paper with ethanol to avoid the inclusion of SiC particles into electrodes. Some samples in the beginning were polished using the current SiC paper. The preparation steps of working specimens are illustrated in Figure 3.1.

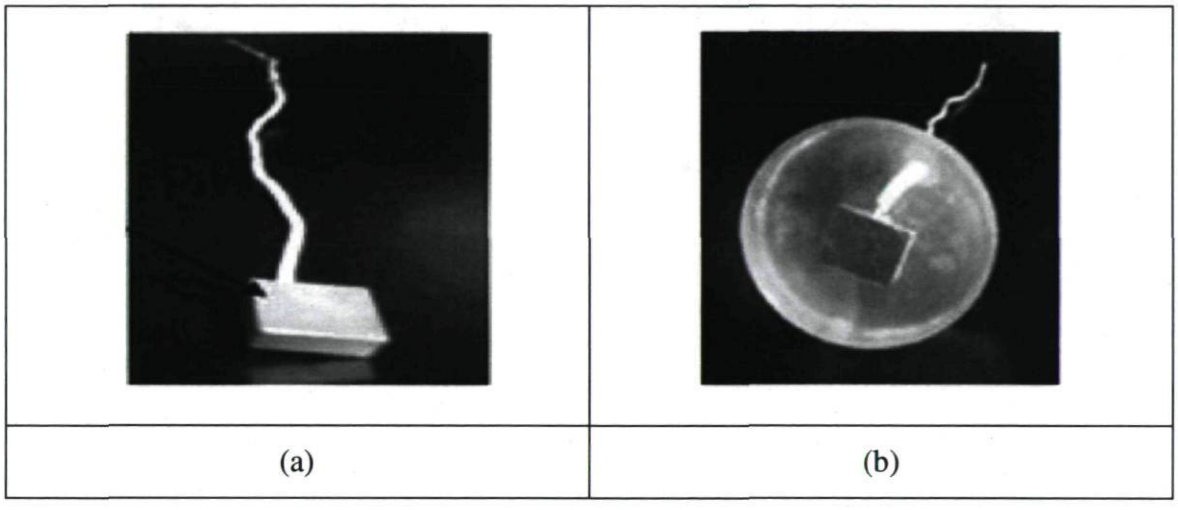

(a) (b)

Figure 3.1. (a) specimen with conducting wire, and (b) specimen embedded in acrylic resin [1].

For cyclic voltammeter, 99.99% pure lead electrodes were made from ~ 9 mm diameter rod and then connected with a plastic isolated copper wire and cast in acrylic resin leaving 0.636 cm^2 exposed area surface.

3.3 Preparation of specimens used for cathode studies

The cathodes were made of aluminum alloy (for current efficiency measurements) or of platinum (for corrosion rate measurements).

The aluminum cathode was a 1.13 cm diameter rod by 1 cm length. The electrical contacts were made by welding plastic isolated copper wire and the piece was cast in

acrylic resin. The exposed area surface was 1 cm^2. Before being introduced into the electrolytic cell, the working surfaces of the anodes and cathodes were ground with SiC abrasive paper (Leco Corporation) down to 600 grit, washed with double distillated water and wiped immediately with tissue paper.

Also, the platinum was cut into small pieces of 1 x 1 x 1 cm then connected with a plastic isolated copper wire and cast in acrylic resin leaving 1 cm^2 exposed area surface.

3.4 Reference electrodes

A reference electrode based mercurous sulphate electrode (MSE, $Hg.Hg_2SO_4/sat.K_2SO_4$, 0.636 versus SHE) and a saturated K_2SO_4 salt bridge were used to keep the reference electrode close to the anode, and avoid any variation of chloride in concentration at the surface.

The conventional reference electrode, a saturated silver chloride electrode $Ag-AgCl/KCl_{sat.}$ (0.202 V versus SHE), was used.

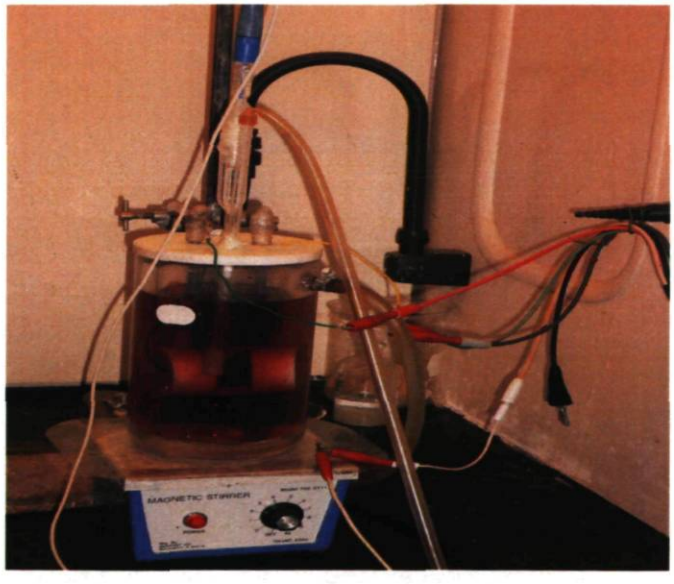

Figure 3.2. Electrolytic cell: one liter double walled beaker with the reference electrode based mercurous sulphate electrode (MSE, $Hg.Hg_2SO_4/sat.K_2SO_4$, 0.636 versus SHE) and a saturated K_2SO_4 salt bridge, working and counter electrode.

3.5 Test media

3.5.1 Preparation of the industrial zinc electrowinning electrolyte

The electrolyte was prepared in laboratory as close as possible in composition to that of the refining industry of Valleyfield, Montreal (Noranda) Quebec, Canada: 60 g/L of Zn^{2+}($ZnSO_4$.7H2O), 180 g/L of H_2SO_4, 8 g/L of Mn^{2+} ($MnSO_4$,H_2O), 250 mg/L of Cl^- and 3 mg/L of Glue. This solution was used to evaluate the performance of the Pb-Ag alloys during and after the polarization at 38°C. Mn^{2+} was added to the electrolyte in some experiments in variable amounts from 4 to 12 mg/L to evaluate its influence. To prepare the test solution in our laboratory, the ions as Zn^{2+}, Mn^{2+} and Cl^- were first added to water, stirred and dissolved completely, then the H_2SO_4 was added to the solution, the Glue was added to the solution only prior to testing to avoid decomposition.

Zinc sulfate ($ZnSO_4 \cdot 7H_2O$), manganese sulfate ($MnSO_4 \cdot H_2O$) from Sigma-Aldrich Fine Chemicals, sodium chloride and sulfuric acid of Merck KGaA were used to prepare the above electrolyte with double distilled water. Gelatin (glue) was the product of BDH Inc. The chemicals meet ACS specifications (except gelatin) and were used as received without further treatment. All stated concentrations of H_2SO_4, Zn^{2+} and Mn^{2+} correspond to the initial concentrations.

3.5.2 Solution for the study of organic additives

Before testing the organic additives, the standard solution was prepared: 60 g/L of Zn^{2+}($ZnSO_4$,$7H_2O$), 180 g/L of H_2SO_4, and 8 g/L of Mn^{2+} ($MnSO_4$,H_2O), with and without 0.01 mg/L of Sb^{3+} or 5 mg/L Ni^{2+}. The chemical products used for the additions of Sb^{3+} and Ni^{2+} are potassium antimonyl tartrate KC_4H_4O.SbO and $NiSO_4$,$6H_2O$ respectively. Then, the following organic additives were added respectively to the standard solution: Malonic acid "MA" (10, 50, 100 and 500 mg/L), Triethyl-benzylammonium chloride "TEBACl" (2 mg/L), Polyethylene glycol 2000 "PEG" (1 mg/L), Perfluoroheptanoic acid "PFHA", and Sodium lauryl sulphate "SLS" (2 mg/L). The effect of these additives has been compared to that of 250 mg/L of Cl^- and 3 mg/L of Glue, generally used in the zinc plant (CEZ) practice at 38°C.

3.5.3 Solution for zinc deposit studies

Zinc is deposited from the electrolyte in presence of glue and antimony, first the standard electrolyte was prepared: 60 g/L of Zn and 180 g/L of H_2SO_4; second the glue (1, 3 and 5 mg/L) was added to this standard electrolyte to test; third the Sb^{3+} (0.0036, 0.0055, 0.01, 0.02, 0.03 mg/L) from potassium antimonyl tartrate $KC_4H_4O.SbO$ was added to the standard electrolyte for testing. Finally, the synergetic effects of glue and antimony were tested in adding the following concentrations of glue and antimony to the standard electrolyte: 1 mg/L of glue with Sb^{3+} = 0.0055, 0.01, 0.02 mg/L, or 3 mg/L of glue with Sb^{3+} = 0.0055, 0.01, 0.02 mg/L.

3.5.4 Solution of 180 g/L H_2SO_4

The acid sulphate solution was used for the hydrogen evolution reaction, and for cyclic voltammetry studies.

3.6 Laboratory simulation of electrolysis and decay

3.6.1. Decay studies

For the corrosion rate measurements: 5 h polarization test at the current density of 50 mA/cm^2 at 38°C was made, then the current was abruptly interrupted and Pb-Ag electrode potential-time curve was recorded during 6 h. Two successive cycles of 5 h galvanostatic polarization, followed by 6 h decay at open circuit potential OCP (reduction or discharge of the anode were carried out). Or 16 h galvanostatic polarization at CD = 50 mA/cm^2 followed by 16 h decay at open circuit potential OCP has been also used.

3.6.2. Electrodeposition

Galvanostatic set-up at current density CD= 500 A/m^2 for 2 h and 24 h deposition time at 38°C at a rotation rate of 60 rpm was used for zinc deposit.

3.7 Electrochemical measurements for corrosion studies

3.7.1 Potentiodynamic polarization studies

The potentiodynamic polarization technique is used to evaluate the corrosion rate of the studied Pb-Ag alloys in the zinc electrolyte with or without $MnSO_4$ at 38°C. The standard ASTM G5 [2] was used to carry out potentiodynamic test and the potentiodynamic curves were traced at 0.166 mV/s scanning rate over a potential range of 50 mV (cathodic polarization -25 mV vs corrosion potential). The reproducibility of the potential values was of the order of ±3~5 % and the reproducibility of the corrosion current values was of the order of ± 4~6 % by potentiodynamic measurements. All the experiments were repeated for three times.

3.7.2 Cyclic voltammetry studies

Cyclic voltammetry was used to investigate the electrochemical behaviour of redox peaks of Pb-Ag alloys. The standard ASTM-61 [3] was used to carry out cyclic potentiodynamic polarization. The cyclic potentiodynamic curves were traced at ranges of 3, 20, 60, 80, 100 and 300 mV/s scanning rate. For Pb-Ag alloy electrodes, the scanning potential range was from -300 to 1800 mV vs OCP. All potentials are given with respect to SHE reference electrode.

3.7.3 Electrochemical noise measurements

The electrochemical noise technique was used to characterize the electrochemical reaction of the lead anode and the influence of silver on the reduction and oxidation reactions on the surface of the lead anode. Also the corrosion behaviour of the Pb-Ag alloys was evaluated by determining the noise resistance (R_n) and the slope and noise intensity of potential, current and ratio of PSD plots.

Electrochemical noise measurements were performed in zinc electrowinning bath for two nominally identical working electrodes (WE) pre-polarized during 24 h at constant 50 mA/cm^2 anodic current density. A set-up of NE in zero resistance ammeter (ZRA) mode was used to obtain information both in potential and current noise. The

electrochemical current noise was measured as the galvanic coupling current between two working electrodes (WE) kept at the same potential. The coupled potential was measured via a reference electrode (Ref.), a saturated silver chloride electrode $Ag,AgCl/KCl_{sat.}$ (0.202 V vs. SHE). Each set of EN records, containing 1024 data points, recorded with a data-sampling rate of 0.1 s at a scan rate of f_s = 10 Hz. A GAMRY® PC4/300 potentiostat was used to log potential and current values. EN experiments and data treatment were conducted using GAMRY ESA400 software for 16 hours immersion period. The data were recorded immediately after the immersion of the working electrodes in the solution. At least, three experiments were made for each specimen tested in this work. All the potential values are given versus standard hydrogen electrode SHE (± 10 mV).

3.7.4 Impedance measurements

Electrochemical impedance was used to determine the involved corrosion mechanism by analyzing the form of plotted Nyquist diagrams. Impedance test allows also to characterize the corrosion behaviour of the studied Pb-Ag alloys by following the evolution of the double layer capacity and charge transfer resistance with the immersion time.

The experimental set-up uses an EG&G PARSTAT 2263 potentiostat/galvanostat controlled by an IBM computer. The electrochemical impedance measurements were carried out using PowerSINE in Electrochemical Power Suite of Advanced Measurement Technology, Inc. over the frequency range from 100 kHz to 100 mHz. The amplitude of the sinusoidal was 10 mV (rms). The reproducibility of the polarization resistance values of impedance during potential decay after 5 h galvanostatic polarization was of the order of ±4~6 %. All the experiments were repeated for three times.

The electrochemical impedance measurements were carried out using a Solartron 1255 high frequency response analyzer and a Solartron 1286 electrochemical interface over the frequency range from 10 kHz to 0.5 Hz. The amplitude of the sinusoidal signals was 10 mV (rms). The software Zplot was used for acquisition of the impedance data.

The Nyquist plots of the impedance data were analyzed using Zview software mainly to calculate the charge transfer resistance during the corrosion process.

3.8 Microstructural analyses

SEM analyses were conducted using JEOL JSM-25s III model Scanning Electron Microscope equipped with a TN 5700 model energy dispersive X-ray analyzer (EDX) to characterize corrosion products. The microstructure of the anode surface was characterized using optical microscope (ZEISS Model). Before analyses, the surface of the anodes was electrochemically polished during 2 min at 100 mA/cm^2 in an etching solution composed of 315 ml of acetic acid, 32 g of sodium acetate and 108 ml of H_2O. After electropolishing, 3:1 acetic acid – H_2O_2 (30%) solution was used to remove the black surface film, then the surface was cleaned with ethanol and air dried.

The chemical composition of the laminated Pb-Ag anodes was analyzed by fluorescence X.

3.9 References

[1] **Amira, S.**, Influence of Microstructure on Corrosion Behaviour and Mechanical Properties of Some Creep Resistant Magnesium Alloys, Ph.D thesis, Laval University, Quebec, Canada, 2008, pp. 177-178.

[2] **ASTM Publication, ASTM G5-94,** Standard Reference Test Method for Making Potentiostatic and Potentiodynamic Anodic Polarization Measurements, Philadelphia, PA, **2001**, vol. 03.02, pp. 54-56.

[3] **ASTM Publication, ASTM G61-86**, Standard Test Method for Conducting Cyclic Potentiodynamic Polarization Measurements for Localized Corrosion Susceptibility of Iron-, Nickel, or Cobalt-Base Alloys. PA, 03.02, 2001, pp. 231-235.

PART 1

Influence of Ag content on the performance of Pb anodes during polarization and decay

(Chapters 4, 5, 6 and 7)

CHAPTER 4

Cyclic voltammetric studies of the behaviour of lead-silver anodes in zinc electrolytes

Cyclic voltammetric studies of the behaviour of lead-silver anodes in zinc electrolytes

W. Zhang[1*], S. Jin[1], E. Ghali[1], G. Houlachi[2]

[1]Department of Mining, Metallurgy and Material Engineering

Laval University, Ste-Foy, Quebec, Canada, G1K 7P4

Wei.Zhang.1@ulaval.ca*

[2]LTE, Hydro-Quebec

600 Avenue de la Mortagne, C.P. 900

Shawinigan, QC, Canada, G9N 7N5

This paper was accepted subject to revision by Journal of Materials Engineering and Performance, ASM, U.S.A, 2007.

4.1 Abstract

Cyclic voltammetry (CV) for lead-silver anodes were performed in an acid zinc sulphate solution with or without Mn^{2+} at 38°C. It has been found that the most redox peaks observed at the lowest sweep rate of 3 mV/s in the sulphate solution could be characterized by the Nernst equation. Bubbling argon into the zinc electrolyte and increasing the potential sweep rates from 3 mV/s to 300 mV/s did not change the shape of the CV diagrams. It was also found that 0.7% silver as alloying element had an important influence on the reactions of Pb-Ag anodes in the zinc electrolyte. Lead-silver alloys were oxidized more easily in sulphuric acid than in the examined zinc electrolyte. The addition of $MnSO_4$ to the zinc electrolyte decreased the numbers of the redox peaks on the curve of CV for lead-silver anode in zinc electrolyte.

Keywords: lead-silver alloy anodes, zinc electrolyte, cyclic voltammetry.

4.2 Introduction

Insoluble anodes are widely used in industrial hydrometallurgical processes. A useful anode material must meet three requirements: electrical conductivity, electrocatalysis and stability. Most hydrometallurgical processes use sulphuric acid solutions. The main anodic reaction is oxygen evolution by decomposition of water. In these solutions, the predominant anode materials have been different lead alloys as anode. However, pure lead has many disadvantages: higher overpotential and more corrosion products. Also, pure lead is a weak material and it tends to creep and warp during use. Therefore, lead must be alloyed in order to improve at least its mechanical properties [1].

Small amounts of Ag (0.7-1.0%) alloyed with lead decreases the oxygen overvoltage and increases the corrosion resistance of material. A well established custom in many electrolytic zinc plants is to use Pb-Ag alloys containing 0.7-1.0% Ag as the anode material [2].

Adding $MnSO_4$ to the zinc electrolyte results in the formation of MnO_2 protective film on the surface of Pb electrode during electrolysis. This helps to minimize the Pb content of the zinc deposits [3].

Cyclic voltammetry has been widely used to investigate the electrochemical behaviour of metal materials. However, the electrochemical behaviour of lead-silver electrodes in aqueous sulphuric acid solution has rarely been investigated using cyclic voltammetry as reported by many researchers [4-6]. For example, Y. Yamamoto et al. [4] have investigated the electrochemical behaviour of pure lead electrode in aqueous sulphuric acid solution and they have studied almost all the peaks of the lead electrodes in the whole potential region of the positive and negative electrodes. They found that several redox peaks appeared concerning the active materials of lead electrode were: $Pb \rightarrow PbSO_4$, $PbO \rightarrow \alpha\text{-}PbO_2$, $PbSO_4 \rightarrow \beta\text{-}PbO_2$, $H_2O \rightarrow O_2$, $PbO_2 \rightarrow PbSO_4$, $PbO \rightarrow Pb$, $PbSO_4 \rightarrow Pb$.

Pavlov et al. [7, 8] suggested that the oxidation of $PbSO_4$ to PbO_2 occurs when the electrode potential is sufficiently high to allow the oxidation of $PbSO_4$. The $PbSO_4$ crystals dissolve as Pb^{2+} and SO_4^{2-} into the solution in the pores of the lead anodic film. The Pb^{2+} ions diffuse to the nearest reaction site where they are oxidised to Pb^{4+} ions. As the Pb^{4+} ions are thermodynamically unstable in solution, they combine with water to form $Pb(OH)_4$ which then is dehydrated to form $PbO(OH)_2$ and finally transferred to PbO_2.

Ijomah [9] observed that the anodic curves (essentially flat within the passive region) failed to confirm the presence of some compounds apparently reduced in the cathodic sweep. Consequently, the anodic curve was fully expanded ten times over the passive range in order to identify any current peaks previously missed on the higher scale and to permit meaningful comparison between different alloys. In the expanded plot, he also found that the current actually wavered in the passive region and some peaks or humps were observed corresponding to formation of lead monoxide (PbO), and lead dioxide ($\alpha\text{-}PbO_2$) beneath the lead sulphate film.

Czerwinski et al. [10] also observed that the redox reactions occurring on the Pb electrode in sulphuric acid solutions are complex and depend on many variables, like the concentration of acid, the sweep rate in CV experiments and temperature. When the lead dioxide, formed at high position potentials, is reduced ($PbO_2 \rightarrow PbSO_4$), a large increase of molar volume is expected and, as a result, the surface cracks, exposing the bare metal.

The surfaces of bare metal are then oxidized. They also found that the change of a sweep rate does not influence to a great extent the shape of CVs at low concentrations of sulphuric acid.

Understanding the electrochemical behaviour of pure lead anode in sulphuric acid should help to improve the performance of Pb-Ag anodes in electrowinning electrolytes.

The cyclic voltammetry has been used to investigate the mechanism of the reactions taking place on Pb-Ag alloy anodes in a sulphuric acid and acidic zinc sulphate electrolytes; it has been shown that with increasing anodic polarization, firstly an insulating film of $PbSO_4$, then conductive layers of PbO_2 are successively formed on the electrode [11].

In this paper we attempt to interpret the peaks appearing on the CV diagrams of lead-silver alloy electrodes in the whole scanned potential region in zinc electrolyte. The main purpose of this work is to characterize each current peak to a corresponding reaction and to examine the influence of various conditions on the position and the heights of these peaks.

4.3 Experimental

4.3.1 Materials and sample preparation

Four types of solution were used in the work, 1) 180 g/dm^2 of H_2SO_4; 2) 60 g/dm^3 of Zn^{2+}($ZnSO_4.7H_2O$), 180 g/dm^3 of H_2SO_4; 3) 60 g/dm^3 of Zn^{2+}, 180 g/dm^3 of H_2SO_4, 250 mg/dm^3 of Cl^- and 3 mg/dm^3 of Glue (Gelatin or glue (G) is an animal protein that consists of a complicated mixture of polypeptides used as levelling agent [12]), 4) 60 g/dm^3 of Zn^{2+}, 180 g/dm^3 of H_2SO_4, 8 g/dm^3 of Mn^{2+}, 250 mg/dm^3 of Cl^- and 3 mg/dm^3 of Glue heated by a flow of thermostated water in the double wall cell (38 ± 0.5°C).

Zinc sulfate ($ZnSO_4 \cdot 7H_2O$), manganese sulfate ($MnSO_4 \cdot H_2O$) from Sigma-Aldrich Fine Chemicals, sodium chloride and sulfuric acid of Merck KGaA were used to prepare the supporting electrolyte with double distilled water. Gelatin (glue) was product of BDH Inc. The chemicals meet ACS specifications (except gelatin) and were used as received

without further treatment. All concentrations of H_2SO_4 and Zn^{2+} stated in this paper are initial concentrations.

The lead-silver anode tested in this work was a laminated Pb-0.0.69%Ag alloys (RSR, Texas, USA). The original surface was removed and only the bulk was used. The cathodes were made of platinum. The Pb-Ag alloy plates were cut into small pieces of 1 × 1 × 1 cm then connected with a plastic isolated copper wire and cast in acrylic resin. The exposed area surface was 1 cm^2, 99.99% pure lead electrodes were made of a 9 mm diameter rod leaving a working surface of 0.636 cm^2. Before being introduced into the electrolytic cell, these working surfaces of the anodes and cathodes were ground with SiC abrasive paper (Leco Corporation) down to 600 grit, washed with double distillated water and wiped immediately with tissue paper.

4.3.2 Experimental setup

The electrolytic cell comprised a one liter double walled beaker containing 800 ml of electrolyte heated by a flow of thermostated water in the double wall (38 ± 0.5°C). The working electrode and the counter electrode were mounted in suitable Teflon made holder and the distance between them was fixed at 2 centimeters. The reference electrode was mercurous sulfate electrode (MSE): Hg, Hg_2SO_4/sat.K_2SO_4 (0.636 V vs. SHE). A saturated K_2SO_4 salt bridge was used to keep the reference electrode close to the cathode. The experimental setup was an EG&G PARSTAT 2263 potentiostat/galvanostat controlled by an IBM computer.

The standard ASTM-61 [13] was used to carry out cyclic potentiodynamic polarization. The cyclic potentiodynamic were traced at 100 mV/s scanning rate. For Pb-Ag alloy electrodes, the range was from -300 to 1800 mV vs OCP. All potentials are given with respect to SHE reference electrode. The reproducibility of the potential values was of the order of ±10-15 mV and the reproducibility of the corrosion current values was also of the order of ±10-15%. All the experiments were repeated for three times.

4.4 Results and discussion

4.4.1 Lead-silver alloy and pure lead in a sulphuric acid

Figure 4.1 shows a cyclic voltammogram of the lead-silver electrode in 180 g dm^{-3} sulphuric acid solution. The potential region investigated ranged from -0.7 V to 2.4 V. There are eight redox peaks on the curve. The electrochemical reactions corresponding to each peak are given as follows based on literature. During the anodic sweep, three oxidation peaks were observed. The oxidation peak I should correspond to reaction (4.1):

$$Pb + SO_4^{2-} \rightarrow PbSO_4 + 2e \qquad (4.1)$$

This reaction leads to the formation of a non - conducting lead sulphate layer, i.e., the passivation of the anode.

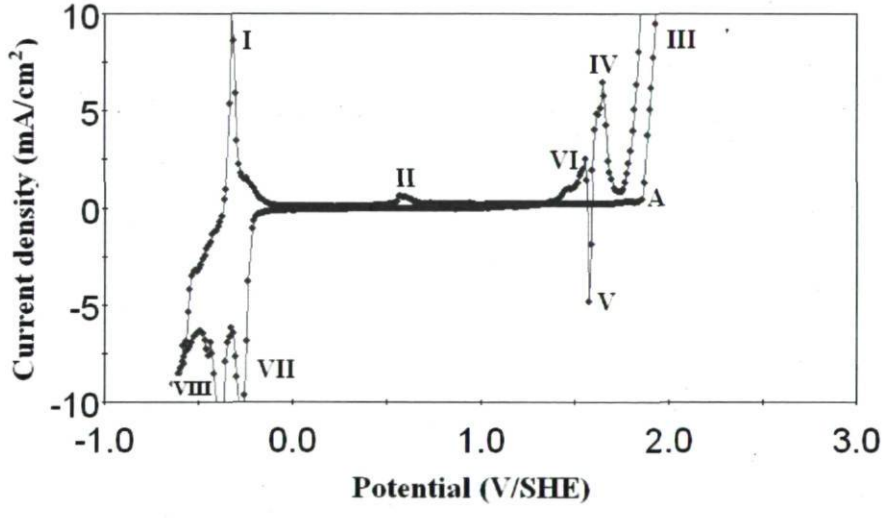

Figure 4.1 Cyclic current-potential curve of the lead-silver alloy anode in a sulphuric acid solution containing 180 g dm^{-3} H_2SO_4 at a scan rate of 3 mV s^{-1}.

The concentration of SO_4^{2-} was considered instead of the activity of SO_4^{2-} since there is no precise data available about the SO_4^{2-} activity. The corresponding Nernst equation is:

$E = E^o - (RT/2F) \ln SO_4^{2-} = -0.356 - 0.0308 \log SO_4^{2-} = - 0.356 - 0.0308 \log 2.25 =$

- 0.367 V [14].

This agrees well with the potential on almost halfway between peak I and its corresponding reduction peak VIII. These peaks can therefore be reliably assigned to anodic formation of lead sulphate by equation (4.1) and its corresponding reduction back to lead.

Following this peak the current drops to a very low value indicative of the attainment of passivity and remained essentially constant at this residual value for a considerable range of potentials (i.e., the passivation region) before rising again owing to the formation of the silver sulfate. Jones and Thirsk [15] stated that Ag_2SO_4 is formed at the this plateau of the curve of CV in sulfuric acid solution and that the Ag_2SO_4 crystals grew mainly parallel to the silver additive surface. So the peak II can correspond to the following reaction:

$$2Ag + SO_4^{2-} = Ag_2SO_4 + 2e \qquad (4.2)$$

The corresponding Nernst equation:

$$E = E^O + RT/2F \ln(Ag^+) + (RT/2F) \ln \alpha_{SO4}^{2-} = 0.62 \text{ V} \quad [15]$$

Deutscher et al. [16] found that region A corresponds to the nucleation and growth of β-PbO_2 from $PbSO_4$.

$$PbSO_4 + 2H_2O \rightarrow PbO_2 + SO_4^{2-} + 4H^+ + 2e \qquad (4.3)$$

The corresponding Nernst equation:

$$E = E^o + (RT/2F) \ln(H^+)^4(SO_4^{2-})^2 = 1.712 - 0.1234 \text{ pH} + 0.0308 \log SO_4^{2-} = 1.794 \text{ V}.$$

The molar volume of β-PbO_2 (25 cm^3 mol^{-1}) is much less than the molar volume of $PbSO_4$ (48 cm^3 mol^{-1}), so gaps are created in outer $PbSO_4$ layer and bare metal is exposed to the acidic solution [16].

The peak III appeared from ~1.8 V and was the highest peak among all the peaks; it was the oxygen evolution on the β-PbO_2 which is a good conductor.

$$2H_2O \rightarrow O_2 + 4H^+ + 4e \qquad (4.4)$$

The corresponding Nernst equation:

$$E = E^o + (RT/4F) \ln(H^+)^4 = 1.23 - 0.0617 \text{ pH} = 1.265 \text{ V}.$$

It is clear that the overpotential of oxygen is very high.

During the reverse sweep, five redox peaks were obtained. When the potential scanned from peak III, the current dropped sharply, the expected reason is that lead dioxide was reduced to sulphate lead, $PbO_2 \rightarrow PbSO_4$. Since the molar volume of $PbSO_4$ is much higher than that of PbO_2, this change in the molar dimensions of the surface layer generates cracks on the electrode surface and the exposure of the metallic lead could then take place: $Pb \rightarrow PbSO_4$. Yamamoto et al. [4] characterized this peak IV with the following reactions:

$$PbO_2 + SO_4^{2-} + 2e + 4H^+ \rightarrow PbSO_4 + 2H_2O \qquad (4.5)$$

And oxidation reaction (4.1).

The left PbO_2 after peak IV continued to form $PbSO_4$ (Equation 4.5) and this introduces peak V.

It is very plausible that the left or new bare lead is oxidized to $PbSO_4$ for peak VI. However, Danel et al. [17] stated that the Peak VI is relative to the oxidation of Pb→PbO #at the potential ~1.5 vs. SHE with overpotential more than 1.3 V.

$$Pb + H_2O \rightarrow PbO + 2e + 2H^+ \qquad (4.6)$$

Finally, the peak VII corresponds to the reduction reaction $PbO \rightarrow Pb$ and the peak VIII corresponds to the reduction reaction: $PbSO_4 \rightarrow Pb$ [4].

The passivity of lead in acid zinc sulphuric electrolyte was primarily due to the presence of a non-conducting lead sulphate film on the metal surface, apparently at a critical surface supersaturation of dissolving Pb^{2+} ions. Two theories, namely, 'solid state' and 'solution-precipitation' had so far been used to explain the phenomenon. In the solid-state mechanism, $PbSO_4$ nucleation was believed to occur directly on the metal surface at a certain critical potential, following by two- or three- dimensional growth until the surface is fully covered. In the solution-precipitation mechanism, however, nucleation of $PbSO_4$ was thought to occur in the solution, followed by its precipitation onto the metal surface. Here, the growth is always three-dimensional, and passivation is by a physical blocking action. The presence of intermediate compounds (i.e. $PbO.PbSO_4$, PbO, and α-PbO_2) beneath the lead sulphate film had been confirmed by Ijomah [9]. It

was believed that a pH gradient existed in the lead sulphate film due to inhibited diffusion through the dense corrosion layer. No anodic peak was recorded for β-PbO_2. The compound was believed to occur simultaneously with oxygen evolution [9].

The cyclic voltammogram of the pure lead electrode in180 g dm^{-3} sulphuric acid solution are represented in Figure 4.2.

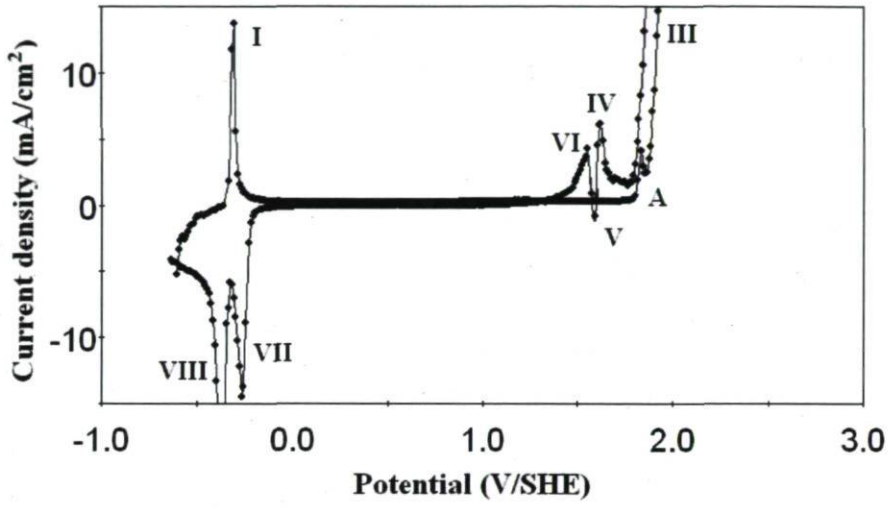

Figure 4.2 Cyclic current-potential curve of the pure lead anode in a sulphuric acid solution containing 180 g dm^{-3} H_2SO_4 at a scan rate of 3 mV s^{-1}.

In this curve, the same peaks as Figure 4.1 were found and redox peaks correspond to the same redox reaction, except absence of peak II. It means that adding 0.7% Ag did not much change the shape of the cyclovoltammograms. However, the current of peak I ($Pb \rightarrow PbSO_4$) of Figure 4.2 is almost 40% higher than that of peak I ($Pb \rightarrow PbSO_4$) of Figure 4.1. As reported by Mahato and Tiedemann [18], the value of peak I can be used to evaluate the corrosion rate of electrode, it means that a higher value of the peak corresponds to higher corrosion rate of the electrode. So the pure lead corrodes more readily than the lead-silver anode in the sulphuric acid solution.

4.4.2 Lead-silver alloy in zinc electrolyte with or without Mn^{2+}

The cyclic voltammogram of the lead-silver alloy electrode in zinc electrolyte without Mn^{2+} is represented in Figure 4.3.

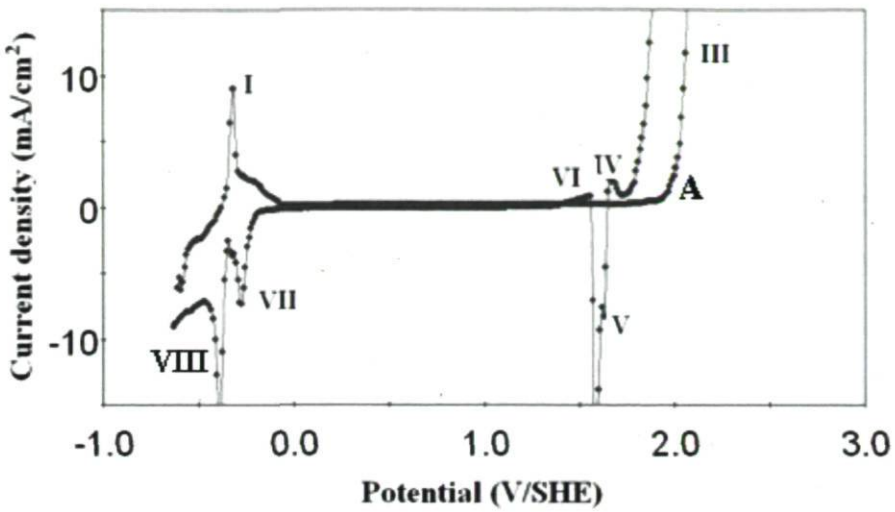

Figure 4.3 Cyclic current-potential curve of the lead-silver alloy anode in zinc electrolyte containing 180 g dm^{-3} H_2SO_4, and 60 g dm^{-3} Zn^{2+}, 250 mg/dm^3 of Cl^- and 3 mg/dm^3 of glue, at a scan rate of 3 mV s^{-1}.

In this curve, seven peaks appeared concerning the lead-silver anode in zinc electrolyte without Mn^{2+}. However, the Ag/Ag^+ peak disappeared since addition of $ZnSO_4$ and glue to the zinc electrolyte suppressed the presence of this peak. The oxidation peak I corresponds to oxidation reaction (4.1).

Region A corresponds to the nucleation and growth of β-PbO_2 from $PbSO_4$ as oxidation reaction (4.3) [18].

The peak III was the highest peak among all the peaks; it corresponds to the oxygen evolution (4.4).

The irregular oxidation peak IV appeared at the outset in reversing the potential scan from a region of the oxygen evolution to the starting potential. This oxidation peak corresponds to bare metal oxidized to sulphate lead (4.5).

The peak V relative to the reduction of PbO_2 into $PbSO_4$; the peak VI should correspond to peak VI in Figure 4.1 that has been explained earlier corresponding to reactions (4.1) and (4.6).

Finally, the peak VII corresponded to the reduction reaction PbO→ Pb and the peak VIII corresponded to the reduction reaction: $PbSO_4$→ Pb [4].

A cyclic voltammogram for the lead-silver alloy anode in the zinc electrolyte with Mn^{2+} is shown in Figure 4.4. There are six redox peaks on the curve.

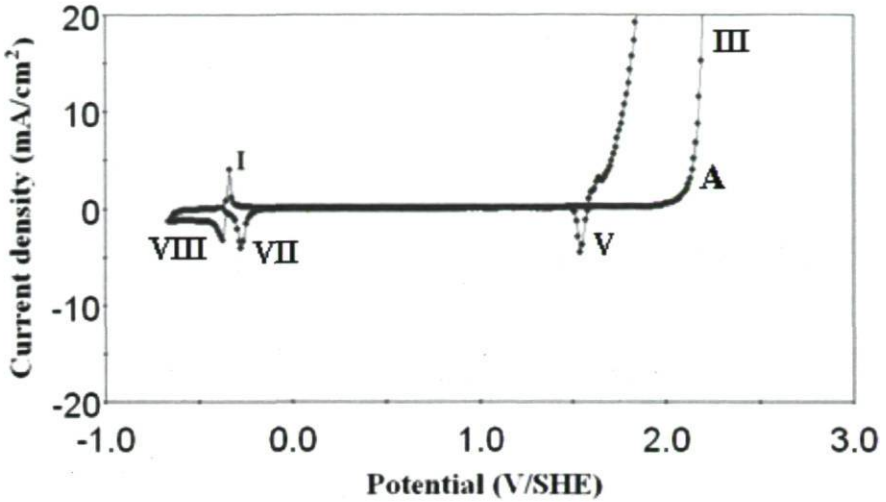

Figure 4.4 Cyclovoltammogram of the lead-silver alloy anode in zinc electrolyte containing 180 g dm^{-3} H_2SO_4, 60 g dm^{-3} Zn^{2+} and 8 g dm^{-3} Mn^{2+}, 250 mg/dm^3 of Cl^- and 3 mg/dm^3 of glue at a scan rate of 3 mV s^{-1}.

As compared to Figure 4.3, two oxidation peaks IV $Pb \rightarrow PbSO_4$ (4.1) and peak VI $Pb \rightarrow PbO$ (4.6) have disappeared. As observing from the experiment, the red product of MnO_4^- and the evolution of oxygen appeared at the same time, so the peak III corresponds to the reactions 4.4 and 4.7, and the standard potential of reaction 4.7 is: 1.52 V/SHE [19]:

$$MnSO_4 + 4H_2O - 5e = MnO_4^- + H_2SO_4 + 6H^+ \quad (4.7)$$

The presense of permanganate ion can give rise to the formation of MnO_2:

$$3MnSO_4 + 2HMnO_4 + 2H_2O = 5MnO_2 + 3H_2SO_4 \quad (4.8)$$

So a dense non-conductive MnO_2 film formed on the surface of anode, the well adherent oxide film MnO_2 increased the thickness and density of oxide layer (PbO_2-MnO_2) which makes the transition of Pb^{2+} ions to the solution difficult and protect the lead anode from corrosion. Then, the Pb contamination of Zn deposit can be reduced because of the Mn^{2+} addition to the zinc electrolyte.

The other redox peaks could be explained as follows: oxidation peak I, $Pb \rightarrow PbSO_4$; reduction peak V, $PbO_2 \rightarrow PbSO_4$, reduction peak VII, $PbO \rightarrow Pb$, and reduction peak VIII, $PbSO_4 \rightarrow Pb$. It was found that the four peaks values were lower than that of the same reaction in Figure 4.3, it means that less Pb is oxidised to $PbSO_4$ compared to that in Figure 4.3, so adding Mn^{2+} to the zinc electrolyte inhibits the corrosion of lead anode.

Figure 4.5 shows the shape change of the cyclic voltammograms of the lead-silver electrode with various sweep rates:

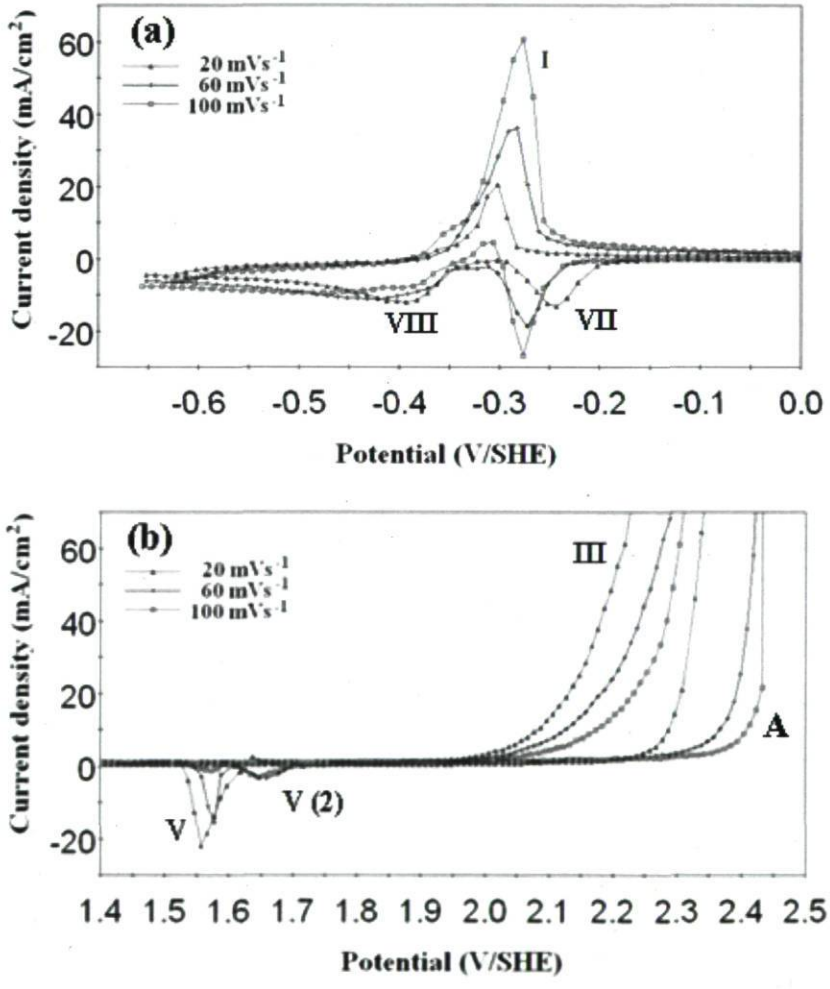

Figure 4.5 Cyclic current-potential curve of the lead-silver alloy anode in zinc electrolyte containing 180 g dm^{-3} H_2SO_4, 60 g dm^{-3} Zn^{2+}, 250 mg/dm^3 of Cl^- and 3 mg/dm^3 of glue, at a scan rate of 20, 60, 100 mVs^{-1} (a) Polarization range: -0.7 to 0 V/SHE; (b) Polarization range: 1.4 to 2.5 V/SHE.

In Figure 4.5, most of redox peaks are the same as those in Figure 4.3 and it was found from Figure 4.5 (a) that the height of oxidation peak I with the sweep rate increase. While in Figure 4.5 (b) at the sweep rate of 60 and 100 mV/s that reduction peak V (2) could be obtained, and this reduction peak was not observed in Figure 4.3 and Figure 4.5 (b) at the sweep rate of 20 mV/s. The peak V (2) is possibly relative to the reduction of PbO_2 into PbO.

Also, the lead alloy anode was in zinc electrolyte containing 180 g dm^{-3} H_2SO_4, 60 g dm^{-3} Zn^{2+}, 250 mg/dm^3 of Cl^- and 3 mg/dm^3 of glue at the sweep rate of 3 mVs^{-1} with bubbling argon only before cyclic voltammetry experiments (5.5 cm^3/s for 800 ml electrolyte). It is observed that bubbling argon into the zinc electrolyte did not change the shape and number of redox peaks on the curve of CV; the reason is that bubbling argon resulted in absence of oxygen in the zinc electrolyte, oxygen having a little influence on oxygen evolution but do not have any influence on other redox equations. Also, adding argon to the zinc electrolyte resulted in stirring the solution, improving the diffusion of ions, and that can influence the effect on the redox equations.

However, when the lead alloy anode was in zinc electrolyte containing 180 g dm^{-3} H_2SO_4, 60 g dm^{-3} Zn^{2+}, 250 mg/dm^3 of Cl^- and 3 mg/dm^3 of glue at the sweep rate of 3 mVs^{-1} with oxygen bubbling (volume of 5.5 cm^3/s for 800 ml electrolyte) before experiment, some redox peaks can be obtaine (Figure 4.6). Comparing the redox peaks of Figures 4.3 and 4.6, a reduction peak B in Figure 4.6 only occurred on the curve. This reduction peak B can correspond to: $O_2 + 4H^+ + 4e \rightarrow 2H_2O$. Also, it was found that the oxidtion peaks I, IV, VI of Figure 4.6 are higher than that of Figure 4.3, while the reduction peak V of Figure 4.6 is lower than that of Figure 4.3, it means that the oxide agent O_2 aerated into the zinc electrolyte is convenient to oxidation peak but inhibits the occurrence of electrochemical reduction peak.

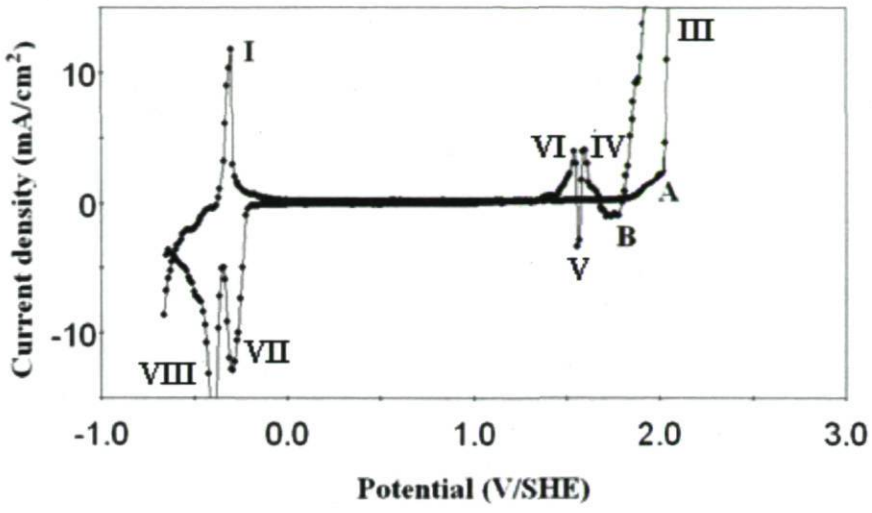

Figure 4.6 Cyclic current-potential curve of the lead-silver alloy anode in zinc electrolyte containing 180 g dm^{-3} H_2SO_4, and 60 g dm^{-3} Zn^{2+}, 250 mg/dm^3 of Cl^- and 3 mg/dm^3 of glue with aerated-oxygen, at a scan rate of 3 mV s^{-1}.

In practice, the electrolyte is always circulated with a certain speed, and it is important to simulate the influence of agitation of the electrolyte on the peaks of redox of lead-silver alloy anodes. Magnetic agitation was carried out by a stirrer (4 cm long 1 cm diameter) at 412 rpm and the obtained diagram is shown in Figure 4.7.

If compared to Figure 4.6 without agitation, the peak B (diffusion controlled peak of dissolved oxygen) disappeared, since agitation accelerated the diffusion of the solution with dissolved oxygen to the interface. Also, it was found that the current value of oxidation peak I of Figure 4.7 corresponding to the quantity of lead ions at the interface was lower than that without agitation of Figure 4.6. The value of reduction peak V of Figure 4.7 was higher than that of Figure 6, since agitation favoured the formation of lead sulphate by diffusion of the sulphuric acid electrolyte to the interface.

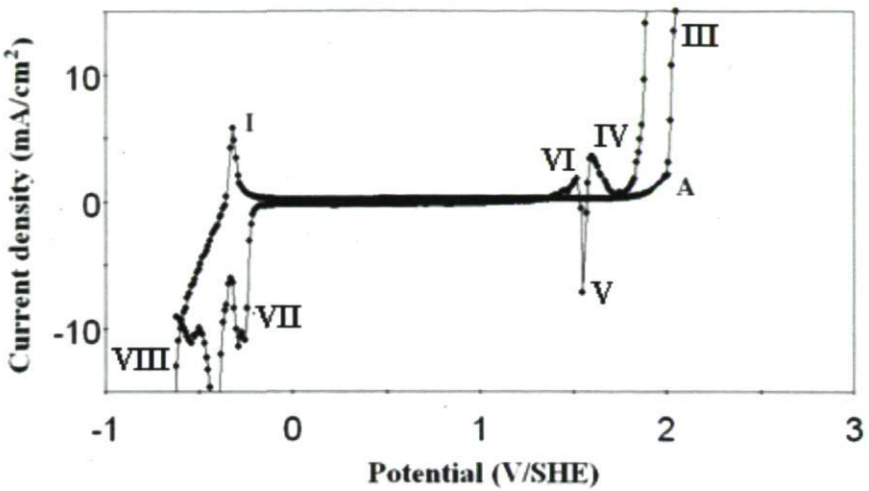

Figure 4.7 Cyclic current-potential curve of the lead-silver alloy anode in zinc electrolyte containing 180 g dm^{-3} H_2SO_4, and 60 g dm^{-3} Zn^{2+}, 250 mg/dm^3 of Cl^- and 3 mg/dm^3 of glue with aerated-oxygen and agitation, at a scan rate of 3 mV s^{-1}.

Figures 4.8 and 4.9 show the effects of the high sweep rate of 300 mVs^{-1} effects on the redox peaks of lead alloy anode in the zinc electrolyte containing 180 g dm^{-3} H_2SO_4, and 60 g dm^{-3} Zn^{2+}.

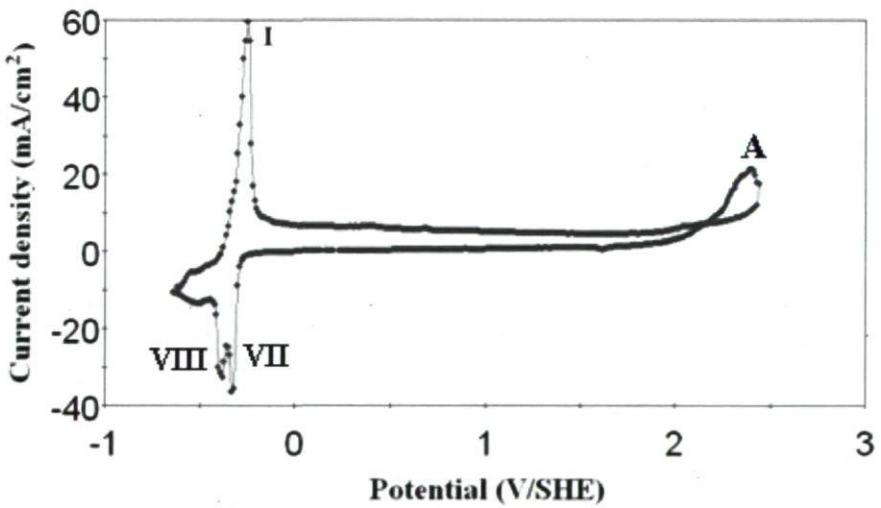

Figure 4.8 Cyclic current-potential curve of the pure lead anode in the zinc electrolyte containing 180 g dm^{-3} H_2SO_4, 60 g dm^{-3} Zn^{2+}, 250 mg/dm^3 of Cl^- and 3 mg/dm^3 of glue at a scan rate of 300 mV s^{-1}.

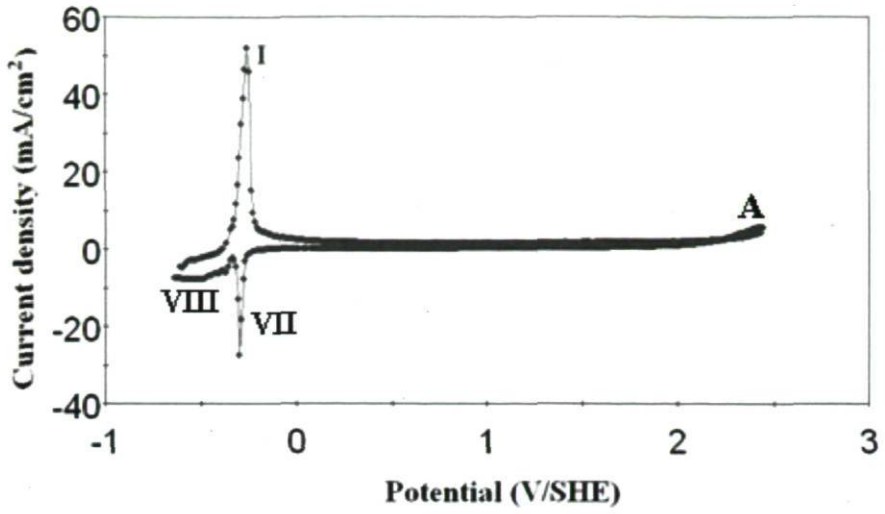

Figure 4.9 Cyclic current-potential curve of the lead-silver alloy anode in the zinc electrolyte containing 180 g dm^{-3} H_2SO_4, 60 g dm^{-3} Zn^{2+}, 250 mg/dm^3 of Cl^- and 3 mg/dm^3 of glue at a scan rate of 300 mV s^{-1}.

In Figures 4.8 and 4.9, oxygen evolution peak could not be obtained, but the oxidation peak of $PbSO_4 \rightarrow PbO_2$ (A) has been found. Also Yamamoto et al. [23] observed that a peak current ascribed to β-PbO_2 formation was clearly detected by cyclic voltammetry. It is then suggested (Figure 4.5) that: at sweep rate from 20 mV/s to100 mV/s, the oxygen evolution peak also overlaps the reaction peak of $PbSO_4 \rightarrow PbO_2$. Comparing Figure 4.8 with Figure 4.9, the current of peak I ($Pb \rightarrow PbSO_4$) of Figure 4.8 is more 10 mA/cm^2 than that of Figure 4.9, also the current of peak A ($PbSO_4 \rightarrow PbO_2$) of Figure 4.8 is more 14 mA/cm^2 than that of peak III of Figure 4.9.

The sweep rates of Figures 4.3, 4.5, 4.8 and 4.9 were increased from 3 mV/s to 300 mV/s, the experiments were performed in the zinc electrolyte containing a sulphuric acid concentration of 1.84 M H_2SO_4. It can be seen from Figures 4.3 to 4.5 that the change of the sweep rates did not influence to a great extent the shape of CV curves. All the cyclic voltammetric curves showed the redox reactions of lead. However in Figures 4.8 and 4.9, different results were obtained; when the sweep rate of cyclic voltammetry reached 300 mV/s, the highest current peak III observed at lower scan rates can not appear, so the oxidation reaction: $O_2 + 4H^+ + 4e \rightarrow 2H_2O$ was disappeared. No visible oxygen evolution was observed on the lead electrode during the cyclic experiments.

It is observed that the height of oxidation peak I increased with the increase of sweep rate but that of the reduction peak V decreased with the same rate in Figure 4.5 (b), this phenomenon was also found by Czerwinski et al. [10]. The reason may be that the higher sweep rate can lead to accelerate oxidation reaction.

From the above results, it is found that CV technique is useful to understand the oxidation and reduction reaction of lead-silver and pure lead in acid solution. Comparing Figure 4.3 with Figure 4.4, following comments could be obtained: the addition of $MnSO_4$ to the zinc electrolyte caused the disappearance of two oxidation peaks of the curve for lead-silver electrode. The reason should be that $MnSO_4$ plays significant role in the anodic process, where it is intimately involved in the formation of oxide layers on Pb-Ag anodes and thus helps to minimize the Pb content of zinc deposits [3].

Comparing Figure 4.1 with Figure 4.2, the current value of peak I ($Pb \rightarrow PbSO_4$) of Figure 4.2 is bigger than that of peak I ($Pb \rightarrow PbSO_4$) of Figure 4.1; it means that pure lead is easier to corrosion than lead-silver anode in zinc electrolyte. Comparing Figure 4.8 with Figure 4.9, the current of peak A ($PbSO_4 \rightarrow PbO_2$) of Figure 4.9 is less than that of peak A ($PbSO_4 \rightarrow PbO_2$) of Figure 4.8, it means that pure lead anode is easier to form PbO_2 layer than lead-silver in zinc electrolyte; so it is found that silver played significant role in the reaction of anodes in zinc electrolyte by CV. The above results are suited for the idea of Umetsu et al [20]: the increase of silver in the alloys results in suppression of anodic oxidation of the materials, decrease, in the anodic potential, the formation of dense oxide layer closely adhering to the electrode and the appearance of ß-PbO_2 in the anodic oxide layer. Also, Pavlov and Rogachev [21] thought that Ag enhances the formation of β-PbO_2 at the oxide solution interface and in the zone close to the metal.

The molar volume of the β-PbO_2 is 25 cm^3mol^{-1}, while the molar volume of the $PbSO_4$ is 48 cm^3mol^{-1}. When the β-PbO_2 was transited to the $PbSO_4$ or the $PbSO_4$ was transited to the PbO_2, these transitions can result in a large increase or decrease of the molar volume of the surface layer, respectively. These changes might cause cracks in the surface layer of lead-silver alloy electrodes, thus exposing a bare metal surface, which is instantly missing to β-PbO_2 at the high anodic potential. As β-PbO_2 is a good conductor the oxygen evolves on surface of β-PbO_2.

Lead-silver had more dissolution peaks and dissolved more readily in sulphuric acid than in zinc electrolyte, because the existing $ZnSO_4$ can help formation of denser layers or lead sulphate of lead-silver alloy in zinc electrolyte than those in sulphuric acid. So it is difficult for lead-silver alloy to break the lead sulphate layer and to oxidize the metallic lead.

4.4.3 Lead-silver alloy in zinc electrolyte during 16 h decay

The Pb-Ag anode sample was immersed 16 h at the OCP in zinc electrolyte following 24 h polarization at CD = 50 mA/cm^2. The period of 16 h potential decay can be divided into four levels: level 1: 1.72-1.66 V/SHE; level 2: 1.66-1.55 V/SHE; level 3: 1.55-0.9 V/SHE; and level 4: 0.9-0.3 V/SHE [22]. The cyclic voltammeter was used to study the electrochemical behaviour of the four levels of Pb-Ag anodes in zinc electrolytic (Figure 4.10).

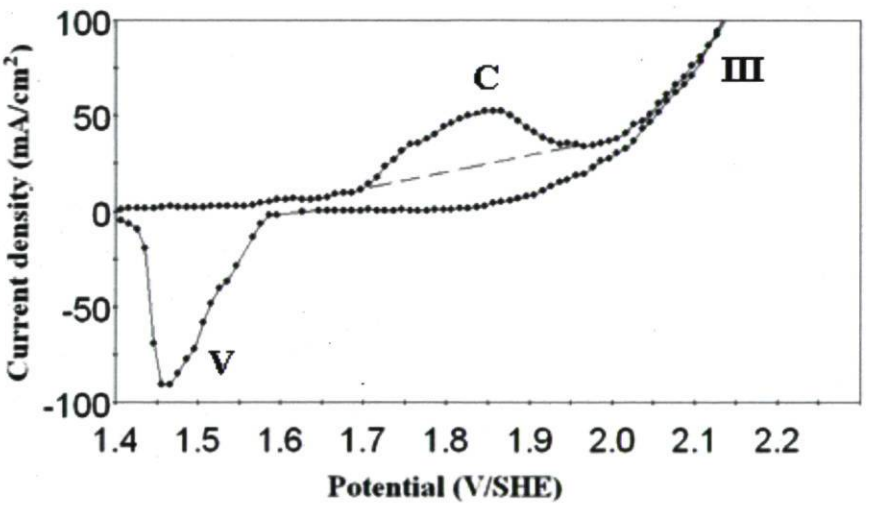

Figure 4.10: Cyclic current-potential curve of the lead-silver alloy anode at the second level at potential 1.62 V and decay of 1 min in a sulphuric acid solution 180 gdm^{-3} H_2SO_4 at a scan rate of 3 mVs^{-1}.

Following anodic polarization, Figure 4.10 shows a cyclic voltammetry diagram after a decay period of ~ 50 second. This corresponds to the second decay period that has been detailed before [22]. The oxidation peaks C and III and a reduction one V can be observed easily on this diagram. The first level is a too short period (30 s) where the formed lead dioxide during anodization is still dominant. At the second level of decay the

most important is that the oxidation peak C corresponds to the oxidation reaction of $PbO.PbSO_4 \rightarrow \alpha\text{-}PbO_2$. During the third level, less $PbO.PbSO_4$ is expected because of its transfer to the stable $PbSO_4$. Obviously, for the 4th level after ~ 128 minutes for Pb-0.7 Ag, this reaction of oxidation of $PbO.PbSO_4$ to PbO_2 cannot be observed in a similar way to that of the second decay level since the residual amount of this compound is too low. It is du to the non thermodynamic stability of this compound at this range of potentials (0.9-0.3 V/SHE). This is already stated by Yamamoto et al. [23]. The oxidation peak III corresponds to the reaction $O_2 + 4H^+ + 4e = 2H_2O$, and the reduction peak V should correspond to $PbO_2 \rightarrow PbSO_4$ as described by Yamamoto et al. [4].

4.5 Conclusions

In this paper, the electrochemical redox behaviour of lead and lead-silver alloy electrodes was investigated in sulphuric acid and zinc electrolyte using cyclovoltammetric method. After characterizing each redox peak, the following conclusions can be drawn:

1. Cyclic voltammetry technique has been used to observe redox peaks, and the associated species or products formed at these peaks could be characterized by chemical and physical methods. This permits to determine the influence of alloying elements such as Ag on the corrosion behaviour of lead anodes.

2. Alloying pure lead with 0.7% Ag for use as anode during zinc electrowinning decreased oxidation peak ($Pb \rightarrow PbSO_4$) by 40% in sulphuric acid zinc electrolyte Also, 0.7% silver as alloying element decreased the height of oxidation peak of ($PbSO_4 \rightarrow \beta\text{-}PbO_2$) by 40%.

3. The change of the sweep rate in CV experiments has an effect on the shape of CV curves, at low sweep rate of 3 mV/s, more redox peaks were observed than that at higher sweep rates. At the high sweep rate of 300 mV/s, the O_2 evolution peak is not visible.

4. Bubbling argon into the zinc electrolyte did not change the shape and number of redox peaks on the curve of CV and the addition of $MnSO_4$ to the zinc electrolyte decreased the redox peaks on the curve for lead-silver anode in zinc electrolyte.

5. During 16 h decay, the oxide peak ($PbO.PbSO_4 \rightarrow \alpha$-$PbO_2$) decreased with the level of decay from second level to fourth level.

4.6 Acknowledgements

The authors are grateful to the Hydro-Quebec, CEZ and the Natural Sciences and Engineering Research Council of Canada (NSERC) for their financial support.

4.7 References

[1] **Ivanov, I., Stefanov, Y., Noncheva, Z., Petrova, M., Dobrev, Ts., Mirkova, L., Vermeersch R. and Demaerel, J.-P.**, Insoluble Anodes Used in Hydrometallurgy: Part I. Corrosion Resistance of Lead and Lead Alloy Anodes, Hydrometallurgy, 57, 2000, pp. 109-124.

[2] **Lander. J. J.**, Silver, Cobalt, and Positive-Grid Corrosion in the Lead-Acid Battery, J. Electrochem. Soc., 105, 1958, pp. 289-292.

[3] **Mackinnon, D. J.**, The Effects of Foaming Agents, and Their Interaction with Antimony, Manganese and Magnesium, on Zinc Electrowinning from Synthetic Acid Sulphate Electrolyte, Hydrometallurgy, 35. 1994. pp. 11-26.

[4] **Yamamoto, Y., Fumino, K., Ueda T. and Nambu, M.**, A Potentiodynamic Study of the Lead Electrode in Sulphuric Acid Solution, Electochemica Acta 37, 1992. pp. 199-203.

[5] **Pavolv, D.**, Processes in Solid State at Anodic Oxidation of A Lead Electrode in H_2SO_4 Solution and Their Dependence on the Oxide Structure and Properties, Electrochima. Acta 23, 1978. pp. 845-854.

[6] **Pavolv D., and Rogachev, T.**, Dependence of the Phase Composition of the Anodic Layer on Oxygen Evolution and Anodic Corrosion of Lead Electrode in Lead Dioxide Potential Region, Electrochim. Acta, 23, 1978. pp. 1237-1242.

[7] **Pavlov, D., Bashtavelova, E., Simonsson, D., Ekdunge, P.**, Processes at the Micro-Level in the Oxidation of $PbSO_4$ to PbO_2 During Charging of Lead/Acid Battery Positive Plates, Journal of Power Sources 30, 1990, pp. 77-97.

[8] **Nguyen, T. K. T.**, Ph.D Thesis, A Study of the Mechanism by Which Cobalt Ions Minimize Corrosion of Lead Alloy Anodes during Electrowinning of Base Metals, University of Queensland, Australia, Chapter 2, 2007, pp. 7-8.

[9] **Ijomah, M. N.C.**, Electrochemical Behavior of Some Lead Alloys, J. electrochem. Soc. 134, 1987. pp. 2960-2966.

[10] **Czerwinski, A., Zelazowska, M., Grden, M., Kuc, K., Milewski, J.D., Nowacki, A., Wojcik, G., Kopczyk, M.**, Electrochemical Behavior of Lead in Sulfuric Acid Solutions, Journal of power Sources, 85, 2000. pp. 49-55.

[11] **Rerolle C. and Wiart, R.**, Kinetics of Pb and Pb---Ag Anodes for Zinc Electrowinning—I. Formation of $PbSO_4$ Layers at Low Polarization, Electrochim. Acta 40, 1995. pp. 939-948.

[12] **Krzewska, S., Pajdowski, L., Podsiadly, H., Podsiadly, J.**, Electrochemical Dtermination of Thiourea and Glue in the Industrial Copper Electrolyte, Metallurgical Transactions B, 1981, Vol. 15B, pp. 451-459.

[13] **ASTM Publication, ASTM G61-86**, Standard Test Method for Conducting Cyclic Potentiodynamic Polarization Measurements for Localized Corrosion Susceptibility of Iron-, Nickel, or Cobalt-Base Alloys. PA, 03.02, 2001, pp. 231-235.

[14] **Barnes S. C. and Mathieson R. T.**, The Potential pH Diagram of Lead in the Presence of Sulphate Ions and Some of Its Implications in Lead-Acid Aattery Studies, in "Batteries" (D. H. Collins, ed.). Pergamon Press, New York. 1963. pp. 41-54.

[15] **Jones P. and Thirsk, H. R.**, An Electrochemical and Structural Investigation of the Processes Occuring at Silver Anodes in Sulphuric Acid, Trans. Faraday Soc., 50, 1954, pp. 732-738.

[16] **Deutscher, R.L., Fletcher, S., Hamilton, J.A.**, Invention of Cyclic Resistometry, Electrochim. Acta 31, 1986. pp. 585-589.

[17] **Danel V., and Plichon, V.**, The Electrochemical Oxidation of Lead in Various H_2O---H_2SO_4 Mixtures—I. Linear Sweep Voltammetry, Electrochemical Acta. Vol 28. 1983. pp. 781-784.

[18] **Mahato B.K., and Tiedemann, W. H.**, Linear Potential Sweep of Lead-Acid Battery Electrodes Containing Trace Te, Sb, As, Co, and Ni, J. Electrochem. Soc. 130, 1983, pp. 2139-2144.

[19] **Pourbaix, M.**, Atlas of Electrochemical Equilibria in Aqueous Solutions. National association of corrosion engineers. Houston, Texas, USA (1974).

[20] **Umetsu, Y., Nozoka H. and Tozawa, K.**, Anodic Behaviour of Pb-Ag Alloys in Sulfuric Acid Solution, Proceedings of the International Symposium on Extract. Metall. Zinc, MMJ, Tokyo, Japan, 1985. pp. 265-279.

[21] **Pavlov, D., Rogachev, T.**, Mechanism of the Action of Ag and As on the Anodic Corrosion of Lead and Oxygen Evolution at the $Pb/PbO_{(2-x)}/H_2O/O_2/H_2SO_4$ Electrode system, Electrochim. Acta 31, 1986, pp. 241-249.

[22] **Zhang, W., Lafront, A-M., Ghali, E., Houlachi, G.**, Influence of Silver Content on Corrosion Resistance of Lead Anodes During Potential Decay by Electrochemical Noise Measurements, METSOC, Development & Perfromance of Sulphur Capture Plants, Sudbury, Ontario, Canada, 48th Annual Conf. of Metallurgists of CIM (2009), pp. 101-115.

[23] **Yamamoto, Y., Matsuoka, M., Kimoto, M., Uemura M., and Iwakura, C.**, Potentiodynamic Reactivation of A Passivated Lead Negative Electrode in Sulphuric Acid, Electrochimica Acta, Vol. 41. No. 3 1996, pp. 439-444.

CHAPTER 5

Effect of silver content in Pb-Ag anodes on the performance of the anodes during zinc electrowinning

Effect of silver content in Pb-Ag anodes on the performance of the anodes during zinc electrowinning

W. Zhang[1*], A.-M. Lafront[1], E. Ghali[1], G. Houlachi[2], G. Monteith[3] and G. Champoux[2]

[1]Department of Mining, Metallurgy and Material Engineering

Laval University, Ste-Foy, Quebec, Canada, G1K 7P4

Wei.Zhang.1@ulaval.ca*

[2]LTE, Hydro-Quebec

600 Avenue de la Mortagne, C.P. 900

Shawinigan, QC, Canada, G9N 7N5

[3]Zinc Électrolytique du Canada Ltée

Valleyfield, Québec, Canada, J6S 4W2

This paper was published in Canadian Metallurgical Quarterly Vol. 48, 2009, pp. 326-337.

5.1 Abstract

The efficiency of the electrowinning process of zinc depends on the performance of oxygen evolution reaction, anode quality and corrosion resistance of lead anodes. Original surfaces of rolled commercial lead-silver anodes were examined using conventional polarization methods in acid zinc sulfate electrolyte with $MnSO_4$ at 38°C. The self-discharge method (potential decay) following 5 h polarization at 50 $mA.cm^{-2}$ was considered to evaluate electrochemical activity, oxygen overpotential and anode stability. The influence of silver content is compared to that of the microstructure, the fabrication process and the composition of the corrosion products. Polished anode samples have also been examined for microstructural and corrosion performance studies. The experiments show that the duration of the plateau at 1600 mV/SHE, the potential level (active corrosion state/corrosion potential region) and the rate $\Delta E_{corr}/\Delta t$ during the decay could be a good indicator to compare the corrosion rates of the anodes in industrial zinc electrolytes.

L'efficacité du procédé d'électrodéposition du zinc dépend de la performance de la réaction d'évolution de l'oxygène, de la qualité de l'anode et de la résistance à la corrosion des anodes de plomb. Les surfaces d'origine des anodes de plomb-argent laminées ont été examinées par les méthodes conventionnelles de polarization dans l'électrolyte acide de sulfate de zinc avec $MnSO_4$ à 38°C. La méthode de décharge libre (évolution du potentiel) après 5 h de polarization à 50 $mA.cm^{-2}$ a été considérée pour évaluer l'activité électrochimique, la surtension de l'oxygène et la stabilité des anodes. L'influence de la teneur en argent est comparée à celle de la microstructure, du procédé de fabrication et de la composition des produits de corrosion. Des échantillons d'anode polie ont aussi été examinés pour des études microstructurales et de performance à la corrosion. Les expériences montrent que la durée du plateau (palier) à 1600 mV/SHE, le niveau de potentiel (stade de corrosion active/région de potentiel de corrosion) et la vitesse $\Delta E_{corr}/\Delta t$ pendant la l'hute du potentiel peuvent être un bon indicateur pour comparer la vitesse de corrosion des anodes dans des électrolytes industriels de zinc.

5.2 Introduction

Insoluble anodes Pb-Ag alloys used in industrial hydrometallurgical processes should possess at least 3 characteristics: high electrical conductivity, good electrocatalytical capability for oxygen evolution with low overpotentials, good stability, very good corrosion and wear resistance [1].

For zinc electrowinning from sulphate acid solutions containing manganese ions, the main oxidation processes including oxygen evolution reaction that take place on the surface of the lead anode are as follows [1]:

$$Pb + SO_4^{2-} \rightarrow PbSO_4 + 2e^- \qquad E° = -0.356\ V/SHE \qquad (5.1)$$

$$2H_2O \rightarrow O_2 + 4H^+ + 2e^- \qquad E° = 1.23\ V/SHE \qquad (5.2)$$

$$PbSO_4 + 2H_2O \rightarrow PbO_2 + H_2SO_4 + 2H^+ + 2e^- \qquad E° = 1.685\ V/SHE \qquad (5.3)$$

$$MnSO_4 + 2H_2O \rightarrow MnO_2 + H_2SO_4 + 4H^+ + 2e^- \qquad E° = 1.26\ V/SHE \qquad (5.4)$$

$$MnSO_4 + 4H_2O \rightarrow MnO_4^- + H_2SO_4 + 6H^+ + 5e^- \qquad E° = 1.52\ V/SHE \qquad (5.5)$$

PbO_2 anodic layer can be formed by electrochemical oxidation of lead electrodes in sulphuric acid solution. A non conducting layer of $PbSO_4$ was formed 1st then it transforms to the well-conducting PbO_2 (Equations 5.1, 5.3). A lead dioxide layer was formed with crystalline structure α- and β-PbO_2 and amorphous structure described as gel-like (hydrated) structure containing structural water or hydrogen species $PbO(OH)_2$ [2]. O_2 evolution starts in a certain number of active centres located in the gel zone of the layer of electrochemically active component PbO_2 (Equation 5.2). The slime MnO_2 and corrosion product PbO_2 protect the lead anode from corrosion (Equations 5.3 and 5.4) [1].

In some industries, there are some power interruptions that last a few hours and they may affect the stability of the anodes. The anodes remain in the electrolyte in the cell while the current is cut off. When the applied current is interrupted in a zinc electrowinning plant lead anodes tend to corrode and this process is similar to the one that takes place in lead acid battery [3]. The anodes seem to be affected during this period of time and as a result high lead contamination of zinc deposit is observed when the current is turned on. The self-discharge of the anode takes place during open circuit

potential OCP. Three potential plateaux are observed in the potential transient curves between in a range of 1600-200 mV corresponding to allotropic transformations for the reduction of PbO_2 to $PbSO_4$. The 1st potential plateau shows a well definite OCP step of PbO_2 hydrogen system around 1600 mV corresponding to the theoretical potential value of the PbO_2/Pb^{2+} equilibrium. This time relates to the amount of PbO_2 present as well as to the difficulty of converting PbO_2 into $PbSO_4$ or a more compact structure [4]. The 2nd and the 3rd plateaux at 1000-900 and 300-200 mV respectively correspond to two electrochemical stages of the reduction of PbO_2 taking place in the gel zones [5] (Equations 5.6, 5.7 and 5.8). Guyen stated that the 2nd plateau corresponds to the reduction of PbO to basic Pb sulphate (Equation 5.9) [4]:

$$PbO_2 + H^+ + e^- \rightarrow PbO(OH) \quad (5.6)$$

$$PbO(OH) + H^+ + e^- \rightarrow Pb(OH)_2 \quad (5.7)$$

$$Pb(OH)_2 + H_2SO_4 \rightarrow PbSO_4 + 2H_2O \quad (5.8)$$

$$2PbO_2 + HSO_4^- + 5H^+ + 4e^- \rightarrow PbOPbSO_4 + 2H_2O \quad (5.9)$$

This cathodic reaction takes place at the oxide surface and the metallic lead in contact with acid through the pores of PbO_2 dissolves (Equation 5.1). Solid $PbSO_4$ formation causes cracks in the protective layer, then lead corrosion continues to take place in considering any available cathodic reaction [5].

The oxide layer of various compositions depends on the electrolyte, the polarization potential and other factors like alloying elements. Ag alloyed in lead anode decreases the oxygen overvoltage and accelerates oxygen evolution on the batteries grids [6]. O_2 evolution is inhibited by silver salt adsorbate like sulphate or permanganate [7]. Ag retards the oxidation of PbO to PbO_2 and enhances the formation of β-PbO_2 in the oxide layer next to the metal [6]. Ag increases also the value of the ratio α/β-PbO_2 and the amount of gel zone in corrosion layer [7].

The oxidation of Pb anode in the Zn electrowinning process influences the anode life and the quality of Zn deposit. The aim of this work is to find an electrochemical parameter able to characterize easily the anode performance. The potential decay or self discharge method (OPC) following 5 h polarization in conjunction with the scanning

electron microscopy technique are considered to evaluate the influence of Ag concentration on the electrochemical activity, O_2 overpotential and corrosion behaviour. The electrochemical measurements and corrosion behaviour are then related to the microstructure and chemical composition of the anodes.

5.3 Experimental procedure

5.3.1 Electrochemical set-up

800 ml of electrolyte containing 60 g/dm³ of Zn^{2+}($ZnSO_4$.7H2O), 180 g/dm³ of H_2SO_4, 8 g/dm³ of Mn^{2+} ($MnSO_4 \cdot H_2O$), 250 mg/dm³ of Cl^- and 3 mg/dm³ of Glue (Gelatin or glue (G) is an animal protein that consists of a complicated mixture of polypeptides and is used as levelling agent [8]) heated by a flow of thermostated water in the double wall (38 ± 0.5°C). The electrolyte was magnetically stirred at 412 rpm during the experiments.

The chemical composition of 6 laminated Pb-Ag anodes used in this work is given in Table 5.1. At least 45 elements were analysed by Fluorescence X and only the elements where the wt% is higher than 0.05% are given. Ag, Ca and Fe contents were analysed quantitatively by atomic absorption technique.

Table 5.1 – Chemical composition (wt %) of the 6 anodes

Anode	Ag (wt %)	Fe (wt %)	Ca (wt %)	Al (wt %)	Mn (wt %)	S (wt %)	Si (wt %)	Ti (wt %)	Zr (wt %)	Pb (wt %)
#1	0.516	0.007	< 0.001	0.29	< 0.05	0.13	1.4	< 0.05	0.21	bal.
#2	0.512	0.007	< 0.001	0.11	< 0.05	0.12	0.4	0.4	0.19	bal.
#3	0.574	0.021	< 0.001	0.09	0.15	0.4	0.29	0.26	0.18	bal.
#4	0.600	0.013	< 0.001	< 0.05	< 0.05	0.08	0.3	0.18	0.22	bal.
#5	0.684	0.015	< 0.001	< 0.05	< 0.05	< 0.05	0.23	0.19	0.2	bal.
#6	0.672	0.009	< 0.001	< 0.05	< 0.05	0.07	0.07	0.25	0.19	bal.

The Pb-Ag alloy anodes plates were cut into small pieces of 1 x 1 x 1 cm then connected with a plastic isolated copper wire and cast in acrylic resin leaving 1 cm² exposed area surface. Two types of working anode, original and polished surfaces were washed with alcohol and dried immediately before being introduced into the electrolytic cell. The polished anode surfaces were obtained ground with 600 soft grid SiC paper with

ethanol to avoid the inclusion of SiC particles into electrodes. Some samples in the beginning were polished using the current SiC paper.

The working electrode and the counter electrode (made of Al for electrowinning test or Pt for corrosion rate measurements) were mounted in suitable Teflon made holder. Their distance was fixed at 2 cm. The reference electrode was mercurous sulphate electrode (MSE, $Hg.Hg_2SO_4/sat.K_2SO_4$) and a saturated K_2SO_4 salt bridge was used to keep the reference electrode close to the anode. The experimental setup was an EG&G PARSTAT 2263 potentiostat/galvanostat controlled by an IBM computer.

5.3.2 Electrochemical methods

A constant 50 mA/cm^2 anodic current density was applied during 5 h then the current was abruptly interrupted and Pb-Ag electrode potential-time curve was recorded during 6 h. Two successive cycles of 5 h galvanostatic polarization at CD = 50 mA/cm^2 followed each time by 6 h decay at open circuit potential OCP (reduction or discharge of the anode) have been used 1) to measure anodic overpotential during anodic polarization and 2) to calculate after each hour decay, the corrosion potential (E_{corr}), corrosion current (i_{corr}) and polarization resistance (R_p) from linear polarization method (potentiodynamic test at 0.166 mV/s scan rate over a potential range of 50 mV (ASTM G5) [9].

Duplicate experimental results have been done from the original surface of the anodes of #1, #2, #4 and #6 at the 1^{st} cycle of polarization, while #3 and #5 were made for one time. Duplicate experimental results have been done from all polished surface at both cycles of polarization.

5.3.3 Surface analysis method

SEM analyses were conducted using JEOL JSM-25s III model Scanning Electron Microscope equipped with a TN 5700 model energy dispersive X-ray analyzer (EDX) to characterize corrosion products. The microstructure of the anode surface was characterized using optical (ZEISS Model). Before analyses, the surface of the anodes was electrochemically polished during 2 min at 100 mA/cm^2 in an etching solution composed of 315 ml of acetic acid, 32 g of sodium acetate and 108 ml of H_2O. After

electropolishing, 3:1 acetic acid – H_2O_2 (30%) solution was used to remove the black surface film, then the surface was cleaned with ethanol and air dried.

5.4 Results

5.4.1 Performance of the anodes

5.4.1.1 Oxygen overpotential

Figure 5.1 shows the anodic polarization potential of anode #6 with original and polished surfaces during the 1st and the 2nd cycle of polarization at 50 mA/cm^2.

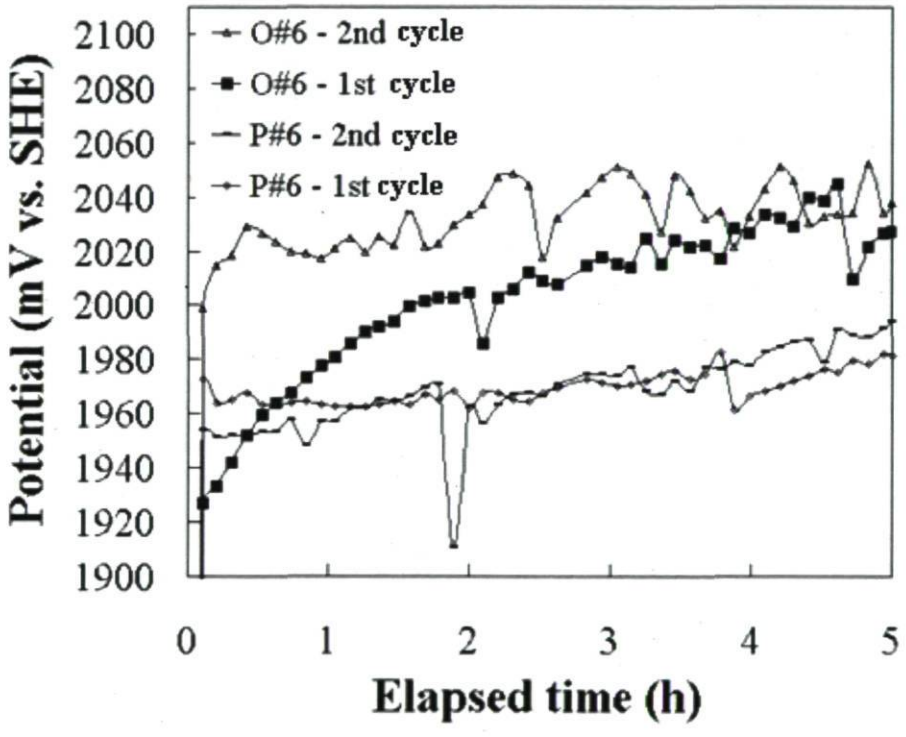

Figure 5.1 - Potential evolution of the original and polished surfaces of anode #6, (O#6) and (P#6), during the 1st and 2nd cycles of 5 h polarization at 50 mA/cm^2 in acid Zn sulphate electrolyte with Mn^{2+} at 38°C.

Average values were obtained in selecting 800 potential measurements starting from the 2nd till the 5th h of polarization. The average values of the original surface of anode #6 at the 1st and 2nd cycles of polarization are 2014 and 2036 mV respectively. The average values of the polished surface of anode #6 at the 1st and 2nd cycles of polarization

is 1966 (±4) and 1973 (±5) mV, respectively, (Figure 5.1). The average potential value is higher for the 2nd cycle of polarization than that of the 1st cycle, around 20 mV for the original surface of the anode and less than 10 mV for that of the polished surface. The average potential value is higher for anode with the original surface than that of the polished surface around 30 mV and 50 mV for the 1st and 2nd cycles of polarization respectively.

The difference between the highest and the lowest average potential values during the period from 1-5 h polarization of the original or the polished surface of the anodes #1, #2, #3, #4, #5 and #6 for the 1st and 2nd cycles of polarization is around 50 mV. It is difficult to find a sequence because some of the average potential differ less than 10 mV. However exception can be due to fall of the corrosion product, or other experimental error, the comparison between the average potential gives 2 groups of potentials from highest to lowest values (#1, #4, #2) and (#6; #3, #5), respectively.

The standard deviation of the reproducibility of the average potential values was of the order of ± 10, 15, 2 and 3 mV, for duplicate experimental results from the original surface of the anodes #1, #2, #4 and #6 respectively at the 1st cycle of polarization (#3 and #5 were made for one time). It was ~ ± 30,. 20 and 1 mV for duplicate experimental results for the 1st cycle of polarization of the polished anode surfaces (#5), (#1, #2) and (#3, #4 and #6), respectively. Also, it was ~ ± 40, 30, 15 and 5 mV for polished anode surfaces (#1), (#2), (#3, #4, #5), (#6), respectively for the 2nd cycle of polarization.

5.4.1.2 Potential transient: open circuit potential (OCP) during discharge (1st hour)

Figure 5.2 shows typical 1 h potential transient at OCP during discharge of anodes #2 and #6 with original surfaces pre-polarized for 5 h at CD = 50 mA/cm^2.

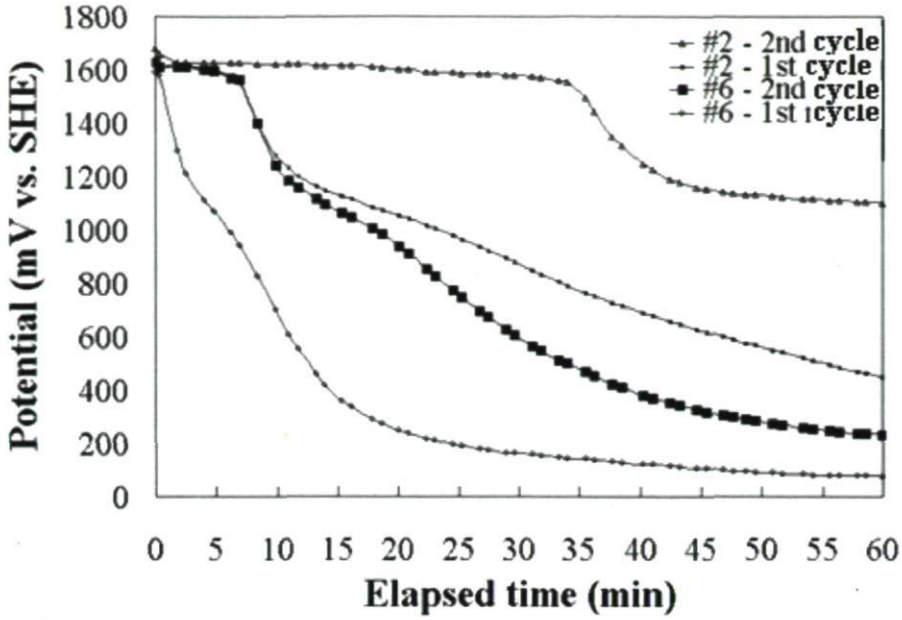

Figure 5.2 – 1 h decay potential transient of original anode surfaces (#2 and #6) at OCP following the 1st and 2nd cycles of 5 h polarization.

After 5 h polarization, the cell current is switched off and the potential remain at a plateau around 1600 mV corresponding to the theoretical potential value of the PbO_2/Pb^{2+} equilibrium. This shows a spontaneous transformation on lead dioxide into lead sulphate because thermodynamically lead dioxide is unstable on the surface of lead in the sulphuric acid solutions [4]. After a certain period of constant positive potential, plateau with duration Δt, the potential dropped down to values around 200 mV showing a stabilization of the potential. The period of plateau and that of the quick change of potentials can correspond to active corrosion state "ACS" since the reaction is accelerated with the reduction of oxides. The last potential can correspond to the total disappearance of PbO_2 and in this region the corrosion potential goes to somewhat more stable values. Since a slight shift versus more active potentials is observed for all the Pb-Ag alloys, this can be called corrosion potential region "CPR" of these specimens and can be different from the potential of lead that has not been submitted to precedent anodic polarization and immerged in the same electrolyte.

After the 1st cycle of polarization, anode #2 shows a long plateau length (11 min) and after this plateau the potential of the electrode drops quite steeply. Anode #6 shows a

short plateau length (1 min) and a gradual decrease of the potential indicating a gradual change in stoichiometry (Figure 5.2).

The length of plateau (duration Δt) is a measure of the time taken to reduce PbO_2 to $PbSO_4$ or it relates to the amount of PbO_2 [4]. This time showing the loss of passivity is between 1 to 11 min and 11 to 48 min for anodes with an original surface after the 1st and 2nd cycles respectively. Δt increases with the time of polarization. After the 2nd cycle of polarization, anodes #2 and #6 show plateau length of about 11 and 36 min, respectively. Anodes with a polished surface show similar range of values however they reach the CPR later than that with original surfaces due to slower slope $\Delta E/\Delta t$. This is an indication of more allotropic changes for polished surfaces or more compact films [10].

After the 1st cycle of polarization, the sequence of the original anodes Δt is from high to low: #2, #1, #4, #5, #3, #6. The CPR is reached after 2 and 3 h for anodes #1 and #2, respectively and after 1 h for the others. After the 2nd cycle of polarization, the sequence and the time to reach the CPR is for original anodes from high to low: #1 (6 h), #2 (4 h), #4 (3 h), #5 (3 h), #3 (3 h), #6 (1 h). The Δt sequence of the polished anodes is from high to low: #4, #1, #6, #2, #5, #3 (not shown).

It can then be suggested that the increasing quantity of Ag in the anode leads to short plateau at ~1600 mV because of less PbO_2 and/or less compact films. It has been stated that higher silver contents lead to the formation of less PbO_2 [6].

5.4.1.3 Anodic behaviour of the anode: E_{corr} and i_{corr} during the decay at open circuit potential (OCP)

Anodes with original surface

Figures 5.3a and b show E_{corr} and i_{corr} calculated each hour during 6 h decay for both successive polarization cycles. 1 to 6 h corresponds to the decay after the 1st cycle of polarization and 7 to 12 h corresponds to the decay after the 2nd cycle of polarization. The CPR is considered to be reached when anodes corrosion potentials are below the dashed line in Figure 5.3a.

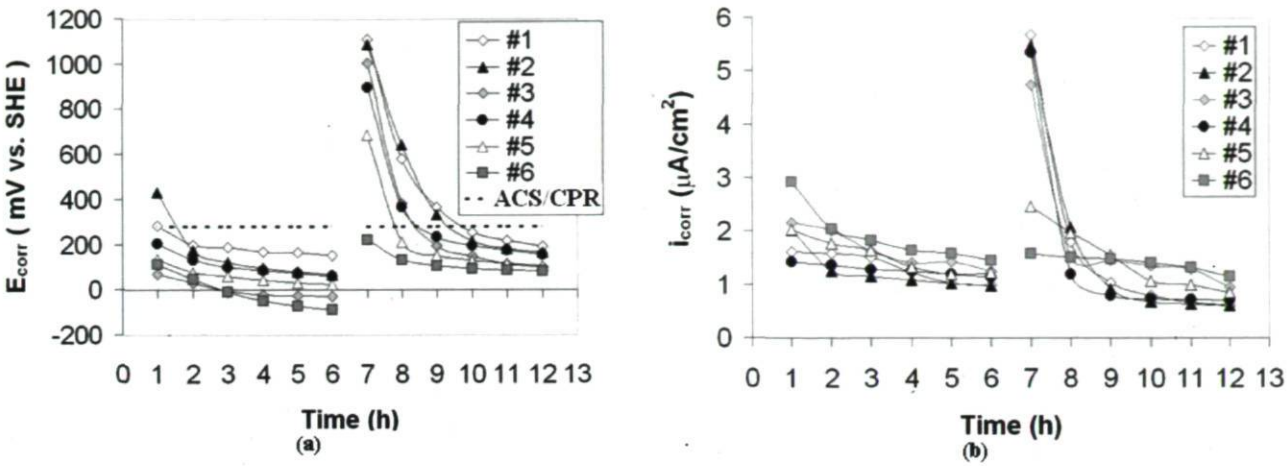

Figure 5.3 – a) E_{corr} vs time and b) i_{corr} vs time for 6 anodes with original surface during 6 h decay after the 1st and 2nd polarization cycles, 1 to 6 h and 7 to 12 h respectively (E_{corr} corrosion potential region "CPR" is < E dashed line).

After 1 h decay following the 1st cycle of 5 h polarization, only the anodes #2 and #1 are in active corrosion state "ACS" (Figure 5.3a). The sequence of E_{corr} and i_{corr} is from low to high: E_{corr} 1st(1 h): #3, #6, #5, #4,. #1(ACS), #2(ACS) and i_{corr} 1st(1 h): #4, #1(ACS), #2(ACS), #5, #3, #6 (Figures 5.3a and b). In the CPR, the lowest E_{corr} 1st(1 h) corresponds to the highest i_{corr} 1st(1 h). After 6 h decay (1st cycle of 5 h polarization), all the anodes are in the CPR and the sequence of E_{corr} and i_{corr} is from low to high E_{corr} 1st(6 h): #6, #3, #5, #4, #2, #1 and i_{corr} 1st(6 h): #1, #2, #4, #5, #3, #6 (Figures 3a and b, respectively).

$\Delta i_{corr}/\Delta t$ follows the same trend as $\Delta E_{corr}/\Delta t$ during the decay (Figures 5.3a and b). The 2nd polarization of the anode in the CPR leads to anode in ACS, E_{corr} 1st(6 h) stays the highest E_{corr} 2nd(1 h) and the lowest i_{corr} 1st(6 h) becomes the highest i_{corr} 2nd(1 h). After 1 h decay following the 2nd cycle of 5 h polarization, all the anodes are in ACS except anode #6. The sequence for E_{corr} 2nd(1 h) and i_{corr} 2nd(1 h) is from low to high: #6, #3(ACS), #5(ACS), #4(ACS), #1(ACS), #2(ACS). In ACS, the highest E_{corr} 2nd(1 h) corresponds to the highest i_{corr} 2nd(1 h). After 6 h decay (2nd cycle of 5 h polarization), all the anode are in a CPR and the sequence of E_{corr} 2nd(6 h) = E_{corr} 1st(6 h) and i_{corr} 2nd(6 h) =

i_{corr} 1st(6 h). The sequence of the best corrosion resistance for anodes with an original surface is: #1 > #2 > #4 > #5 > #3 > #6 (Figures 5.3a and b).

Some results deduced from Figure 5.3 are summarized in Table 5.2:

Table 5.2 – Corrosion potentials and corrosion current rates of two original surfaces of anodes after polarization for both cycles the 1st and the 6th h of decay

Anode	Polarization cycles	E_{corr} (mV vs. SHE)		i_{corr} (μA/cm^2)	
		1st h	6th h	1st h	6th h
#2	1st	433	67	2.02	0.98
	2nd	1089	165	5.46	0.60
#6	1st	112	-87	2.93	1.46
	2nd	222	82	1.59	1.16

The corrosion potential values at similar decays increase at the 2nd cycle of polarization (Figure 5.3a and Table 5.2). After the 2nd cycle of polarization, the corrosion current value at the 1st h decay increases because anodes are not in the CPR and decreases at 6 h decay. However, for anode #6 i_{corr} 2nd(1 h) < i_{corr} 1st(1 h) because this anode was also in the CPR at the 1st h decay of the 2nd cycle of polarization.

Anodes with the polished surface

Figures 5.4a and b show E_{corr} and i_{corr} calculated each hour of 6 h decay for both successive polarization cycles. 1 to 6 h corresponds to the decay after the 1st cycle of polarization and 7 to 12 h corresponds to the decay after the 2nd cycle of polarization.

Examining profoundly the Figures 5.3 and 5.4, it can be deduced that anode corrosion rates can be compared when they are in the same state as defined (active corrosion state or corrosion potential region as defined by the corrosion potential values). It can be underlined that anodes with polished surface have more difficulty to attend the CPR generally and the comparative sequence is hard to deduce. The sequence of anodes with polished surfaces for i_{corr}1st(6 h) CPR is from low to high: #2, #5, #3 which confirms the sequence of that of original samples.

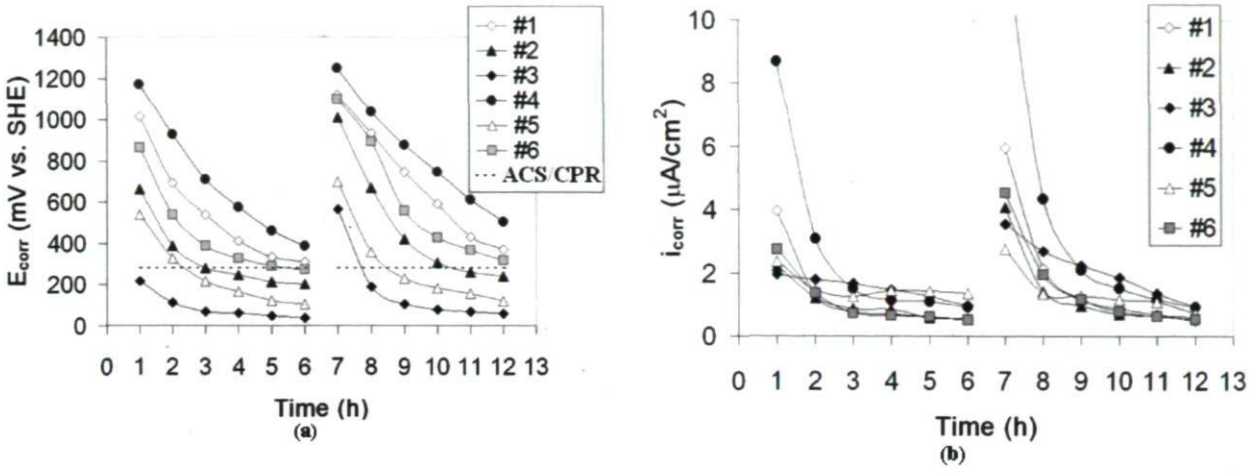

Figure 5.4 – a) E_{corr} vs. time and b) i_{corr} vs. time for anodes with polished surface over 6 h decay after the 1st and 2nd polarization cycles, 1 to 6 h and 7 to 12 h respectively (E_{corr} corrosion potential region "CPR" is < E dashed line).

Table 5.3 shows the sequence of all the anodes with original and polished surfaces in the CPR or ACS states for both cycles of polarization and 6 h decay:

Table 5.3 – E_{corr} and I_{corr} sequence in corrosion potential region and active corrosion state for both cycles of polarization and 6 h decay

E_{corr} sequence (CPR or ACS)	E_{corr} 1st(6 h)	<	E_{corr} 2nd(6 h)	<	E_{corr} 1st(1 h)	<	E_{corr} 2nd(1 h)
I_{corr} sequence: All E_{corr} in CPR	i_{corr} 2nd(6 h)	<	i_{corr} 1st(6 h)	<	i_{corr} 2nd(1 h)	<	i_{corr} 1st(1 h)
E_{corr} 1st2nd(6 h) CPR / E_{corr} 1st2nd(1 h) ACS	i_{corr} 2nd(6 h)	<	i_{corr} 1st(6 h)	<	i_{corr} 1st(1 h)	<	i_{corr} 2nd(1 h)
All E_{corr} in ACS	i_{corr} 1st(6 h)	≤	i_{corr} 2nd(6 h)	<	i_{corr} 1st (1 h)	<	i_{corr} 2nd(1 h)

In the CPR, the i_{corr} values are lowered both by the number of cycles and by the duration of the reduction time at OCP. E_{corr} values are lowered by the duration of the reduction time only. The transversal long arrows (Table 5.3) show that less positive potentials lead to higher corrosion rates. During the ACS, the i_{corr} and E_{corr} values are lowered by the duration of the reduction time. The vertical short arrows indicate that low potentials lead to low corrosion rates (Table 5.3).

5.4.1.4 Comparison of corrosion current values of anodes with the original and polished surface

The i_{corr} values after the 1st and the 6th h of decay following the 2nd cycle of polarization have been chosen to compare the corrosion values of original and polished surfaces because at this time of decay most of the anodes are already in ACS and in CPR of OCP, respectively, (Figures 5.5a and b).

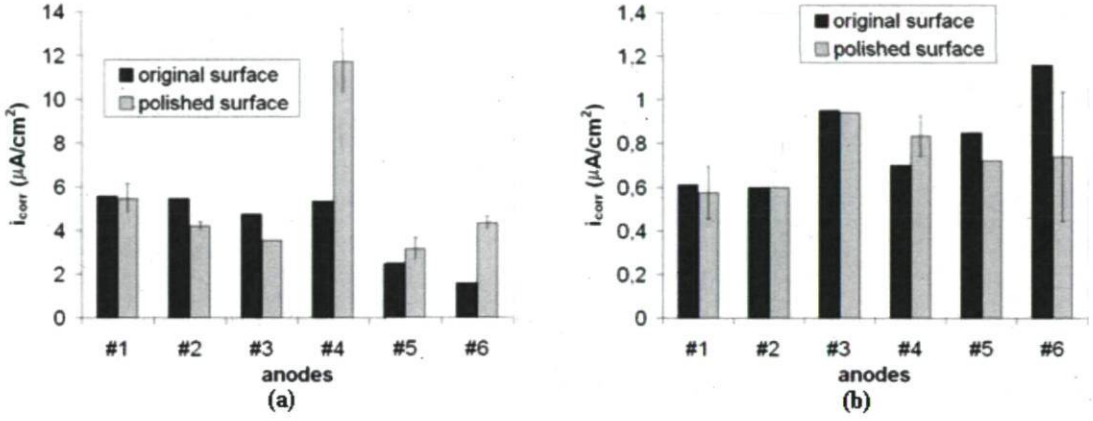

Figure 5.5 – a) i_{corr} 2nd(1 h) (active corrosion state at OCP) and b) i_{corr} 2nd(6 h) (corrosion potential region at OCP) values of 6 anodes with original and polished surfaces. The error bars represent the standard deviation for duplicate experiments.

For the 1st h of decay after the 2nd cycle of polarization, the sequence of the i_{corr} is from low to high: #6 (1.59), #5 (2.47), #3 (4.75), #4 (5.35), #2 (5.46), #1 (5.58) μA/cm^2 and #5 (3.12 ± 0.51), #3 (3.54), #6 (4.20 ± 0.2), #2 (4.32 ± 0.3), #1 (5.4 ± 0.6), #4 (11.74 ± 1.47) μA/cm^2 for anodes with original and polished surfaces, respectively, (Figure 5.5a). Since anode #6 with original surface is in CPR, its lower i_{corr} values than that of anode #6 with polished surface can be well understood. It seems also that the polished surface of anode #4 has an extreme high i_{corr} values and that may be due to the polishing effect technique of lead anodes. The best corrosion resistance performance of anodes with polished or original surfaces in ACS is: #5 > #3 > #2> #1. The difference between i_{corr} maximum and minimum values is ~ 3 and the average value is 4.5 μA/cm^2 (Figure 5.5a).

It can be noticed that the scale in the Figure 5b is 10 times lower than that of Figure 5.5a. For the 6th h of decay after the 2nd cycle of polarization, the sequence of the i_{corr} is from low to high: #1 (0.61), #2 (0.60), #4 (0.70), #5 (0.85), #3 (0.95), #6 (1.16) $\mu A/cm^2$ and #1 (0.57 ± 0.12), #2 (0.60), #5 (0.72), #6 (0.74 ± 0.29), #4 (0.83 ± 0.09), #3 (0.94) $\mu A/cm^2$ for anode with original and polished surface respectively (Figure 5.5b). In a CPR, similar i_{corr} values are obtained for both type of surface except for anode #6. Duplicate experiments for anodes #2, #3, #5 with polished surface give reproducible results and the reproducibility for anodes #1, #4, #6 is ± 0.12, 0.09 and 0.29 $\mu A/cm^2$, respectively. Moreover anodes #1, #4, #6 with polished surface are not in CPR, so the results of the polished anode surfaces in the CPR could be compared with that of the original anodes. The best corrosion resistance performance of the anodes with polished or original surfaces in the CPR is: #1 > #2 > #5 > #3. The difference between i_{corr} extreme values is ~ 0.35 and the average value is 0.75 $\mu A/cm^2$ (Figure 5.5b).

5.4.2 Characterisation studies

5.4.2.1 Microstructure of the polished anodes

Figure 5.6 shows the micrograph of Pb-Ag alloys anodes

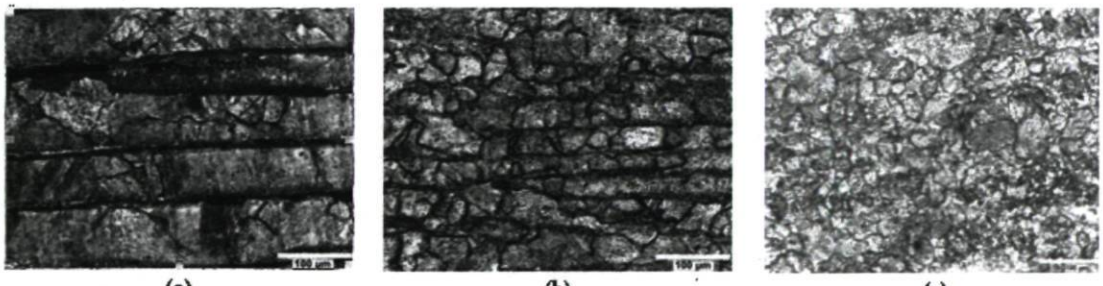

Figure 5.6 - Optical micrographs of Pb-Ag anodes a) #2, b) #3 and c) #6.

Concerning the anodes of Pb-Ag alloys, Figure 5.6 shows that large amounts of the 2nd phase (Ag-Pb eutectic) are located in grain and some regions along the grain boundary (dark color). Grain boundary precipitations are also observed when the grain seems to lead to a layered distribution for anodes #2 and #3 (Figures 5.6a and b). It can

be suggested that the quality of rolling is inferior for anode #6 (Figure 5.6c) and anodes #1, #4 and #5 (not shown). This can be influenced by the rolling process [11].

Anode #2 (as well as anode #1) shows a coarse grain structure (Figure 5.6a). Anode #3 shows a finer grain than anode #2 and has the most homogenous grain structure in size (Figure 5.6b). Anode #6 shows the finest grain structure (Figure 5.6c). The microstructure indicates that the grain size of the Pb-Ag is refined with increasing Ag content. The uniform and fine grain structure will corrode more uniformly [11].

5.4.2.2 SEM morphology and EDX and XRD analyses

SEM associated with X-Rays diffraction analyses, XRD, is used to identify the formation of anode slime and corrosion product on the Pb-Ag anodes. Figure 5.7 shows the SEM micrograph of anode surface film formed on Pb-Ag alloy by anodic polarization at 50 mA/cm^2: 1) for 5 h (Figure 5.7a) and 2) for two cycles of 5 h followed by 6 h decay each time (Figure 5.7c). EDX analysis of different phases has been done.

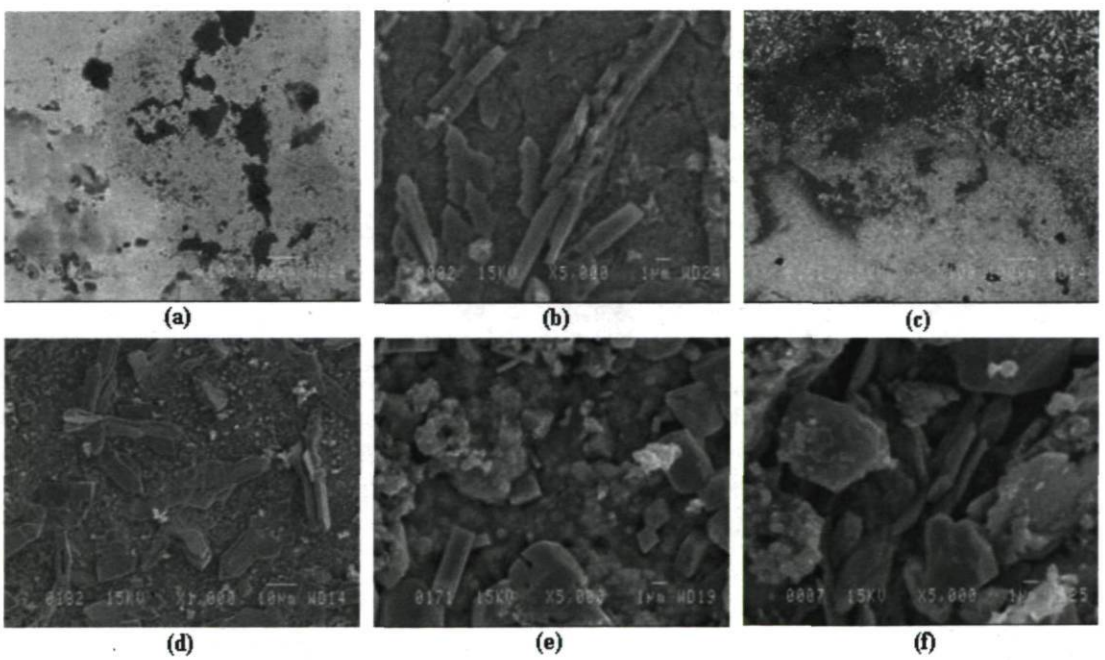

Figure 5.7 – a) Backscattered electron BSE micrograph of anode oxide formed on polished surface of anode #3 after 5 h polarization at 50 mA/cm^2, b) Scanning Electron Micrograph SEM of the grey part in a, c) BSE micrograph of anode oxide formed on

polished surface of anode #1 after 2 cycles of 5 h polarization followed by 6 h decay, d) SEM of the white part in c, e) SEM of grey part in c, and f) SEM of white-grey part in c.

Three different areas characterized by black, grey and white colors are present on the backscattered electron micrograph "BSE" of Pb-Ag alloys with polished surface after 5 h oxidation at 50 mA/cm^2 (Figure 5.7a) or after two cycles of 5 h oxidation at 50 mA/cm^2 followed by 6 h decay each time (Figure 5.7c).

After 5 h oxidation at 50 mA/cm^2, the outer part of the oxide layer is made of a thick layer of anodic amorphous slime MnO_2 poorly adherent, black area in Figure 5.7a. On some part of the top of this layer, white phase under black phase giving a grey area in Figure 5.7a, there are some crystals plate crystals PbO_2 around 2-3 μm in size (Figure 5.7b). The sublayer is made of agglomerates of submicronic tiny rounded crystals, white area in Figure 5.7a. The EDX spectrum contains peaks of Pb, O, S, Mn. May be Pb oxide coexists with trace of MnO_2. XRD measurements show Pb, $PbSO_4$, αPbO_2 and βPbO_2 phases.

After 2 cycles of 5 h oxidation at 50 mA/cm^2 followed by 6 h decay each time, anodic amorphous slime MnO_2 poorly adherent remains on the outer layer (black area). This layer is cracked due to internal stress. On some part of the top of this layer there are some plate crystals (white area) $PbSO_4$ around 20 μm in size (Figure 5.7d). The sublayer is made of 3 different phases: agglomerates of submicronic tiny rounded crystals for polished anodes (Figure 5.7e) or hexagonal plate crystal for polished anode (Figure 5.7f) (white-grey area, where EDX spectrum contains peaks of Pb, O, Mn indicating possible presence of Pb_2MnO_4 crystals); crystals of αPbO_2 with rhombic symmetry or of βPbO_2 with tetragonal symmetry; and prismatic crystals of $PbSO_4$ around 5 μm in size. XRD measurements confirm the presence of Pb and $PbSO_4$ phases. It is worthy to mention that the original surface leads to the same results as polished one.

5.5 Discussion

The results show that potential values during the anodic polarization (O_2 overpotential) decreases of about 50 mV with an increase of Ag content from 0.5 to 0.7 % in the Pb-Ag anodes (#1, #2) and (#5, #6), respectively. Anodes # 3 and #4 (Pb-Ag 0.57 and 0.6%)

show the same tendency as the 2 group of anodes (#5, #6) and (#1, #2) respectively showing the difficulty to establish rigorous sequence.

It is interesting to investigate the type of corrosion control during decay. At ACS, at the high level of potential plateau and high corrosion rates, the lead dioxide is reduced easily and this leads to anodic control. The passage to the CPR, where lead oxides and dioxides are disappearing and dissolved oxygen is becoming much less, the cathodic reaction becomes mostly that of the simple H_2 evolution reaction that leads to a cathodic control. In the same time, there is formation of non-conductor lead sulphate layer leading to limited anodic sites in the pores (pseudo-passive state) giving finally a mixed anodic and cathodic control.

If the quantity of Ag increases from 0.5 to 0.7%, in the "ACS" the potential shifts to more active values (less positive) and less corrosion currents corresponding typically to a relative more cathodic control since the 0.7% Ag anodes have less lead dioxide and less plateau duration. In absence of PbO_2 or in the CPR, the shift of potential goes to more active values as before but the corrosion rates shift to higher values due to the increasing galvanic cells that is proportional to Ag content.

At the end of the 6^{th} h decay after the 2^{nd} cycle of polarization, the polished anode surfaces show a sub-layer of tiny crystals instead of well–crystallised plates for original anode surfaces because they have reached the CPR later than the anodes with the original surface. Moreover, i_{corr} of the polished surface in the ACS state is slightly lower than that of the original surface because the crystal structure promotes higher i_{corr} than the amorphous one. The strong i_{corr} observed for anode #4 with polished surface could be due to polishing and contamination with SiC. Moreover, very probably that anode #4 has not been rolled efficiently as compared to other anodes and it is admitted that the rolling process decreases i_{corr}.

Because chemical analyses do not show significant difference between the anodes except for the Ag content, the rolling process and the grain size could explain certain differences in the electrochemical behaviour. The absence of visible rolling process could be responsible for the lack of reproducibility for anode #6 with polished surface. The relatively well rolling process giving more homogeneous structure could be responsible

for the behavior of anode #3 (Figure 5.6) close to that of the anode #5 and #6 containing higher Ag content. Further work is suggested to clarify the mechanism of corrosion and evaluate the influence of more than 2 cycles of polarization and decay. It is also suggested that the decay period can be limited in the case of several cycles to 2 h decay adopted frequently in the practice of zinc electrolysis.

It can be then stated that the effects of the relative increase of silver content in the lead anode lead to relative approximate increase of silver phases (~ 20 to 40%), that changes the performance of the anode during its life service, influences mainly the oxygen evolution reaction during electrowinning and decreases the hydrogen overpotential during decay.

5.5 Conclusions

Considering the approach of two successive cycles of 5 hours galvanostatic polarization at 50 mA/cm^2, followed by 6 hours decay at Open Circuit Potential "OCP" to examine the performance of the Pb-Ag anodes in zinc electrowinining, the following conclusions can be deduced:

1. An increase of silver content from 0.5, 0.6 to 0.7% in the Pb-Ag alloy #1< #2<#3<#4< #6<#5 leads to the following consecutive effects:

a- The decrease of the overpotential of O_2 evolution of about 50 mV at the 1st and 2nd cycles of polarization. The average of polarization potential gives 2 groups of potential values: the highest potential values (#1, #4; #2) and the lowest potential (#6; #3, #5). The O_2 overpotential values are increased of ~ 20 mV for the original surface as compared to the polished one and also during the 2nd cycle of polarization.

b- The decrease of the plateau duration during the decay at 1600 mV vs. SHE of about 10 and 25 min for the 1st and the 2nd cycles of polarization respectively leads to:

- A decrease of E_{corr} ~ 450 mV corresponding to a decrease of the corrosion current of ~ 3 $\mu A/cm^2$ during the reduction of PbO_2 corresponding to the active corrosion state at potential from ~ 1600 to 250 mV.

- A decrease of E_{corr} ~ 150 mV corresponding to an increase of the corrosion current 0.35 $\mu A/cm^2$ during the total reduction of PbO_2 to $PbSO_4$ corresponding to the corrosion potential region at potential lower than 250 mV.

2. The duration of the plateau at 1600 mV, the potential level and the rate $\Delta E_{corr}/\Delta t$ during the decay (which follows the same trend as $\Delta i_{corr}/\Delta t$) could be a good indicator to compare the corrosion rates of the anode.

3. During active corrosion state, higher Ag content promotes the best corrosion resistance, however, at the corrosion potential region of potentials slightly increasing corrosion rates have been observed with increasing silver content.

4. At OCP, both corrosion potential and current values are lowered by the reduction time. The corrosion rate values are lowered at the 2^{nd} cycle only when the corrosion region is reached.

5. Some observed differences in the obtained results were due to blistering, shear cracking, flaking or even fall of the corrosion products, different microstructure, and experimental errors and also due to the different corrosion products obtained during the general non-uniform corrosion on the surface of Pb-Ag anodes.

5.7 Acknowledgements

The authors are grateful to the Hydro-Quebec, CEZ and the Natural Sciences and Engineering Research Council of Canada (NSERC) for their financial support. Mrs M. Larouche, M. Ferland and J. Frenette (U.L.) are highly appreciated for their professional technical participation.

5.8 References

[1] **Ivanov, I., Stefanov, Y., Noncheva, Z., Petrova. M., Dobrev, Ts., Mirkova, L., Vermeersch R. and Demaerel, J.-P.**, Insoluble Anodes Used in Hydrometallurgy Part I. Corrosion Resistance of Lead and Lead Alloy Anodes Part II. Anodic Behaviour of Lead and Lead-Alloy Anodes, Hydrometallurgy, Vol. 57, 2000, pp. 109-124, 125-139.

[2] **Pavlov, D.,** The Lead-Acid Battery Lead Dioxide Active Mass: A Gel-Crystal System with Proton and Electron Conductivity, Journal of Electrochem. Society, Vol. 139, 1992, PP. 3075-3080.

[3] **Cifuentes, G., Cifuentes L. and Crisostomos, G.**, A Lead-Acid Battery Analogue to In Situ Anode Degradation in Copper Electrometallurgy, Corrosion sciences, Vol. 40, No. 2-3, 1998, PP. 225-234.

[4] **Nguyen, T. K. T.**, A Study of the Mechanism by which Cobalt Ions Minimize Corrosion of Lead Alloy Anodes during Electrowinning of Base Metal, Ph.D. Thesis, University of Queensland, Australia, 2007, PP. 2-11. 4-18.

[5] **Zerroual, L., Fitas, R., Djellouli B. and Chelali, N.**, Relationship Between Water Departure and Capacity Loss of α and β-PbO_2 Using An All Solid-State System: Estimation of Proton Diffusion Coefficient, Journal of power sources, Vol. 158, 2006, PP. 837-840.

[6] **Monahov, B., Pavlov D. and Petrov, D.**, Influence of Ag As Alloy Additive on the Oxygen Evolution Reaction on Pb/PbO_2 Electrode, Journal of Power Sources, Vol. 85, 2000, PP. 59-62.

[7] **Rerolle C. and Wiart, R.**, Kinetics of Oxygen Evolution on Pb and Pb-Ag Anodes During Zinc Electrowinning, Electrochimica Acta, Vol. 41, No. 7/8, 1996, PP. 1063-1069.

[8] **Krzewska, S., Pajdowski, L., Podsiadly, H., Podsiadly, J.**, Electrochemical Dtermination of Thiourea and Glue in the Industrial Copper Electrolyte, Metallurgical and Materials Transactions B, 1981, Vol. 15B, pp. 451-459.

[9] **ASTM. ASTM G5-94.** Standard Reference Test Method for Making Potentiostatic and Potentiodynamic Anodic Polarization Measurements, Philadelphia. PA, Vol. 03.02, 2001, PP. 58-69.

[10] **Lupi C. and Pilone, D.**, New Lead Alloy Anodes and Organic Depolariser Utilization in Zinc Electrowinning, Hydrometallurgy, Vol. 44, 1997, PP. 347-358.

[11] **Petrova, M., Noncheva, Z., Dobrev, Ts., Rashkov, St., Kounchev, N., Petrov, D., Vlaev, St., Mihnev, V., Zarev, S., Georgieva, L., Butilleni, D.**, Investigation of

the Process of Obtaining Plastic Treatment and Electrochemical Behaviour of Lead Alloys in Their Capacity As Anodes During the Electroextraction of Zinc I Behavior of Pb-Ag, Pb-Ca and Pb-Ag-Ca Alloys, Hydrometallurgy, Vol. 40, 1996, pp. 293-318.

CHAPTER 6

Influence of silver content on corrosion resistance of lead anodes during potential decay by electrochemical noise measurements

Influence of silver content on corrosion resistance of lead anodes during potential decay by electrochemical noise measurements

W. Zhang[1]*, A-M. Lafront[1], E. Ghali[1], and G. Houlachi[2]

1. Department of Mining, Metallurgical and Materials Engineering, Laval University, Quebec, QC, Canada, G1K 7P4.

* Corresponding author. Tel: (418) 656-7777, ext. 4871, Fax: (418) 656-5343.

wei.zhang.1@ulaval.ca

2. Hydro-Québec research institute, Shawinigan, QC, Canada, G9N 7N5.

This paper was published in METSOC, Development & Perfromance of Sulphur Capture Plants, Sudbury, Ontario, Canada, 48th Annual Conf. of Metallurgists of CIM (Aug. 23-26, 2009), pp. 101-115.

6. 1 Abstract

The potential decay of three lead anodes containing 0.5-0.7% Ag was investigated by electrochemical noise measurements "ENM" using the zero resistance ammeter set-up (ZRA) after polarization at 50 mA/cm^2 in zinc sulphate-manganese acid electrolyte at 38°C. Intense variations of potential and current values can be observed on the three specimens during the first hour of decay followed by constant current and very slight oscillations in potential values. A starting plateau and another typical one can be identified as function of their appearance and potential. Obtaining several parameters in situ by ENM is beneficial to characterize the decay from high positive to stationary open circuit potentials. The amplitude variation-oscillation of $\Delta E/\Delta t$ during the decay follows a certain pattern as a function of the plateau and decay time; however that of $\Delta I/\Delta t$ is almost similar from one level to another of which can suggest certain corrosion rate pattern. Analyses of time and frequency domain of ENM indicate that the corrosion rates of the typical plateau have certain different characteristics from that of the following region of potential decay. The typical plateau had higher corrosion rate "$1/R_n$", higher slope of ratio "S_r" than that in its following decay period. It is then assumed that the corrosion behaviour of lead anodes during their potential decay can be better understood by ENM studies.

6.2 Introduction

It is widely known that lead anodes used in electrowinning can corrode when the current is switched on after an interruption. This phenomenon can be explained in terms of the loss of the anode passivity that takes place in absence of the applied current. Electrochemical (anodic and cathodic) and chemical reactions take place spontaneously on the anode surface, leading to lead corrosion and dissolution of the lead (IV) dioxide layer and this can be inspired partially from the literature concerning lead-acid battery [1]. The lead-acid battery derives its power from the electrochemical energy released during the conversion of PbO_2 to $PbSO_4$ on the positive plate and Pb to $PbSO_4$ on the negative plate. In general, electrochemically prepared lead dioxides are non-stoichiometric and

exhibit high electrochemical activity, whereas chemical forms are nearly stoichiometric and are reputed to be inactive [2].

The potential decay following polarization for lead anode for zinc electrowinning could be assimilated to the discharge of positive lead/acid battery plate. During the decay, there are several reactions that will form the plateau on the potential decay curve. First, the PbO_2 formed by the polarization for lead anode immediately reacts to form lead (II) sulfate: $PbO_2 + 4H^+ + SO_4^{2-} + 2e^- \rightarrow PbSO_4 + 2H_2O$ [3]. At the end of discharge, $PbSO_4$ will block further discharge of PbO, and the remaining PbO_2 will be electrochemically inactive, i.e., $PbSO_4[PbO_2]$ is formed, and the potential will fall [3]. Second, the remaining PbO_2 will be reduced to Pb_3O_4 or PbOOH and PbOOH can be reduced to $PbSO_4$ [4, 5].

On polarization of lead electrode during electrowinning, PbO_2 is formed on the anode in H_2SO_4 solution at the potentials more than positive 1.0 V (vs. Hg/Hg_2SO_4 electrode), oxygen is evolved as a result of the reaction: $H_2O \rightarrow 1/2O_2 + 2H^+ + 2e^-$. The rate of O_2 evolution depends on the potential, the temperature and the nature and concentration of alloying additives used [6]. As the oxide phase stays in direct contact with concentrated sulfuric acid since the oxide film is porous, the metallic lead is also in contact with acid and dissolves. Solid lead sulfate has been shown to form during discharge of a battery. The following reaction spontaneously takes place at pores: $Pb + SO_4^{2-} \rightarrow PbSO_4(s) + 2e^-$ [1].

EN measurements have been widely used for the characterization and monitoring of corrosion processes during the last 20 years including the analysis of different types of systems [7]. Electrochemical noise technique can be used for monitoring without disturbing the system under investigation. In addition, it is more sensitive to localized corrosion processes than some traditional techniques, which produce little information. In the literature, two methods for the mathematical treatment of electrochemical noise have been frequently implemented: the statistical method in time domain and the spectral method in frequency domain. Last, EN can provide more information of corrosion than conventional technique [8].

The analysis of electrochemical noise data can be performed in both time and frequency domains. In the time domain the most interesting parameter is the noise resistance, R_n, which can be associated with the polarization resistance, R_p [7]. In the frequency domain the spectral noise resistance, R_{sn}, defined as the square-root of the ratio of power spectral densities (PSD) of potential and current fluctuations can be compared with the magnitude of the electrochemical impedance at the same frequency [9]. The spectral analysis method is typically used to show noise signals as power spectral density (PSD) in the frequency domain [10, 11]. In recent years, the theory of electrochemical noise has been further developed to consider factors such as methods for trend removal, different transient shapes and electrode asymmetry, detection of localised and pitting corrosion, and partition of current fluctuations between different electrodes [11].

The corrosion products from lead anode in the zinc electrowinning process influence the quality of zinc deposit. The aim of this work is to use the electrochemical noise to characterize the electrochemical reaction of the lead anode and the influence of silver on the reduction and oxidation reactions on the surface of the lead anode.

6.3 Experimental conditions

6.3.1 Electrochemical set-up

Electrochemical noise measurements were performed using a set-up in electrochemical noise (EN) mode of zero resistance ammeters (ZRA). Two identical specimens were used as the working electrode and a saturated silver chloride electrode as the reference electrode Ag, $AgCl/KCl_{sat}$ (0.202V/SHE), respectively. The electrochemical current noise was measured as the galvanic coupling current between two identical working electrodes (WE) kept at the same potential. A potentiostat GAMRY model PC4/750 linked to a personal computer was used to log potential; and current values sampled at a scan rate of 10 Hz for 102.4 s giving a total of 1024 readings. EN experiments and data treatment were calculated using the GAMRY ESA400 software [7]. The noise data were collected for 16 h immersion of the working electrodes by ENM in the solution following 24 h polarization at CD = 50 mA/cm^2.

Noise data were also transformed into the frequency domain using Fast Fourier Transformed (FFT) algorithm and presented as power spectral density (PSD) calculated in a frequency domain from 5×10^{-2} to 5 Hz.

6.3.2 Material and electrolyte

800 ml of electrolyte containing 60 g/dm³ of Zn^{2+}($ZnSO_4 \cdot 7H_2O$), 180 g/dm³ of H_2SO_4, 8 g/dm³ of Mn^{2+} ($MnSO_4 \cdot H_2O$), 250 mg/dm³ of Cl^- and 3 mg/dm³ of Glue was heated by a flow of thermostated water in the double wall (38 ± 0.5°C). The electrolyte was magnetically stirred at 412 rpm during the experiments by a stirrer (4 cm long 1 cm diameter).

The chemical composition of 3 laminated Pb-Ag anodes used in this work is given in Table 6.1. At least 45 elements were analysed by Fluorescence X and only the elements where the %wt is higher than 0.05% are given. Ag, Ca and Fe contents were analysed quantitatively by atomic absorption technique.

Table 6.1 – Chemical composition (wt%) of the 3 anodes

Anode	Ag (wt %)	Fe (wt %)	Ca (wt %)	Al (wt %)	Mn (wt %)	S (wt %)	Si (wt %)	Ti (wt %)	Zr (wt %)	Pb (wt %)
0.5%Ag	0.516	0.007	< 0.001	0.29	< 0.05	0.13	1.4	< 0.05	0.21	bal.
0.6%Ag	0.600	0.013	< 0.001	< 0.05	< 0.05	0.08	0.3	0.18	0.22	bal.
0.7%Ag	0.672	0.009	< 0.001	< 0.05	< 0.05	0.07	0.07	0.25	0.19	bal.

The Pb-Ag alloy anodes plates were cut into small pieces of 1×1×1 cm then connected with a plastic isolated copper wire and cast in acrylic resin leaving 1 cm² exposed area surface. The polished surfaces of anodes were washed with alcohol and dried immediately before being introduced into the electrolytic cell. The polished anode surfaces were obtained ground most of the time with 600 soft grid SiC paper with ethanol to avoid the inclusion of particles into electrodes.

6.4 Results and discussion

6.4.1 Potential and current transient

6.4.1.1 Potential decay by ZRA during 16 h discharge

The potential decay was investigated by electrochemical noise "ENM" using the zero resistance ammeter set-up (ZRA). Figure 6.1 shows typical potential decay and current transient curves of three lead anodes containing 0.5-0.7% Ag for 16 h after polarization at 50 mA/cm^2 in acid zinc sulphate-manganese electrolyte at 38 °C. The measurements of the potential decay of the three Ag lead anodes were carried out by ENM. Generally, the reproducibility of the potential measurements during the decay was ~ ±5 mV for duplicates or triplicates. The potential evolution depends on the alloy and shows different stages. For example, considering the potential decay of 0.5% Ag-Pb anode, two plateaux "ab" and "de", quick decay "bc" and slow decay "cd" can be observed.

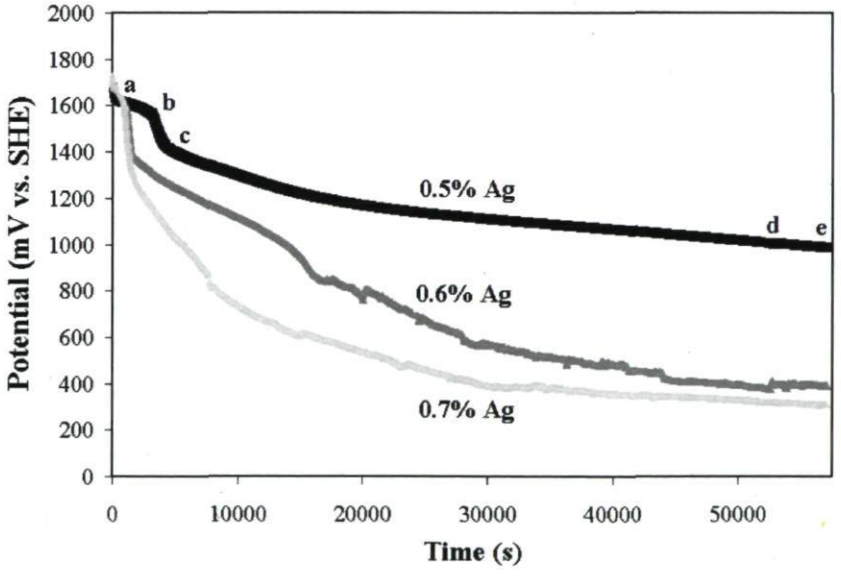

Figure 6.1: Potential decay transient curves of three lead anode specimens 0.5% Ag, 0.6% Ag and 0.7% Ag representing the trend during 16 h (57600 s) immersion time respectively following 16 h polarization at 50 mA/cm^2 in zinc electrolyte solution and 38 °C.

Figure 6.1 shows that anode 0.5% Ag lead anode had the longest first plateau at a potential ~ 1650 mV (SHE) if compared to the two other anodes: 0.6% and 0.7% Ag lead

anodes. This plateau shows a spontaneous transformation on lead dioxide into lead sulphate because thermodynamically lead dioxide is unstable on the surface of lead in the sulphuric acid solution [1]. After 16 h decay, it was found that 0.7% Ag lead anode had the lowest potential (the most active) followed by 0.6%, 0.5% Ag lead anodes. The potential of 0.6%, 0.7% Ag lead anode at the end of 16 h decay is around 400 and 300 mV/SHE which can correspond to the total disappearance of corrosion products and stabilization by $PbSO_4$, while the potential of 0.5% Ag lead anode at the end of 16 h decay is around 800 mV which corresponds very probably to the appearance of $Pb(OH)_2$ [1]. More corrosion products can be observed on the surface of the 0.5% Pb anode during 16 h decay, and its potential dropped slowly during decay, the potential at the end of 16 h decay was kept at 1.0 V (SHE) ~ 600 mV higher than that of the other anodes with higher silver content. Higher silver in 0.7% Ag lead anode resulted in less corrosion products during polarization and the potential was decreased quicker and reached 0.3 V (SHE) at the end of 16 h decay. There may be also a certain difference in the type or microstructure of these components.

EN data analysis in the time domain involves the calculation of the noise resistance R_n which was determined in the time domain, as the ratio of the standard deviation of potential noise, σ_v, to that of current noise, σ_I, ($R_n = \sigma_v / \sigma_I$). This parameter can be used to calculate the corrosion rate, assuming that it is equivalent to the polarization resistance R_p [11]. To obtain the detailed results of the potential decay of the lead anodes containing 0.5%, 0.6%, and 0.7% Ag, the potential decay and $1/R_n$ with time were plotted together. Figure 6.2 shows a typical example of potential decay and corrosion rate with time ($1/R_n$) of 0.7% Ag lead anode. The potential decay behaviours of 0.6% and 0.7% Ag lead anodes were very similar to each other but different from that of 0.5% Ag lead anode.

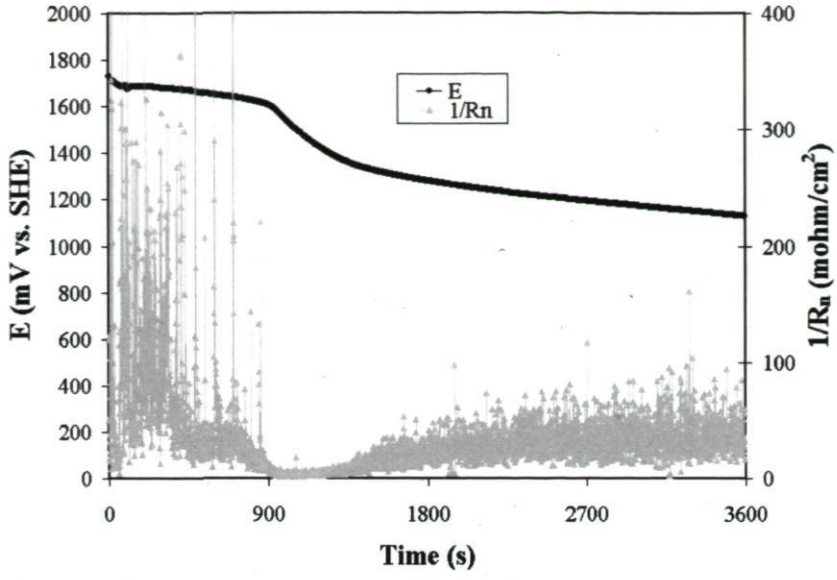

Figure 6.2 Electrochemical noise data of potential and $1/R_n$ with time of 0.7% Ag lead anode during first 3600 s (1 h) immersion period following 16 h polarization at 50 mA/cm^2 in zinc electrolyte solution at 38°C.

Figure 6.2 shows that the corrosion rate ($1/R_n$) is the highest at the typical long plateau, and then it is the lowest at the quick decay region, after the quick decay, the corrosion rate ($1/R_n$) increased again, so combining the potential decay with corrosion rate ($1/R_n$), it is very easy to identify the plateau. It was found that there is higher corrosion rate ($1/R_n$) in the place of plateau ($PbO_2 \rightarrow PbSO_4$, etc.) than that in the place of decay.

Also, it was found in Figure 6.2, after a typical plateau, the potential drops sharply, and the corrosion rate of the potential decay becomes very low, then after this quick decay, the corrosion rate becomes high again. The possible reasons are that the surface of the Ag lead anode during the quick potential decay was covered by $PbSO_4$ or $PbSO_4(PbO_2)$ and thus increasing corrosion resistance, but after this quick decay, the lead sulphate deposit can be cracked because of its high important volume compared to that of PbO_2. It is also possible to reduce PbO_2 in presence of H^+ ions to form PbO that can be hydrated: $PbO + H_2O \rightarrow Pb(OH)_2$ [4].

6.4.1.2 Corrosion rate ($1/R_n$) with time

Figure 6.3 shows the inverse of R_n that is proportional to the corrosion rate which was calculated as the average values of 1 h based on every second record.

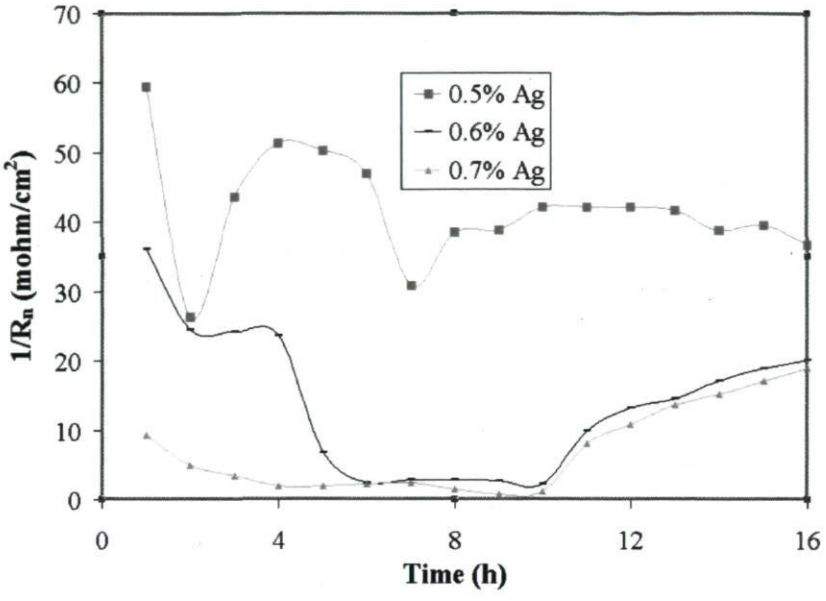

Figure 6.3: Evolution of corrosion rate "$1/R_n$" of lead anodes containing 0.5%, 0.6%, and 0.7% Ag as recorded during 16 h immersion period in the zinc electrolyte.

It was found that the lead anode containing lowest silver 0.5% Ag had the highest corrosion rate among the three samples; while lead anode containing highest silver had the lowest corrosion among the three specimens. It was found that lead anodes 0.5% Ag had one peak from 3 to 7 h that should correspond to the approximately plateau of potential decay at the third level.

Also, it was found that 0.6% and 0.7% Ag lead anodes had higher corrosion rates after 10 h than that at 5-9 h, this can be explained by less coverage products, alteration and disintegration of corrosion products, for example: the passive film ($PbSO_4$ and $MnSO_4$, MnO_2) on the surface of the two specimens was broken and the fresh metal surface appeared, so the corrosion rates of the fresh surfaces were higher than before. This is very possibly accompanied by the change of the reduction reaction to that of hydrogen ions in presence of the solution saturated by atmospheric oxygen on the cathodic sites of the lead surface instead of PbO_2 reduction.

The corrosion rate of 0.6% Ag lead anode is much higher than that of 0.7% Ag lead anode for the first 5 h. However, the corrosion rates of these two anodes are almost the same from 6 h to the end since the surface of the two samples were covered by $PbSO_4$ in a similar way very possibly.

To understand the characteristics of the 16 h decay, the period can be divided to four levels for the three specimens since other authors have suggested different reactions corresponding to different periods of the decay [1-5], it can be observed in Figures 6.1 and 6.2 that each level has different behaviour, the range of the four levels is as follows: level 1: 1.72 – 1.66 V/SHE, level 2: 1.66 – 1.55 V/SHE, level 3: 1.55 – 0.9 V/SHE, level 4: 0.9 – 0.3 V/SHE.

6.4.2 Fluctuations of the potential and current noise during the 16 h decay

As function of time, the potential and current noise measurements were recorded simultaneously and the data were analysed in time. During the immersion period, some typical transients were observed and various transients indicate different corrosion mechanisms [12]. Examples of typical raw data obtained after trend removal are shown in Figures 6.4 and 6.5.

It can be observed that the scale of potential and current is smaller than that of Figure 6.1 since the dc trend was removed [9]. 20 s domain can be considered for each range of potential and current fluctuations. Concerning the potential and current transients of 0.7% Ag lead anode, it can be seen that the high amplitude of fluctuations of potential and current are the greatest for 0.7% Ag lead anode in the zinc electrolyte at the first level of potentials, and that active potentials lead to higher current densities. At 340 s (first level of potentials), a sharp drop down of potential has been observed, accompanied by a sharp rise in current at the same time, the high amplitude variation of potential and current suggested specially metastable pitting for 0.7% Ag lead anode [10, 11]. However, it is very plausible that it is caused by oxygen bubble evolution at the high level of potentials after the reaction: $2H_2O \rightarrow 4H^+ + O_2 + 4e^-$. Visual observation of the tested sample showed the appearance of oxygen bubble on the surface of the electrode during especially the 1st level of potentials.

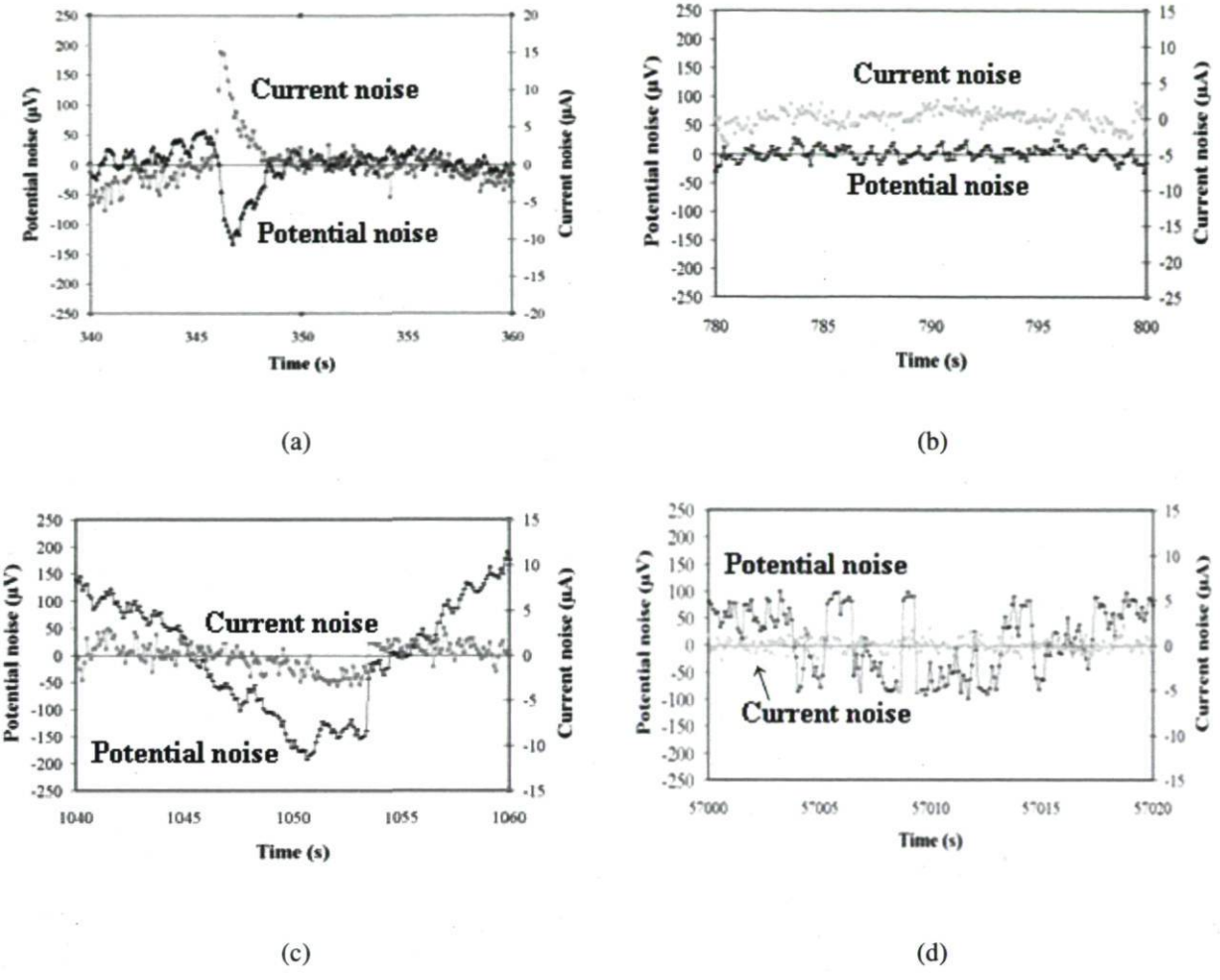

Figure 6.4: 20 s of the fluctuations of potential and current noise of 0.7% Ag lead anode at (a) 1st, (b) 2nd, (c) 3rd, and (d) 4th level.

For the other levels (780 s, 1040 s, 57000 s), the potential-time record starting at 780 s showed a very frequent repetition rates of potential fluctuations with equal and low amplitude of the order of 40 μV. The potential-time record of 1040 s showed high amplitude of potential variation of big peak at 1040 s (quick decay of the third level). The 1040 s fluctuation of potential is much larger than that at 780 s (second level) and 57000 s (plateau of fourth level), meaning that quick decay had highest variation of the potential value at this time (1040 s). The amplitudes of potential variation of the typical plateau (780 s) were always from -20 to 20 μV, and lowest among the four levels. Also, potential-time of 57000 s (fourth level of potentials) showed several high amplitude and high frequency oscillations with several peak transients; and the transients were

associated to localised film breakdown repair events over the metal surface [13]. This shows that the difference in amplitude variations of potential suggested differences in corrosion mechanism. Also, the amplitudes of current variation of the three levels are small and stable. The current-time record of 57000 s showed equal and low amplitude of current fluctuation, it means possibly that a white noise pattern was observed, indicating passive state [12]. Fluctuations of potential and current seem to be independent.

Figure 6.5 shows 20 s of the fluctuation of potential and current noise of 0.5% Ag lead anode at the second and third levels since the decay of 0.5% Ag lead anode did not show the first and fourth levels.

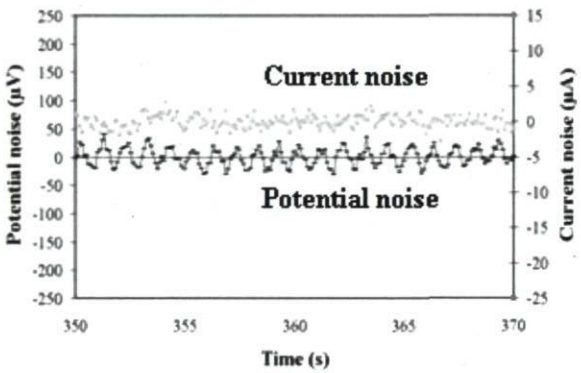

(a)

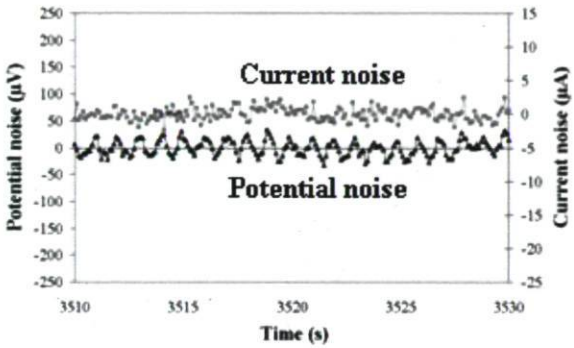

(b)

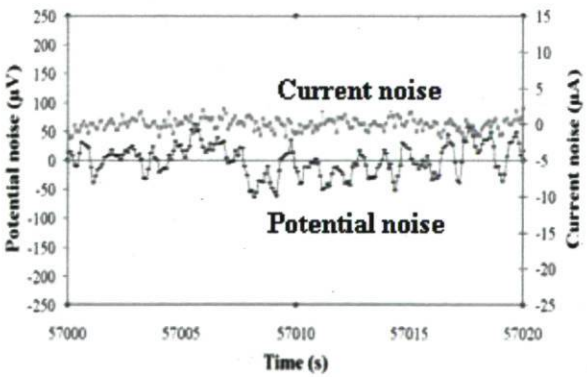

(c)

Figure 6.5: 20 s of the fluctuations of potential and current noise of 0.5% Ag lead anode concerning the 2nd level (a); the quick decay at the beginning (b) and at the end (c) of the 3rd level in the zinc electrolyte at 38 ^{O}C.

The potential variation of 0.5% Ag lead anode at the potential value of 1.62 V/ SHE was considered; a region of 20 s at the 350 s of 0.5% Ag lead anode in Figure 6.5 (a) (second level) is compared to that of the same potential of 0.7% Ag lead anode at 780 s. Effectively, the potential of 0.5% Ag lead anode has more frequent repetition of fluctuations with smoother and equal amplitudes than that of 0.7% Ag lead anode. It is very interesting to find that there is a smooth fluctuation of potential noise at the potential value of 1.50 V/SHE presenting the quick decay at the beginning of the 3rd level (Figure 6.5 (b)), this can be compared to that of the same potential of 0.7% Ag lead anode at 1040 s, but the potential of 0.7% Ag lead anode (Figure 6.4 (c)) has bigger peak with high amplitude potential variation. Generally, the 0.5% Ag lead anode containing lower silver had higher overpotentials for the electrochemical reactions at 350 s at the second level than that of 0.7% Ag content. The corrosion rate of 0.5% Ag lead anode is higher than that of 0.7% due to the important quantities of corrosion products that gives the longest reduction of lead oxide plateau at level two. However, the current variations of current with time ($\Delta I/\Delta t$) of 0.5% Ag and 0.7% Ag lead anodes are close.

Figure 6.5 (c) shows the fluctuations of potential and current of 0.5% Ag lead anode at the end of decay (57000 s). The potential-time record shows that the amplitude of the potential fluctuation of 0.5% Ag lead anode of the order of 10 μV less than that of 0.7% Ag lead anode at the end of decay (57000 s) of the order of 20 μV. It was also found that several oscillation peaks are smaller than that of 0.7% Ag lead anode at 57000 s. The smaller peak transients are associated to much less pits on the surface of 0.5% Ag lead anode than 0.7% Ag lead anode. It can be admitted then that the stationary corrosion potential of 0.5% Ag-Pb anodes shows higher corrosion rate than that of 0.7% Ag anode ($1/R_n$ = ~ 42 mohm and ~13 mohm corrosion rate, respectively, (Figure 6.2). The frequent galvanic cells and less overpotentials for hydrogen cathodic reactions on silver components of 0.7% Ag-Pb could be the reason for the more intense localized corrosion of this anode. Visual examination of the surface did not distinguish the localized corrosion morphology of 0.7% Ag lead anode, very possibly because 16 h period of decay is not long enough. However, corrosion of 0.5% Ag anodes was in presence of more important and thicker corrosion products on the surface.

Comparison of the fluctuations of potential and current of the three specimens showed that the amplitude variation-oscillation of $\Delta E/\Delta t$ during the decay follows a certain pattern as a function of the plateau and decay time; however that of $\Delta I/\Delta t$ is almost similar from one level to another in spite of the difference in the current density values, except for the first level of the anode 0.7% Ag.

6.4.3 Frequency analysis of 0.5% and 0.7% Ag anode during the 16 h decay

The PSD plots and the spectral noise plots were fitted to:

$\log PSD_V = A_V + S_V \log f$, $\log PSD_I = A_I + S_I \log f$, $A_r = A_v - A_i$, $S_r = S_v - S_i$

where S_v and A_v, S_i and A_i, S_r and A_r are respectively the slope and the noise intensity of potential, current and ratio of PSD plots [7].

6.4.3.1 Frequency analysis of 0.7% Ag lead anode at the four levels

The data of PSD analysis of 0.7% Ag lead anode at the four levels are shown in Table 6.2 and the PSD plot current of 0.7% Ag lead anode is shown in Figure 6.6 (a). For each level, one point is chosen for first, second, third and fourth levels, 340, 780, 1040 and 57000 s points respectively; around this point, three ranges (20 s) had been analysed, and the average values are considered.

Table 6.2 - Average of 20 s of the chose points of 0.7% Ag lead anode observed at the four levels

Frequency parameter	First level 340 s	Second level 780 s (~typical plateau)	Third level 1040 s (quick decay)	Fourth level 57000 s
E (V vs. SHE)	1.68	1.62	1.50	0.31
I (μA)	-810	43.1	36.9	89.4
$1/R_n$(mohm)	156	17.9	5.1	19.9
R_n (ohm)	13	63	245	65
A_v	-8.86(±0.09)	-11.14(±0.08)	*	-7.78(±0.07)
A_i	-10.35(±0.1)	-13.00(±0.1)		-13.12(±0.11)
A_r	1.49(±0.07)	1.86(±0.06)		5.34(±0.08)
S_v	-3.53(±0.05)	-1.05(±0.05)		-1.11(±0.04)
S_i	-3.01(±0.04)	-1.06(±0.04)		-0.70(±0.05)
S_r	-0.52(±0.04)	0.01(±0.05)		-0.61(±0.03)

* Trending is difficult because of strong drift due to potential variation.

Table 6.2 shows that the parameters of time domain and PSD of potential, current and ratio. It is interesting to compare the $1/R_n$ of the four levels from the parameters of time domain; the $1/R_n$ of the point of 340 s is around 30 times higher than that of 1040 s. The possible reason is that amount of PbO_2 was reduced to $PbSO_4$ at 340 s, and the Pilling – Bedworth molar volume ratio of $PbSO_4/PbO_2$ = 1.9: 1 [14], and so a large of fresh Pb base surface appeared showing a very high corrosion rate at 210 s.

Table 6.2 shows that the absolute magnitudes of PSD current and potential slopes are large around (S_v -3.5, S_i -3.0) at 340 s (first level) if compared to that of other levels. As suggested by Cheng et al. and other authors, it is very possible to have localised corrosion if the absolute magnitudes of S and S_i are around 3.0 [9, 10, 11]. So this can be due possibly to metastable pitting or oxygen evolution. More silver content (0.7% Ag) in the lead anode resulted in less PbO_2 formation and more silver content lead to more cathodic sites for the attack by chloride ion in the zinc electrolyte or to much more quick dissolution of formed basic lead compounds at 340 s. Also, it was found that the absolute magnitude of PSD current slopes of 0.7% Ag lead anode at the fourth levels (57000 s) was the lowest one showing possibly the active corrosion state of the high silver anode at open circuit potential. The first and fourth levels show the absolute magnitudes of PSD characteristic of localized corrosion while that of the second level are specific possibly for uniform corrosion since the S_r is about 0 [15].

The intensity of PSD current of the first level (-10.4) is higher than that of the other two levels (-13.0, -13.1) respectively), it is then evident that the first level is more active than the other levels. Also, the intensity of PSD ratio "A_r" increased from first level to second and then to fourth.

6.4.3.2 Frequency analysis of the typical plateau and its following decay of 0.5% Ag lead anodes

Table 6.3 shows the average values of electrochemical noise data in the frequency domain of the typical plateau, the following decay and at the end of 16 h decay of the 0.5% Ag lead anodes in zinc electrolyte, and the PSD plot current of 0.7% Ag lead anode is shown in Figure 6.6 (a).

Table 6.3 shows that the intensities of the PSD potential and current of quick decay are higher than that of the following plateau; however, the A_r of the plateau is higher than that of the following quick decay. Also, the absolute magnitude of the slopes of PSD potential and current of the quick decay around (-0.8, -0.7 respectively) were higher than that of the following typical plateau around (-0.4, -0.6 respectively), and the typical plateau had higher slope ratio "S_r" than that observed in the following period. It was clear that the corrosion rate ($1/R_n$) of the plateau was much higher than that of the following decay.

Table 6.3 - Average of 20 s of the typical plateaux and their following decay of 0.5% Ag lead anode

Frequency Parameter	Second level 350 s (typical plateau)	Third level 3510 s (quick decay)	Third level 57000 s
E (V vs. SHE)	1.62	1.50	0.99
I (μA)	187	71.5	82.3
$1/R_n$(mohm)	42.7	20.2	43.9
R_n(ohm)	31.6	55.5	26.6
A_v	-11.17(±0.05)	-11.09(±0.04)	-10.28(±0.06)
A_i	-12.73(±0.05)	-12.56(±0.05)	-13.07(±0.05)
A_r	1.56(±0.02)	1.47(±0.06)	2.79(±0.04)
S_v	-0.42(±0.03)	-0.83(±0.03)	-1.62(±0.03)
S_i	-0.58(±0.04)	-0.71(±0.07)	-0.67(±0.03)
S_r	0.16(±0.03)	-0.11(±0.06)	-0.95(±0.02)

Also, Table 6.3 shows that the absolute magnitude of PSD potential at the end of the third level is higher than that of the quick decay and the typical plateau, and the absolute S_r at the end of the third level (57000 s) is much higher than that of quick decay and typical plateau. It means that the 0.5% Ag lead anode became active at the end of the decay, the potential may drop down and go to 4^{th} level if the decay time is longer than 16 h.

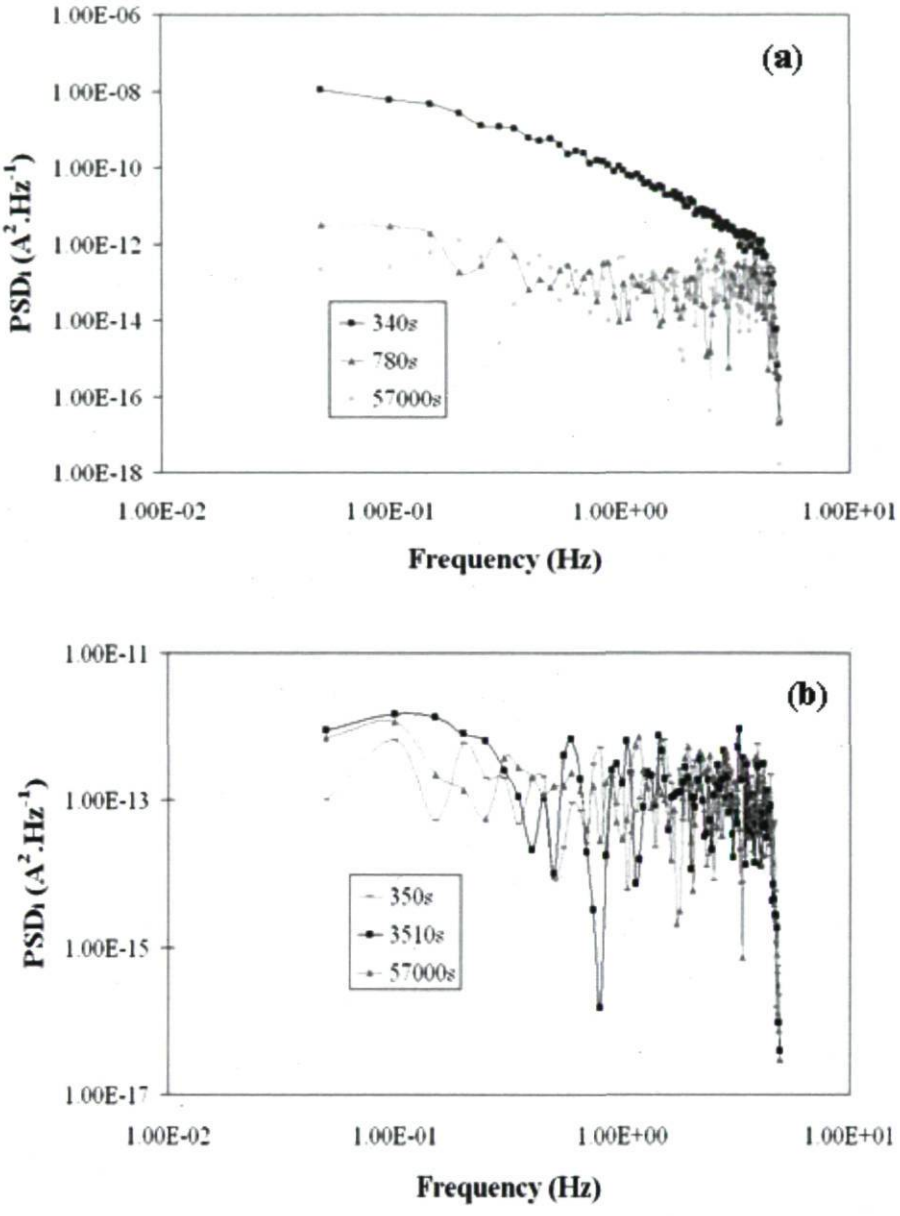

Figure 6.6: PSD_i plots for (a) 0.7% Ag for 20 s of the three levels observed at 340 (1st level), 780 (2nd level), 57000 s (3rd level) and (b) 0.5% Ag lead anode for 20 s of the two levels observed at 350 s (2nd level), 3510 s, 57000 s (3rd level) in zinc electrolyte.

Comparison of data of frequency analysis of 0.5% and 0.7% Ag lead anodes from Tables 6.2 and 6.3, it was also found that the current density of the typical plateau of the lead anode containing 0.5% Ag was higher than that containing 0.7% Ag. The ratio intensity of the typical plateau of the lead anode containing 0.7% Ag was higher than that containing 0.5% Ag. Comparison of the slopes of PSD of the typical plateaux of the two

specimens, it was also found that the absolute magnitudes of the slopes of current and potential PSD of 0.5% Ag lead anode are also lower than that of 0.7% Ag lead anode. It means that 0.5% Ag lead anode should be possible to enter into the passive state [13], while 0.7% Ag lead anode is much quicker to potential and current decay than that of 0.5% Ag lead anode. However, the absolute magnitudes of the PSD potential "S_v" of 0.5% Ag lead anode at the end of 16 h decay (57000 s) are higher than that of 0.7% Ag lead anode, while the values of the PSD current "S_i" of 0.5% is slightly lower than that of 0.7% Ag lead anode. This means that 0.5% Ag lead anode can show localised type of corrosion as that of 0.7% Ag lead anode at the end of 16 h decay.

The absolute magnitudes of PSD slopes of the two Ag lead anodes can correspond to different corrosion reactions and/or corrosion types. Comparing the parameters of the electrochemical noise, it is then found that electrochemical noise is a good technique to investigate the influence of silver on the corrosion rate of lead anodes.

6.4.4 Four levels during the 16 h potential decay

The characteristics of the four levels of the three samples are described in Table 6.4. This is based on the above results.

The three specimens (0.5%, 0.6%, 0.7% Ag lead anodes) at the four levels during 16 h decay in zinc electrolyte had different electrochemical reactions. Some authors, for example: S.C. Barnes and R.T. Mathieson (1963) [4], J. Garche et al. (1990) [3], and G. Cifuentes et al. (1998) [1] found that certain electrochemical reactions that can correspond to the potential decay at each level, and the results are shown in the following. All E° standard potential values at 25°C and at atmospheric pressure are given for reduction reaction for the sake of comparison.

Table 6.4 - The characteristics of the four levels of the three samples (0.5%, 0.6% and 0.7% Ag lead anodes) during 16 h decay in the zinc electrolyte at 38°C.

Potential level (times)	Potential values (V vs. SHE)	Description			$1/R_n$ (mohm.cm^{-2})			Morphology
		0.5% Ag	0.6% Ag	0.7% Ag	0.5% Ag	0.6% Ag	0.7% Ag	
Level 1 after 100s transfer	1.72-1.66	No observed	Short plateau (20s)	Short plateau (30s)	/	41.5±0.2	9.8±0.3	O_2 evolution, small cracks in coating
Level 2	1.66-1.55	Long plateau	Long plateau and short quick decay	Long plateau + Quick decay	48.2±0.3	11.2±0.3	8.1±0.4	Big cracks in coating, more $PbSO_4$
Level 3	1.55-0.9	Limited to 500 mV Quick + slow decay +OCP (1.0V vs. SHE)	Quick decay +slow decay	Quick decay +slow decay	42.1±0.4	7.8±0.2	4.3±0.3	Corrosion products Pb_3O_4, PbO(OH), $PbSO_4$
Level 4	0.9-0.3	Not observed	Plateau stationary +OCP	Plateau stationary +OCP	/	13.5±0.4	12.8±0.3	Black $PbSO_4$ layer

The first level: from the potential 1.72 to 1.66 V (SHE), the cathodic reaction is: $PbO_2 + SO_4^{2-} + 4H^+ + 2e^- \rightarrow PbSO_4 + 2H_2O$ $E^\circ = 1.712$ V (SHE) [4]. The dominating anodic reaction is: $H_2O \rightarrow 2H^+ + 1/2O_2 + 2e^-$ $E^\circ = 1.23$ V (SHE).

The second level: from the potential 1.66 to 1.55 V (SHE), the cathodic reaction is: $PbO_2 + HSO_4^- + 3H^+ + 2e^- \rightarrow PbSO_4 + 2H_2O$, $E^\circ = 1.655$ V (SHE) [4]. The anodic reaction is: $Pb + SO_4^- \rightarrow PbSO_4(s) + 2e^-$ [1]. It is very interesting to note that the potential dropped down sharply following the typical plateau in the second level for the three specimens (0.5%, 0.6%, 0.7% Ag lead anodes). This drop in the same level and the different jumps from level to level can be caused by:

- Disappearance of lead dioxide for example and/or change in its microstructure or its transfer to other solid intermediates, leading then to a change in the reduction

reaction. Also, replacement of the oxygen evolution reaction should occur to another oxidation one more favourable at lower potentials.

- There are three types of possible overpotentials (transfer of the electron, concentration and ohmic resistance) that are characteristic of the different oxidation and reduction reactions and products. This should be different at the start especially in the first 10-20 minutes as compared to that after 16 h of decay because of the difference in species close to the anode at the moment of decay from that changing at the open circuit potential as function of time. Diffusion of species can change the properties of the interface as the variation of pH or the activity (concentration) of soluble reactants or products after Nernst equation and thermodynamic considerations [16].

The third level: from the potential 1.55 to 0.9 V (SHE), the cathodic reaction is: $3PbO_2 + 4H^+ + 4e^- \rightarrow Pb_3O_4 + 2H_2O$ $E^\circ = 1.12$ V (SHE) [16] or $PbO_2 + H^+ + e^- \rightarrow PbO(OH)$ [5]. The anodic reaction is: $Pb + SO_4^{2-} \rightarrow PbSO_4(s) + 2e^-$ [1]. The following cathodic reaction: $2PbO_2 + HSO_4^- + 5H^+ + 4e^- \rightarrow PbO{\bullet}PbSO_4 + 3H_2O$, $E^\circ = 1.375$ V (SHE) can be the main one in this level only when the $PbO{\bullet}PbSO_4$ is stable at relatively high pH values that are reached temporarily at the interface after electrolysis and in absence of strong agitation (pH 8-9 at standard conditions) [3].

The fourth level: from the potential 0.9 to 0.3 V (SHE), the cathodic reaction is the conventional cathodic reaction in presence of oxygen. Also, $PbO(OH) + H^+ + e^- \rightarrow Pb(OH)_2$ [5] can occur since it is more exothermic than hydrogen evolution and this can be followed by the chemical reaction: $Pb(OH)_2 + H_2SO_4 \rightarrow PbSO_4 + 2H_2O$.

The main cathodic and anodic reactions of four levels of the three samples (0.5%, 0.6%, 0.7% Ag lead anodes) in the zinc electrolyte during 16 h are plotted in Figure 6.7. It should be added that the different levels of standard potential E^o of the four mentioned reduction potentials confirm the existence of these consecutive four stages or levels of reduction. This is also supported by the fact that after anodic polarization, the SO_4^{2-} is the abundant ion at the metal interface during the 1st level while the hydrogen ion arrives to the decayed electrode late at the 3rd level because it is mainly controlled by diffusion.

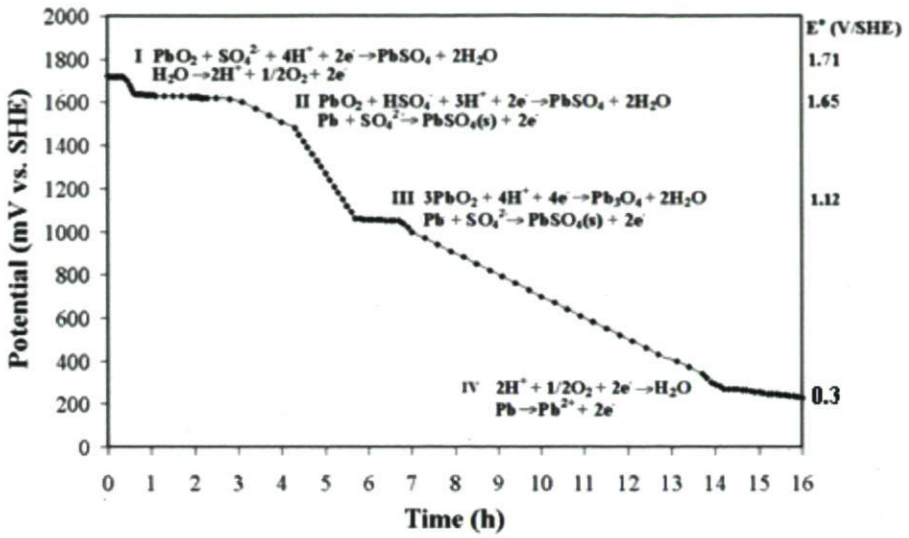

Figure 6.7: The main thermodynamic reduction and oxidation reactions at every stage of the four potential levels during 16 h inspired from the behaviour of the three Ag-Pb anodes. The reduction potentials (E°) are given for every level at standard conditions.

6.5 Conclusions

It has been observed in this study that during the frequent decay periods of the anodes in the industry (2 h/every week, and 16 h/every month generally), the first hour and even the first 15 minutes (for 0.6 and 0.7% Ag of lead anodes) constitutes the most active reduction of the formed PbO_2 during polarization. A theoretical and laboratory scale experimental approach of potential decay of Ag lead anodes during these 16 h suggested the following:

- The main reduction and oxidation reactions for four identified stages can be suggested during the 16 h decay based on thermodynamic and past electrochemical considerations of discharge of lead battery electrodes. The different levels of E° of the four mentioned reduction and oxidation potentials confirm the existence of these consecutive four stages or levels of decay (discharge and/or corrosion).
- Different fluctuations of potential pattern referred to different corrosion types. The amplitude variation-oscillation of $\Delta E/\Delta t$ during the decay follows a certain pattern as a function of the plateau, decay time; however the $\Delta I/\Delta t$ is almost similar from one

level to another in spite of the difference in the current density absolute values, except for the first level.

- The absolute magnitude of power spectral density "PSD" slopes of the three Ag lead anodes can correspond to different corrosion reactions and/or corrosion types. Comparing the parameters of the electrochemical noise, it is then found that electrochemical noise is a good technique to investigate the influence of silver on the corrosion rate of lead anodes. 0.5% Ag lead anode shows uniform corrosion at the beginning (first 1 h) and localised corrosion at the end of the 16 h decay, while 0.7% Ag lead anode shows high localised corrosion at the beginning followed possibly by uniform corrosion and then back to localised corrosion.
- It was found that the typical plateau had higher corrosion rate "$1/R_n$" and higher slope ratio "S_r" than that obtained during the following decay period. PSD can be used to determine the corrosion type during the decay.
- There is enough evidence from electrochemical noise measurements of existing difference in corrosion performance between the 0.5% and 0.7% Ag-Pb anodes. It can be admitted that 0.5% Ag-Pb anode has more corrosion products during polarization or electrolysis and this is shown by important plateau at the average value of 1.61 V/SHE for the longest time (45 min); while 0.7% Ag lead anode showed more active galvanic cells at the beginning of decay (11-16 h of the decay) that can correspond to more localised corrosion because of more abundant silver content.
- The characteristics of the four levels show that each level has different corrosion products and morphology.

6.6 Acknowledgements

The authors are grateful to the Hydro-Quebec, CEZ and the Natural Sciences and Engineering Research Council of Canada (NSERC) for their financial support.

6.7 References

[1] **Cifuentes, G., Cifuentes L. and Crisostomo, G.**, A Lead-Acid Battery Analogue to In Situ Anode Degradation in Copper Electrometallurgy, corrosion science, Vol 40, No. 2-3, 1998, pp. 225-234.

[2] **Zerroual, L., Fitas, R., Djellouli B. and Chelai, N.**, Relationship between Water Depature and Capacity Loss of α and β-PbO_2 Using An All Solid-State System: Estimation of Proton Diffusion Coefficient, Journal of power sources, Vol.158, 2006, pp. 837-840.

[3] **Garche, J.**, Passivation of the Positive Electrode of the Lead/Acid Battery: A Consequence of Self-Discharge, Journal of power sources, Vol. 30, 1990, pp. 47-54.

[4] **Barnes, S.C., Mathieson, R.T.**, The Potential pH Diagram of Lead in the Presence of Sulphate Ions and Some of Its Implications in Lead-Acid Battery Studies, in "Batteries", D. H. Collins, (Ed). Pergamon Press, New York, 1963, pp. 41-54.

[5] **Fitas, R., Chelali, N., Zerroual, L., Djellouli, B.**, Mechanism of the Reduction of α- and β-PbO_2 Electrodes Using An All-Solid-State System, Solid state ionics, Vol. 127, 2000, pp. 49-54.

[6] **Monahov, B., Pavlov, D., Petrov, D.**, Influence of Ag As Alloy Additive on Oxygen Evolution Reaction on Pb/PbO_2 Electrode, Journal of power source, Vol. 85, 2000, pp. 59-62.

[7] **Lafront, A-M., Zhang, W., Jin, S., Tremblay, R., Dube, D., Ghali, E.**, Pitting Corrosion of AZ91D and AJ62x Magnesium Alloys in Alkaline Chloride Medium Using Electrochemical Techniques, Electrochimica Acta 51, 2005, pp. 489-501.

[8] **Xiao, H., Mansfeld, F.**, Evaluation of Coating Degradation with Electrochemical Impedance Spectroscopy and Electrochemical Noise Analysis, J. Electrochem. Soc. Vol. 141, 1994, pp. 2332-2339.

[9] **Bierwagen, G.P.**, Calculation of Noise Resistance from Simultaneous Electrochemical Voltage and Current Noise Data, J. Electrochem. Soc. Vol. 141, 1994, pp. L155-162.

[10] **Cheng, Y. F., Luo, J.L., Wilmott, M.**, Spectral Analysis of Electrochemical Noise with Different Transient Shapes, Electrochemica Acta, Vol. 45, 2000, pp. 1763-1771.

[11] **Gouveia-Caridade, C., Isabel, M., Pereira, S., Brett, C. M. A.**, Electrochemical Noise and Impedance Study of Aluminium in Weakly Acid Chloride Solution, Electrochimica Acta, Vol. 49, 2004, pp. 785–793.

[12] **Cuevas-Arteaga, C., Porcayo-Calderon, J.**, Electrochemical Noise Analysis in Frequency Domain and Determination of Corrosion Rates for SS-304 Stainless Steel, Materials science and engineering A 435-436, 2006, pp. 439-446.

[13] **Girija, S., Kamachi Mudali, U., Raju, V. R., Dayal, R. K., Khatak, H. S., Raj, B.,** Determination of Corrosion Types for AISI Type 304L Stainless Steel Using Electrochemical Noise Method, Materials Science and Engineering A 407, 2005, pp. 188-195.

[14] **Deutscher, R.L., Fletcher, S., Hamilton, J.A.**, Invention of Cyclic Resistometry, Electrochim. Acta, Vol. 31, 1986, pp. 585-589.

[15] **Lee C.C. and Mansfeld, F.**, Analysis of Electrochemical Noise Data for A Passive System in the Frequency Domain, Corrosion science, Vol. 40, No. 6, pp. 959-962.

[16] **Pourbaix, M.**, Altas of Electrochemical Equilibrium in Aqueous Solution, NACE, Houston, TX, 1974, pp. 141-145.

CHAPTER 7

Electrochemical impedance spectroscopy evaluation of the corrosion behaviour of Pb-Ag alloys

Electrochemical impedance spectroscopy evaluation of the corrosion behaviour of Pb-Ag alloys

W. Zhang[1*], M. Bounoughaz[2], E. Ghali[1], G. Houlachi[3]

[1]Department of Mining, Metallurgy and Material Engineering

Laval University, Ste-Foy, Quebec, Canada, G1K 7P4

Wei.Zhang.1@ulaval.ca*

2 Department de Chimie, Faculte des Sciences,

Universite de Boumerdes, Algerie

[3]LTE, Hydro-Quebec

600 Avenue de la Mortagne, C.P. 900

Shawinigan, QC, Canada, G9N 7N5

This paper will be sent to Hydrometallurgy

7.1 Abstract

One Pb-0.56%Ag anode was studied by electrochemical impedance spectroscopy « EIS » in typical acid zinc sulphate electrolyte containing $MnSO_4$ to evaluate its electrochemical activity during and after electrolysis. Galvanostatic polarization under 50 mA/cm^2 and at 38°C was carried out for 5 h and a potential decay period of 6 h was evaluated. During the first hour of potential decay the diffusion process controlled the electrochemical reaction and during the following period of potential decay (2 h to 6 h) the double layer and film capacities decreased with immersion time. However, the surface layer and the charge transfer resistances increased with time.

7.2 Introduction

Zinc electrowinning industry requires high quality anodes with high corrosion resistance to produce high purity metal [1]. High quality anode means that the anode has high corrosion resistance to minimize dissolution of corrosion products into the electrolyte, and to achieve required purity of zinc deposits. However, the use of Pb electrode has some problems; for example, the co-deposition of lead corrosion products in the zinc deposit at the cathode decreases the purity, and the high oxygen overpotential on pure lead results in high cell voltage and low energy efficiency. Due to these problems, there is always an interest in finding ways to improve lead anode performance and minimize corrosion and overpotential problems [1]. Also, in zinc industries, there are periods of break time when current is cut off, (for example, 2 hours once a week and 12-16 hours every 3 months) which influence the stability of the anodes. The process of lead anode corrosion (in zinc electrowining electrolyte) on open-circuit (during current interruption for maintenance) following anodic polarization is analogous to the self-discharge of lead acid batteries following the charging state. Zhang et al. [2] found that there are four levels corresponding to different electrochemical reactions during the 16 h of potential decay and corrosion after the polarization.

Electrochemical impedance spectroscopy (EIS) is a powerful tool to study corrosion kinetics and corrosion mechanism of the Pb-Ag anode. Also, the electrochemical impedance spectroscopy (EIS) is one of the best methods to study the

electrochemical double layer properties and provides an opportunity for an *in situ* microstructural characterization of the PbO_2/electrolyte interphase [3].

7.3 Experimental setup

800 ml of electrolyte containing 60 g/dm³ of Zn^{2+}($ZnSO_4.7H_2O$), 180 g/dm³ of H_2SO_4, 8 g/dm³ of Mn^{2+} ($MnSO_4,H_2O$), 250 mg/dm³ of Cl^- and 3 mg/dm³ of Glue (Gelatin or glue (G)) is an animal protein that consists of a complicated mixture of polypeptides and is used as levelling agent [4]) heated by a flow of thermostated water in the double wall (38 ± 0.5°C). The electrolyte was magnetically stirred at 412 rpm during the experiments by a stirrer (4 cm long 1 cm diameter). The Pb-Ag alloy anode (Pb-0.56%Ag) plates were cut into small pieces of 1 x 1 x 1 cm then connected with a plastic isolated copper wire and cast in acrylic resin leaving 1 cm² exposed area surface. The polishing surface of working anode was washed with alcohol and dried immediately before being introduced into the electrolytic cell. The polished anode surfaces were obtained ground with 600 soft grid SiC paper with ethanol to avoid the inclusion of SiC particles into electrodes. Some samples in the beginning were polished using the current SiC paper.

The anodes used in this work were made of laminated Pb-0.56% Ag alloy anode, its chemical composition is given in Table 7.1

Table 7.1 - Chemical composition (wt%) of the Pb-0.56% Ag lead alloy anode

Anodes	Ag	Zr	Ca	Al	Au	Fe	Cu	Ba	Ni	W	S	Pb
#3	0.56	0.24	0.06	<0.05	<0.01	<0.05	<0.05	<0.05	<0.05	<0.05	<0.05	bal.

The working electrode and the Pt counter electrode were mounted in suitable Teflon made holder. Their distance was fixed at 2 cm. The reference electrode was mercurous sulphate electrode (MSE, Hg, Hg_2SO_4/sat.K_2SO_4) and a saturated K_2SO_4 salt bridge was used to keep the reference electrode close to the anode. All the potentials mentioned in this paper are converted to standard hydrogen electrode (SHE).

The electrochemical impedance measurements were carried out using a Solartron 1255 HF frequency response analyzer and a Solartron 1286 electrochemical interface over the frequency range from 10 kHz to 0.5 Hz. The amplitude of the sinusoidal signals was 10 mV (rms). The software Zplot was used for piloting the impedance experiments

and acquisition of the impedance data. The Nyquist plots of the impedance data were analyzed using Zview software mainly to calculate the charge transfer resistance during the corrosion process.

The electrochemical impedance measurements were carried out using galvanostatic mode for 5 hours, i.e., a constant current and temperature (50 mA/cm^2 and 38 °C) was imposed on the anodes and a small alternative signal was added to the constant current during impedance measurements. The impedance of the alternative signal was measured as a function of frequency.

The measurement of electrochemical impedance at open circuit potential started immediately. During the first hour potential decay, every eight minutes of decay is followed by impedance measurement for two minutes.

For each hour of potential decay, the measurement of electrochemical impedance at open circuit potential was conducted five times during two minutes at the end of every hour (2-6 hours). This was carried out six times for six consecutive hours.

7.4 Results and discussion

7.4.1 Electrochemical behaviour of Pb-Ag alloy anode during polarization

During the 5 h polarization at 50 mA/cm^2 and 38°C, the curve of potential with time was recorded; the result is shown in Figure 7.1. It was observed that the potential increased with time for the period 1-5 hours (Figure 7.1).

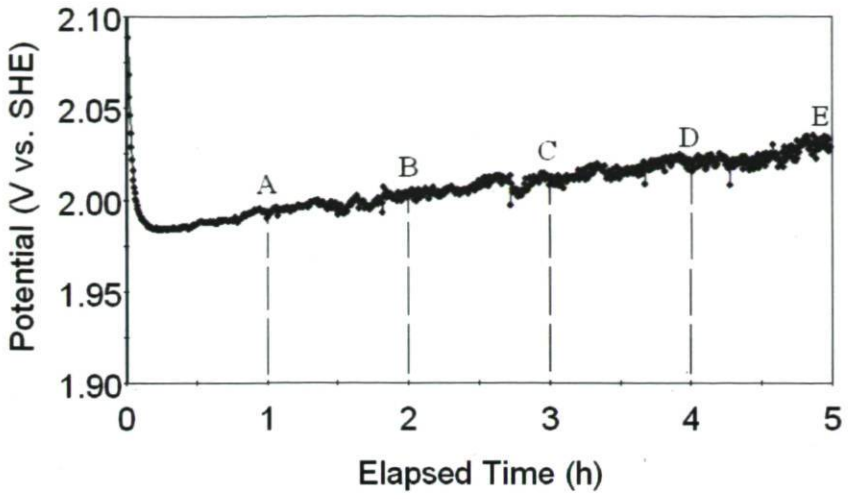

Figure 7.1 Potential for oxygen evolution reaction on the Pb-0.56% Ag anode at a current density of 50 $mAcm^{-2}$ and 38°C in the zinc electrolyte. A: 1993 mV, B: 2003 mV, C: 2011 mV, D: 2022 mV, E: 2029 mV.

Figure 7.2 shows the Nyquist plot of the electrochemical impedance for oxygen evolution reaction on Pb-Ag alloy anode (rate determining step of the kinetic process at the given potential). It can be seen from Figure 7.2 that the Nyquist plot for Pb-Ag alloy anode has a small semicircle; this semicircle should correspond to the electrochemical reaction of the oxygen evolution [5]:

$$M + H_2O_{ad} \rightarrow MOH_{ad} + H^+ + e^- \quad (7.1)$$

$$MOH_{ad} \rightarrow MO_{ad} + H^+ + e^- \quad (7.2)$$

$$2M\ O_{ad} \rightarrow M + O_2 \quad (7.3)$$

where M is the surface of metal.

According to the oxygen evolution mechanism, the steps (7.1) (7.2) are the electrochemical reactions, and the step (7.3) is chemical reaction. When the overpotential is relative low, oxygen evolution reaction is electrochemical control reation, which means that increasing of overpotential will increase the reaction current density. However, when the overpotential becomes relative high, the current density will reach a so-called "limiting current" since the step (7.3) becomes the rate-determining step and it is not affected by applied overpotential. In this experiment, it is likely step (7.3) is in control.

The PbO_2 is formed on the surface of Pb-Ag alloy anode which is a semi-conductor oxide film at the same time. The inductance in the Nyquist plots is probably related to the adsorbed oxygen. An equivalent circuit shown in Figure 7.3 is suggested to simulate the electrochemical process of the oxygen evolution reaction (the rate determining step). R_S corresponds to the electrolyte resistance between the electrode surface and the salt bridge tip. R_1 corresponds to the charge transfer resistance of the oxygen evolution reaction and the electrode surface oxide layer resistance, since the first part does not change under certain conditions, the change of R_1 should be related to the thickness and the properties of the surface layer. CPE_1 is constant phase elements related to the apparent double layer capacitance (C_{dl}) for the oxygen evolution reaction.

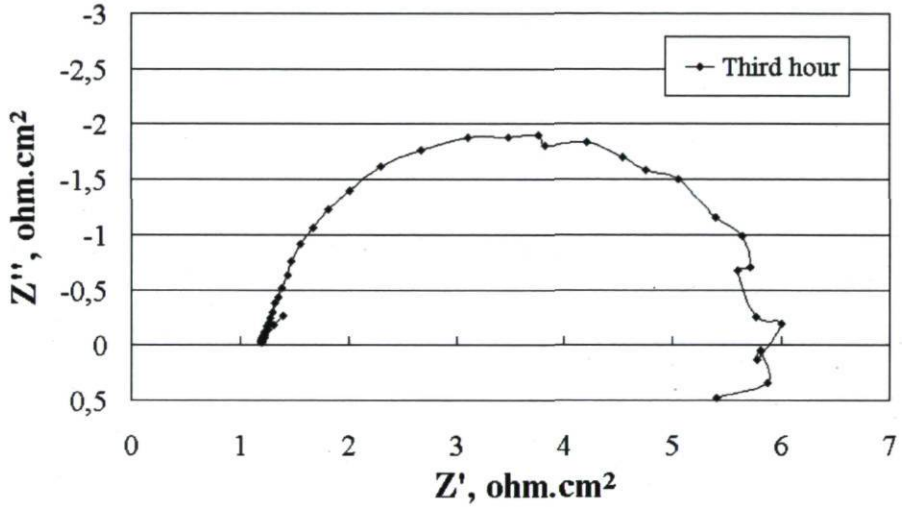

Figure 7.2 – Nyquist plots of electrochemical impedance on the lead-silver alloy anode in the zinc electrolyte at 38°, 50 mA/cm^2 for an hour polarization such as the third hour.

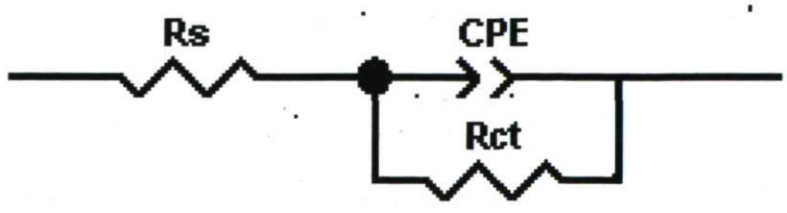

Figure 7.3 – Equivalent circuit proposed for fitting the experimental data of electrochemical impedance measurements of oxygen evolution reaction on lead-silver alloy anodes.

The calculated resistance and capacitance values are given in Table 7.2.

Table 7.2 – Comparison of the parameters of the equivalent circuit of the oxygen evolution reaction on Pb-0.56%Ag alloy anode measured by electrochemical impedance

Time (h)	R_S (Ω cm^2)	R_{ct} (Ω cm^2)	C_{dl} (mF/cm^2)
1	1.11	4.06	11.99
2	1.19	4.68	14.47
3	1.31	5.06	16.02
4	1.47	5.54	19.17
5	1.62	5.74	23.79

It can be seen from Table 7.2 that the surface layer resistance, the charge transfer resistance and the apparent double layer capacitance increase with polarization time. It is admitted that the increase in PbO_2 layer thickness leads to higher values of R_{ct}. The value of Rct is small under the high overpotential polarization confirms that the oxygen evolution reaction is not electrochemical control. The large value of apparent double layer capacity (in mF/cm^2 level) is mainly contributed by oxygen adsorption described in step (7.3).

It should be noted that in Figure 7.1, the Nyquist plot has an inductance at low frequencies. This inductance may be related to the removal of oxygen on the anode surface by step (7.3) and change of oxide film of the Pb surface. Two phenomena may be considered: one is that the oxygen is a strong oxidant, it can diffuse across the oxide layer and attack the metal substrate to form more oxide, this accelerates the corrosion rate of the anode [5]; the second is that this inductance apparently correponds very possibly to oxide dissolution.

7.4.2 Corrosion behaviour of Pb-Ag alloy anode during decay

After 5 h galvanostatic polarization, the potential decay was recorded; a schematic presentation of the 6 hours potential decay of the Pb-Ag alloy anode is shown in Figure 7.4.

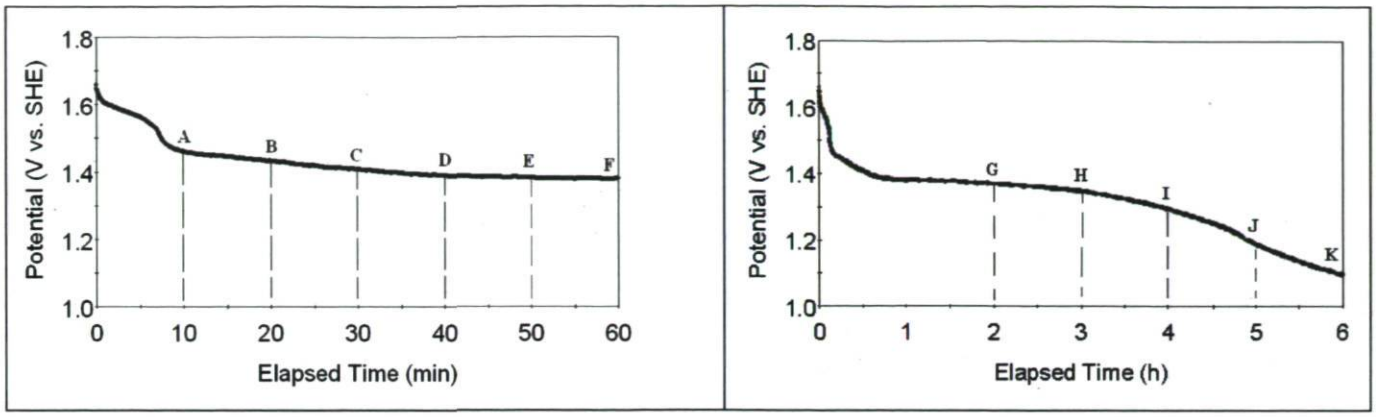

Figure 7.4- Potential decay of the Pb-0.56%Ag following 5 hours of galvanostatic polarization at 50mA/cm^2 in acid zinc sulphate electrolyte.

It is observed from Figure 7.4 that the potential dropped very quickly at the first few minutes, then the rate of potential decay was slower than before, as reported by Zhang et al. [2]. This potential decay can be divided to four levels. For the first and second level during the first 10minutes, the dominating reactions are:

$$PbO_2 + SO_4^{2-} + 4H^+ + 2e^- \rightarrow PbSO_4 + 2H_2O \quad (7.4)$$

$$PbO_2 + HSO_4^- + 3H^+ + 2e^- \rightarrow PbSO_4 + 2H_2O \quad (7.5)$$

For the third level during the periods from 10 to 60 minutes then up to 6 hour, the electrochemical reactions are as following [3, 6]:

$$PbO_2 + H_2O \rightarrow PbO(OH)_2 \quad (7.6)$$

$$PbO_2 + H^+ + e^- \rightarrow PbO(OH) \qquad E^\circ = 1.49\ V \quad (7.7)$$

$$2PbO_2 + HSO_4^- + 5H^+ + 4e \rightarrow PbOPbSO_4 + 3H_2O \qquad E^\circ = 1.375\ V \quad (7.8)$$

$$PbO_2 + 2H^+ + 2e \rightarrow PbO + 2H_2O \qquad E^\circ = 1.107\ V \quad (7.9)$$

At the beginning time (From 10 min to 1h), the oxide film layer contains mainly $PbO(OH)_2$ and PbO(OH) which are colloid and gel conductive, at this time, the oxide film layer has many pores, the ions can pass these pores, it indicated a diffusion control. Then (1 h to 6 h) there are main products of $Pb(OH)_2$, PbO and $PbSO_4$ which are low conductive or no-conductive [3], the oxide film layer is thickness and non-porous, and the thickness of oxide film increased with the decay time, so the charge transfer resistance increased.

The fourth level corresponding to complete formation of lead sulphate on the Pb-0.56% Ag anode was not identified during 6 h of decay because of the relative important of the quantity of corrosion products formed during polarization.

During the first hour of potential decay, six points (A-F) were considered to do the impedance measurements, since the decay rate of the potential at the first hour is very quick, it is very possible that certain electrochemical reactions were at these places [2]. Then, (G-K) five points were carried out by impedance measurements during the following 5 hours (from 2-6 h).

Figure 7.5 illustrates the Nyquist plots for the corrosion impedance of Pb-Ag alloy specimen as a function of immersion time. It can be observed that the size of the capacitive semi-circle of the Nyquist plots increases with time. Since the diameter of the capacitive semi-circle is directly proportional to the charge transfer resistance (R_{ct}) for the electrochemical corrosion process, the growing of the semi-circle means that the corrosion resistance increased and the corrosion current decreased with time. Also, it was found that the Warburg impedance (diffusion control) existed at low frequencies because the mass transport of the electroactive species may limit the electron-transfer process.

As reported by Deutscher et al. [7], the PbO_2 was reduced to $PbSO_4$ during the potential decay, while the molar volume of β-PbO_2 (25 cm^3 mol^{-1}) is much less than the molar volume of $PbSO_4$ (48 cm^3 mol^{-1}) and PbO(OH), so gaps are created in the outer $PbSO_4$ layer and bare metal is exposed to the acidic solution and the diffusion of Pb^{2+} passed through the gaps of $PbSO_4$ and PbO_2 layer.

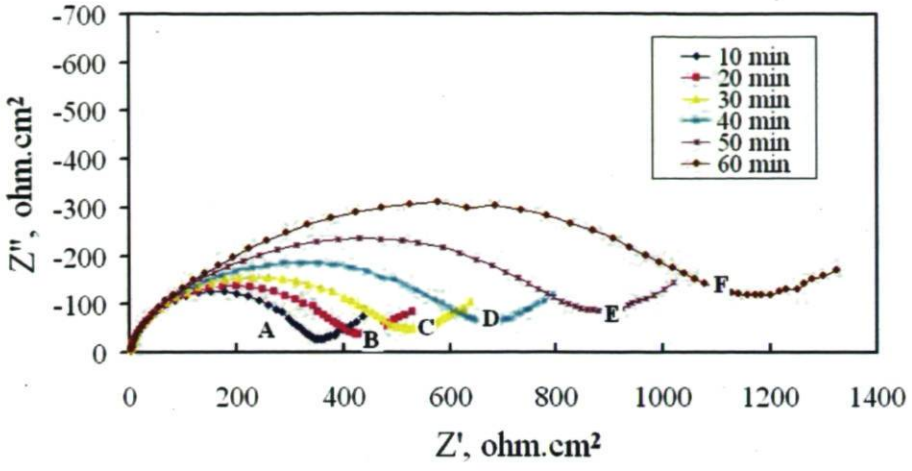

Figure 7.5 - Nyquist plots of corrosion impedance of the Pb-0.56% Ag alloy specimen as a function of immersion time in the zinc electrolyte at 38°C after 5 h polarization. The potentials versus SHE are at the elapsed times A: 1459 mV, B: 1432 mV, C: 1407 mV, D: 1389 mV, E: 1382 mV, F: 1378 mV.

An equivalent circuit shown in Figure 7.6 was used to calculate the charge transfer resistance, Warburg impedance and other parameters.

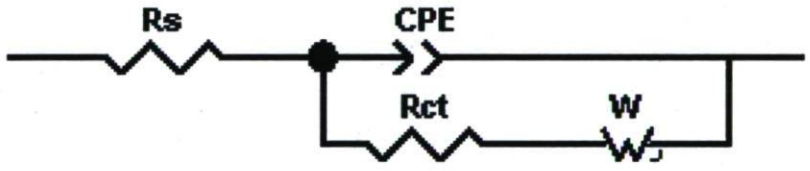

Figure 7.6- Equivalent circuit of the corrosion cell: R_s = electrolyte resistance, R_{ct} = charge transfer resistance, CPE = constant phase element related to double layer capacity, W_o = Warburg impedance.

The values of the charge transfer resistance and Warburg impedance are showed in Table 7.3, the values of R_S was nor considered since it is the resistance of the electrolyte that is constant in these conditions. It was observed that the double layer capacity decreased with the immersion time, meaning that the rate of the diffusion of the ions was decreased. This can correspond to a decrease of the attached ions that are very close to the metal surface.

Table 7.3 - R_{ct}, C_{dl}, Warburg impedance values of the Pb-0.56%Ag alloy specimen as a function of immersion time in the zinc electrolyte at 38°C after 5 h polarization for different times

Time (min)	R_{ct} ($\Omega.cm^2$)	C_{dl} (F/cm^2)	W-R ($\Omega.cm^2$)	C_w (F/cm^2)
10	345.1	1.36e-5	593.2	49.82
20	418.6	1.21e-5	693.7	59.84
30	507.8	1.12e-5	810.3	82.13
40	633.4	1.04e-5	1005.6	84.99
50	830.7	1.02e-5	1391.5	133.41
60	1091.9	1.01e-5	2623.8	623.24

Figure 7.7 gives the evolution of the charge transfer resistance and the Warburg impedance with time. It is clear that the charge transfer resistance changed synchronously with the variation of Warburg resistance. The increase of the charge transfer resistance signifies a decrease of corrosion current, while the increase of the Warburg resistance can be due to a decrease in the pores of the surface film, leading to a control of the diffusion of Pb^{2+} ions. Also, it can be observed that the W-R is larger than R_{ct} indicating a diffusion control. This may be due to a concentration depletion or accumulation layer of reactant/product. As reported by Zhang et al. [2], less Ag content in the Pb-Ag alloy anodes resulted in more PbO_2 on the surface of Pb-Ag alloy anode during its polarization, and during the decay of Pb-Ag alloy anodes after polarization, more PbO_2 resulted in slower rate of the potential decay of the Pb-Ag alloy anode. It can be admitted then that the process of PbO_2 reduction to $PbSO_4$ lasted more than 1 hour since only 0.56% Ag is contained in the Pb-0.56%Ag alloy anode.

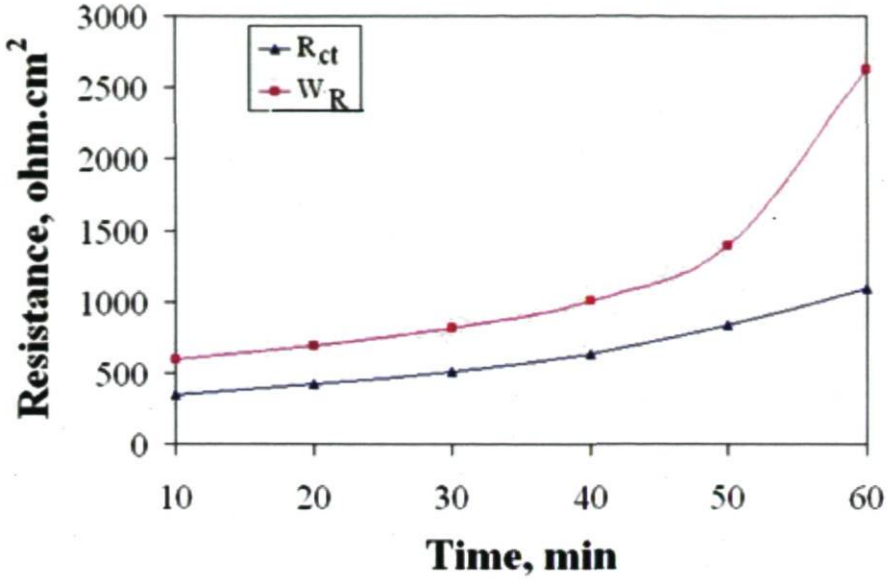

Figure 7.7 – Evolution of R_{ct} and Warburg resistance of the Pb-0.56%Ag alloy specimen as a function of immersion time in the zinc electrolyte at 38 °C after 5 h polarization.

Figure 7.8 illustrates the Nyquist plots of the corrosion impedance of Pb-0.56%Ag alloy specimen during the 5 hours decay immersion time (from 2 to 6 h).

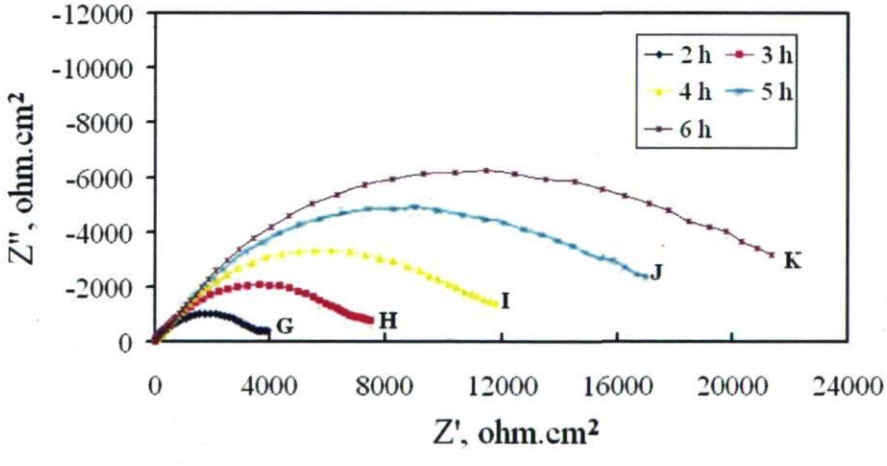

Figure 7.8 - Nyquist plots of corrosion impedance of the Pb-0.56%Ag alloy specimen as a function of the 6 h potential decay immersion time in the zinc electrolyte at 38 °C after 5 h polarization. The potentials versus SHE are at the elapsed times G: 1368 mV, H: 1347 mV, I: 1296 mV, J: 1186 mV, K: 1094 mV.

An equivalent circuit fitted for Figure 7.8 shown in Figure 7.9 was used to calculate the charge transfer resistance, surface film resistance and other parameters.

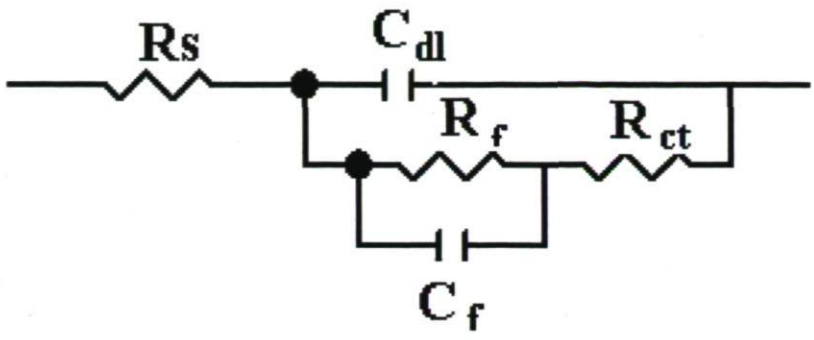

Figure 7.9 - Equivalent circuit of the corrosion cell: R_s = electrolyte resistance, R_{ct} = charge transfer resistance, R_f = surface film resistance, C_{dl} = double layer capacity, C_f = film capacity.

The values of the charge transfer and surface film resistances are shown in Table 7.4. The values of R_S werenot considered since it is not relatively important in the examined electrolyte. The film capacity decreased with the immersed time, it is due to the PbO_2 reduction to $PbSO_4$. Also, the double layer capacity decreased with the decay time since the low potential resulted in less Pb^{2+} ions attached to the surface of double layer.

Table 7.4 - R_{ct}, R_f, C_{dl} and C_f values of the Pb-0.56%Ag alloy specimen as a function of immersion time in the zinc electrolyte at 38 °C after 5 h polarization for different times

Time (h)	R_f ($\Omega.cm^2$)	C_f (F/cm^2)	R_{ct} ($\Omega.cm^2$)	C_{dl} (F/cm^2)
2	687.4	2.56e-6	3931	1.69e-5
3	813.9	2.07e-6	7729	1.35e-5
4	923.3	1.71e-6	12568	1.17e-5
5	1024	1.43e-6	18799	1.11e-5
6	1110	1.17e-6	24190	1.02e-5

It can be observed from Figure 7.10 that the surface film resistance increases with immersion time. This increase of R_f caused by the thickness of $PbSO_4$ film increase, it means that there is more $PbSO_4$. It is clear that the charge transfer resistance changed synchronously with the variation of surface film resistance. It was also found that the charge transfer resistance increased since less Pb^{2+} corroded from the Pb alloy anode and

these Pb^{2+} ions were difficult to pass through the thick and passive $PbSO_4$ layer (low conductive) [3].

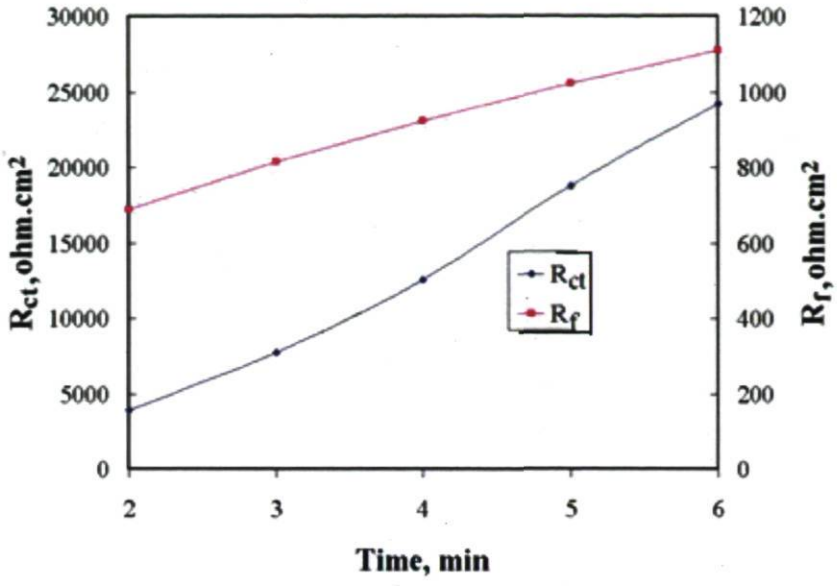

Figure 7.10 – Evolution of R_{ct} and R_f of the Pb-0.56%Ag alloy specimen as a function of immersion time (2-6 h) in the zinc electrolyte at 38°C after 5 h polarization.

7.5. Conclusions

The following conclusions can be deduced from this study:

- During the polarization, the surface layer resistance, the charge transfer resistance and the double layer capacitance increase with polarization time.
- During the first hour potential decay after 5 h polarization:

The Warburg process controls the electrochemical reaction. The resistance of the electrochemical reaction of Pb-Ag consists of Warburg resistance and the charge transfer resistance, which increased with the immersion time.

- The potential decay during the period from the second to sixth hour:

The double layer capacity and the film capacity decreased with the immersion time.

The surface layer resistance and the charge transfer increased with time.

7.6. Acknowledgements

Our deep thanks go to Drs Gordon Gu and Jian Li (CANMET Materials Technology Laboratory, Natural Resources Canada) for their interest and participation in reviewing this work.

7.7. References

[1] **Yu P., and O'Keefe, T.J.**, Evaluation of Lead Anode Reactions in Acid Sulfate Electrolytes. I. Lead Alloys with Cobalt Additives, Journal of the Electrochemical Society, 146, 1999, pp. 1361-1369.

[2] **Zhang, W., Lafront, A-M., Ghali, E., Houlachi, G.**, Influence of Silver Content on Corrosion Resistance of Lead Anodes During Potential Decay by Electrochemical Noise Measurements, METSOC, Development & Perfromance of Sulphur Capture Plants, Sudbury, Ontario, Canada, 48th Annual Conf. of Metallurgists of CIM, 2009, pp. 101-115.

[3] **Kirchev, A., Delaille, A., Perrin, M., Lemaire, E., Mattera, F.**, Studies of the Pulse Charge of Lead-Acid Batteries for PV Applications Part II: Impedance of the Positive Plate Revisited, Journal of Power Sources 170, 2007, pp. 495-512.

[4] **Krzewska, S., Pajdowski, L., Podsiadly, H., Podsiadly, J.**, Electrochemical Dermination of Thiourea and Glue in the Industrial Copper Electrolyte, Metallurgical and Materials Transactions B, 1981, Vol. 15B, pp. 451-459.

[5] **Zha,Q.**, An Introduction to the Kinetics of Electrode Processes, Kexue Chubanshe, Beijing, China, 1987, pp. 369-375.

[6] **Zerroual, L., Fitas, R., Djellouli B. and Chelai, N.**, Relationship between Water Depature and Capacity Loss of α and β-PbO_2 Using An All Solid-State System: Estimation of Proton Diffusion Coefficient, Journal of power sources, Vol.158, 2006, pp. 837-840.

[7] **Deutscher, R.L., Fletcher, S., Hamilton, J.A.**, Invention of Cyclic Resistometry, Electrochim. Acta 31, 1986. pp. 585-589.

PART 2

CHAPTER 8

Influence of $MnSO_4$ addition on the performance of different lead-silver alloys during polarization and decay periods

8.1 Introduction

Even though lead is the anode material of choice in many major electrowinning processes, such as copper, zinc, and manganese, there are some difficulties in their use that can create problems; one is concerned with the incorporation of lead corrosion products in the deposit at the cathode which decrease the purity. Also the oxygen overpotential is relatively high that increases the cell voltage and decreases energy efficiency. Due to these problems there is always interest in finding ways to improve anode performance and minimize the corrosion and overpotential problems [1].

Small amounts of Ag (0.7-1.0%) alloyed with lead decrease the oxygen overvoltage, and increase the corrosion resistance of material. A well established custom in all electrolytic zinc plants is to use Pb-Ag alloys containing 0.7-1.0 percent Ag as the anode material. The resulting benefits are a longer anode life and a lower Pb content in the cathodic zinc [2, 3]. It is generally acknowledged that zirconium has an excellent resistance to corrosion in acid sulphate solution due to the formation of a layer of its metal oxide [4]. According to Charlesby [5] the anodic passivation film is made up of cubic ZrO_2 in the case of polarization in dilute acid sulphate. The addition of ~ 0.1% Ca in this ternary alloy hinders the transfer of Pb in the cathode [6]. Also, addition of ~ 0.1% Ca content resulted in a decrease in the electrode potential for the alloy anodes containing silver [7].

The electrochemical behaviour of the anode of the zinc electrowinning is very important for the anodic reactions as well as for the quality of zinc deposit. Potentiodynamic measurements, galvanostatic and impedance spectroscopic techniques were used to investigate the electrochemical behaviour of three Pb-Ag alloys and one Pb-Ag-Ca alloys with different miscrostructures. By comparing these results, the lead electrode for the zinc electrowinning industry having the lowest corrosion rate, the lowest overpotential and best stability during polarization, after polarization (potential decay) and at the open-circuit potential studies could be chosen.

The aim of this work is to use the electrochemical measurements to study the performance of different Pb-Ag anodes in presence of 8g/L $MnSO_4$ as in the industrial

practice during and after electrowinning. Also, once the best anode composition is identified, different additions of $MnSO_4$ (4 g/L- 12 g/L) to the electrolyte were tested.

8.2. Experimental

8.2.1 Materials and sample preparation

The composition of the electrolyte used in this work is as follows: Zn^{2+} 60 gdm^{-3}; H_2SO_4 180 gdm^{-3}; Mn^{2+} 8 gdm^{-3}; Cl^- 250 $mgdm^{-3}$; Glue 3 $mgdm^{-3}$.

Zinc sulphate ($ZnSO_4 \cdot 7H_2O$), manganese sulphate ($MnSO_4 \cdot H_2O$) from Sigma-Aldrich Fine Chemicals, sodium chloride and sulphuric acid of Merck KGaA were used to prepare the supporting electrolyte with double distilled water. Gelatin (glue) was product of BDH Inc. The chemicals meet ACS specifications (except gelatin) and were used as received without further treatment. All concentrations of H_2SO_4 and Zn^{2+} stated in this paper are initial concentrations.

The anodes used in this work were made of laminated Pb-Ag and Pb-Ag-Ca alloys. The anode #1 is a Pb-0.25%Ag-0.1%Ca alloy; the anodes #2 and #3 are Pb-0.6%Ag alloys, while anode #4 is a Pb-0.7%Ag alloy. Their chemical composition is given in Table 8.1.

Table 8.1 Chemical composition (wt%) of the four commercial lead alloy anodes

Anodes	Ag	Zr	Ca	Al	Au	Fe	Cu	Ba	Ni	W	S	Pb
#1	0.25	0.22	0.1	<0.05	<0.01	<0.05	<0.05	<0.05	<0.05	0.10	0.12	bal.
#2	0.60	0.23	0.05	<0.05	<0.01	<0.05	<0.05	<0.05	<0.05	0.10	0.09	bal.
#3	0.56	0.24	0.06	<0.05	<0.01	<0.05	<0.05	<0.05	<0.05	<0.05	<0.05	bal.
#4	0.69	0.22	0.05	<0.05	<0.01	<0.05	<0.05	<0.05	<0.05	<0.05	<0.05	bal.

The middle bulk and original surface of the four anodes were used. The cathodes were made of platinum for corrosion rate measurements. The Pb-Ag alloy anodes plates were cut into small pieces of 1 × 1 × 1 cm then connected with a plastic isolated copper wire and cast in acrylic resin. The electrical contacts were made with plastic isolated copper wires and the piece was cast in acrylic resin. The exposed area surface was 1 cm^2. Before being introduced into the electrolytic cell, all working surfaces of the anodes and cathodes were ground with SiC abrasive paper (Leco Corporation) down to 600 grit,

washed with double distillated water and wiped immediately with tissue paper, however, comparison of the polished surfaces and original ones were conducted only for polarized samples followed by one hour potential decay.

8.2.2 Experimental setup

The electrolytic cell comprised a one litre double walled beaker containing 800 ml of electrolyte heated by a flow of thermostated water in the double wall (38 ± 0.5°C). The working electrode and the counter electrode were mounted in suitable Teflon made holder and the distance between them was fixed at 2 cm. The reference electrode was mercurous sulphate electrode (MSE): Hg, Hg_2SO_4/sat.K_2SO_4. A saturated K_2SO_4 salt bridge was used to keep the reference electrode close to the anode. The experimental setup was an EG&G PARSTAT 2263 potentiostat/galvanostat controlled by an IBM computer. The electrochemical impedance measurements were carried out using PowerSINE in Electrochemical PowerSuite of Advanced Measurement Technology, Inc. over the frequency range from 100 kHz to 100 mHz. The amplitude of the sinusoidal was 10 mV (rms). The reproducibility of the polarization resistance values of impedance during potential decay after 5 h galvanostatic polarization was of the order of ±4~6 %. All the experiments were repeated for three times.

The measurements of the overpotentials of the four polished anodes were carried out by galvanostatic polarization at a current density of 50 mA cm^{-2} at 38°C. The standard ASTM G5 [8] was used to carry out potentiodynamic test, the potentiodynamic curves were traced at 0.166 mV/s scanning rate over a potential range of 50 mV (cathodic polarization -25 mV vs. corrosion potential). The reproducibility of the potential values was of the order of ±3~5 % and the reproducibility of the corrosion current values was of the order of ± 4~6 % by potentiodynamic measurements. All the experiments were repeated for three times.

8.3. Results and discussion

8.3.1 Overpotential for the oxygen evolution reaction (ORE) on the four polished anodes in acid zinc sulphate electrolyte with 8 gdm^{-3} Mn^{2+} and without $MnSO_4$ addition

Generally, industrial acid zinc sulphate electrolyte contains 100 mg dm^{-3} MnO_4^-. It is then necessary to study the anodic corrosion behaviour in zinc electrolyte containing manganese sulphate. 8 gdm^{-3} Mn^{2+} in the form of $MnSO_4 \cdot H_2O$ was added to the acid zinc sulphate electrolyte [9]. After five hours of electrolysis at 50 $mAcm^{-2}$ using Pb-Ag alloy anodes, the solution became purple-red because of the formation of permanganate ions. Then the potential decay and the polarization experiments were carried out to measure the corrosion potential and corrosion current.

Figure 8.1 represents the overpotentials of anodic reaction of the four polished anodes in acid zinc sulphate electrolyte containing 8 gdm^{-3} Mn^{2+} with time. The oxygen overpotentials at 50 $mAcm^{-2}$ were determined by subtracting the ohmic drops (obtained by ac impedance technique) and the calculated reversible potentials (1.264 V vs. SHE) from the measured electrode potential values.

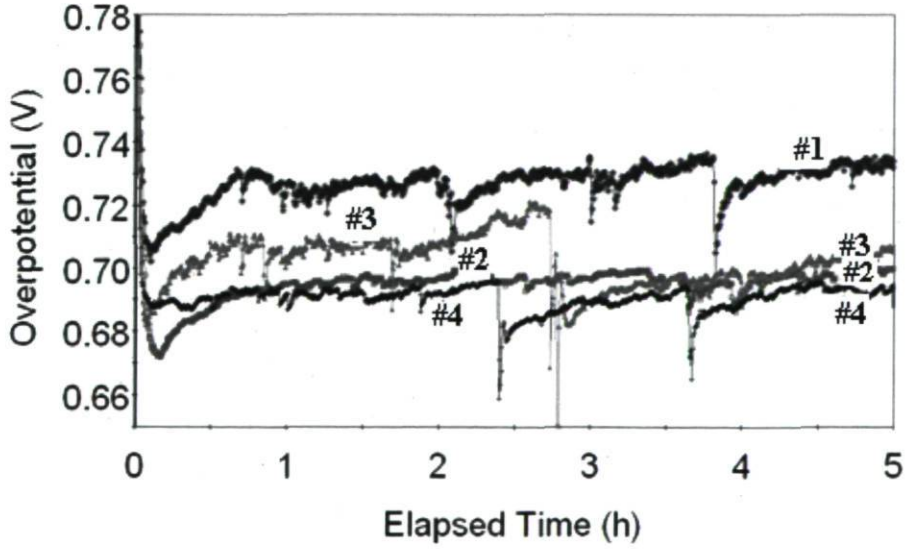

Figure 8.1 Overpotentials for oxygen evolution reaction on the four polished anodes (anodes #1, #2, #3, #4) at a current density of 50 $mAcm^{-2}$ in acid zinc sulphate electrolyte containing 8 gdm^{-3} Mn^{2+}.

At the end of the electrolysis, the overpotentials of the anodes #4, #2, #3 and #1 were 689, 697, 706, and 742 mV as average values for all cycles, respectively. In the beginning, there were remarkable fluctuations, but after 5 h immersion, it is clear that anode #1 had much higher overpotential than anode #3 followed very closely by anodes #2 and #4. There were inversion of the order and some fluctuations as for example the overpotential of anode #2 was lower than that of anode #4 during the first hour, however, after 5 h electrolysis, the overpotential of anode #2 was slightly higher than that of #4.

As shown in Figure 8.1, the curves of the four polished anodes have remarkable potential fluctuations due probably to repeated formation and breakdown of the anode film. For example, a conductive PbO_2 is formed and then followed by non-conductive MnO_2 on the surface of the polished anodes, when non-conductive MnO_2 gradually covers the surface of the anode, current density of the small uncovered parts of the anode surface increases rapidly, and this causes the anode film breakdown into the electrolyte. This cycle could repeat itself.

The overpotentials for the four polished anodes were measured at a current density of 50 $mAcm^{-2}$ in acid zinc sulfate electrolyte without $MnSO_4$ addition for five hours. The curves of overpotentials vs. time are shown in Figure 8.2.

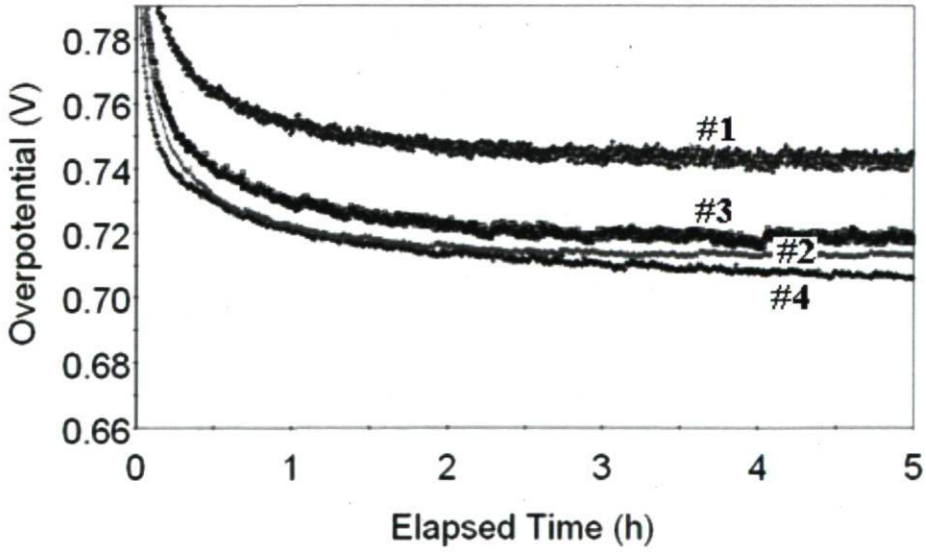

Figure 8.2 Overpotentials for OER on the four polished anodes (anodes #1, #2, #3, #4) at a current density of 50 $mAcm^{-2}$ in acid zinc sulphate electrolyte without $MnSO_4$ addition.

The curves of the four polished anodes had the same trend, but fluctuations are less important due possibly to the absence of Mn^{2+} ions. At the end of the electrolysis, the overpotentials of the anodes #4, #2, #3 and #1 were 712, 725, 733 and 753 mV, respectively. The anode #4 had the highest activity for OER among the four polished anodes, followed by anodes #2, #3 and #1. Anode #1 contains much less silver than the other three anodes, and silver alloyed with lead decreases the oxygen overvoltage, so it had much higher overpotential than anodes #2, #3 and #4. The other three anodes #2, #3 and #4 had almost the same silver content, and their overpotentials were relatively close to each other in this case.

Comparing Figure 8.1 to Figure 8.2, overpotentials of the four anodes #1 through #4 in the electrolyte without Mn^{2+} were higher 11, 28, 27 and 23 mV than that of the four anodes in the electrolyte with 8 gdm^{-3} Mn^{2+}, respectively, the difference between them being considered little.

8.3.2. Corrosion behaviour after polarization

8.3.2.1. Potential decay and corrosion rate after 5h polarization in acid zinc sulphate electrolyte with 8 gdm^{-3} Mn^{2+} and without $MnSO_4$ addition

After galvanostatic polarization, the corrosion potential decay of one hour was recorded, then potentiodynamic measurements (linear polarization resisstance) were performed to measure the corrosion potential (E_{corr}) and corrosion current (i_{corr}). These tests were followed by second hour potential decay and another potentiodynamic measurement. The potential decay curves of the four polished anodes following 5 h polarization in acid zinc sulphate electrolyte containing 8 gdm^{-3} Mn^{2+} are shown in Figure 8.3. The corrosion potential (E_{corr}) and corrosion current (i_{corr}) of the four polished anodes #1 - #4 after one hour and the second hour potential decay following 5 h galvanostatic polarization at 50 $mAcm^{-2}$ in the zinc electrolyte containing 8 gdm^{-3} Mn^{2+} and without $MnSO_4$ addition were shown in Tables 8.2 and 8.3, respectively.

Figure 8.3 showed that the potential of anode #3 drop slowly and had a longest potential plateau among the four samples around 1600 mV corresponding to the theoretical potential value of the PbO_2/Pb^{2+} equilibrium. This shows a spontaneous

transformation of lead dioxide into lead sulphate because thermodynamically lead dioxide is unstable on the surface of lead in the sulphuric acid solution [10]. The potentials at the end of 1 hour for the anodes #3, #1, #2 and #4 were 1180, 645, 590 and 414 mV vs. SHE, respectively. After the galvanostatic polarization, the higher potential leads to the higher corrosion rate for all anodes in a bath with and without $MnSO_4$ addition (Tables 8.2 and 8.3).

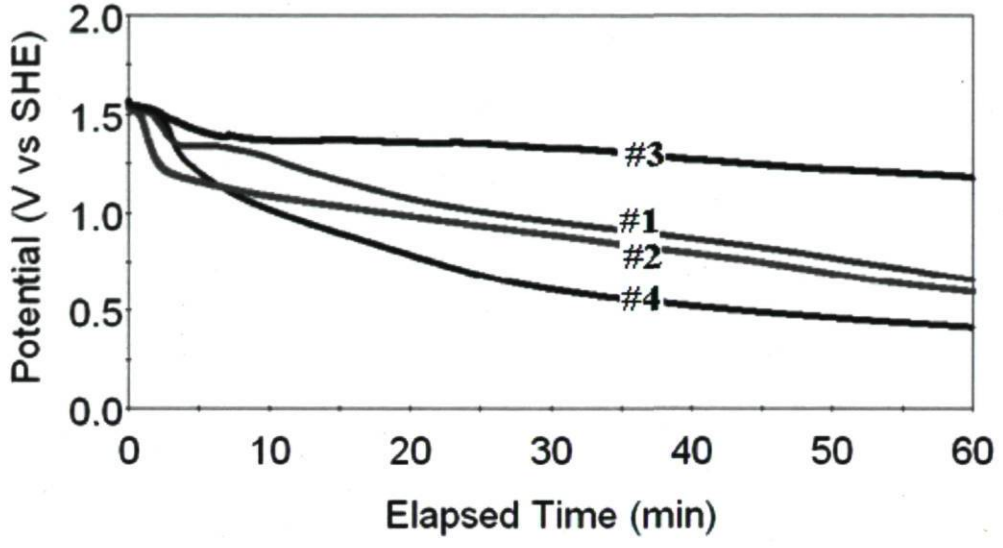

Figure 8.3. Potential decay of the four polished anodes (anodes #1, #2, #3, #4) following 5 hours of galvanostatic polarization at 50 $mAcm^{-2}$ in acid zinc sulphate electrolyte containing 8 gdm^{-3} Mn^{2+}.

Table 8.2 Corrosion potentials and corrosion currents of the four polished anodes #1 through #4 after one hour and the second hour potential decay following 5 h galvanostatic polarization at 50 $mAcm^{-2}$ in the zinc electrolyte containing 8 gdm^{-3} Mn^{2+} at 38°C

Anodes	E_{corr} (mV vs. SHE)		i_{corr} (μAcm^{-2})	
	One hour decay	Second hour decay	One hour decay	Second hour decay
#3	1174	1036	12.46	8.65
#1	640	367	3.93	2.36
#2	584	339	3.28	2.04
#4	407	305	2.73	1.78

Seen from Table 8.2, after one hour and the second hour potential decay following 5 h galvanostatic polarization, the anode #4 had the lowest corrosion potential and corrosion current among the four polished anodes, followed by the anodes #2, #1 and #3. It means that the anode #4 had the best corrosion resistance. Also the corrosion rates of four polished anodes decrease when the potential decay time increases.

It can be observed from Table 8.3 that the corrosion rate of the anode #4 were still the lowest among the four polished anodes in the electrolyte without $MnSO_4$ addition, followed by anodes #2, #1 and #3. Also the corrosion potentials and corrosion rates of one hour decay for the four polished anodes are higher than that of second hour decay.

Table 8.3 Corrosion potentials, corrosion currents of the four polished anodes #1 through #4 after one hour and two hour potential decay following 5 h galvanostatic polarization at 50 $mAcm^{-2}$ in acid zinc sulphate electrolyte without $MnSO_4$ addition at 38°C

Anodes	$\mathbf{E_{corr}}$ (mV vs. SHE)		$\mathbf{i_{corr}}$ (μAcm^{-2})	
	One hour decay	Second hour decay	One hour decay	Second hour decay
#3	1257	1128	18.02	9.37
#1	989	612	7.43	3.59
#2	872	558	5.84	2.96
#4	764	476	5.07	1.81

Comparing Tables 8.2 and 8.3, it is found that the four polished anodes in acid zinc sulphate electrolyte containing 8 g dm^{-3} Mn^{2+} had lower corrosion rates than those in the acid zinc sulphate electrolyte without $MnSO_4$ addition, the reason should be:

The electrolyte contains Mn^{2+} which reacts on the anode [6]:

$$MnSO_4 + 2H_2O - 2e = MnO_2 + H_2SO_4 + 2H^+ \qquad E_O = 1.28\ V/SHE \qquad (8.1)$$

$$MnSO_4 + 4H_2O - 5e = MnO_4^- + H_2SO_4 + 6H^+ \qquad E_O = 1.52\ V/SHE \qquad (8.2)$$

$$3MnSO_4 + 2HMnO_4 + 2H_2O = 5MnO_2 + 3H_2SO_4 \qquad (8.3)$$

So a dense non-conductive MnO_2 film formed on the surface of anode, the well adherent oxide film MnO_2 increased the thickness and density of oxide layer (PbO_2-MnO_2) which makes the transition of Pb^{2+} ions to the solution difficult and protect the

lead anode from corrosion. The dissolution of Pb anode is limited at the pores of protective layer. As a result of the protective action of the layer produced in presence of manganese ions the purity of the cathodic metal increases.

8.3.2.2. EIS measurement of polarization resistance of the four polished anodes after 5 hours electrolysis followed by the potential decay in zinc electrolyte with 8 gdm^{-3} Mn^{2+} without $MnSO_4$ addition

In this work, when the working electrode was introduced into the cell, the galvanostatic polarization was started immediately and was preformed for 5 hours, then the corrosion potential decay tests was done, after one hour of the potential decay, the measurements of electrochemical impedance at open circuit potential were carried out and the polarization resistances were calculated. These tests were followed by another potential decay of one hour and a subsequent EIS measurement. This sequence was conducted over four cycles of impedance measurements.

Figure 8.4 displays the Nyquist plots of the fourth cycle of EIS measurement after the galvanostatic polarization at 50 $mAcm^{-2}$ for the four polished anodes in acid zinc sulphate electrolyte containing 8 gdm^{-3} Mn^{2+}.

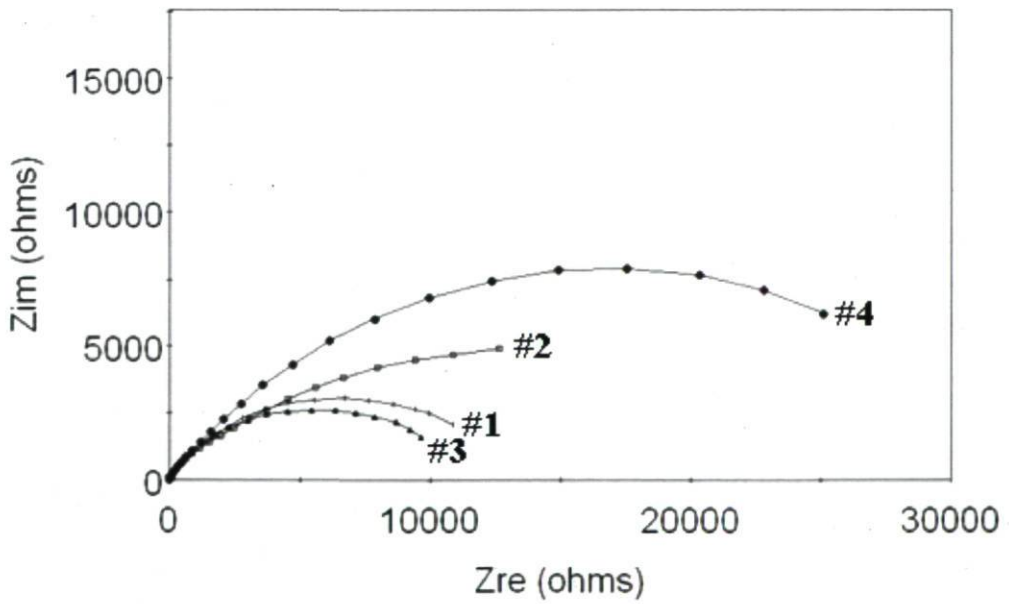

Figure 8.4 Nyquist plots of the four polished anodes (anodes #1, #2, #3, #4) after the galvanostatic polarization at potential decay time after the fourth hour (cycle) in acid zinc sulphate electrolyte containing 8 gdm^{-3} Mn^{2+} at 38°C.

The data of the four cycles obtained by fit circle of "PowerSINE" software are shown in Table 8.4. The anode #4 had the highest polarization resistance among the four anodes, followed by anodes #2, #1, #3.

Table 8.4 Data of polarization resistance of the four anodes obtained from the Nyquist plots for the four cycles in the zinc electrolyte containing 8 gdm^{-3} Mn^{2+} at $38^{O}C$

Anodes	Polarization resistance (R_p, $K\Omega \cdot cm^2$)			
	1 h	2 h	3 h	4 h
#3	6.67	10.87	14.98	13.35
#1	11.73	15.64	19.87	17.65
#2	13.43	19.89	29.30	35.48
#4	20.38	36.06	42.45	38.89

Comparing Tables 8.2 and 8.4, it can be seen that the polarization resistances measured by EIS for the four anodes had a same trend as those of potentiodynamic measurements in the electrolyte containing 8 gdm^{-3} Mn^{2+}.

The Nyquist plots of the fourth cycle EIS measurement after the galvanostatic polarization at 50 $mAcm^{-2}$ for the four polished anodes in acid zinc sulphate electrolyte without $MnSO_4$ addition are shown in Figure 8.5. It is observed that the semi-circle for anode #4 is the biggest followed by that for anodes #2, #1 and #3.

The data of the four cycles are shown in Table 8.5. It can be seen that the anode #4 had the highest polarization resistance among the four polished anodes in acid sulphate electrolyte without $MnSO_4$ addition, followed by anodes #2, #1 and #3.

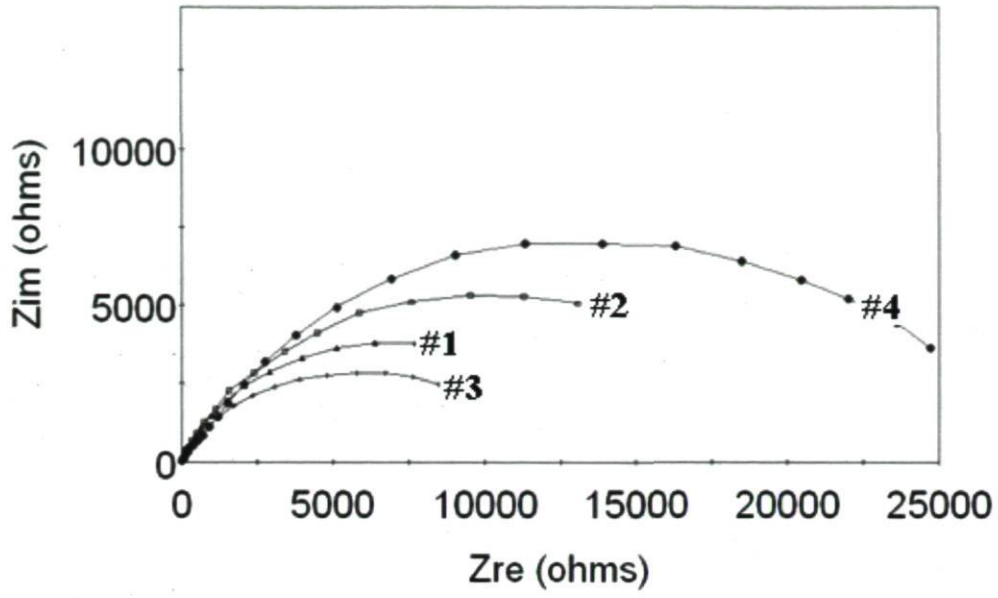

Figure 8.5. Nyquist plots of the four polished anodes (anodes #1, #2, #3, #4) at potential decay time after the fourth hour (cycle) after the galvanostatic polarization at 50 $mAcm^{-2}$ in acid zinc sulphate electrolyte without $MnSO_4$ addition.

Table 8.5 Polarization resistances of the four polished anodes obtained from the Nyquist plots for the fourth cycles in the zinc electrolyte without $MnSO_4$ addition at 38°C

Anodes	Polarization resistance (R_p, $K\Omega \cdot cm^2$)			
	1 h	2 h	3 h	4 h
#3	4.41	8.77	13.67	11.46
#1	11.22	13.88	16.16	14.56
#2	12.97	19.33	19.57	22.33
#4	17.25	28.03	27.03	32.34

Comparing Tables 8.4 and 8.5, it is found that the four polished anodes in the acid zinc sulphate electrolyte containing 8 g dm^{-3} Mn^{2+} had higher polarization resistance than those in acid zinc sulphate electrolyte without $MnSO_4$ addition. It can also be stated that the anode #4 had the highest polarization resistance, followed by anodes #2, #1, #3.

8.3.3. Some key parameters

8.3.3.1. Effect of Mn^{2+}concentration

The electrochemical behaviour of the polished anode #4 was conducted in acid zinc sulphate electrolyte containing 4, 6, 10 and 12 gdm^{-3} Mn^{2+} around 8 gdm^{-3}, respectively, to investigate the effect of Mn^{2+}concentration on the oxygen evolution reaction (OER) and the corrosion rate.

The overpotentials of the polished anode #4 in acid zinc sulphate electrolyte with the variation of concentrations 8, 10 and 12 gdm^{-3} Mn^{2+} were shown in Figure 8.6 (the overpotentials of the polished anode #4 in acid zinc sulphate electrolyte with the variation of concentrations 4 and 6 gdm^{-3} are almost the same as that of 8 gdm^{-3}).

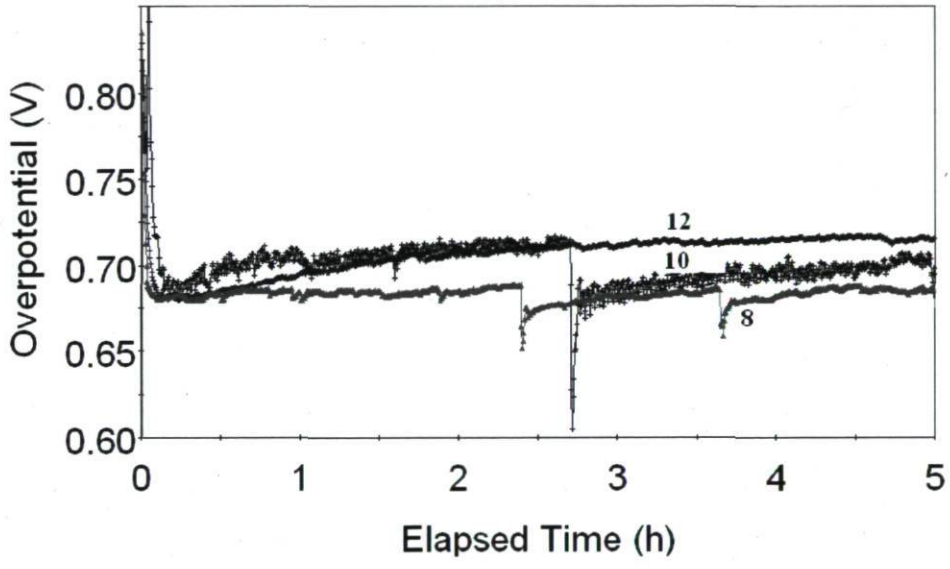

Figure 8.6. Comparison of overpotentials of the polished anode #4 galvanostatically polarized at 50 $mAcm^{-2}$ in acid zinc sulphate electrolyte containing 8, 10 and 12 gdm^{-3} Mn^{2+} at 38°C.

It is seen from Figure 8.6 that the polished anode #4 in acid zinc sulphate electrolyte with 12 gdm^{-3} Mn^{2+} had higher OER overpotential than that in lower Mn^{2+} concentration solutions. At the end of electrolysis, the overpotentials of the polished anode #4 in the electrolyte with the variation of concentrations for 4, 6, 8, were almost the same (693, 691, 689), while for 10 and 12, the overpotentials began to rise sensibly (713 and 728 mV respectively). It is very possible that Mn^{2+} reacted on the anode, the

potential decreases as result of the depolarization effect during the oxidation of Mn^{2+} on the anode and moreover, the potential increase as a result of the formation of a protective layer composed of Mn oxides - MnO_2 [6].

Corrosion rates of the four polished anodes after the galvanostatic polarization followed by the potential decay at various immersion times were calculated by the linear polarization resistance method, the results are shown in Table 8.6.

Table 8.6 Corrosion rates of the polished anode #4 in acid zinc sulphate electrolyte at 38°C for different immersion times

Immersion time after 5 h electrolysis (h)	Corrosion current density at different temperatures ($\mu A cm^{-2}$)			
	Mn^{2+}(4 gdm^{-3})	Mn^{2+}(6 gdm^{-3})	Mn^{2+}(10 gdm^{-3})	Mn^{2+}(12 gdm^{-3})
1	4.31	3.65	2.59	2.45
2	2.35	1.82	1.58	1.46
3	1.79	1.54	1.23	1.13
4	1.43	1.32	1.18	1.07
5	1.31	1.22	0.93	0.78

As shown in Table 8.6, the corrosion rate of the polished anode #4 in the electrolyte decreases with Mn^{2+} increase, since the reason is that Mn^{2+} and MnO_4^- plays significant role in the anodic process [11]. For example: the concentrations of Mn^{2+} added to acid zinc sulphate electrolyte increased from 4 to 6, 10 and 12 dm^{-3}, the corrosion current of anode #4 at 1 hour immersion time after 5 h electrolysis decreased ~ 15.3%, 39.9% and 43.2%, respectively. When anode #4 was in electrolyte with polarization, PbO_2 formed on the surface of this anode, however, the protective PbO_2 had pores, Pb dissolved readily through the pores. After the equations 8.1, 8.2 and 8.3, the presence of Mn^{2+} and MnO_4^- in the electrolyte cause formation of a thin layer of MnO_2 on the anode. This layer becomes more dense and adherent as the concentration of Mn^{2+} is increased and acted as an additional physical barrier to protect the Pb-Ag substrate from corrosion.

Figure 8.7 shows the combination of the results of polished anode # 4 in Figure 8.6 (concerning the overpotentials at the end of electrolysis) and in Table 8.6 (the first line: corrosion currents at 1 hour immersion time).

It is seen from Figure 8.7, at the high concentrations of Mn^{2+} (10 and 12 gdm^{-3}), the overpotentials at the end of electrolysis of the polished anode #4 in acid sulphate electrolyte increased rapidly with the increase of concentrations of Mn^{2+}, while the corrosion current at 1 hour immersion time after 5 hour electrolysis of the polished anode #4 in acid sulphate electrolyte decreased sharply with the increase of concentrations of Mn^{2+} at the low concentrations of Mn^{2+} (4, 6 and 8 gdm^{-3}). It seems then that a dense non-conductive, well adherent oxide film of MnO_2 increased the thickness and density of oxide layer (PbO_2-MnO_2) and increased the overpotential [6].

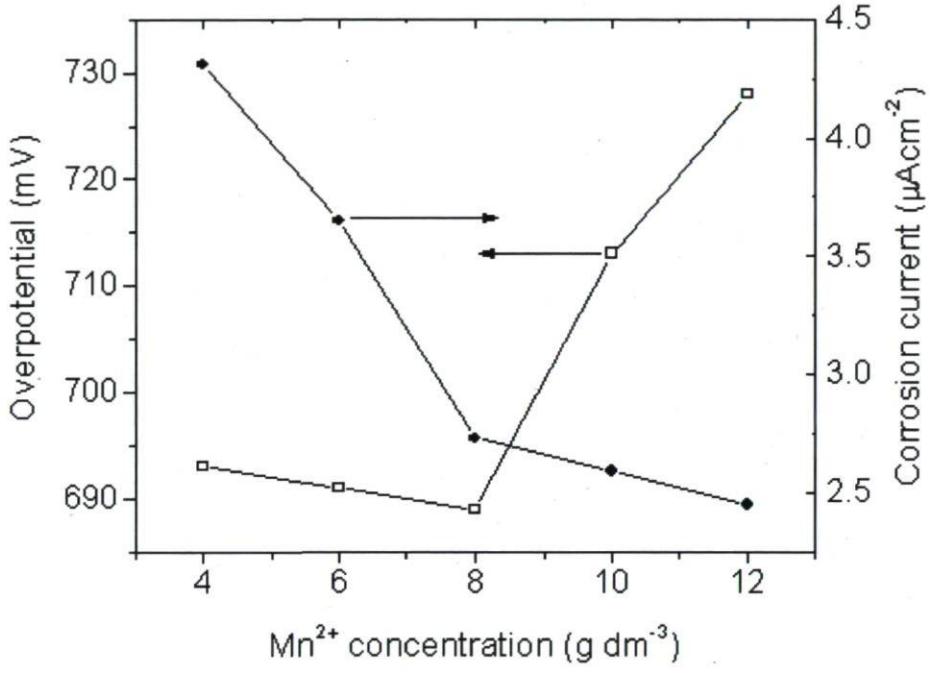

Figure 8.7. Overpotentials after 5 hour electrolysis of the polished anode #4 galvanostatically polarized at 50 $mAcm^{-2}$ and corrosion currents after 1 hour potential decay in acid zinc sulphate electrolyte containing 4, 6, 8, 10 and 12 gdm^{-3} Mn^{2+} at 38°C.

8.3.3.2 Effect of current density

The current density is an important factor for electrochemical behaviour of the polished anode #4 in acid zinc sulphate electrolyte containing 8 gdm^{-3} Mn^{2+}; the corrosion current of anode #4 was determined at different current densities.

From Table 8.7, it can be seen that the corrosion rates of anode #4 in acid zinc sulphate electrolyte containing 8 gdm^{-3} Mn^{2+}during potential decay increased much with the current density of previous galvanostatic polarization experiments from 40 to 50 and much less from 50 to 60 mA/cm^2. It is very possible that more current density during polarization resulted in more PbO_2, and consequently, more PbO_2 was reduced to $PbSO_4$.

Table 8.7 Corrosion rates of the polished anode #4 after the galvanostatic polarization at different current densities in the zinc electrolyte containing 8 gdm^{-3} Mn^{2+} at 38°C

Galvanostatic polarization current density $mAcm^{-2}$	Corrosion current density (μAcm^{-2})				
	1 h	2 h	3 h	4 h	5 h
40	2.31	1.57	1.25	1.19	0.86
50	2.73	1.78	1.34	1.25	1.04
60	3.19	1.97	1.53	1.41	1.28

8.3.3.3. Effect of temperature

The corrosion behaviour of the polished anode #4 was conducted at different temperatures. From Table 8.8, the corrosion rates of anode #4 increase with the temperature increase. The above results confirm the results of Ivanov et al. [6] showing that in presence of Mn^{2+}, the corrosion rate increases significantly with increasing temperature for Pb-Ag alloys.

Table 8.8 Corrosion rates of the polished anode #4 in acid zinc sulphate electrolyte containing 8 gdm^{-3} Mn^{2+} at different temperatures

Immersion time after 5 h electrolysis (h)	Corrosion current density at different temperatures (μAcm^{-2})		
	25°C	38°C	55°C
1	1.48	2.73	3.42
2	1.37	1.78	2.12
3	1.22	1.34	1.95
4	1.01	1.25	1.70
5	0.89	1.04	1.51

Higher temperature during polarization caused the formation of more PbO_2. Also, higher temperature resulted in the acceleration of the reduction reaction during decay after polarization.

8.3.4. Influence of mechanical polishing on polarization followed up by 1 h potential decay

Before the four anodes were polished, there is an oxide film formed on the original surface. The four original surfaces of the anodes were polarization for 5 h followed by one hour potential decay, and then potentiodynamic measurements were carried out; the results are shown in Table 8.9.

Comparing the Tables 8.3 and 8.9 of corrosion current of one hour decay, it can be stated that the four original anodes had lower corrosion currents than that of the four polished anodes in acid zinc sulphate electrolyte without $MnSO_4$ addition. The original oxide film on the surfaces of the four anodes can protect the anodes from corrosion.

Table 8.9 Corrosion potential, corrosion current of the four original anodes #1 - #4 after one hour potential decay following 5 h galvanostatic polarization at 50 $mAcm^{-2}$ in acid zinc sulphate electrolyte without $MnSO_4$ addition at 38°C

Anodes	E_{corr} (mV/SHE)	i_{corr} (μAcm^{-2})
#3	1000	5.77
#1	682	4.84
#2	546	3.97
#4	325	3.86

Comparable experiments are carried out in the electrolyte containing 8 gdm^{-3} Mn^{2+}, the same trend was observed, however, the addition of $MnSO_4$ made the difference between the original and polished samples much less clear.

From the above results, the polished surfaces show that anode #4 had the best corrosion resistance among the four anodes during galvanostatic control in the bath containing permanganate ion at a current density of 50 $mAcm^{-2}$ and 38°C and during the decay period of potential after 5 h galvanostatic polarization in the bath with and without

permanganate ions, and #3 had the worst corrosion resistance among the four anodes. Since anodes #4 has the highest silver content among the four anodes, #2 and #3 have the same silver content (0.56-0.60 approximately), but #2 has the much better performance than #3, it is very possible that the microstructure of anode #3 is causing its worst performance.

Hine et al. [12] found that addition of Ag can decrease the corrosion rates and overpotentials of Pb-Ag alloy anodes, the more addition of Ag is, the lower the corrosion rates and overpotentials are; the optimum Ag content was 1-2% from the economic point of view in Pb-Ag alloys. However, other conditions also could influence the corrosion rates and overpotentials of Pb-Ag alloys, as reported by Prengaman and Siegmund [13], in rolled anodes since the texture was oriented in the rolling direction, producing a grain structure even more difficult to corrode and to form an adherent layer of PbO_2. For example: RSR Technologies has developed a method to produce a surface on the anode, through controlled rolling and alloying, to which a hard, dense layer PbO_2 adheres very quickly. So the different level of roll during fabrication can influence the microstructure of these four Pb-Ag alloys.

It is also found that anode #1 had the lest silver content among the four anodes, although addition of silver at the range of 0.5-1.0% is good at decrease the corrosion rate but the polished surface of anode #1 had higher corrosion resistance than that of anode #3 during potential decay after 5 hours galvanostatic polarization, it should be noted that anode #1 had more Ca content that could have an effect on the corrosion rates of Pb-Ag alloys (+0.04 % difference, anode #1 with oxide layer).

Umetsu et al. [7] found that alloying of calcium $< 0.1\%$ in Pb-0.2-0.3%Ag resulted in depression of anodic oxidation of anode slowly; however, alloying of calcium $< 0.1\%$ in Pb-0.6-0.7% Ag alloys resulted in drastic depression of anodic oxidation of the alloys during polarization. In a word, silver suppresses the anodic oxidation of the material and converts the main oxide from α-PbO_2 into β-PbO_2 and calcium encourages the growth of β-PbO_2 crystals at lower (~ 0.2-0.3%) Ag-content in the Pb-Ag-Ca tertiary alloy anodes during polarization, and β-PbO_2 is an anodic oxide layer of large idiomophic crystals in tight arrangement; β-PbO_2 oxide layer has lower potential and corrosion rate

than α-PbO_2 in same condition [7]. So addition of 0.1% Ca in this Pb alloy anode #1 can decrease much corrosion rate of anode #1 and result that the corrosion rate of anode #1 was less than that of anode #3 containing 0.06% Ca during 1 and 2 h potential decay after 5 h galvanostatic polarization at 50 mA cm^{-2} and 38^{O}C.

8.4. Conclusions

The following conclusions can be drawn from this study:

a. At a current density of 50 $mAcm^{-2}$ and 38°C in a bath with $MnSO_4$ addition, the polished surface of the anode #4 has the lowest overpotential followed closely by that of anodes #2 and #3 and then anode #1.

b. Overpotentials of the four anodes #1 through #4 in the electrolyte without Mn^{2+} were higher 11, 28, 27 and 23 mV than that of the four anodes in the electrolyte with 8 gdm^{-3} Mn^{2+} respectively.

c. Addition of manganese sulphate from 4 to 8 gdm^{-3} Mn^{2+} to the bath gave almost the same overpotentials and then increased for 10 and 12 for the anode #4.

d. During the potential decay period:

- The original anodes had lower corrosion current than the polished anodes in acid zinc sulphate electrolyte without $MnSO_4$ addition.
- With the temperature and current density increase, the corrosion rates of Pb-Ag anodes increased.
- The four polished anodes in the acid zinc sulphate electrolyte containing $MnSO_4$ addition had lower corrosion rates than those in acid zinc sulphate electrolyte without $MnSO_4$ addition. Also the corrosion rate of Pb-Ag alloy anode decreases with the $MnSO_4$ addition.
- The corrosion rates of the four anodes decrease with the potential decay time.
- The values of more positive (higher) decay potentials lead to higher corrosion rates for all anodes with polished surface in a bath with and without $MnSO_4$ addition for short decay periods.

- The results of EIS measurements show that the anode #4 had the highest polarization resistance among the four anodes, followed by the anodes #2, #1 and #3 in a bath with and without $MnSO_4$ addition.

e. The excessive quantity of calcium (0.12%) in Pb-Ag 0.25% anode showed generally higher overvoltages during electrolysis, if compared to 0.06% Ca and Pb-0.56% Ag content of another anode. However, it showed better corrosion rates during short decay periods in spite of the lower silver content.

8.5 References

[1] **Yu P. and O'Keefe, T.J.**, Evaluation of Lead Anode Reactions in Acid Sulfate Electrolytes. I. Lead Alloys with Cobalt Additives, J. Electrochem. Soc., 146, 1999, pp. 1361-1369.

[2] **Lander, J. J.**, Silver, Cobalt, and Positive-Grid Corrosion in the Lead-Acid Battery, J. Electrochem. Soc., 105, 1958, pp. 289-292.

[3] **Tikkanen M.H. and Hyvarinen, O.**, On the Anodic Behaviour of Pb-Ag Alloys in Sulfuric Acid Solutions, Proc. Int. Congr. Metai. Corros., Meeting data 1969, 1972, 4th, pp. 669-675.

[4] **Pourbaix, M.**, Atlas of Electrochemical Equilibria in Aqueous Solutions, National association of corrosion engineers. Houston, Texas, USA, 1974.

[5] **Charlesby, A.,** Ionic Currents in Thin Films of Zirconium Oxide Les Courants Ioniques Dans De Minces Couches D'oxyde De ZirconiumIonenströme in Dünnen Zirkonoxydfilmen, Acta Met., 1, 1953, pp. 340-347.

[6] **Ivanov, I., Stefanov, Y., Noncheva, Z., Petrova, M., Dobrev, Ts., Mirkova, L., Vermeersch R. and Demaerel, J.-P.,** Insoluble Anodes Used in Hydrometallurgy Part I. Corrosion Resistance of Lead and Lead Alloy Anodes, Hydrometallurgy, 57, 2000, pp. 109-124.

[7] **Umetsu, Y., Nozoka H. and Tozawa, K.**, Anodic Behaviour of Pb-Ag Alloys in Sulfuric Acid Solution, Proceedings of the International Symposium on Extract. Metall. Zinc, MMJ, Tokyo, Japan, 1985, pp. 265-276.

[8] **ASTM Publication, ASTM G5-94**, Standard Reference Test Method for Making Potentiostatic and Potentiodynamic Anodic Polarization Measurements, Philadelphia, PA, vol. 03.02, 2001, pp. 54-59.

[9] **Jin, S., Ghali E. and Houlachi, G.**, Effect of Sandblasting and Shot-Peening on the Corrosion Behavior of Pb-Ag Alloy Anodes in Acid Zinc Sulfate Electrolyte at 38°C, Environment degradation of materials and corrosion control in metals, (Eds: J. Luo, M. Elboudjani, D. Shoesmith, and P.C. Patnaik), Met-Soc, CIM, Montréal, Canada, 2003, pp. 459-470.

[10] **Nguyen, T. K. T.**, A Study of the Mechanism by which Cobalt Ions Minimize Corrosion of Lead Alloy Anodes During Electrowinning of Base Metal, Ph.D Thesis, University of Queensland, Australia, 2007, pp. 2-11, 4-18.

[11] **MacKinnon, D.J.**, The Effects of Foaming Agents, and Their Interaction with Antimony, Manganese and Magnesium, on Zinc Electrowinning from Synthetic Acid Sulphate Electrolyte, Hydrometallurgy, 35, 1994, pp. 11-26.

[12] **Hine, F., Ogata Y., and Yasuda, M.**, Consumption of Lead-Silver Alloy Anodes in Sulfuric Acid Solution, B. Electrochem., 4(1), 1988, pp. 61-65.

[13] **Prengaman R.D. and Siegmund, A.**, New Wrought Pb-Ag-Ca Anodes for Zinc Electrowinning to Protective Oxide Coating Rapidly, LEAD-ZINC 2000, (Eds: J.E. Dutrizac, J.A. Gonzalez, D.M. Henke, S.E. James and A.H.-J. Siegmund), Warrendale, PA: The Metallurgical Society of AIME, 2000, pp. 589-597.

PART 3

Effect of organic additives on current efficiency of zinc deposit

(Chapters 9 and 10)

CHAPTER 9

Influence of malonic acid and triethylbenzylammonium chloride on Zn electrowinning in zinc electrolyte

Influence of malonic acid and triethylbenzylammonium chloride on Zn electrowinning in zinc electrolyte

W. Zhang[1*], A-M. Lafront[1], E. Ghali[1], and G. Houlachi[2]

1. Dept. of Mining, Metallurgical & Materials Engineering, Laval University, Quebec, Canada, G1K 7P4.

2. Hydro-Québec Research Institute, Shawinigan, QC, Canada, G9N 7N5.

* Corresponding author. Tel: (418) 656-7777, ext. 4871, Fax: (418) 656-5343.
wei.zhang.1@ulaval.ca

This paper was published in Hydrometallurgy, Vol. 99, 2009, pp. 181-188.

9.1 Abstract

The influence of malonic acid and other additives has been investigated during the electrowinning of zinc from acid sulphate solutions containing manganese ions. It was found that adding malonic acid "MA" increased the current efficiency and decreased the anodic and cathodic potentials and the cell voltage in the standard electrolyte. Adding malonic acid to the industrial electrolyte containing antimony impurity also led to an increase in the current efficiency. Triethyl-benzylammonium chloride "TEBACl" was the best additive to improve current efficiency in presence of 5 mg/L Ni^{2+} impurity and it also counteracted the deleterious effect of Sb^{3+} better than the other additives such as polyethyleneglycol, sodium lauryl sulphate, perfluoro-heptanoic acid and malonic acid were not as good as glue and chloride ion together. Adding 2 mg/L of "TEBACl" to sulphuric acid solution in presence of nickel ions increased the cathodic potential of hydrogen evolution on the zinc deposit, much more than that of 100 mg/L "MA".

Keywords: Zinc electrowinning; Malonic acid; Triethyl-benzylammonium chloride;

Current efficiency; Electrode potential; Hydrogen evolution.

9.2. Introduction

During the electrowinning of zinc sulphate electrolytes, there are two main reactions in competition on the cathode, one is zinc deposit, and the other is hydrogen evolution. In the pure zinc electrolyte, over 90% of the total reaction corresponds to the zinc deposit. Cachet and Wiart [1] explained the strong interaction between H^+ and Zn^{2+} in terms of a model based on a competition between the autocatalytic production of an adsorbed intermediate, Zn^{+}_{ads} and adsorption of H_{ads} that acts primarily as an inhibitor. The hydrogen evolution reaction (HER) is one of the most frequently studied electrochemical reactions because of its importance in different applied areas. It takes place on zinc in two steps with the involvement of one intermediate electrochemical reaction i.e. $H^+ + e \rightarrow H_{ads}$ followed by $H_{ads} + H^+ + e \rightarrow H_2$ that constitutes the slow step [2].

The electrolyte often contains some metal ion impurities, such as Ni, Co, Sb, Ge, etc, more electropositive than zinc, and their presence can be very detrimental. This results in a deterioration of zinc deposit quality, a decrease in current efficiency (CE), and an alteration of cell voltage (CV). These impurities can accelerate the parallel process of hydrogen evolution due to the lower overvoltage of discharge of H_3O^+ on Ni, Co, Cu sites on the surface or the formation of unstable hydrides with Sb, Ge, and As [3]. It has been proposed that a certain amount of hydrides is sufficient to initiate a process known as "zinc redissolution" [4]. Antimony (III) has been recognised as one of the most deleterious and toxic impurities. Hydrogen evolution creates a local redistribution of the current showing structural defects in the form of pits [5-7].

Organic additives are widely employed to counteract the harmful effects of these metallic impurities. In combination with some glue, antimony also plays a beneficial role producing optimum current efficiency and acceptable surface morphology of the deposit [8-11]. Glue is the most common organic additive used industrially. Nevertheless, some authors have investigated the use of other additives like ammonium ion, various polyols and also anionic additives like perfluorocarboxylic acid and alkyl sulphates as alternatives to glue.

Triethyl-benzylammonium chloride (TEBACl C_6H_5-CH_2-N-$(C_2H_5)_3Cl$) and other additives such as polyethylene glycol (PEG HO-$(CH_2$-CH_2-$O)_n$-H), perfluoro-heptanoic acid (PFHA $C_6F_{13}COOH$), and sodium lauryl sulphate (SLS $C_{12}H_{25}SO_4$) have been selected to be studied in this work because some authors have reported on their beneficial effect either alone or in combination on current efficiency (CE) in presence of antimony [4, 8, 9, 11-17]. They have been used also in different electrowinning bath conditions such as that of Zinc Électrolytique du Canada Ltd. "CEZ" conditions but most of the investigations used electrolytes without Mn^{2+}.

Triethyl-benzylammonium chloride "TEBACl" can be adsorbed on the cathodic surface and block the active sites. Ivanov [4] stated that it decreases the screening effect of hydrogen bubbles responsible for the formation of local galvanic cells, and increases the induction period for the dissolution of deposited zinc in nickel-containing solution

under galvanostatic control. Polyethylene glycol "PEG" has a strong inhibitive effect on the cathodic zinc deposition reaction; this effect is associated with adsorption of a monolayer of PEG molecules that collapse into spheres. Moffat et al. [16] observed that PEG interacts synergistically with Cl^- and Cu^+ to form a passive film that inhibits the electro-deposition of metal. Adding perfluoroheptanoic acid "PFHA" to the electrolyte suppresses hydrogen evolution during zinc electro-deposition by blocking the active sites through adsorption [15]. The adsorption is not caused by electrostatic attraction but by the organic group of the acid. Sodium lauryl sulphate "SLS" reduces the interfacial tension and leads to the incorporation of protons at the interface favouring proton reduction and modification of the interfacial pH [8-10].

The decrease in current efficiencies with the increase of glue concentrations has also been observed by other workers and is generally attributed to the surface coverage of the cathode by a strongly adsorbed additive layer [13]. Such a layer increases the interfacial viscosity and thereby decreases the mass transfer and zinc deposition rates [8]. It has been shown that an induction period of more than 1 h exists before cobalt and nickel begin to have an effect on current efficiency of zinc deposit. After the induction period, the current efficiency decreases rapidly with time. Addition of triethyl-benzylammonium chloride or other additives can increase the induction time and decrease hydrogen evolution [11].

Malonic acid belongs to the polyacid family. The effect of malonic acid on zinc electrowinning has been studied by Jin et al. [18]. They found that adding 500 mg/L malonic acid $CH_2(COOH)_2$ to the acid electrolyte gave excellent current efficiency 94.8% and decreased the cell potential 51 mV during 12 hours of electrowinning. However, adding 500 mg/L is too excessive since malonic acid is expensive as compared to glue. Gamburg et al. [19] added malonic acid to the electrolyte designed for deposition of nickel coating to increase the buffer properties of the electrolyte and to decrease the passivation of nickel anode. The deposits could be obtained over a wide range of deposition times and current densities with high current efficiency in comparison to boric and succinic acid electrolyte. In this work, a rather long period of 24 h deposition is

considered because this leads to more precise CE% determination without the need to adjust the electrolytic bath.

The objectives of this study are to investigate the influence of malonic acid, triethyl-benzylammonium chloride and other additives on the current efficiency, anodic and cathodic potentials, cell voltage and deposit morphology during the electrowinning of zinc. In particular, the acid sulphate solutions contained Mn^{2+} in the presence of different metallic impurities such as Sb^{3+} and Ni^{2+} and are employed at typical operational conditions. Based on preliminary tests and previous investigations, attention was given to examine the influence of malonic acid concentration in the electrolyte to determine the optimum concentration to use. The effect of malonic acid is also examined in the presence of Sb^{3+} ions and/or industrially used additives such as glue and chloride ion. The influence of the two promising additives MA and TEBACl on the competing hydrogen evolution reaction "HER" in the same operational conditions of electrowinning are also examined, with and without antimony, as it is frequently present as an impurity in the electrolyte.

9.3 Experimental

9.3.1 Electrolyte

Experiments were done in 800 ml of synthetic standard acid electrolyte "AE" containing 60 g/L Zn^{2+} ($ZnSO_4$,$7H_2O$), 180 g/L H_2SO_4, and 8 g/L Mn^{2+} ($MnSO_4.H_2O$) or only 180 g/L H_2SO_4 for the hydrogen evolution reaction. In this work, manganese ions were added to simulate the practical conditions considering their beneficial influence on the electowinning process. The effect of some additives on current efficiency and cell voltage were studied in acid electrolyte and acid electrolyte containing impurities (0.01 mg/L Sb^{3+} from potassium antimony tartrate $KC_4H_4O.SbO$ or 5 mg/L Ni^{2+} from $NiSO_4.6H_2O$). Four different concentrations of malonic acid (MA) were chosen 10, 50, 100 and 500 mg/L. Four other additives with fixed concentrations giving highest CE% were chosen: 2 mg/L TEBACl, 1 mg/L of polyethylene glycol 2000 (PEG), 10 mg/L perfluoroheptanoic acid (PFHA), 2 mg/L sodium lauryl sulphate (SLS). The effect of these additives were

compared to that of 250 mg/L Cl^- and 3 mg/L glue, generally used in the zinc plant (CEZ) practice.

9.3.2 Measurements methods

Two galvanostatic experimental set-ups were employed at a current density of CD = 500 A/m^2 for 24 h deposition time at 38°C with stirring at a rotation rate of 60 rpm. No adjustment of composition of the electrolytic bath was carried out during the 24 h. The first set-up was used to measure the cathodic potential and current efficiency, while the second set-up was used to obtain the anodic potential and current efficiency as duplicates. The cell voltage were calculated as (anodic potential – cathodic potential). The electrodes were mechanically polished with emery paper down to grit 1000. A three electrodes setup comprising: $1cm^2$ aluminum cathode Al 1100 (or 1 cm^2 Zn deposit on aluminum for the hydrogen evolution reaction), 1 cm^2 Pb-0.6 wt% Ag alloy polished anodes and the reference electrodes ($Ag,AgCl/KCl_{sat}$) or ($Hg, Hg_2SO_4/sat.K_2SO_4$) were used for first or second set-ups respectively. All the potential values are given versus SHE.

Some experiments were made in duplicate and triplicate and only experiments which were made in triplicate are considered for error bars statistical evaluation as shown in the corresponding figures. The two used set-ups gave the same trend but did not match in absolute values.

The current efficiency was calculated as CE% = (W.F.n/I.t.M) x100%; where W is the weight of deposit (g), n is the number of e^-, F is the faraday constant, M is a molecular weight, I is the total cell current (A) and t is the time of deposition.

SEM analyses were conducted using JEOL JSM-25s III model Scanning Electron Microscope to characterize the zinc deposit.

9.4. Results and discussion

9.4.1. Malonic acid and MA with glue and chloride ion

9.4.1.1 Malonic acid

The effect of 0, 10, 50, 100 and 500 mg/L MA on CE% and on the anodic, cathodic potentials and cell voltage during the 24 h deposit is shown in Figures 9.1, and 9.2, respectively.

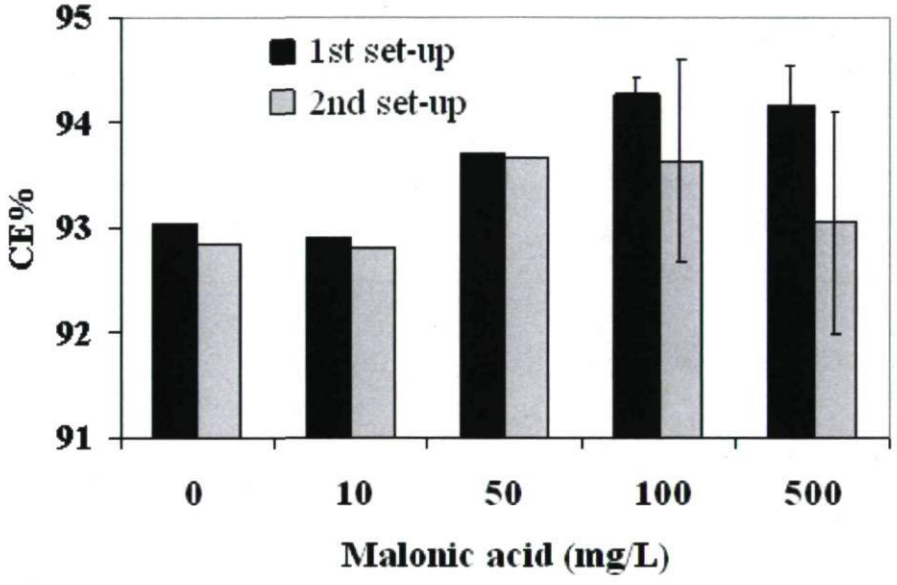

Figure 9.1: CE% of Zn deposit from electrolyte containing different concentrations of MA after 24 hours deposition from the first and the second set-ups.

The addition of MA to the zinc electrolytic resulted in increasing the CE% with the best increase of 1.2% and 0.8% found for the addition of 100 mg/L MA after the first and second set-ups, respectively. Addition of 500 mg/L did not show any advantage for CE% and could be considered as excessive. Error bars indicate the difficulty to have reproducible results with the second set-up for current efficiencies for the concentrations of 100 and 500 mg/L MA. The different results from the two set-ups might be due to the rate of Zn^{2+} diffusion to the cathode, since there were slight differences in stirring rates (± 10%) and in the positions of the electrode in the glass container.

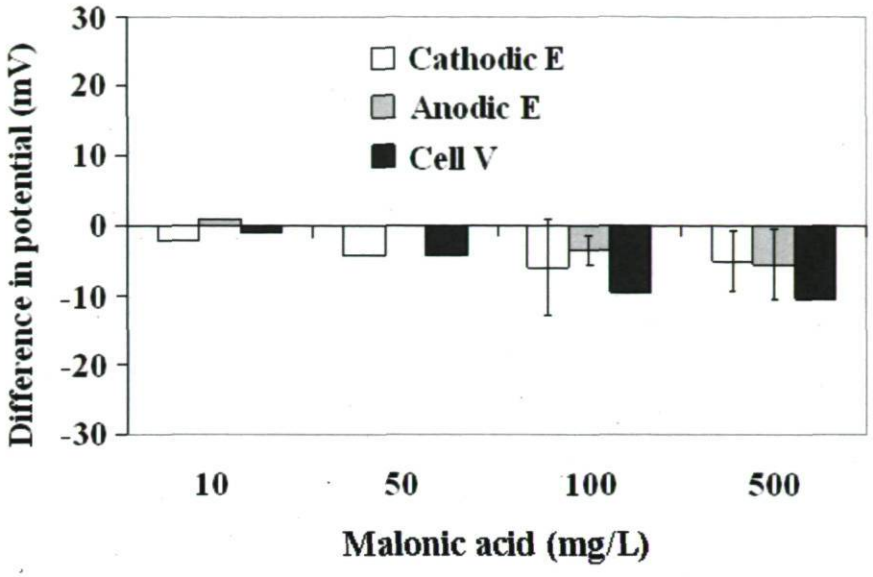

Figure 9.2: The difference in potential of the Zn cathode, Pb anode and cell voltage after 24 hours of electrolysis for added malonic acid with reference to electrolyte without additive.

Figure 9.2 shows that the differences in cathodic and anodic potentials and in cell voltage values were less than 10 mV, with more decrease in potential observed with the increase in MA concentration. Again, the addition of 100 mg/L MA gave the best decrease of cathodic potential around 5 mV, whilst 500 mg/L MA gave almost the same decrease of total cell voltage ~ 10 mV. Therefore, it seems that 100 mg/L MA will be the optimum addition, subject to thorough economical assessment.

The addition of malonic acid increases the current efficiency of zinc deposit since it complexes with impurities of the electrolyte, such as iron (II) from the anode and also decreases H_2 evolution. It was also found that during the 24 hours of electrolysis with addition of 10 and 50 mg/L MA, the solution became deep violet red colour; indicating the production of MnO_4^-. However, during electrowinning with 100 mg/L MA or more, the solution remained colourless indicating that there was no MnO_2 mud precipitation formed at the anode, nor traces of MnO_4^-. Jin et al. [18] found that the presence of MnO_4^- in the electrolyte can decrease the current efficiency whilst Berka et al. [20] stated that malonic acid reduces the permanganate ion and increases the current efficiency according to the following equation:

$$HOOC\text{-}CH_2\text{-}COOH + 2MnO_4^- \rightarrow (COOH)_2^{2-} + CO_2 + 2MnO(OH)_2 \text{ --------- (9.1)}$$

9.4.1.2 Malonic acid with glue + Cl^-

Figure 9.3 shows the effect of addition of MA (100 mg/L), glue+Cl^- (3 mg/L, 250 mg/L respectively), and the addition of MA+glue+Cl^- on the CE% of zinc deposition from the standard acid electrolyte and from the electrolyte containing Sb^{3+} (0.01mg/L).

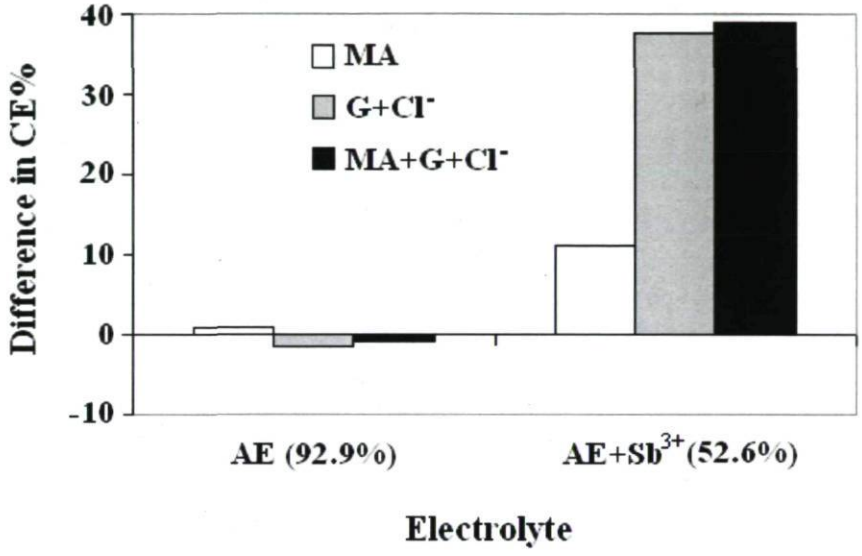

Figure 9.3: The effect on CE% of additives MA, glue+Cl^- and MA+glue+Cl^- in the standard acid electrolyte without and with 0.01 mg/L Sb^{3+} - relative to CE% without additives.

In the acid electrolyte, the addition of MA increased the CE by 1% whilst the addition of glue+Cl^- and MA+glue+Cl^- to the electrolyte, decreased the CE by 2.3% and 1.1% respectively. However, all the additives had much more positive effect on increasing the rather poor CE% of 52.6% in the electrolyte containing Sb^{3+}. The addition of MA had less effect than that of glue+Cl^- and the combination of 100 mg/L MA with glue+Cl^- only marginally increased the CE by a further 1.2%.

Adding 0.01 mg/L of Sb^{3+} to the electrolyte decreased zinc CE% to 52.6% because antimony ions facilitate H_2 evolution and accelerate the localised corrosion of deposited zinc even while cathodically polarized. The mechanism of the interaction of antimony and glue in solution or at the cathode surface cannot be elucidated. At the

optimum combination levels, the presence of one additive modifies the controlling effect of the other, but not to the extent that platelet refinement is eliminated [13].

There are two proposed mechanisms to explain the decrease of the CE due to the presence of impurities in the zinc electrolyte [21]. They are:

(i) the reduction of H^+ on co-deposited impurities with low hydrogen overpotentials (high exchange current density) combined with localized cell corrosion.

(ii) continuous co-deposition and evolution of H_2 on zinc without preferential areas of zinc corrosion.

The latter mechanism may involve interaction between the impurities and H^+ in the double layer without the impurities actually depositing cathodically on zinc, e.g. the decomposition of hydrides formed in the double layer would provide an alternate path for hydrogen evolution. For antimony impurity, Mackinnon et al. [22] chose the second mechanism since Sb has never been found in the deposit, and only very small concentrations in the electrolyte are required for them to become active. Also, antimony has fairly high hydrogen overpotential and would not be expected to be particularly harmful when deposited in the metallic state.

Figure 9.4 shows the effect of the above additive combinations on the difference in cathodic and anodic potentials and cell voltage.

In the standard electrolyte, the cathodic and anodic potentials and cell voltage were -945, 1962 and 2907 mV, respectively. The addition of MA slightly decreased the cathodic and anodic potential by 6 and 4 mV, respectively, whilst the addition of glue+Cl^- hardly affected the cathodic potential but increased the anodic potential by 14 mV. Further addition of MA had little effect. In the electrolyte containing Sb^{3+}, the cathodic and anodic potentials and cell voltage were -880, 1960 and 2840 mV, respectively. The addition of the three additives increased the cathodic and to a lesser extent the anodic potentials and hence the cell voltage was 40-50 mV higher.

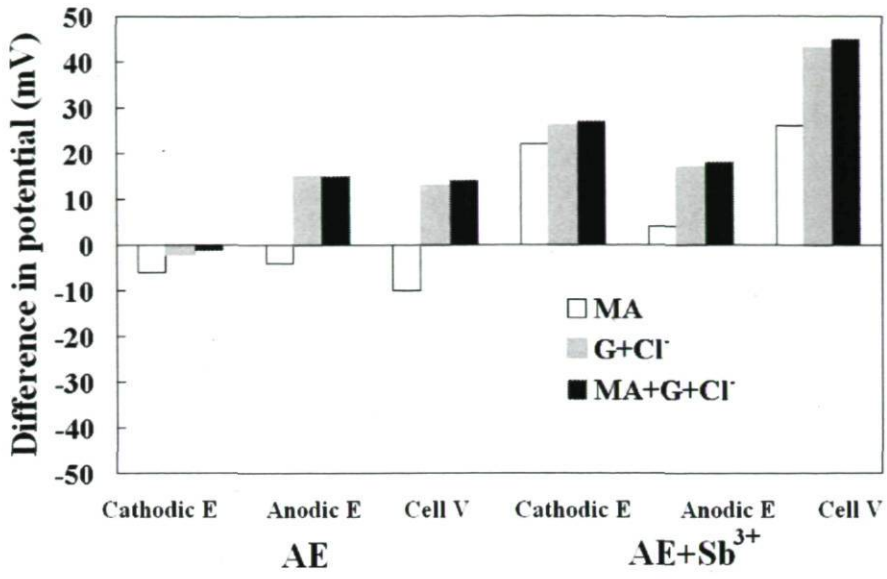

Figure 9.4 Differences in cathodic Zn, anodic Pb potentials and cell voltage in electrolyte with and without 0.01 mg/L Sb3+ containing MA, glue+Cl^- and MA+glue+Cl^- - relative to values without additives.

9.4.2. Influence of TEBACl, MA and other additives as compared to glue

The effect of TEBACl (2 mg/L) and MA (100 mg/L) as well as other additives such as PEG (1 mg/L), PFHA (10 mg/L) and SLS (1 mg/L) were added to the standard zinc electrolyte with and without antimony to examine CE%, anodic, cathodic potentials, and cell voltage. The optimum concentrations of TEBACl, PEG, PFHA and SLS were considered after the literature [8-10, 14-17] and some preliminary laboratory experiments (not shown). The chosen concentrations of these additives were the optimum concentrations added to electrolyte to get the best current efficiency. Figure 9.5 shows their influence on CE% and Figures 9.6 and 9.7 show their influence on anodic Pb, cathodic Zn potentials and cell voltage as compared to that of glue+Cl^- (3 mg/L + 250 mg/L). Again, the comparison is made with respect to electrolyte with or without 0.01 mg/L Sb^{3+} in Figures 9.6 and 9.7.

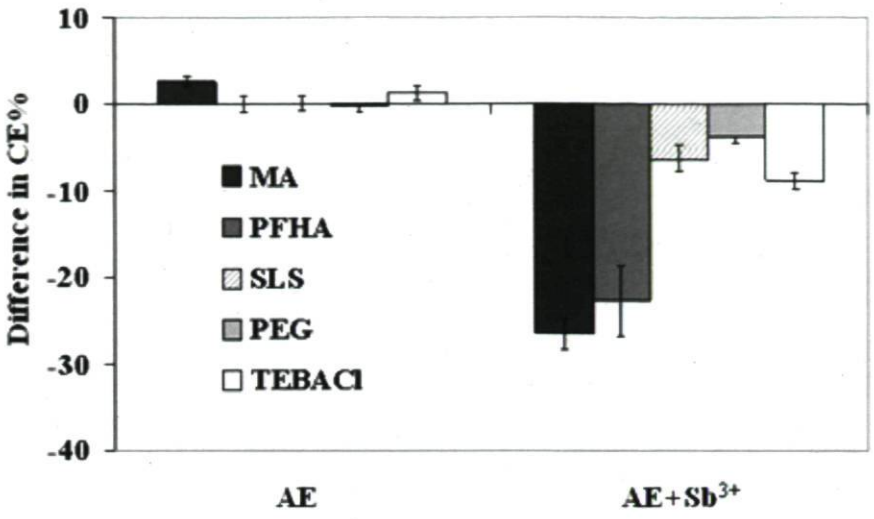

Figure 9.5 Influence of five further additives on CE% of zinc deposit as compared to that with added glue (3 mg/L) + Cl^- (250 mg/L) - with or without 0.01 mg/L Sb^{3+}.

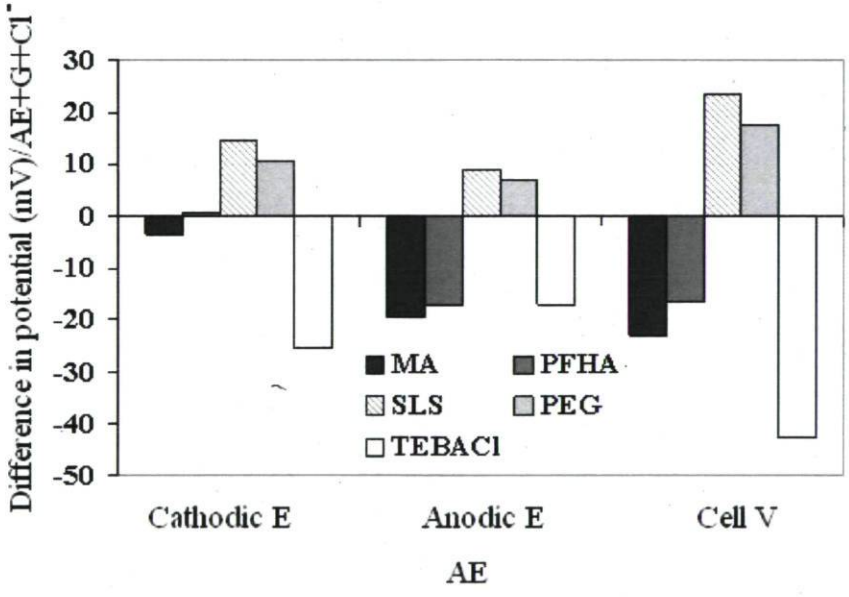

Figure 9.6 Influence of five further additives on anodic Pb, cathodic Zn potentials and cell voltage as compared to that with added glue (3 mg/L) + Cl^- (250 mg/L).

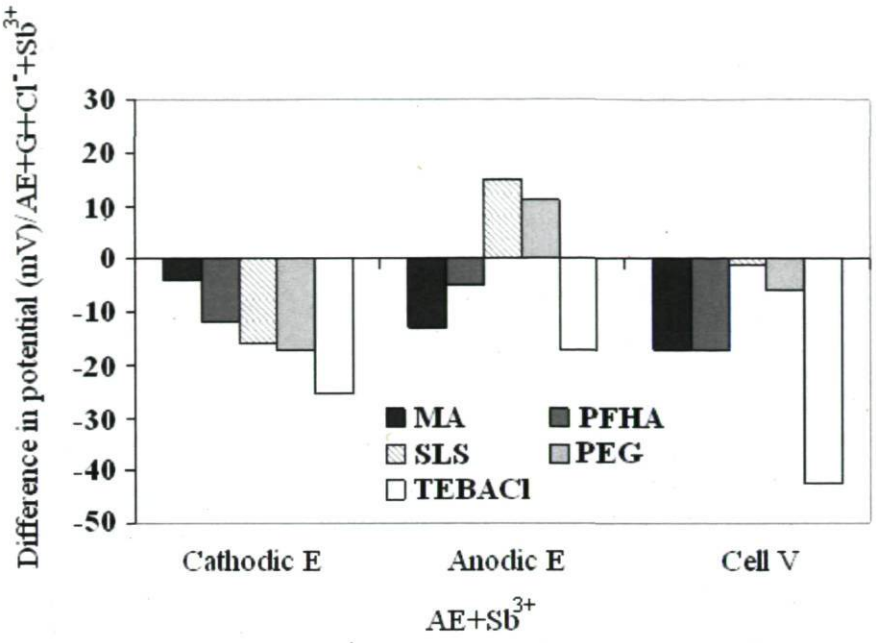

Figure 9.7 Influence of five further additives on anodic Pb, cathodic Zn potentials and cell voltage as compared to that with added glue (3 mg/L) + Cl^- (250 mg/L) in electrolyte with Sb^{3+}.

With reference to acid electrolyte containing glue G + Cl^-, the further addition of malonic acid "MA" increased CE% by 2.5 (±0.5)%, while it decreased the cell voltage by 23 mV. The addition of perfluoroheptanoic acid "PFHA" did not change the CE% (±0.8) but decreased the cell voltage by 17 mV; whilst the addition of sodium lauryl sulphate "SLS" again did not change the CE% (±0.7) but increased the cell voltage by 23.5 mV. Similarly, the addition of polyethyleneglycol PEG hardly changed CE% and increased the cell voltage by 17.5 mV. Finally, the addition of Triethyl-benzylammonium chloride "TEBACl" increased CE by 1.3 (±0.8)% and decreased the cell voltage by 42.5 mV (Figures 9.5 and 9.6).

A similar comparison with acid electrolyte containing Sb^{3+} as well as glue + Cl^- found much larger changes in CE% but similarly small changes in voltage. The further addition of MA decreased CE by 26.5 (±1.8)% and the cell voltage by 17 mV; whilst PFHA decreased CE by 22.8 (±4.0) % and the cell voltage by 17 mV; SLS decreased CE by 6.1 (±1.8)% and the cell voltage by 1 mV; PEG decreased CE by 3.9 (±0.6)% and the

cell voltage by 6 mV and finally TEBACl decreased CE by 8.9 (±1)% and the cell voltage by 26 mV (Figures 9.5 and 9.7).

Clearly, the addition of malonic acid to the standard acid electrolyte led to better current efficiency than that of other additives. However, MA counteracted the deleterious antimony impurity less than the other four additives. The possible reason is that MA is not well adsorbed on the surface compared to other additives to form a strongly adsorbed additive layer that can complex with harmful metallic impurities. Among the tested additives, PEG added to an electrolyte containing Sb^{3+} seems to be the best additive to give the highest CE% but it is not as good as glue. Whilst TEBACl (2 mg/L) added to an electrolyte with and without Sb^{3+} appears to be the best additive for decreasing cell voltage.

The effect of glue, MA and TEBACl on the Ni^{2+} impurities has also been tested and the results are shown in Table 9.1.

Table 9.1 Current efficiencies of zinc deposit, cathodic Zn and anodic Pb potentials determined at 50 mA/cm^2 in different electrolytes (stirred at 38°C during 24 h electrowinning with Pb-0.6%Ag alloy anode)

Electrolyte *	First set-up			Second set-up			Cell voltage (mV)	
	CE (%)	Cathodic potential vs. SHE (mV)		CE (%)	Anodic potential vs. SHE (mV)		Average	ΔV
		Average	ΔV		Average	ΔV		
AE + G + Cl^- + 5 mg/l Ni^+	12.7±3.2	-910±6	0	11.5±2.9	1988±10	0	2898	0
AE + 2 mg/l TEBACl + 5 mg/l Ni^+	91.6±0.7	-919±2	-9	91.3±0.5	1970±6	-18	2889	-9
AE + 0.1 g/l malonic + 5 mg/l Ni^{2+}	20.5±2.5	-914±5	-4	20.1±2.7	1966±2	-22	2880	-18

* AE: Standard electrolyte; G : Glue; TEBACL : Triethylbenzylammonium chloride.

It can be deduced from Table 9.1 that the presence of 5 mg/L of Ni^+ in the industrial electrolyte (glue + Cl^-) led a very low CE% of 12.1 (0.6)%. However, the addition of MA and TEBACl to a standard electrolyte containing 5 mg/L Ni^{2+}, increased

the CE by 8.2 (±0.4)% and 79.3 (±0.4)% respectively. The CE% of the zinc deposit in an electrolyte containing 5 mg/L Ni^{2+} and 2 mg/L TEBACl was very satisfactory (91.6%) and the cell voltage decreased by 9 mV. It means that TEBACl counteracts the deleterious effect of Ni^{2+} better than glue.

As previously reported by Stefanov and Ivanov [6], during the electrowinning of zinc from acid sulphate electrolytes in presence of nickel ions, redissolution of deposited metal takes place due to nickel co-deposits which forms numerous galvanic micropairs with zinc and facilitates H_2 evolution. However, the addition of surface active agents decreases the surface tension and increases the cathodic potential of zinc deposit, leading to the formation of small hydrogen bubbles, easier separation of zinc deposit from the cathode surface and increasing induction time to prevent zinc deposit dissolution.

The nature of induction period in the course of zinc redissolution in the presence of nickel ions has been explained by the action of the hydrogen bubbles arising on the areas of co-deposited zinc and nickel. The increase in the induction period and beneficial effect of triethyl-benzylammonium chloride "TEBACl" in nickel-containing electrolytes has been related to a decrease in the screening effect of hydrogen bubbles where local galvanic cells can be generated [7]. Concerning current efficiency, it is found that MA is less harmful on Ni^{2+} than glue and chloride, since malonic acid is a buffering and complexing agent in the electrolyte, so it can counteract the deleterious effect of Ni^{2+} [19].

9.4.3. SEM morphology

SEM was used to examine the formation of zinc deposit; and typical images are shown in Figure 9.8.

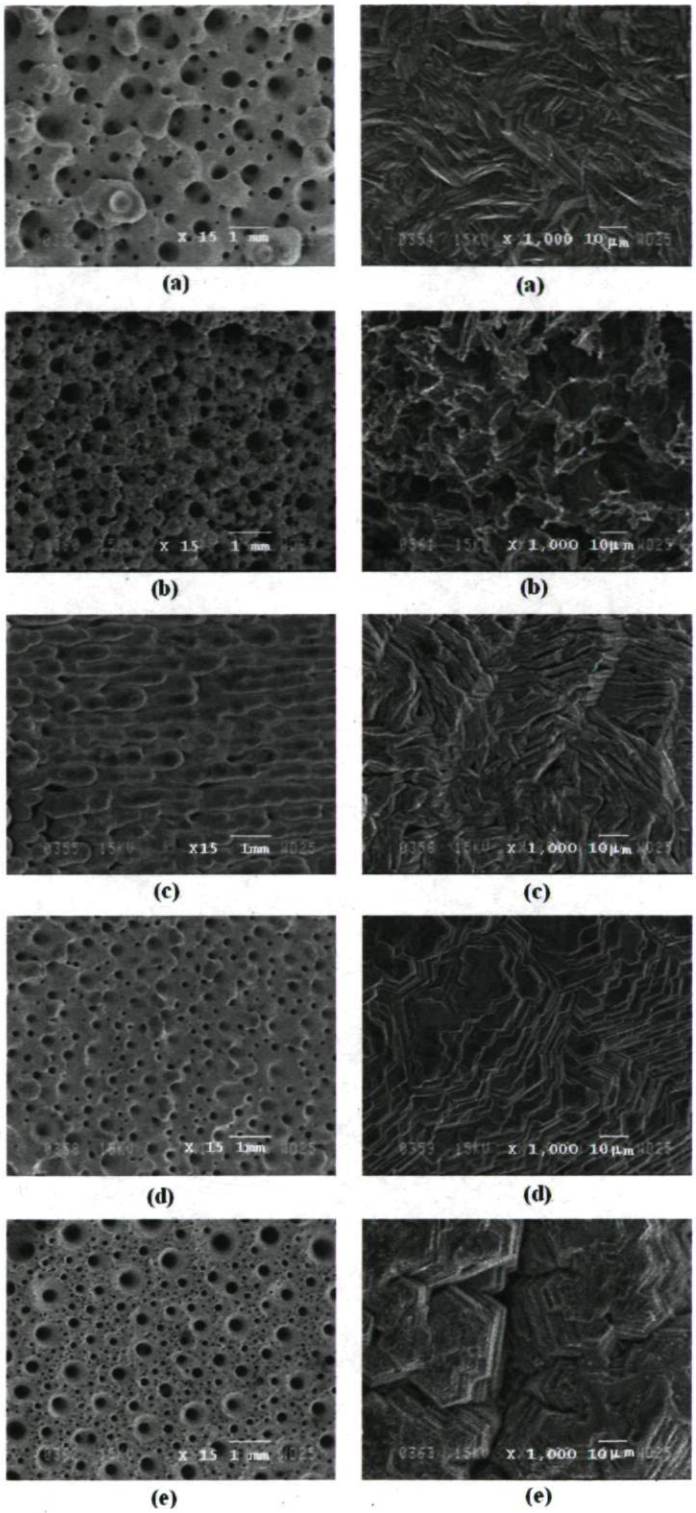

Figure 9.8: SEM morphology of 24 hours zinc deposition from acid sulphate electrolyte containing different additives (a) MA, (b) MA + Sb^{3+}, (c) Glue + Cl^- + Sb^{3+}, (d) Glue + Cl^- + Ni^{2+}, (e) TEBACl + Ni^{2+} at 50 mA/cm^2 and 38°C.

The addition of MA to the standard acid electrolyte caused the production of deposits with many pores or holes (Figure 9.8a). The observed bubbles were formed and developed at specific sites on the electrode surface that led to the existence of circular holes. Sharply defined zinc platelets were aligned at intermediate angles to the aluminum cathode (Figure 9.8a). The presence of antimony in the electrolyte with MA led to an increased number of circular holes with decreased diameter (Figure 9.8b). Strong dissolution took place at the edge of the crystal grain leading to a strong corroded structure (Figure 9.8b).

Zinc deposits from the electrolyte containing glue + Cl^- and Sb^{3+} showed compact nodules (Figure 9.8c). The nodules consisted of hexagonal zinc platelets aligned at intermediate angles to the aluminium cathode (Figure 9.8c). Short tiny needles appeared in the edges of the platelets (not shown).

Electrolytes containing Ni^{2+} instead of Sb^{3+} as impurity showed a zinc deposit with numerous holes (Figure 9.8d). The deposit had a basal orientation of its crystal and the hexagonal zinc crystals were poorly defined. They had varying grain size with some degree of zinc dissolution (Figure 9.8d).

Finally, the zinc deposit from the electrolyte containing Ni^{2+} and TEBACl as an alternative additive to glue showed less numerous but bigger pores (Figure 9.8e) and well defined hexagonal platelet parallel to the substrate (Figure 9.8e). It appeared that very small crystallites were formed on the bigger crystal platelets (not shown). Tripathy et al. [14] have observed a similar phenomenon in the case of combination of TEBACl and Sb^{3+} instead of Ni^{2+} that gave the optimum CE%.

Finally, the SEM morphology studies of 24 hours zinc deposits from acid sulphate electrolyte containing different additives showed that the addition of both TEBACl and Ni^{2+} was the best choice.

9.4.4. Influence of MA and TEBACl on hydrogen evolution on Zn in H_2SO_4

9.4.4.1 Influence of MA

The cathodic polarization curves are shown in Figure 9.9 concerning two baths with and without malonic acid. Current densities on the Zn surface in the two baths increased

slowly at potential -0.8 V/SHE, close to the open circuit potential under the same conditions of zinc electrolysis. This shows the important zone of polarization resistance for hydrogen evolution reaction on Zn deposit as cathode. As the potential became more negative, the current densities on the Zn surface in the two baths increased. The current on the Zn deposit in sulphuric acid solution (180 g/L H_2SO_4) was more significant than that in the same solution containing 100 mg/L MA at the same potentials. The difference in current density became more significant with increasing negative potentials. Diffusion overpotential was limiting the current density at high cathodic potentials in the presence of MA (limiting current plateau) due to the employed agitation rate. From Figure 9.9, it is clear that the addition of MA results in a higher overpotential for H_2 evolution, which is benefical to zinc deposition and it will increase CE% of zinc deposit.

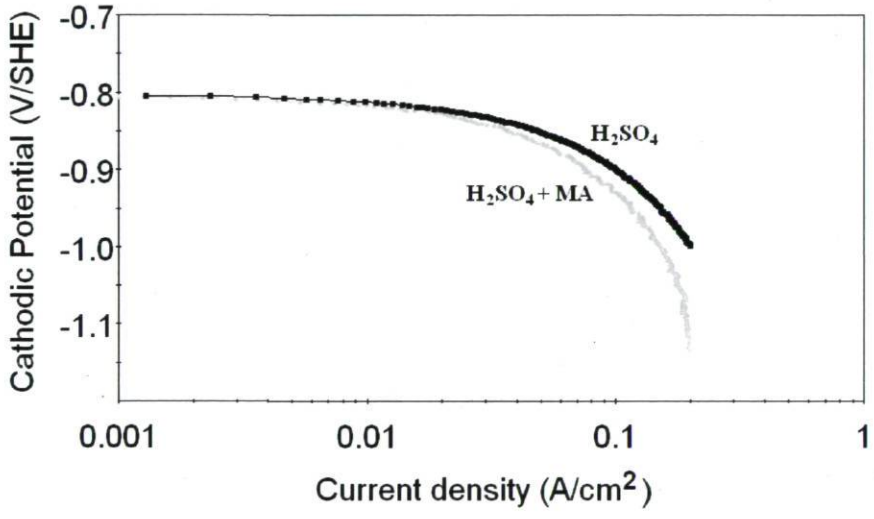

Figure 9.9: Potentiodynamic cathodic polarization curves of Zn electrode in 180 g/L H_2SO_4, and 180 g/L H_2SO_4 + 100 mg/L MA at 38°C.

The cathodic polarization curves of the hydrogen evolution reaction of the Zn deposit as a function of electrolysis time were carried out at the current densities of 40, 50, 60 mA/cm² over four minutes. The overpotentials of the hydrogen evolution reaction were determined by subtracting the ohmic drop (obtained by ac impedance technique) and the calculated reversible potentials of hydrogen evolution reaction (0.034 V vs. SHE) from the measured electrode potential values.

Figure 9.10 shows that the difference increases with the increase of the current densities at 38°C for the examined time period. It can be observed that overpotential "Δη" during the first 50 seconds was more significant than that at the end with and without malonic acid. It is possible that the formed "Beilby layer" with superficial non conducting metal oxides and impurities after mechanical polishing could be the origin of these temporary high initial overpotentials. Galvanostatic studies, which reflected more the electrowinning process conditions, confirmed the potentiodynamic polarization studies.

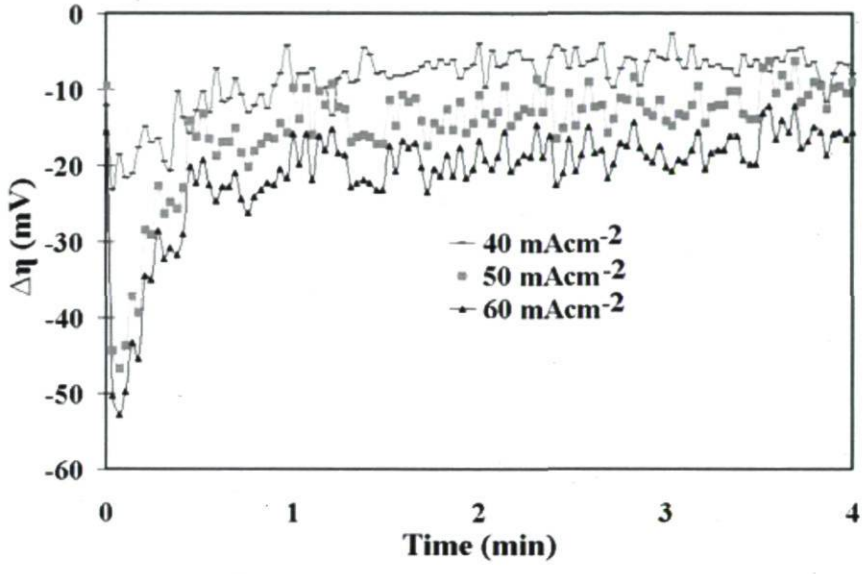

Figure 9.10: Difference Δη between the overpotentials of H_2 evolution reaction on Zn deposit in H_2SO_4 with and without MA at 38°C.

9.4.4.2 Influence of TEBACl and MA

Figure 9.11 shows the cathodic potential of the hydrogen evolution reaction on Zn deposit as cathode in 180 g/L H_2SO_4 at the current density of 50 mA/cm^{-2} at 38°C for H_2SO_4, H_2SO_4 + TEBACl or MA and for H_2SO_4 + Ni + TEBACl or MA.

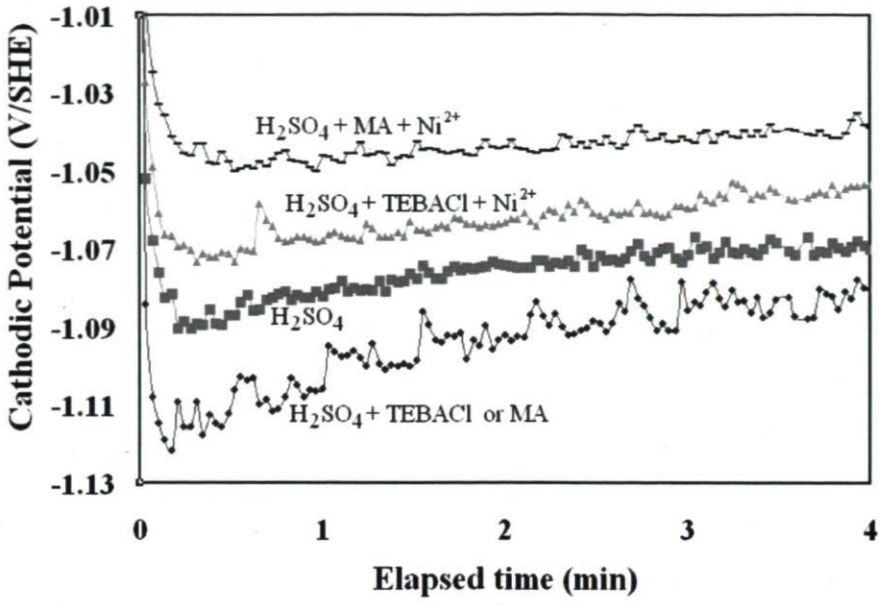

Figure 9.11: Comparison of cathodic potentials on Zn deposit at constant current density of 50 mA/cm^{-2} and 38°C in (a) 180 g/L H_2SO_4, (b) 180 g/L H_2SO_4 + 2 mg/L TEBACl (c) 180 g/L H_2SO_4 + 2 mg/L TEBACl + 5 mg/L Ni^{2+}, and (d) 180 g/L H_2SO_4 + 100 mg/L MA + 5 mg/L Ni^{2+}.

After 4 min of electrolysis at the current density of 50 mA/cm^{-2}, the addition of 2 mg/L TEBACl increased the cathodic potential by more negative 11 mV and this was very close to that of MA (10 mV). Thus, the addition of MA or TEBACl led to reduce the hydrogen evolution and hence increase the CE% of zinc deposition. In presence of 5 mg/L Ni^{2+} lower cathodic overpotentials of hydrogen evolution were obtained in presence of the two additives. However, the difference in hydrogen overpotential ($\Delta\eta$) for TEBACl was about 20 mV higher or more negative than that of MA (Figure 9.11). The addition of MA has much less effect on polarization of hydrogen evolution reaction in presence of Ni^{2+} than TEBACl as mentioned by Cachet et al. [7].

9.5. Conclusions

Considering 24 hours of galvanostatic polarization of zinc electrowinning in acid sulphate electrolyte at 50 mA/cm^2, the following conclusions can be deduced:

1. Among the examined additives, the use of PEG and TEBACl seems to be better than anionic PHFA and SLS. Cationic TEBACl decreased the cell voltage by ~42 mV in

comparison to that of glue + Cl^-. The morphology of zinc deposit from the standard electrolyte + TEBACl + Ni^{2+} was a well defined hexagonal platelet parallel to the substrate. Addition of MA to the standard electrolyte led to a zinc deposit characterized by the presence of platelets aligned at intermediate angles.

2. The optimum concentration of malonic acid appears to be 100 mg/L. The addition of 100 mg/L MA in the acid electrolyte containing 60 g/L Zn^{2+}, 180 g/L H_2SO_4, and 8 g/L Mn^{2+}, increased the CE by 3.3% and decreased the cell voltage by about 20 mV as compared to the standard electrolyte containing glue + Cl^- (3 and 250 mg/L respectively).

3. In electrolytes containing 0.01 mg/L Sb^{3+}, it is recommended 100 mg/L MA should be present with the current industrial additives since this combination improved the CE% by ~1% as compared to that of glue + Cl^- alone.

4. The current efficiency of zinc deposit in the standard electrolyte solution containing 5 g/L Ni^{2+} was too low to consider but increased to ~91% with the addition of TEBACl.

5. 100 mg/L MA and 2 mg/L TEBACl added to H_2SO_4 solution at galvanostatic imposed fixed current densities showed an increase of the cathodic hydrogen evolution potential on zinc of about 8-14 mV. In presence of 5 mg/L Ni^{2+}, the addition of TEBACl led to higher (more negative) hydrogen evolution potentials compared to that of malonic acid.

9.6 Acknowledgements

The authors are grateful to the Hydro-Quebec, CEZ and the Natural Sciences and Engineering Research Council of Canada (NSERC) for their financial support. The authors are grateful to Mr Gary Monteith (Canadian Electrolytic Zinc) and Gilles Champoux (Hydro-Quebec, Montreal) for their fruitful discussions in the conception, realization and participation in this project.

9.7 References

[1] **Cachet C., Wiart, R.**, Zinc Deposition and Passivated Hydrogen Evolution in Highly Acidic Sulphate Electrolytes: Depassivation by Nickel Impurities. J. Applied Electrochemistry 20, 1990, pp. 1009-1014.

[2] **Zhang, X. G.**, Corrosion and Electrochemistry of Zinc, Schulich Science & Engineering, Plenum, 1996, ISBN: 0306453347.

[3] **Bozhkov, C., Petrova, M., Rashkov, St.**, Nickel and Cobalt Synergism Effect in Zinc Electrowinning from Sulphate Electrolytes. Journal of Applied Electrochemistry 22, 1992, pp. 73-81.

[4] **Ivanov, I.**, Increased Current Efficiency of Zinc Electrowinning in the Presence of Metal Impurities by Addition of Organic Inhibitors, Hydrometallurgy 72, 2004, pp. 73-78.

[5] **Rashkov, S., Petrova, M., Bozhkov, C.**, The Effect of Nickel on the Mechanism of the Initial Stages of Zinc Electrowinning from Sulphate Electrolytes. Part I. Investigations on A Spectrally Pure Aluminium Cathode, Journal of Applied Electrochemistry 20, 1990, pp. 11-16.

[6] **Stefanov, Y., Ivanov, I.**, The Influence of Nickel Ions and Triethyl-benzylammonium Chloride on the Electrowinning of Zinc from Sulphate Electrolytes Containing Manganese Ions, Hydrometallurgy, 64, 2002, pp. 193-203.

[7] **Cachet, C., Wiart, R., Ivanov, I., Stefanov, Y., Rashkov, S.**, Mechanism of the Reverse Dissolution of Zinc in the Presence of Nickel Part II: Influence of Triethylbenzylammonium Chloride, Journal of Applied Electrochemistry 24, 1994, pp. 713-718.

[8] **Tripathy, B. C., Das, S. C., Hefter, G. T., Singh, P.**, Zinc Electrowinning from Acidic Sulfate Solutions Part I: Effects of Sodium Lauryl Sulfate. Journal of Applied Electrochemistry 27, 1997, pp. 673-678.

[9] **Tripathy, B.C., Das, S.C., Misra, V.N.**, Effect of Antimony (III) on the Electrocrystallisation of Zinc from Sulphate Solutions Containing SLS. Hydrometallurgy 69, 2003, pp. 81-88.

[10] **Recéndiz, A., Gonzàlez, I., Nava, J. L.**, Current Efficiency Studies of the Zinc Electrowinning Process on Aluminum Rotating Cylinder Electrode (RCE) in

Sulfuric Acid Medium: Influence of Different Additives, Electrochimica Acta 52, 2007, pp.6880-6887.

[11] **Stefanov, Y., Ivanov, I., Rashkov, S.**, Electro-Extraction of Zinc from Sulphate Slectrolytes Containing Antimony and Hydroxyethylated-butyne-2-diol-1,4. Part 1: Deposition on An Aluminium Cathode Containing Iron Impurities, Hydrometallurgy 44, 1997, pp. 71- 81.

[12] **Ivanov, I., Stefanov, Y.**, Electroextraction of Zinc from Sulphate Electrolytes Containing Antimony and Hydroxyethylated-butine-2-diol-1,4 Part 2: Deposition on A Specpure Aluminium Cathode. Hydrometallurgy 64, 2002, pp. 111-117.

[13] **Robinson, D. J., O'Keefe, T. J.**, On the Effects of Antimony and Glue on Zinc Electrocrystallization Behaviour. J. Applied Electrochemistry 6, 1996, pp. 1-7.

[14] **Tripathy, B. C., Das, S. C., Hefter, G. T., Singh, P.**, Zinc Electrowinning from Acidic Sulphate Solutions Part II: Effects of Triethyl-benzylammonium Chloride, Journal of Applied Electrochemistry 28, 1998, pp. 915-920.

[15] **Tripathy, B. C., Das, S.C., Singh, P., Hefter G.T., Misra, V.N.**, Zinc Electrowinning from Acidic Sulphate Solutions Part IV: Effects of Perfluorocarboxylic Acids. Journal of Electroanalytical Chemistry 565, 2004, pp. 49-56.

[16] **Moffat, T.P., Wheeler, D., Josell, D.**, Electrodeposition of Copper in SPS-PEG-Cl Additives System, I. Kinetic Measurements Influence of SPS, Journal of Electrochemical Society 151(4), 2004, pp. C262-C271.

[17] **Ballesteros, J.C., Diaz-Arista, P., Meas, Y., Ortega, R., Trejo, G.**, Zinc Electrodeposition in the Presence of Polyethylene Glycol 20000. Electrochemica Acta 52, 2007, pp. 3686-3696.

[18] **Jin, S., Ghali, E., St-Amant, G., Houlachi, G.**, Effect of Some Polyols and Organic Acids on the Current Efficiency and the Cell Voltage During Zinc Electrowinning, in Hydrometallurgy 2003: (Eds: C. Young, A. Alfantazi, C.

Anderson, A. James, D. Dreisinger, and B. Harris), TMS, Warrendale, PA, USA, Vol. 2, 2003, pp. 1219-1231.

[19] **Gamburg, Y.D., Grosheva, M.Y., Biallozor, S., Hass, M.**, The Electrochemical Deposition of Nickel from Electrolytes Containing Malonic Acid. Surface and Coatings Technology 150, 2002, pp. 95-100.

[20] **Berka, A., Korinkova M., Barek, J.**, The Deterimination of Organic Substances by the Oxidation with Permanganate XVIII. The Oxidation of Malonic Acid. Microchemical Journal 20, 1975, pp. 353-359.

[21] **Fukubayashi, H., O'Keefe T.J., Clinton, W.C.**, Effect of the Impurities and Additives on the Electrowinning of Zinc, US Bureau of Mines Report of Investigations, RI 7966, 1974, pp. 26-32.

[22] **MacKinnon, D.J., Brannen, J.M., Fenn, P.L.**, Characterization of Impurity Effectsin Zinc Electrowinning from Industrial Acid Sulphate Electrolyte. Journal of Applied Electrochemistry 17, 1987, pp. 1129-1143.

CHARTER 10

Effect of gelatin and antimony on zinc electrowinning by electrochemicalnoise

Effect of gelatin and antimony on zinc electrowinning by electrochemical noise

A-M. Lafront[1],W. Zhang[1*], E. Ghali[1] and G.Houlachi[2]

[1]Department of Mining, Metallurgy and Material Engineering

Laval University, Ste-Foy, Quebec, Canada, G1K 7P4

Wei.Zhang.1@ulaval.ca*

[2]LTE, Hydro-Quebec

600 Avenue de la Mortagne,C.P. 900

Shawinigan, QC, Canada, G9N 7N5

This paper was published in Canadian Metallurgical Quertarly Vol. 48, 2009, pp. 337-346.

10.1 Abstract

The influence of additive (gelatin), impurity (antimony) or a combination of both gelatin and antimony on zinc electrowinning in sulphuric acid electrolytes was investigated by electrochemical noise measurements. This study was oriented to examine the utility of using electrochemical noise "EN" technique to characterize the electrowinning process and the deposit structure morphology during electrolysis and complement the scanning electronic microscope studies "SEM". The electrochemical noise analysis in the time domain (skewness and kurtosis parameters) was successful to reveal the combined effect of different concentrations of gelatin and antimony on zinc electrowinning process. Skewness and kurtosis slope values around 0 mean that the distribution of data is symmetric around the mean value and the shape is similar to that of the normal distribution, seem corresponded to the best combination of the synergetic effect of impurity and additive for higher current efficiency, lower overpotentials, better smooth and compact deposits.

L'influence de l'additif (gélatine), de l'impureté (antimoine) ou de la combinaison des deux gélatines et antimoine sur l'électrodéposition du zinc à partir d'électrolyte d'acide sulfurique a été étudiée par la technique de la mesure du bruit électrochimique. Cette étude est orientée pour examiner l'utilité d'utiliser la technique du bruit électrochimique "EN" pour caractériser le procédé d'électrodéposition et la morphologie de la structure du dépôt pendant l'électrolyse en complément des études au microscope électronique à balayage. L'analyse du bruit électrochimique dans le domaine du temps (les paramètres skewness et kurtosis) est un succès pour révéler l'effet combiné des différentes concentrations de gélatine et d'antimoine sur le procédé d'électrodéposition du zinc. Les valeurs de la pente de skewness et kurtosis autour de 0, signifiant que la distribution des données est symétrique autour d'une valeur moyenne et que la forme est similaire à une distribution normale semblent correspondre à la meilleure combinaison de l'effet synergétique de l'impureté et l'additif pour l'efficacité de courant la plus élevée, les plus basses surtensions et les meilleurs dépôts lisses et compacts.

10.2 Introduction

Two of the principal problems encountered in electrowinning zinc from acid sulphate electrolytes are (a) maintaining high current efficiency and low energy consumption, (b) producing more smooth level deposits at high current densities [1]. Low current efficiencies during zinc reduction process have been generally stated due to hydrogen evolution [2]. In spite of costly purification steps, the zinc electrolyte is always contaminated with various metal ion impurities that decrease the current efficiency and lead to low deposit quality [3] and thus organic additives are widely employed to counteract their harmful effects [4]. Antimony (III) has been recognised as one of the most deleterious and toxic solution impurities, but at the same time, it also plays a beneficial role when combined with some organic additives producing optimum current efficiency and acceptable surface morphology of the deposits [5]. The addition of animal gelatin (glue) to the zinc electrolyte used in zinc electrowinning plant serves several purposes [6]. Gelatin increases zinc deposition polarization, decreases the current efficiency and reduces the deposit grain size. Certain combinations of antimony and gelatin optimize zinc deposition current efficiency [7].

There is a relationship between the zinc deposit structure and current efficiency, and this suggests that proper control of crystal growth could yield high current efficiencies (≥90%) and longer plating cycles. Although the effects of impurities and addition agents on current efficiency are well established, their effects on zinc deposit morphology, orientation and smoothness have only recently begun to receive some attention. Scanning electron microscope (SEM) is an essential means to characterize the often rough deposit surfaces [4].

Addition of gelatin and antimony to the zinc electrolyte has great influence on the overpotential of zinc deposit. The effects of antimony, gelatin or combinations of the two were previously particularly identified and quantitatively evaluated employing ex-situ cyclic voltametric technique (CV) [6]. This technique has shown that the Nucleation Overpotential region (NOP) (difference between *the crossover potential,* the start of the dissolution, and the point at which Zn begins to deposit) could be a useful parameter to identify the best gelatin and antimony ratio [8]. Gelatin addition shows a gradual

proportional increase of NOP. Antimony addition shows a significant decrease in the NOP reflecting the strong depolarizing effect of Sb. For each Sb concentration there is an optimum gelatin value at which the current efficiency "CE" is maximum, for instant, when Sb concentrations at 0.02 and 0.04 mg/L the corresponding concentrations of gelatin are 5 and 20 mg/L, respectively. Such correlation can be observed between CE and NOP for zinc deposition in a way that the CE was maximal when the NOP of the initial cell electrolyte was 756-766 mV/SHE, and /or NOP of the final cell electrolyte was 736-746 mV/SHE [8].

Electrochemical noise (EN) is a new and more sensitive in-situ electrochemical tool that can provide complementary information about the deposit structure, and monitor the deposit quality during electrolysis. Electrocrystallization studies have been reported in the literature for a number of electroplating systems [9-14], including that of silver and copper deposition [10]. The growth mechanism of silver electrodeposition has been analysed in the frequency domain of EN [15]. In the case of zinc electroplating which can lead to spongy, compact or dendritic deposits, the experimental study of the electrocrystallization current allows to establish some close correlations between the deposit morphology and the noise power measured in the low frequency range and with wavelet analyses [15-17]. In our laboratory, preliminary EN statistical approach has been successfully used to identify copper electrorefining conditions leading to nodulation [18-19].

The aim of this study is to consider an electrochemical technique that can evaluate the effect of the presence of impurity or additive in the electrolyte on the morphology of zinc deposit. This technique will also be useful in monitoring the evolution of the quality of the deposit. In this context, the recent developments in Electrochemical Noise Measurements "ENM" and Analyses "ENA" would make them appropriate tools. Analysis of the potential noise in the time domain is carried out to see the effect of the additive (gelatin) or the impurity (antimony) or both on the quality of the deposit. This is supplemented by scanning electron microscopy. In addition, current efficiency and cathodic potential measurements are determined after 2 hours of galvanostatic experiments since these are important parameters for energy savings.

10.3 Experimental conditions

Electrochemical noise measurements were performed using a set-up in electrochemical noise (EN) mode of galvanostatic at current density CD= 500 A/m^2 for 2 h deposition time, at 38°C. A 3 electrodes set-up was used (Al 1100 cathode, Pt anode and Ag, AgCl/KCl sat. reference electrode). Experiments were done in 1) standard electrolyte "SE" composed of 60 g/L of Zn and 180 g/L of H_2SO_4 and was considered as reference electrolyte, 2) SE + gelatin (1, 3 and 5 mg/L), 3) SE + Antimony-tartrate $KSbC_4H_4O_7 0.5 H_2O$ (Sb^{3+}) (0.0036, 0.0055, 0.01, 0.02, 0.03 mg/L) and 4) SE + combination of gelatin+ Sb^{3+}, such as 1 mg/L of gelatin with Sb^{3+} = 0.0055, 0.01, 0.02 mg/L and 3 mg/L of gelatin with Sb^{3+} = 0.0055, 0.01, 0.02 mg/L were tested.

The current efficiency was calculated as CE% = (WFn/ItM)×100%; where W is the weight of deposit (g), n is the number of e^-, F is the faraday constant, M is a molecular weight, I is the total cell current (A) and t is the time of deposition.

A GAMRY® PC4/300 potentiostat was used to log potential and current values. EN experiments and data treatment were conducted using GAMRY® ESA400 software. Electrochemical noise measurement records, containing 1024 data points, were collected at 102.4 points per second at a scan rate of f_s = 10 Hz. At least 2 or 3 experiments have been done for each experimental condition.

Electrochemical noise analyses of the potential signal have been done in the time domain (skewness and kurtosis). Skewness and kurtosis are indicative of the shape character of the distribution of electrochemical noise data. For normal distribution, skewness and kurtosis have values around 0 [20]. The skewness or skew is a dimensionless measure of the symmetry of the distribution of data around the mean value of the data [21]. Skewness should be zero when the distribution of data is symmetric around the mean value. A positive skew implies that there is a tail in the positive direction, and a negative skew implies that there is a tail in the negative direction.

$$\text{Skewness} = \frac{1}{N}\sum_{k=1}^{N}\left(\frac{E_n[k]-\bar{E}}{\sqrt{E_n[k]^2}}\right)^3 \qquad (10.1)$$

Kurtosis is a dimensionless measure of whether data are peaked or flat relative to a normal distribution. Kurtosis of zero implies that the distribution has a shape similar to that of the normal distribution. A positive kurtosis implies a more sharply peaked distribution than the normal distribution, while a negative kurtosis implies a more flat topped distribution than the normal distribution.

$$\text{Kurtosis} = \frac{1}{N}\sum_{k=1}^{N}\left(\frac{E_n[k]-\overline{E}}{\sqrt{E_n[k]^2}}\right)^4 - 3 \qquad (10.2)$$

where N is the number of points in the time record, $\overline{E}$ is the mean potential, and $E_n(k)$ is the potential of function of time at each instant k.

The average skewness and kurtosis were calculated after each 1000 s of zinc deposition time for a total of 7200 s (2 hours) and the starting period of 120 s was not considered. This time corresponds to the charge of the electrodes [21].

10.4 Results and discussions

10.4.1 Current efficiency CE% and cathodic potential

Figure 10.1 shows the CE (%) obtained with different concentrations of G, Sb^{3+} and G + Sb^{3+}.

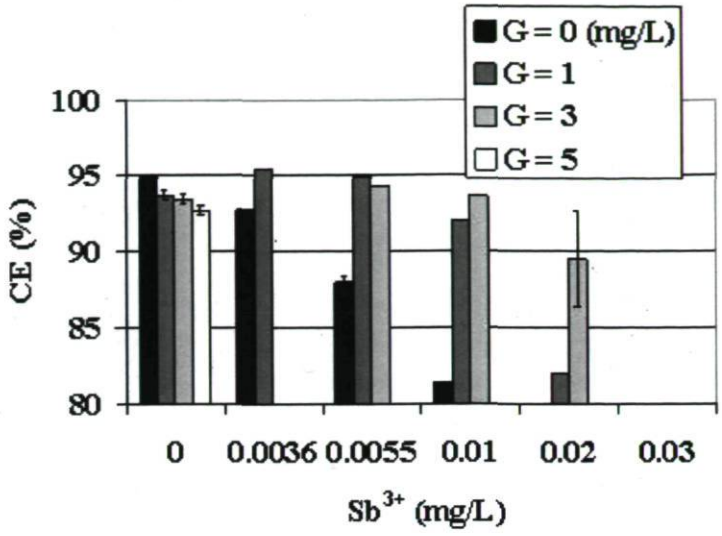

Figure 10.1-CE (%) after 2 hours of deposition at current density CD= 500 A/m^2 for electrolyte containing antimony and gelatin (Sb^{3+} + G), (0, 0.0036, 0.0055, 0.01, 0.02, 0.03 mg/L) and (0, 1, 3, 5 mg/L), respectively. Some experiments have been done 4 times and results are represented as error bars.

Figure 10.2 shows the cathodic potential obtained with different concentrations of G, Sb^{3+} and G+Sb^{3+}.

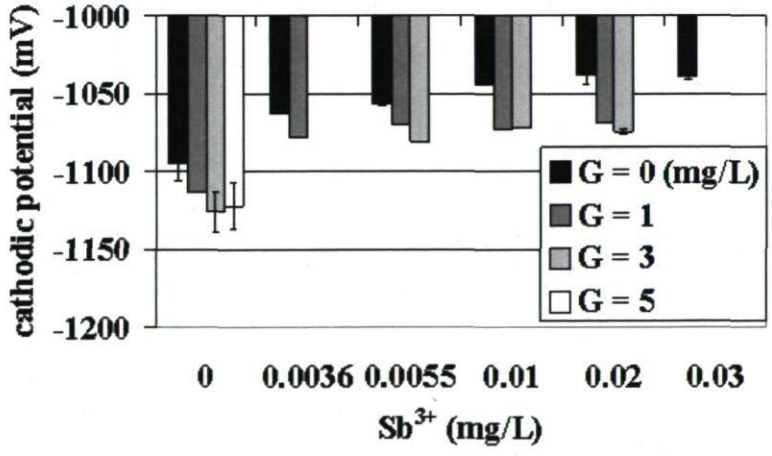

Figure 10.2-Cathodic potentials after 2 hours deposition at current density CD= 500 A/m^2 for electrolyte containing antimony and gelatin (Sb^{3+} + G), (0, 0.0036, 0.0055, 0.01, 0.02, 0.03 mg/L) and (0, 1, 3, 5 mg/L), respectively. (More negative values due to gelatin addition correspond to higher overpotentials). Some experiments have been done 4 times and results are represented as error bars.

10.4.1.1 Effect of gelatin addition to the standard electrolyte

The increase of G concentration from 1 to 5 mg/L leads to a decrease of CE of about 2.6 % (Figure 10.1) and an increase of cathodic potential of about 26 mV (Figure 10.2) in considering the obtained results in SE as a base. The decrease in CE (%) with increasing gelatin concentrations has been observed frequently and is usually ascribed to blocking of the deposition process by adsorption of the additive on the cathode surface [1].

10.4.1.2 Effect of Sb^{3+} addition to the standard electrolyte

The increase of Sb^{3+} from 0.0036 to 0.03 mg/L leads to a decrease of CE of about 50 % (Figure 10.1) and a decrease of cathodic potential of about 60 mV (Figure 10.2) as compared to that obtained in the SE. The reproducibility of CE at low Sb^{3+}, 0.0036, 0.0055 and 0.01 mg/L is about ±0.14, ±0.47 and ±1.13 %, respectively. However, the reproducibility of CE at high Sb^{3+}, 0.02 and 0.03 mg/L is about ±24.60 and ±25.54 %, respectively. The decrease of the CE can be due to the formation of unstable hydrides with Sb^{3+} accelerating the parallel process of hydrogen evolution on zinc without preferential areas of zinc corrosion [22].

10.4.1.3 Synergetic effet of G + Sb^{3+}

To examine better the synergetic effect of antimony ions and gelatin additions, it is interesting to compare the obtained results first to that corresponding to the basic standard electrolyte, and then to that obtained in SE+G = 1 or 3 mg/L.

The addition of different quantities of antimony to SE + 1 or 3 mg/L of gelatin shows the following results in considering the obtained results in SE electrolyte as reference: The addition of 0.0036 and 0.0055 mg/L of Sb^{3+} to G = 1 mg/L gives an increase of CE of about 0.7 and 0.2 %, respectively (Figure 10.1) and a decrease of E_c of about 22 and 30 mV, respectively (Figure 10.2); while the addition of 0.01 and 0.02 mg/L of Sb^{3+} with G=1 mg/L gives rise to a decrease of CE of about 3 and 13 %, respectively (Figure 10.1) and a decrease of E_c of about 28 and 31 mV, respectively (Figure 10.2). The addition of 0.0055 and 0.01 mg/L of Sb^{3+} to G = 3 mg/L gives a decrease of CE of about 0.4 and 1 %, respectively (Figure 10.1) and a decrease of E_c of about 20 and 28

mV, respectively (Figure 10.2). The addition of 0.02 mg/L of Sb^{3+} to G = 3 mg/L gives a decrease of CE of about 7.5 % (Figure 10.1) and a decrease of E_c of about 25 mV (Figure 10.2).

The comparison to the results in presence of galatin alone with respect to SE+G = 1 mg/L or SE+G = 3 mg/L can be considered also (Figures 10.1 and 10.2). However, it can be stated that the addition of low concentration of G = 1 mg/L to low concentrations of Sb^{3+} (0.0055 mg/L) gives a slight increase of CE% in comparison to the addition of G = 3 mg/L to low Sb^{3+}. The addition of high concentration of G = 3 mg/L to high 0.01 and 0.02 mg/L of Sb^{3+} gives an increase of CE% of about 2 and 5, respectively, in comparison to the addition of low G = 1 mg/L.

It can be stated that suitable synergetic effect of glue and Sb^{3+} increased the current efficiency for zinc deposit. The best increase of CE of about 0.7% (0.0036 mg/L of Sb^{3+} and G = 1 mg/L) has been obtained in the studied conditions.

10.4.2 EN analyses and morphology

Table 10.1 shows the S and K values and slopes from EN analyses for specific antimony and gelatin concentration associated with the morphology obtained by Scanning Electron Microscopy (SEM).

Table 10.1-S and K value and slope as function of gelatin and antimony concentration

Sb mg/L	G mg/L	CE %	Ec (mV)	S value	K value	S slope	K slope	SEM
0	0	94.7	-1093	>0	>0	0.77	5.33	Figure 10.4a
0	3	93.2	-1119	>0	>0	0.71	4.10	Figure 10.4b
0	5	92.6	-1130	>0	>0	0.79	5.5	Not shown
0.0055	0	87.8	-1057	<0	>0	-0.76	6.76	Figure 10.6a
0.03	0	60.9	-1042	<0	>0	-0.21	1.45	Figure 10.6b
0.0055	1	94.9	-1070	<0	≤0	-0.13	0.034	Figure 10.9a
0.0055	3	94	-1083	>0	>0	-0.23	0.321	Not shown
0.01	3	93.6	-1063	>0	>0	-0.44	0.104	Not shown
0.02	3	87.2	-1073	<0	>0	-0.35	0.617	Figure 10.9b

From Table 10.1, it can be deduced as example that the addition of glue alone from 3 to 5 mg/L, the S slope increases from 0.77 to 0.79; while the addition of antimony alone from 0.0055 to 0.3 mg/L, the K slope decreases from 6.76 to 1.45.

Figures 10.3, 10.5, 10.7 and 10.8 show the average of EN analyses (skewness and kurtosis values) for duplicate experiments. Figures 10.4, 10.6 and 10.9 show the specific SEM morphology of zinc deposit (500X) obtained at the end of 2 hours electrolysis at CD = 50 mA/cm^2 and 38°C.

10.4.2.1 Gelatin effect

Figure 10.3 shows the EN analyses for SE + G (G = 1, 3, 5) mg/L.

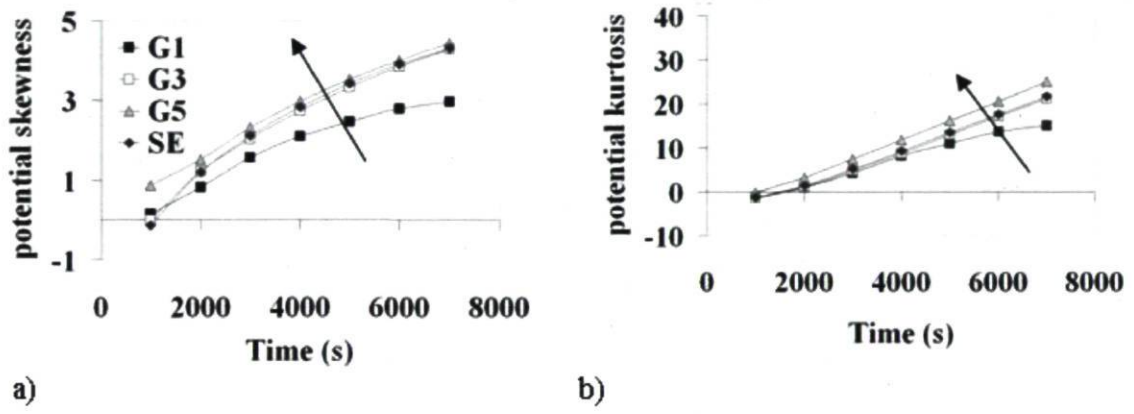

Figure 10.3-Average of a) Skewness and b) Kurtosis of the cathode deposit at current density CD= 500 A/m^2 in the SE + G (G = 1, 3, 5 mg/L, respectively) for duplicate experiments (the arrow shows the increase of gelatin concentration in SE).

Positive skewness and kurtosis values which increase quasi linearly (slope) with the time of deposition have been obtained for SE and SE containing gelatin (Figures 10.3a and 10.3b).

Positive skewness and kurtosis values increase more rapidly with the time of deposition and an increase of gelatin concentration (Table 10.1). This means that both positive slopes (skewness and kurtosis) increase with an increase of gelatin (Figures 10.3a and 10.3b).

For standard electrolyte SE, the duplicate experiment gives reproducible results of about ±0.27 and ±2.17 for skewness and kurtosis. For G = 1, 3 and 5 mg/L, the duplicate experiments give reproducible results for skewness of about ±0.34, ±0.12 and ±0.07, respectively, and for kurtosis of about ±1.89, ±0.75 and ±0.74, respectively.

Figure 10.4 shows the specific SEM of zinc deposit (500X) obtained at the end of 2 hours electrolysis at CD = 50 mA/cm^2 and 38°C.

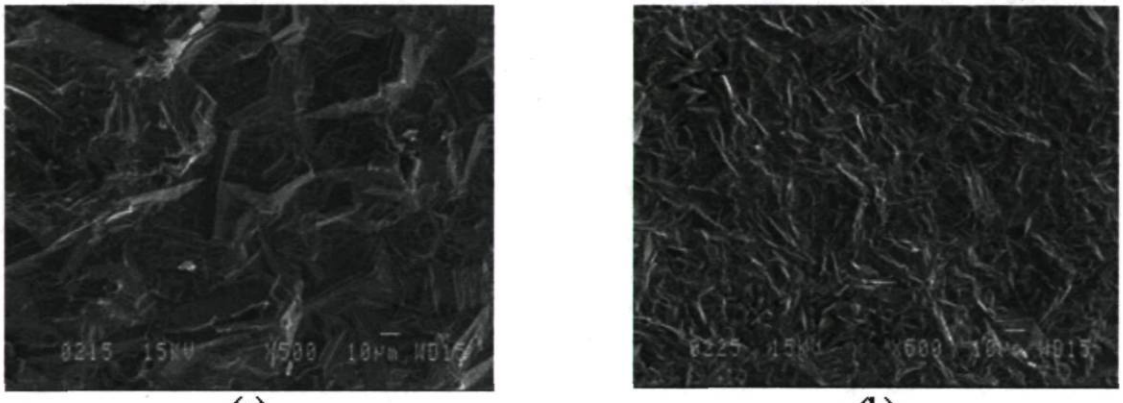

(a) (b)

Figure 10.4-SEM photomicrographs of the cathode deposit at current density CD= 500 A/m^2 in (a) SE at E_c = -1093 mV with CE = 94.7 %, (b) SE + G = 3 mg/L at E_c = -1119 mV with CE = 93.2 %.

The zinc deposit consists of well defined hexagonal platelets of varying size randomly oriented, the hexagonal platelets are aligned at low angle to the Al cathode [22] (Figure 10.4a). G = 3 mg/L influences the size but not the shape of the crystals on the electrodeposited zinc. It reduces the platelet size and gives smoother deposit than SE (Figure 10.4b). Porosity (depressions or pits) observed in the surface (not shown) is due to adherent hydrogen bubbles.

The distribution of data is not symmetric around the mean value distribution (a tail in the positive direction, positive S slope) and it is peaked than a normal distribution leading to a smooth, porous and non oriented deposit (Figures 10.4a and 10.4b). Lower S and K slopes is obtained for G =1 mg/L leading to smoother deposit (not shown). The distribution behaviour of the data becomes also less symmetric and more peaked with the increase of gelatin concentration leading to nodular deposit (highest S and K slopes,

Table 10.1). The distribution behaviour of the data becomes less symmetric and more peaked with the increase of time of deposition showing that the deposit is not good.

10.4.2.2 Antimony effect

Figure 10.5 shows the EN analyses for SE + Sb^{3+} (0.0055, 0.02, 0.03 mg/L).

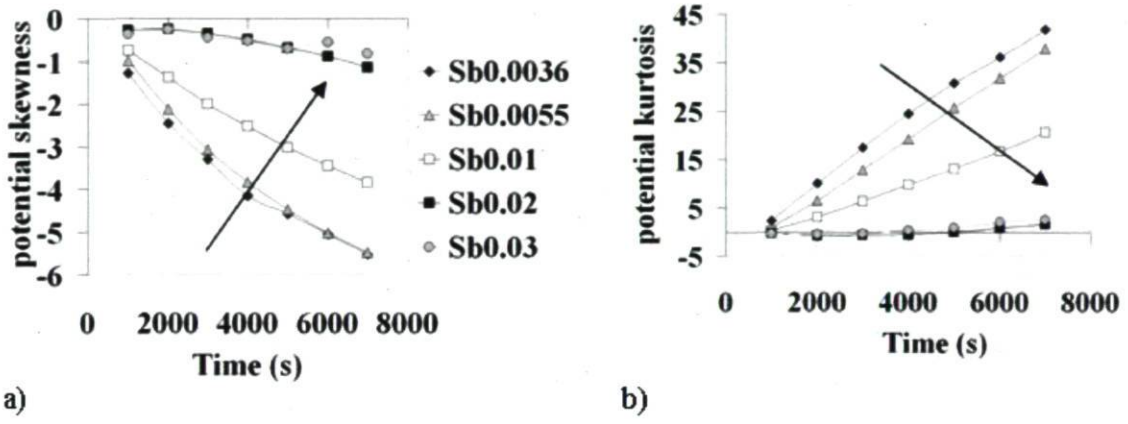

a) b)

Figure 10.5-a) Average of Skewness and b) Kurtosis of the cathode deposit at current density CD= 500 A/m^2 in the SE + Sb^{3+} (0.0055, 0.02, 0.03 mg/L respectively) for duplicate experiments. The arrow shows the increase of Sb^{3+} concentration in SE.

Negative skewness and positive kurtosis values which increase quasi linearly (slope) with the time of deposition have been obtained for SE containing Sb^{3+} (Table 10.1 and Figure 10.5).

Skewness and kurtosis absolute values decrease more rapidly with the time of deposition with the increase of Sb^{3+} concentration. Skewness and kurtosis values reach the 0 for some experiments with high concentrations of Sb^{3+} (0.02 and 0.03 mg/L). This means that both negative skewness and positive kurtosis slopes decrease with an increase of Sb^{3+} concentration (Table 10.1 and Figures 10.5a and 10.5b).

For Sb^{3+} = 0.0036, 0.0055, 0.01, 0.02 and 0.03 mg/L, the duplicate experiments give reproducible results for skewness of about ±0.04, ±0.10, ±0.72, ±0.46 and ±0.70, respectively and for kurtosis of about ±2.65, ±1.69, ±4.49, ±0.97 and ±2.63, respectively.

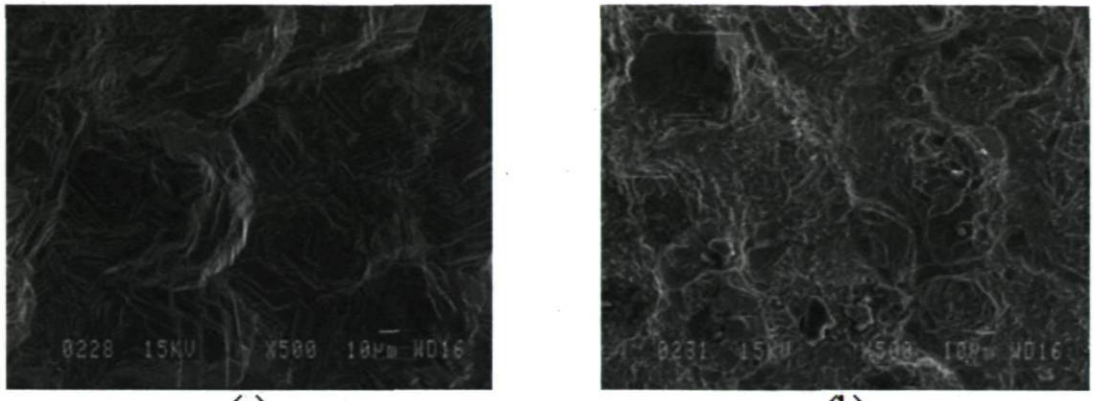

(a) (b)

Figure 10.6-SEM photomicrographs of the cathode deposit at current density CD= 500 A/m^2 in (a) SE + Sb^{3+} = 0.0055 mg/L at E_c = -1057 mV with CE = 87.8%, (b) SE + Sb^{3+} = 0.03 mg/L at E_c= -1042 mV with CE = 60.9%.

The addition of low concentration of antimony (0.0055 mg/L) to the SE doesn't modify the shape and the size of the crystals (platelets) but it modifies their arrangement, since towers of platelets were formed (orientation). Porosity of the surface disappears, however the surface is rough due to towers of platelets (Figure 10.6a). The presence Sb^{3+} = 0.03 mg/L initiates the process of zinc re-dissolution. The deposit with Sb^{3+} = 0.03 mg/L shows that zinc crystals were poorly defined (the platelet edges appeared rounded) and a needle-like morphology was observed (Figure 10.6b).

The distribution of data is not symmetric around the mean value distribution (a tail in the negative direction) and it is peaked than a normal distribution leading to a rough, compact and oriented deposit (Figure 10.6a). The distribution behaviour of the data becomes less symmetric and more peaked with the increase of time of deposition. The distribution behaviour of the data becomes more symmetric and less peaked with the increase of antimony concentration due to the dissolution process (disappearance of tower of platelets). The deposit is less rough and the slopes decrease (Table 10.1). The distribution behaviour of the data becomes less symmetric and more peaked with the increase of time of deposition showing that the deposit is not good (Figure 10.6b).

10.4.2.3 Antimony and gelatin effect

Figure 10.7 shows the EN analyses for SE + Sb^{3+} (0.0036, 0.0055, 0.02, 0.03 mg/L) + G = 1 mg/L.

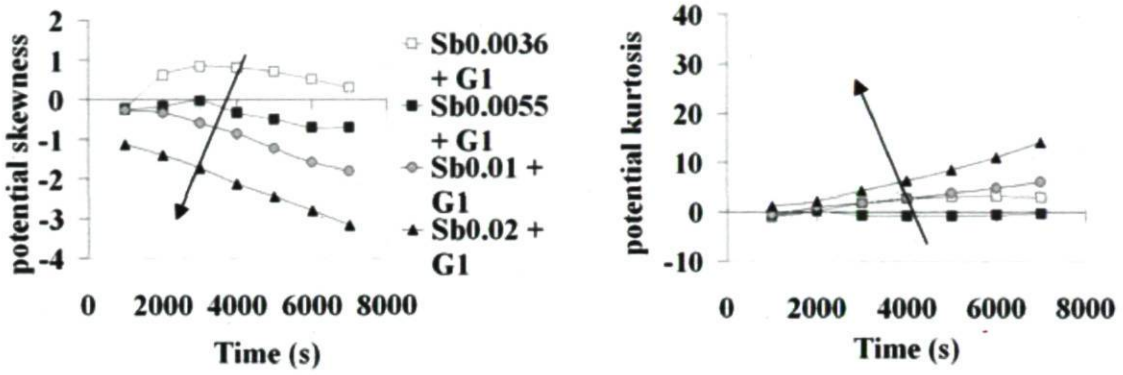

a) b)

Figure 10.7-a) Average of Skewness and b) Kurtosis of the cathode deposit at current density CD= 500 A/m^2 in the SE + Sb^{3+} (0.0036, 0.0055, 0.02, 0.03 mg/L respectively) + G = 1 mg/L for duplicate experiments (the arrow shows the increase of Sb^{3+} concentration in SE+G = 1 mg/L).

The addition of increasing concentrations of Sb^{3+} (0.0036, 0.0055, 0.01, 0.02 mg/L) to SE containing 1 mg/L of gelatin leads to a change from positive to negative skewness value, an increase of the slope for skewness (0 to negative values) (Figure 10.7a), and an increase of the slope for kurtosis (0 to positive values) (Figure 10.7b). This means that both slopes negative and positive, skewness and kurtosis, respectively, increase with an increase of Sb^{3+} in SE + G = 1 mg/L going to an "antimony type" behaviour for G1 + 0.01Sb^{3+} and G1 + 0.02Sb^{3+}. The skewness and kurtosis values obtained for Sb^{3+} = 0.02 mg/L + G1 looks like the ones obtained for Sb^{3+} = 0.01 mg/L (Figures 10.5 and 10.7). The slope around 0 gives the best combination of gelatin and antimony (synergetic effect). Positive values of skewness and kurtosis (G1 + Sb^{3+} = 0.0036 mg/L) give better CE (95.5 %) than negative values of skewness and kurtosis (G1 + Sb^{3+} = 0.0055 mg/L) (CE = 94.9 %).

For G = 1 mg/L + Sb^{3+} = 0.0036, 0.0055, 0.01 and 0.02 mg/L, the duplicate experiments give reproducible results for skewness of about ±0.72, ±0.13, ±1.05 and ±0.23, respectively, and for kurtosis of about ±1.00, ±0.4, ±3.32 and ± 1.64, respectively.

Figure 10.8 shows the EN analyses for SE + Sb^{3+} (0.0036, 0.0055, 0.02, 0.03 mg/L) + G = 3 mg/L.

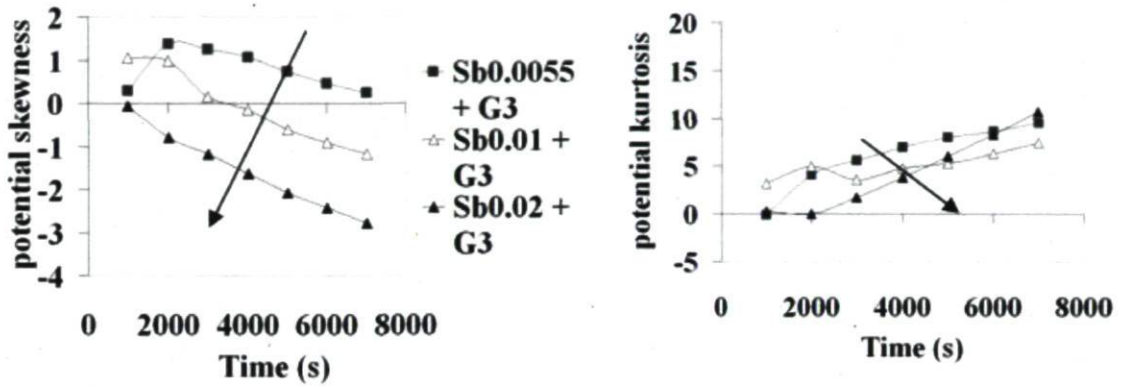

Figure 10.8-a) Average of Skewness and b) Kurtosis of the cathode deposit at current density CD= 500 A/m^2 in the SE + Sb^{3+} (0.0036, 0.0055, 0.02, 0.03 mg/L respectively) + G = 3 mg/L for duplicate experiments. The arrow shows the increase of Sb^{3+} concentration in SE+G = 3 mg/L.

The addition of increasing concentrations of Sb^{3+} (0.0036, 0.0055, 0.01, 0.02 mg/L) to SE containing 3 mg/L of gelatin leads to a change from positive to negative skewness value, an increase of the slope for skewness towards negative values, and an increase of the slope for kurtosis towards positive values (Figure 10.8). This means that both negative and positive slopes, skewness and kurtosis, respectively, increase with an increase of Sb^{3+} in SE + G = 1 mg/L going to an "antimony type" behaviour for G3 + $0.02Sb^{3+}$.

G3 + $0.0055Sb^{3+}$ skewness and kurtosis behaviour looks like G1 + $0.0036Sb^{3+}$ (Figures 10.5 and 10.8).

For G = 3 mg/L + Sb^{3+} = 0.0055, 0.01 and 0.02 mg/L, the duplicate experiment gives reproducible results for skewness of about ±1.05, ±1.14 and ±0.64, respectively, and for kurtosis of about ±2.38, ±3.10 and ±3.39, respectively.

The addition of G = 1 mg/L to SE + Sb^{3+} = 0.0055 mg/L did not modify the shape and the size of the crystals (platelets) but did modify their arrangement in comparison with Figure 10.6a giving structure that can be described as pyramidal (Figure 10.9a), however it appears more compact as compared to that containing 0.0055 mg/L Sb^{3+} (Figure 10.6a). Surface is less rough than that in Sb^{3+} only.

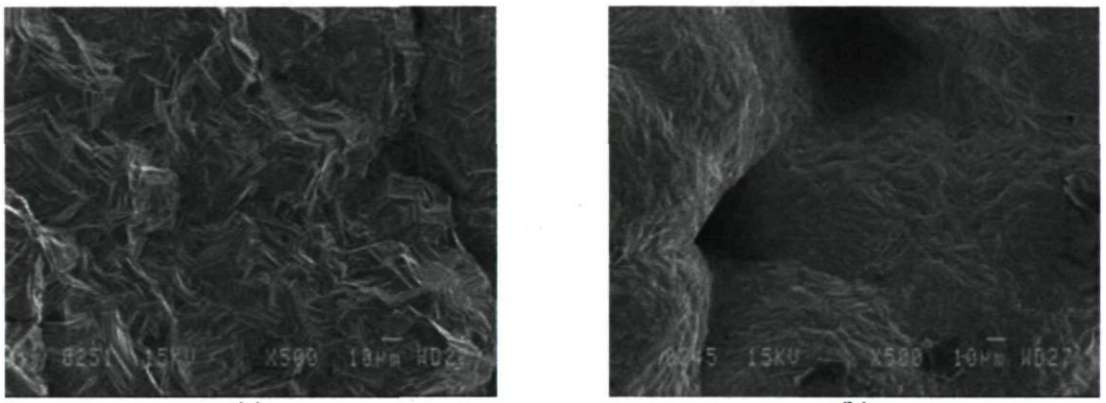

(a) (b)

Figure 10.9-SEM photomicrographs of cathode deposit at current density CD= 500 A/m^2 in (a) SE + Sb^{3+} = 0.0055 mg/L + G = 1 mg/L at E_c= -1070 mV with CE = 94.9 %, (b) SE + Sb^{3+} = 0.02 mg/L + G =3 mg/L at E_c = -1073 mV with CE = 87.2%.

The addition of G = 3 mg/L to SE + Sb^{3+}=0.0055 mg/L looks like the experiments made with G=3mg/L alone (Figure 10.4b).The surface roughness is between glue (Figure 10.4b) and antimony (Figure. 10.6a) alone. Deposit morphology of the addition of G = 3 mg/L to SE + Sb^{3+} = 0.01 mg/L looks like Figure 10.9b, however spongy structure appears on the edge giving uneven deposit on the edge (not shown). The addition of a higher quantity of glue (3 mg/L) to high concentration of antimony (0.02 mg/L) produces a corroded zinc deposit, increases the number of holes leading to a spongy structure (Figure 10.9b). It seems that G = 3 mg/L cannot control the negative effect of Sb^{3+} = 0.02 mg/L.

A competition occurs between gelatin and antimony. Antimony has a tendency to shift the S and K value to negative part in distribution data and the contrary is observed for gelatin (Table 10.1). Smooth and porous deposit occurring with gelatin is in competition to compact and rough deposit obtained with antimony. If imbalanced gelatin

and antimony ratio occurs the deposit could look like the one obtained for gelatin or antimony. If there is not enough antimony to compensate the effect of gelatin, the deposit could become porous (Figure 10.9b). Also, if there is not enough gelatin to compensate the effect of antimony, the deposit could become corroded (not shown).

For appropriate concentrations of gelatin and antimony, the slope of S and K are low (S and K values become very low, Table 10.1) and the distribution of data becomes symmetric around the mean value and has a shape similar to that of the normal distribution, the deposit is smooth and compact as the one obtained in Figure 10.9a. The distribution behaviour of the data doesn't change a lot with the increase of time of deposition. High concentrations of antimony such as (0.02 mg/L) leads to more negative values of skewness and more positive values of kurtosis, and this signals low current efficiency and the morphology of the deposit is bad, showing big pores (Figure. 10.9b).

Comparing Table 10.1 and Figures 10.4, 10.6, and 10.9, it can be obtained that the distribution of high non- symmetric (positive) and peaked shape data (high positive S and K, respectively) indicates the presence of high gelatin concentration that leads to rough nodular deposit. The distribution of high non- symmetric (negative) and peaked shape data (high negative S and high positive K, respectively) indicates the presence of antimony concentration that leads to rough and compact deposit (tower of platelets). The distribution of low non- symmetric (positive) and peaked data (positive S and K, respectively) indicates the predominance of gelatin concentration that leads to smooth porous deposit.

The distribution of low non- symmetric (negative) and peaked data (negative S and K, respectively) indicates the predominance of high antimony concentration that leads to redissolution of deposit (Figure 10.1 and 10.5). The distribution of symmetric data around the mean value with a similar shape to that of the normal distribution (S and K around 0, respectively) leads to the best morphology and current efficiency (Figure 10.1 and 10.7).

10.5 Conclusions

Adding gelatin alone such as 1 mg/L to the standard bath resulted in smoother electrodeposited zinc. This corresponds to an increase of cathodic potential and decrease of CE%. An increase of both positive skewness and kurtosis slopes with the quantity of added G has been observed. The best CE%, the most negative E_c values and the lowest slopes were found for 1 mg addition of G/L.

Adding antimony alone over 0.01 mg/L to the bath resulted in bad zinc deposit, the process known as zinc re-dissolution was observed. The EN skewness and kurtosis slope values were around 0 monitoring a strong dissolution of zinc. Considering the solutions that contain antimony, the concentation of Sb^{3+} of 0.0036 mg/L gives the least decrease on CE%. Generally, a decrease of CE% and a decrease of cathodic potential are accompanied by a decrease of both EN negative and positive skewness and kurtosis slope values respectively as deduced from this study.

The conventional tools of investigation and EN measurements showed that the same trend is found as that of gelatin type behaviour alone, for high quantities of G = 1, 3 mg/L and low antimony concentrations (0.0036, 0.0055 mg/L); also antimony type behaviour alone has been found for high concentrations of antimony as Sb^{3+} = 0.02 mg/L and low gelatin concentrations (1 mg/L).

The synergetic effect of gelatin and Sb consists in the decrease of cathodic potential and CE% giving skewness and kurtosis slope values around 0 showing that skewness and kurtosis values slightly different from 0 corresponds to the best current efficiency and less overpotentials. It can be stated then that the distribution of symmetric data around the mean value having the shape similar to that of the normal distribution (S and K are around 0) signals the best smooth and compact deposit.

Considering the relative lower overpotentials, the best current efficiency, the quantity of added chemicals and possible influence on the morphology of the deposit, it seems appropriate to recommend 0.0036 Sb^{3+} and G = 1 mg/L as the best combination for the synergetic effect. EN analyses in the time domain monitored this trend and thus it

could be a powerful tool to detect the best combination of gelatin and antimony leading to better CE%.

10.6 Acknowledgements

The authors are grateful to Gill Champoux from the Hydro-Quebec and Gary Monteith from CEZ for their interest and fruitful discussions, CEZ and the Natural Sciences and Engineering Research Council of Canada (NSERC) for their financial support. Andre Ferland is highly appreciated for his professional technical participation.

10.7 References

[1] **Robinson, D. J., O'Keefe, T. J.**, On the Effects of Antimony and Glue on Zinc Electrocrystallization Behaviour, Journal of applied electrochemistry, vol. 6, 1976, pp. 1-7.

[2] **Gabe, D.R.**, The Role of Hydrogen in Metal Electrodeposition Processes, J. Appl. Electrochem., vol. 27, 1997, pp. 908-915.

[3] **Mackinnon, D. J., Brannen, J. M.**, Zinc Deposit Structures Obtained from High Purity Synthetic and Industrial Acid Sulphate Electrolytes with and without Antimony and Glue Additions, Journal of Applied electrochemistry, vol. 7, 1977, pp. 451-459.

[4] **Tripathy, B. C., Bhattacharya, L. N., Gopalakrishna, P., Das, S. C.**, The Role of Organic Additives in Zinc Electrowinning, Trans. Indian Inst. Met., vol. 5, 1998a, pp. 303-314.

[5] **Cachet, C., Wiart, R.,** Zinc Deposition and Passivated Hydrogen Evolution in Highly Acidic Sulphate Electrolytes: Depassivation by Nickel Impurities, J. Appl. Electrochem., vol. 20, 1990, pp. 1009-1014.

[6] **Kerby, R. C., Jackson, H. E., O'Keefe, T. J. and Wang, Y-M.**, Evaluation of Organic Additives for Use in Zinc Electrowinning, Metall. Trans.B, vol. 8, 1977, pp. 661-668.

[7] **Ivanov, I., Stefanov, Y.**, Electroextraction of Zinc from Sulphate Electrolytes Containing Antimony and Hydroxyethylated-butine-2-diol-1,4, Part 2: Deposition on A Specpure Aluminium Cathode, HydrometallurgY, 64, 2002, pp. 111-117.

[8] **Mackinnon, D. J., Morrison, R. M., Mouland J. E. and Warren, P. E.**, The Effects of Antimony and Glue on Zinc Electrowinning from Kidd Creek Electrolyte, Journal of Applied Electrochemistry, vol. 20, 1990, pp. 728-736.

[9] **Budevski, E., Obretenov, W., Bostanov, W., Staikov, G., Doneit, J., Juttner K. and Lorentz, J.**, Noise Analysis in Metal Deposition—Expectations and Limits. Electrochimica Acta, vol. 34(8), 1989, pp. 1023-1029.

[10] **Cachet, C., Gabrielli, C., Huet, F., Keddam M. and Wiart, R.**, Growth Mechanism for Silver Electrodeposition—A Kinetic Analysis by Impedance and Noise Measurements, Electrochimica Acta, vol. 28(7), 1983, pp. 899-908.

[11] **Bostanov, V., Obretenov, W., Staikov, G., Roe D. K. and Budevski, E.**, Rate of Crystal Growth by 2D Nucleation in the Case of Electrocrystallization of Silver, Journal of Crystal Growth, vol. 52, 1981, pp. 761-765.

[12] **Budewski, E., Bostanoff, W., Witanoff, T., Stoinoff, Z., Kotzewa A. and Kaischew, R.**, Keimbildungserscheinungen An Versetzungsfreien (100)-Flächen Von Silbereinkristallen, Electrochimica Acta, vol. 11, 1966, pp. 1697-1707.

[13] **Budevski, E., Fleischma, M., Gabrielli C. and Labram, M.**, Statistical Analysis of the 2-D Nucleation and Electrocrystallization of Silver, Electrochimica Acta, vol. 28, 1983, pp. 925-931.

[14] **Blanc, G., Gabrielli C. and Keddam, M.**, Measurement of the Electrochemical Noise by A Cross Correlation Method, Electrochimca Acta, vol. 20, 1975, pp. 687-689.

[15] **Blanc, G., Gabrielli. C., Keddam M. and Wiart, R.**, Experimental Study of the Relationships between the Electrochemical Noise and the Structure of the Electrodeposits of Metals, Electrochimica Acta, vol. 23, 1978, pp. 337-340.

[16] **Yank, Z. N., Zhang, Z., Leng, W. H., Ling K. and Zhang, J. Q.**, In-Situ Monitoring of Nickel Electrodeposit Structure Using Electrochemical Noise Technique, Transaction of non ferrous materials Society of China, vol. 16(1), 2006, pp. 209-216.

[17] **Zhang, Z., Leng, W. H., Cai, Q. Y., Cao F. H. and Zhang, J. Q.**, Study of the Zinc Electroplating Process Using Electrochemical Noise Technique, Journal of Electroanalytical Chemistry, vol. 578(2), 2005, pp. 357-367.

[18] **Veilleux, B., Lafront, A-M., Ghali E., and Roberge, P. R.**, The Use of Electrochemical Noise Measurements to Detect Bad Copper Electrorefining Conditions, Journal of Applied Electrochemistry, vol. 33, 2003, pp. 1093-1098.

[19] **Safisadeh, F., Lafront A-M and Ghali, E.,** Monitoring the Quality of Copper Deposition by Statistical and Frequency Analyses of Electrochemical Noise, METSOC 2007 (46th Conference of Metallurgists) Cu2007 the 6th International Copper/Cobre Conference, August 25-30, 2007, Toronto, Ontario, Canada, pp. 533-544.

[20] **Zaveri, N., Sun, R., Zufelt, N., Zhou, A., Chen, Y.**, Evaluation of Microbially Influenced Corrosion with Electrochemical Noise Analysis and Signal Processing, Electrochemical Acta, vol. 52, 2007, pp. 5795-5807.

[21] **Cottis, R., and Turgoose. S.**, Electrochemical Impedance and Noise, in corrosion testing made easy, Cottis R and S.Turgoose edited by NACE International, Houston, Texas, USA, 1999.

[22] **Mackinnon, D. J., Brannen J. M. and Fenn, P. L.**, Characterization of Impurity Effects in Zinc Electrowinning from Industrial Acid Sulphate Electrolyte, Journal of Applied Electrochemistry, vol. 17, 1987, pp. 1129-1143.

CHAPTER 11

General conclusions

According to the research work of this thesis, the following conclusions can be drawn.

General conclusions:

Higher silver content of Pb-Ag anodes has the lower overpotential during polarization and the lower corrosion rate during short potential decay periods after polarization. During polarization, addition of manganese sulphate from 4 to 8 g/L Mn^{2+} to the bath gave almost the same overpotentials and then increased for 10 and 12 for the electrode Pb-0.69% Ag. Malonic acid and Triethyl-benzylammonium chloride were added to the zinc electrolyte containing antimony to increase the current efficiency. Electrochemical Noise Analyses in the time domain monitored the synergetic effect of Gelatin and and is a powerful tool to detect the best combination of G and Sb^{3+}leading to better CE%.

Active and Corrosion Potential levels can be observed during the decay after electrolysis and it has been shown that each level has different corrosion products. Active corrosion state "ACS" or High corrosion rate for more Ag leads to less PbO_2 and less i_{corr}. In the Corrosion potential region "CRP" or Low corrosion rate, more Ag leads to more galvanic cells and very slightly higher i_{corr}.The shape of fluctuations during decay by electrochemical noise in situ of anode potential refers to different corrosion mechanisms such as uniform and localised corrosion.

11.1 Anode choice and performance:

11.1.1 Cyclic voltammetry studies of Pb-Ag alloys

Pure lead and 0.7% Pb-Ag alloy anode were examined by cyclic voltammetry in zinc electrolyte:

- Cyclic voltammetry technique has been used to observe redox peaks, and the associated species or products formed at these peaks could be characterized by chemical and physical methods. This permits to determine the influence of alloying elements such as Ag on the corrosion behaviour of lead anodes.
- Alloying pure lead with 0.7% Ag for use as anode during zinc electrowinning decreased oxidation peak ($Pb \rightarrow PbSO_4$) by almost 40% in sulphuric acid zinc

electrolyte. Also, 0.7% silver as alloying element decreased the height of oxidation peak of ($PbSO_4 \rightarrow \beta$-PbO_2) by ~ 40%.

- The change of the sweep rate in CV experiments has an effect on the shape of CVs, at low sweep rate of 3 mV/s, more redox peaks were observed than that at higher sweep rates. At the high sweep rate of 300 mV/s, the O_2 evolution peak is not visible.
- Bubbling argon into the zinc electrolyte did not change the shape and number of redox peaks on the curve of CV and the addition of $MnSO_4$ to the zinc electrolyte decreased the redox peaks on the curve for lead-silver anode in zinc electrolyte. (Chapter 4)

11.1.2 Performance of Pb-Ag alloy anodes

Three Pb-Ag alloys (0.5%, 0.6% and 0.7%) were studied using different techniques and related to the composition and microstructure of these alloys, the three alloys were cold rolled (laminated) anodes. The electrochemical measurements were used in comparison with the traditional electrochemical techniques such as optical microscopy, scanning electron microscopy (SEM) and X-ray analysis were utilized to analyze the microstructure and corroded surface of specimens in order to provide useful and complementary data and explanations.

11.1.2.1 Application of two successive cycles of polarization

Three Pb-Ag alloys were evaluated by two successive cycles of 5 hours galvanostatic polarization at 50 mA/cm^2 and 38°C, followed by 6 hours decay at Open Circuit Potential "OCP" to examine the performance of the Pb-Ag anodes in zinc electrowinining, the following conclusions can be deduced. An increase of silver content from 0.5, 0.6 to 0.7% in the Pb-Ag alloy #1< #2<#3<#4< #6<#5 leads to the following consecutive effects:

Decrease of overpotential The decrease of the overpotential of O_2 evolution of about 50 mV at the 1st and 2nd cycles of polarization. The average of polarization potential gives 2 groups of potential values: the highest potential values (#1, #4; #2) and the lowest

potential (#6; #3, #5). The O_2 overpotential values are increased of ~ 20 mV for the original surface as compared to the polished one and also during the 2nd cycle of polarization.

Decay and reduction of PbO_2 The decrease of the first plateau period during the decay at 1600 mV vs. SHE for the second level after about 10 and 25 min for the 1st and the 2nd cycles of polarization, respectively, leads to:

- A decrease of E_{corr} ~ 450 mV corresponding to a decrease of the corrosion current of ~ 3 $\mu A/cm^2$ during the reduction of PbO_2 corresponding to the active corrosion state at potential from ~ 1600 to 250 mV.
- A decrease of E_{corr} ~ 150 mV corresponding to an increase of the corrosion current 0.35 $\mu A/cm^2$ during the total reduction of PbO_2 to $PbSO_4$ corresponding to the corrosion potential region at potential lower than 250 mV.
- The duration of the plateau at 1600 mV, the potential level and the rate $\Delta E_{corr}/\Delta t$ during the decay (which follows the same trend as $\Delta i_{corr}/\Delta t$) could be a good indicator to compare the corrosion rates of the anode.
- Some observed differences in the obtained results were due to blistering, shear cracking, flaking or even fall of the corrosion products, different microstructure, and experimental errors and also due to the different corrosion products obtained during the general non-uniform corrosion on the surface of Pb-Ag anodes.

Active corrosion state Higher Ag (0.7%) content promotes the best corrosion resistance. However, at the corrosion potential region of potentials, slightly increasing corrosion rates (from 0.6 $\mu A/cm^2$ of 0.5%Ag-Pb anode to 0.70 $\mu A/cm^2$ of 0.7%Ag-Pb anode) have been observed with increasing silver content. At OCP, both corrosion potential and current values are lowered by the reduction time. The corrosion rate values are lowered at the 2nd cycle only when the corrosion region is reached. (Chapter 5)

11.1.2.2 Decay studies after 24 h polarization

It has been also observed in this study that during the frequent decay periods of the anodes in the industry (2 h/every week, and 16 h/every month, generally), the first hour and even the first 15 minutes (for 0.6 and 0.7% Ag of lead anodes) constitutes the most active reduction of the formed PbO_2 during polarization. After 24 h polarization in the zinc electrolyte at 38°C and 50 mA/cm^2, a theoretical and laboratory scale experimental approach of potential decay of Ag lead anodes during these 16 h can lead to the following statements:

- The main reduction and oxidation reactions for four identified stages can be suggested during the 16 h decay based on thermodynamic and past electrochemical considerations of discharge of lead battery electrodes. The different levels of E° of the four mentioned reduction and oxidation potentials confirm the existence of these consecutive four stages or levels of decay (discharge and/or corrosion).

- Different fluctuations of potential pattern referred to different corrosion types. The amplitude variation-oscillation of $\Delta E/\Delta t$ during the decay follows a certain pattern as a function of the plateau, decay time. However the $\Delta I/\Delta t$ is almost similar from one level to another in spite of the difference in the current density absolute values, except for the first level.

- The absolute magnitude of power spectral density "PSD" slopes of the three Ag lead anodes can correspond to different corrosion reactions and/or corrosion types. Comparing the parameters of the electrochemical noise, it is then found that electrochemical noise is a good technique to investigate the influence of silver on the corrosion rate of lead anodes. 0.5% Ag lead anode shows uniform corrosion at the beginning (first 1 h) and localised corrosion at the end of the 16 h decay, while 0.7% Ag lead anode shows high localised corrosion at the beginning followed possibly by uniform corrosion and then back to localised corrosion.

- It was found that the typical plateau had higher corrosion rate "$1/R_n$" and higher slope ratio "S_r" than that obtained during the following decay period. PSD can be used to determine the corrosion type during the decay.
- There is enough evidence from electrochemical noise measurements of existing difference in corrosion performance between the 0.5% and 0.7% Ag-Pb anodes. It can be admitted that 0.5% Ag-Pb anode has more corrosion products during polarization or electrolysis and this is shown by important plateau at the average value of 1.61 V/SHE for the longest time (45 min); while 0.7% Ag lead anode showed more active galvanic cells at the beginning of decay (11-16h of the decay) that can correspond to more localised corrosion because of more abundant silver containing phases.
- The characteristics of the four levels show that each level has different corrosion products and morphology. (Chapter 6)

11.1.2.3 Electrochemical activity

One lead anode containing 0.56 Ag was studied by electrochemical impedance spectroscopy (EIS) with $MnSO_4$ additions to evaluate their electrochemical activity, during potential decay period after 5 h of electrolysis.

During the first hour potential decay after 5 h polarization:

The Warburg controls the electrochemical reaction. The resistance of the electrochemical reaction of Pb-Ag consists of Warburg resistance and the charge transfer resistance, the Warburg resistance and the charge transfer resistance increased with the immersed time.

The potential decay during the period from the second to sixth hour:

- The double layer capacity and the film capacity decreased with the immersion time.
- The surface layer resistance and the charge transfer increased with time. (Chapter 7)

11.1.2.4 Polarization resistance

One Pb-0.25%Ag+0.1% Ca alloy anode and three commercial Pb-0.6~0.7% Ag alloys anodes were studied by conventional electrochemical methods and electrochemical impedance spectroscopy (EIS) in acid zinc sulphate electrolyte with and without $MnSO_4$ additions to evaluate their activity and corrosion behaviour after 5 electrolysis at a current density of 50 $mAcm^{-2}$ and 38°C:

During the potential decay period:

- The results of EIS measurements show that the anode with the highest Ag (0.69%) content had the highest polarization resistance among the four anodes, followed by the anodes containing 0.6% Ag, 0.25% Ag+0.1% Ca, and 0.56% Ag content in a bath with and without $MnSO_4$ addition.
- With the temperature and current density increase, the corrosion rates of Pb-Ag anodes increased.
- The four polished anodes in the acid zinc sulphate electrolyte containing $MnSO_4$ addition had lower corrosion rates than those in acid zinc sulphate electrolyte without $MnSO_4$ addition. Also the corrosion rate of Pb-Ag alloy anode decreases with the $MnSO_4$ addition.
- The corrosion rates of the four anodes decrease with the potential decay time.
- The values of more positive (higher) decay potentials lead to higher corrosion rates for all anodes with polished surface in a bath with and without $MnSO_4$ addition for short decay periods.
- The excessive quantity of calcium (0.12%) in Pb-Ag 0.25% anode showed generally higher overvoltages during electrolysis, if compared to 0.06% Ca and Pb-0.56% Ag content of another anode. However, it showed better corrosion rates during short decay periods in spite of the lower silver content. (Chapter 8)

11.2 Better additives for electrolyte

Considering 24 hours of galvanostatic polarization of electrowinning in acid sulphate electrolyte at 50 mA/cm^2, the following conclusions can be deduced:

- Among the examined additives, the use of cationic ions (PEG and TEBACl) seems to be better than anionic ones (PHFA and SLS). Cationic additives as (TEBACl) decreased the cell voltage ~ 42 mV in comparison to that of Glue + Cl^-. The morphology of zinc deposit from the standard electrolyte + TEBACl + Ni^{2+} was a well defined hexagonal platelet parallel to the substrate. Addition of MA to the standard electrolyte led to a zinc deposit characterized by the presence of platelets aligned at intermediate angles to aluminum cathode.

- The best of the four examined concentrations of malonic acid seems to be 100 mg/L for CE%, however 500 mg/L had a slightly higher effect than 100 mg/L for cell voltage only. The addition of 100 mg/L malonic acid, "MA", in acid electrolyte AE (containing 60 g/L of Zn^{2+}($ZnSO_4$,$7H_2O$), 180 g/L of H_2SO_4, and 8 g/L of Mn^{2+} ($MnSO_4$,H_2O), increased the CE by 2.5 % and decreased the cell voltage by about 20 mV as compared to the standard electrolyte containing G+Cl^- (3 and 250 mg/L respectively).

- In a solution containing 0.01 mg/L of Sb^{3+} (AE+Sb^{3+}) , it is recommended that malonic acid (100 mg/L) should be in presence of the industrial current additives Glue and chloride (250 mg/L of Cl^- and 3 mg/L of Glue) since this combination improved the CE% by about 1% as compared to that of G+Cl^-alone.

- The current efficiency of zinc deposit in the standard solution containing 5 g/L Ni^{2+} was around 91% due to the addition of TEBACl while that of G+Cl^- was too little to consider.

- 100 mg/L Malonic acid and 2 mg/L TEBACl added to H_2SO_4 acid at galvanostatic imposed current densities 40, 50, 60 $mAcm^{-2}$ and 50 $mAcm^{-2}$ respectively showed an increase of the catholic hydrogen evolution potential for about 8-14 mV in the stationary state. In presence of nickel ions (5 mg/L Ni^{2+}), the addition of TEBACl has led to higher polarization potentials (more negative) of the hydrogen evolution reaction on Zn deposit in acid solution than that of malonic acid. (Chapter 9)

11.3 Synergetic effect of additives in situ

- Adding gelatin alone such as 1 mg/L to the standard bath resulted in smoother electrodeposited zinc. This corresponds to an increase of cathodic potential and decrease of CE%. An increase of both positive skewness and kurtosis slopes with the quantity of added G has been observed. The best CE%, the most negative E_c values and the lowest slopes were found for 1 mg addition of G/L.

- Adding antimony alone over 0.01 mg/L to the bath resulted in bad zinc deposit, the process known as zinc re-dissolution was observed. The EN skewness and kurtosis slope values were around 0 monitoring a strong dissolution of zinc. Considering antimony containing solutions, 0.0036 mg/L of Sb^{3+} gives the least decrease on CE%. Generally, a decrease of CE% and a decrease of cathodic potential are accompanied by a decrease of both EN negative and positive skewness and kurtosis slope values, respectively, as deduced from this study.

- The conventional tools of investigation and NE measurements showed that the same trend is found as that of gelatin type behaviour alone, for high quantities of G = 1, 3 mg/L and low antimony concentrations (0.0036, 0.0055 mg/L); also antimony type behaviour alone has been found for high concentrations of antimony as Sb^{3+} = 0.02 mg/L and low gelatin concentrations (1 mg/L).

- The synergetic effect of gelatin and Sb consists in the decrease of cathodic potential and CE% giving skewness and kurtosis slope values around 0 showing that skewness and kurtosis values slightly different from 0 corresponds to the best current efficiency and less overpotentials. It can be stated then that the distribution of symmetric data around the mean value having the shape similar to that of the normal distribution (S and K are around 0) signals the best smooth and compact deposit.

- Considering the relative lower overpotentials, the best current efficiency, the quantity of added chemicals and possible influence on the morphology of the deposit, it seems appropriate to recommend 0.0036 Sb^{3+} and G = 1 mg/L as the best combination for the synergetic effect. EN analysis in the time domain

monitored this trend and thus it could be a powerful tool to detect the best combination of gelatin and antimony leading to better CE%. (Chapter 10)

CHAPTER 12

Future work

Long time potential decay of Pb-Ag alloy anode

In this thesis, the potential of Pb-Ag alloy anode was decay 16 h after 24 hours polarization. It is very interesting to investigate the potential decay of Pb-Ag alloy for one week to try to find the corrosion form on the surface of Pb-Ag alloy.

Scanning reference electrode technique

The Scanning Reference Electrode Technique (SRET) has proven to be an effective analytical tool in the characterization of materials at the liquid-solid interface. It has the ability to measure micro-galvanic potentials close to the surface of materials, and it allows in-situ examination (mapping) and quantification, on a microscopic scale, of electrochemical activity as it occurs, Also SRET has been shown to offer a technique for studying localized corrosion including pitting, inter-granular corrosion, and stress-corrosion cracking. It is very interesting to analyse localized corrosion of the Pb-Ag alloy anode by SRET and it is suggested to work in the weak acid solution with aggressive ambient (Cl^- ion) to simulate the corrosion phenomena, imposing different values of current on the experimental samples.

Electrochemical impedance evaluation of the corrosion behaviour of the Pb-Ag alloy anode

Impedance measurement is powerful tool to characterize the corrosion behaviour for Pb-Ag alloy anode in the zinc electrolyte; it will be very interesting to use the method of impedance to measure the resistance for each group of Pb-Ag alloy anode and to determine the corrosion current, also to better understand the process of the potential decay of Pb-Ag alloy anode.